UNIVERSIDAD COMPLUTENSE DE MADRID

FACULTAD DE CIENCIAS QUÍMICAS

TESIS DOCTORAL

Evaluación del potencial de las nanopartículas de Se en aplicaciones biomédicas mediante el uso de herramientas (bio)analíticas y tecnologías ómicas

MEMORIA PARA OPTAR AL GRADO DE DOCTOR

PRESENTADA POR

Héctor Estévez Sánchez

DIRECTOR

José Luis Luque García

UNIVERSIDAD COMPLUTENSE

DE MADRID

FACULTAD DE CIENCIAS QUÍMICAS

Programa de Doctorado en Química Avanzada

TESIS DOCTORAL

Evaluación del potencial de las nanopartículas de Se en aplicaciones biomédicas mediante el uso de herramientas (bio)analíticas y tecnologías ómicas

MEMORIA PARA OPTAR AL GRADO DE DOCTOR
PRESENTADA POR

Héctor Estévez Sánchez

Director

José Luis Luque García

Madrid, 2024

Agradecimientos

Como cualquier camino que merezca la pena, este no ha sido uno que haya andado solo. Sirvan estas líneas para reconocer la ayuda de todas aquellas personas que me han acompañado en él.

El mayor agradecimiento que puedo dedicar es a Jose. Formalmente: José Luis Luque García, director de esta Tesis Doctoral, al que hoy tengo el privilegio de llamar amigo antes que director.
Un buen día me abriste las puertas del despacho y me hablaste de ciencia. No has dejado de abrirme puertas desde aquel día, para que sea un buen científico, y para que descubra el mundo. Siento verdadera admiración por la agilidad y forma en la que eres capaz de pensar en ciencia, para la ciencia y para la vida. Entiendo que este es un caso especial puesto que, a pesar de toda tu ayuda en la universidad, es incomparable con lo mucho que atesoro la amistad que me has regalado. Has estado presente cuando empezaba a conocer a la que hoy es mi mujer. Estuviste cuando no podía moverme del hospital. Y, tanto Sandor como tú, habéis estado para disfrutar de la vida y hacer de vuestra casa, la nuestra. Nunca podré agradecértelo suficiente.

Este trabajo se ha llevado a cabo en el Departamento de Química Analítica de la Facultad de Ciencias Químicas. Mi reconocimiento a todos sus integrantes por construir un entorno donde muchos como yo hemos podido desarrollar nuestro trabajo. A María Pedrero, gracias por su dedicación infinita al interés general. Gracias a Miriam por su diligencia siempre, y a Isabel por su cariño, a quien nunca “le pisaré lo fregado”.

A los investigadores de los centros en los que he complementado el trabajo: muchas gracias. A Rafa Prados, por dedicarme su tiempo en Bilbao y su buena disposición siempre para enseñarme a trabajar con bacterias. De igual manera agradecer a Blanca González sus aportaciones en el diseño y síntesis de materiales, y también a Raquel Sánchez, Angélica, y Sonia Castillo por posibilitar los ensayos *in vivo*.

Cuando entré en el laboratorio de QBA por primera vez, no sabía cuántas experiencias tan buenas viviría gracias a todos los compañeros que han trabajado, literalmente, "codo con codo" conmigo.

Gracias en primer lugar a Estefi, una fuerza inagotable de la naturaleza dedicada en cuerpo y alma a la pasión por investigar. Gracias por acompañarme en todo lo científico, pero por supuesto por estar para todo lo demás. Hoy ya eres madre, y ese corazón tuyo es aún más grande.

A Mabel. Es bonito pensar que fuiste tú la que me enseñaste a sintetizar lo que sería el núcleo de mi trabajo, las SeNPs, y hoy te has convertido en amiga.

Gracias de igual modo a Pablo, Javier Espadas, Mari, Sandra y a Carlos, porque compartimos, además de ciencia, comedia. Por el ejemplo de prudencia y disciplina, mi agradecimiento a Andrés y a Guille. Mi camino ha sido mucho más sencillo trabajando a vuestro lado, me alegra haber descubierto a la persona detrás del investigador. Gracias a Pilar y a Roberto, por completar un muy buen equipo en el tramo final y hacerlo más agradable. A Cris, muchas gracias. Por humanizar el trabajo, por saber entender, y por saber disfrutar. Ha sido siempre un desahogo compartir contigo.

Al final del pasillo encontré lo que sería "mi otra casa", me integré en el grupo más heterogéneo y humano que podía imaginar. Un refugio

compuesto por Ana, Antonio, Bea, Dani, Fran, Hugo, Íñigo, Jorge, Susana Víctor y Sandra. Estaré y seguiréis estando, estoy seguro.

Pocos en número, fuertes en espíritu. Gracias a mis amigos Douglas, Ximo, Miguel, y Víctor. Este paso también es por vosotros, contad conmigo para todos los que deis vosotros siempre. A Cristina y a Belén, por haceros (bastante) mejores.

Agradezco mucho a Raúl y a Almudena por querer y por saber compartir. La lumbre que más calienta.

En todo este camino he ampliado mi familia. Gracias a Lucía, José Luis, Carlos, y demás "Jiménez y Falcaos" por nutrir cuerpo y alma. A mi tía Toñi y a mi tío Fernando, por el cariño y los buenos mimbres, gracias.

Por toda mi familia. Va por ti, tío Manolo, y por ti también Dolores, os echamos mucho de menos.

Soy Héctor por Oresti y por Luis. Mis padres. Mi mano derecha nunca se enterará de lo que hace la izquierda, y no haré mudanza en tiempos de crisis. Gracias por mis libros, mis croquetas, por el teatro, y por el Atleti. Cuando era pequeño pensaba que erais superhéroes, pero ahora que sé que sois humanos me gustáis incluso más.

Os quiero muchísimo.

Sandra, mi compañera de vida. Siento verdadera admiración por tu tesón, por tu bondad, y por ese espíritu sin límites de celebrar las cosas verdaderamente importantes. Gracias por coger mi mano aquel día, y no volverla a soltar ni en este camino, ni en ningún otro.

Tu risa sigue pareciéndome lo más bonito que veré nunca.

Te quiero.

La elaboración de la presente Tesis Doctoral ha sido posible gracias a la concesión de una contrato FPI (PRE2018-08419) dentro del programa estatal para contratos predoctorales para la formación de doctores/as contemplada en el Subprograma Estatal de Formación, del Programa Estatal de Promoción del Talento y su Empleabilidad, en el marco del Plan Estatal de Investigación Científica y Técnica e Innovación 2017-2020, en régimen de concurrencia competitiva y aplicando los principios de publicidad y objetividad.

La presente Tesis Doctoral se ha realizado en el Departamento de Química Analítica de la Facultad de Ciencias Químicas de la Universidad Complutense de Madrid (UCM) gracias al proyecto de investigación CTQ2017-85673-R titulado "Desarrollo y caracterización funcional mediante técnicas analíticas y -ómicas de nuevos nanosistemas híbridos como herramienta frente a cáncer y tuberculosis" concedido al grupo de investigación en Química Bioanalítica que dirige el profesor José Luis Luque García.

Tabla de contenidos

Resumen 14

Abstract 20

Objetivos 26

Objectives 30

I. Introducción 35

1.1 Selenio 37

1.1.1. Características propiedades, y especies 37

1.1.2. Selenio y salud 40

1.2. Nanotecnología y Nanomedicina 48

1.2.1. Nanomateriales: clasificación y propiedades 48

1.2.2. Nanomateriales mesoporosos de sílice 55

1.2.3. Nanomedicina y cáncer 60

1.2.4. Nanomedicina y tuberculosis 65

1.3. Técnicas -omicas 68

1.3.1. Transcriptómica 68

1.3.2. Proteómica 71

1.3.3. Metabolómica 74

II. Parte experimental 78

Capítulo 1. Evaluación del potencial antitumoral de las SeNPs 80

1.1. Effects of chitosan-modified selenium nanoparticles on cell proliferation, apoptosis and cell cycle pattern: comparison with other selenospecies 82

1.2. Transcriptome analysis identifies novel mechanisms associated with the antitumor effect of chitosan-stabilized selenium nanoparticles 104

1.3. Unraveling the mechanisms of Ch-SeNPs cytotoxicity against cancer Cells: insights from targeted and untargeted metabolomics....130

1.4. Combination of SILAC-based quantitative proteomics and selective enrichment of nuclear proteins to gain insight into the molecular mechanisms responsible for the antitumor effect of selenium nanoparticles. *In-vivo* validation in a murine melanoma model....160

Capítulo 2. Diseño y síntesis de un nuevo nanosistema híbrido con base de SeNPs con potencial antitumoral....189

2.1. Mesoporous silica nanoparticles functionalized with transferrin for target-oriented delivery of selenium nanoparticles: Deepening into the action mechanisms....186

Capítulo 3. Evaluación del potencial de las SeNPs micobactericida....232

3.1. Antimycobacterial effect of selenium nanoparticles on Mycobacterium tuberculosis....236

III. Discusión integradora....250

IV. Conclusiones....258

Anexos

A.I. Glosario de abreviaciones....263

A.II. Técnicas analíticas y bioanalíticas **267**

AII.1. Técnicas de caracterización analítica 268

AII.2. Técnicas bioanalíticas 273

A.III. Producciones científicas derivadas y comunicaciones a congresos **292**

A.III.1. Artículos científicos derivados 293

A.III.2. Otros artículos científicos 294

A.III.3. Capítulos de libro 295

A.IV. 4. Comunicaciones a congresos 295

Resumen

El selenio, así como un gran número de elementos y sustancias químicas, han sido estudiados con relación a los efectos que son capaces de producir en un contexto bioquímico. Aunque la naturaleza química es un factor crucial en su aplicabilidad como agentes quimioterapéuticos, la forma y dimensiones en la que se presentan es igual de decisiva. Gracias a la irrupción de la nanotecnología, así como del desarrollo de técnicas bioanalíticas y de caracterización, los avances en el estudio de las propiedades de nuevos materiales han evolucionado exponencialmente. Concretamente, una de las áreas que ha experimentado una mayor revolución es la nanomedicina.

El cáncer es, desde hace décadas, una de las enfermedades con mayor mortalidad del planeta, superando los 10 millones de defunciones anuales. Se define por una serie de cambios mutagénicos en las células que multiplican exponencialmente su crecimiento.
Su tratamiento es principalmente cirugía, radioterapia, y quimioterapia. A pesar de que los avances en esta última son muy considerables, suele apoyarse en tratamientos sistémicos. Puesto que el fármaco no se absorbe específicamente, las dosis suelen ser mayores de las teóricamente necesarias, y los efectos secundarios suelen tener un precio muy alto para los pacientes.

El selenio ha sido apreciado clásicamente por sus propiedades antioxidantes, Si bien, en numerosos estudios, también se ha sugerido su potencial quimioterapéutico. Por este motivo, en la presente Tesis Doctoral, en primer lugar se comparó el comportamiento de nanopartículas de selenio elemental (SeNPs), con el de otras formas de selenio más estudiadas, tanto orgánicas como inorgánicas, en una serie de estudios bioanalíticos en células de hepatocarcinoma (HepG2). Además

de estudios preliminares de viabilidad, proliferación y muerte celular, se exploraron ciertos marcadores claves en rutas metabólicas importantes como la apoptosis o el control del ciclo celular. Las SeNPs exhiben un comportamiento claramente diferente al resto de especies evaluadas. Son capaces de reducir la viabilidad y proliferación celular, y no inducen apoptosis, sino que inhiben parcialmente una de las ciclinas dependientes de kinasa que controlan la entrada del ciclo celular hacia mitosis. Esta inhibición parcial, además de confirmar a las SeNPs como potencial agente en quimioterapia, es un indicador de que afectan selectivamente a las células cancerígenas, ya que tienen un metabolismo mucho más rápido.

Una vez confirmado el potencial antitumoral de las SeNPs, se planteó profundizar en los mecanismos moleculares del efecto de las SeNPs en células cancerígenas. A través de múltiples estrategias -ómicas (transcriptómica, proteómica y metabolómica) se pudo obtener un conocimiento muy valioso acerca de cómo las SeNPs son capaces de modular, inhibir o activar diferentes rutas celulares cuya participación en procesos cancerígenos es fundamental.

El estudio de transcriptómica, además de confirmar la inhibición parcial de Cdk1 observada por Western Blot, reveló un gran número de alteraciones en tránscriptos con una participación muy significativa en el ciclo celular como por ejemplo CDKN1A, CDC25, o CDCA2, entre otros. Otro gran número de genes alterados son considerados supresores tumorales como BTG3 o DUSP5, o inhibidores de la proliferación celular como DUSP5. Cabe mencionar también la colección de genes asociados a la inducción del fenotipo senescente encontrados alterados, como por ejemplo SERPINE-1, CCL-20 o MMP3. De formas complementaria, se

analizó específicamente la expresión de uno de los marcadores más claros de senescencia; la β-galactosidasa. Las células expuestas a SeNPs expresaron unos niveles de enzima iguales a los del control positivo de senescencia.

Por su parte, la combinación del estudio de metabolómica dirigida y no dirigida, resultó en un conocimiento mucho más profundo acerca de los mecanismos biomoleculares relacionados con el efecto citotóxico de las SeNPs. La metabolómica dirigida reveló alteraciones muy significativas en el metabolismo energético después de la exposición a las nanopartículas (niveles de ATP, ADP, NAD^+), provocando la disrupción del ciclo de los ácidos tricarboxílicos. Se probaron, gracias a la metabolómica no dirigida, las conclusiones previas acerca del ciclo celular, así como una deriva metabólica hacia la glicólisis como ruta alternativa o la inducción de hipoxia como consecuencia de la exposición a SeNPs.

Dado que gran parte de los datos recabados apuntaban a que la acción de las SeNPs era especialmente significativa en el núcleo celular, se diseñó un experimento SILAC (proteómica cuantitativa) a través del cual profundizar en dicha afección. Además de confirmarse el potencial antitumoral de las SeNPs por rutas celulares ya observadas, se descubrieron nuevas potenciales dianas terapéuticas como PLEC, SUMO2 o RSU1. Complementariamente, se empleó la qPCR para validar algunas dianas relativas al ciclo celular.

Por último, se comprobó la efectividad de las SeNPs en un modelo *in vivo* (murino). El tamaño de los tumores a los que se le administró una dosis de SeNPs fue significativamente menor al de aquellos sin tratar, sin

mostrar ningún signo de efectos secundarios derivados del mismo, confirmándose así nuevamente el potencial de las SeNPs en un ambiente *in vivo* más complejo.

Sin embargo, el desarrollo de un potencial fármaco tiene como compromiso, además de ser capaz de exhibir sus propiedades terapéuticas, el respetar el entorno biológico evitando o limitando efectos secundarios nocivos. Por ello, una parte importante de la presente Tesis Doctoral se centró en diseñar y sintetizar un nuevo nanomaterial que pudiera dirigirse de forma selectiva al tumor, que fuese biocompatible, y cuya base farmacológica fueran las SeNPs. El vehículo químico elegido fueron las nanopartículas de sílice mesoporosa, que proporcionan un andamiaje ideal para la funcionalización con ligandos de vectorización. La transferrina resultó ser idónea tanto para conseguir un targeting efectivo en células cancerígenas, como para nuclear las SeNPs.

De igual forma, se realizaron estudios enfocados a comprobar la capacidad de este nanosistema para, no solo potenciar la acción quimioterapéutica de las SeNPs, sino también para dirigirlas específicamente a las células cancerígenas y entender los mecanismos moleculares implicados. Se comprobó la efectividad de la transferrina como ligando de targeting comparando células que no expresan receptores de transferrina en su membrana, con las HepG2, que sí los expresan. Además, se realizaron estudios de viabilidad celular y ciclo celular por citometría de flujo.

Los estudios siguientes trataron nuevamente de profundizar en los mecanismos moleculares responsables de la quimioterapia. La transcriptómica y los estudios de senescencia confirmaron la alteración de

muchos de los elementos alterados por acción de las SeNPs, y además permitieron el descubrimiento de otros nuevos

Finalmente, se planteó el estudio de la capacidad del nanosistema en modelos *in vivo* (embriones de pollo). Nuevamente, el comportamiento del material fue muy prometedor ya que la exposición al nanosistema consiguió reducir en un 70% el crecimiento de un tumor altamente agresivo triple negativo de cáncer de mama (MDA-MB-231).

Además de evaluar el potencial antitumoral de las SeNPs, también se decidió estudiar su potencial capacidad bactericida frente a tuberculosis. La prevalencia y capacidad de mutación y adaptación de esta enfermedad sigue creciendo, así como la urgencia por encontrar materiales bactericidas específicos.

Las SeNPs demostraron ser muy efectivas en la inhibición del crecimiento bacteriano, tanto de la cepa inocua Mycobacterium smegmatis como en *Mycobacterium tuberculosis*. Los ensayos de TEM y cryo-TEM probaron un gran compromiso de la integridad de la pared bacteriana y la extrusión del material citoplasmático a causa de la exposición a las mismas.

Abstract

Selenium, along with a large number of elements and chemicals, has been studied concerning the effects it can produce in a biochemical context. While chemical nature is a crucial factor in its applicability as chemotherapeutic agents, the form and dimensions in which they appear are equally decisive. Thanks to the emergence of nanotechnology, as well as the development of bioanalytical and characterization techniques, advances in studying the properties of new materials have evolved exponentially. Specifically, one of the areas that has experienced a significant revolution is nanomedicine.

Cancer has been one of the deadliest diseases on the planet for decades, surpassing 10 million deaths annually. It is defined by a series of mutagenic changes in cells that exponentially increase their growth. Its treatment primarily involves surgery, radiotherapy, and chemotherapy. Despite considerable advances in the latter, it often relies on systemic treatments. Since the drug is not specifically absorbed, doses are usually higher than theoretically needed, and the side effects often come at a high cost to patients.

Selenium has traditionally been appreciated for its antioxidant properties. However, it has recently been suggested that it may have chemotherapeutic capacity. For this reason, the general aim of this research work was to compare the behavior of selenium nanoparticles (SeNPs) with that of other more common forms of selenium, both organic and inorganic, in a series of bioanalytical studies in hepatocarcinoma cells (HepG2). In addition to preliminary studies on viability, proliferation, and cell death, certain key markers in important metabolic pathways, such as apoptosis or cell cycle control, were explored. SeNPs exhibited a unique behavior against HepG2 cells. They can reduce cell viability and proliferation, and do not induce apoptosis. Instead, they partially inhibit

one of the cyclin-dependent kinases that control the cell cycle's entry into mitosis. This partial inhibition, in addition to confirming SeNPs as a potential chemotherapeutic agent, is an indicator that they selectively affect cancer cells, as these cells have a much faster metabolism.

Once the antitumor potential of SeNPs was confirmed, the second step was to delve into the molecular mechanisms of the effect of SeNPs on cancer cells. Through multiple omics strategies (proteomics, genomics, metabolomics, and transcriptomics), valuable knowledge was obtained about how SeNPs can modulate, inhibit, or activate different metabolic pathways crucial in cancer processes.

The transcriptomic study, in addition to confirming the partial inhibition of Cdk1 observed by Western Blot, revealed numerous alterations in transcripts significantly involved in the cell cycle, such as CDKN1A, CDC25, or CDCA2, among others. Another set of altered genes included tumor suppressors like BTG3 or DUSP5, as well as cell proliferation inhibitors like DUSP5. There were also several altered genes associated with the induction of the senescent phenotype, such as SERPINE-1, CCL-20, or MMP3. Additionally, the expression of one of the clearest markers of senescence, β-galactosidase, was analyzed, showing levels comparable to the senescence control in cells exposed to SeNPs.

The combination of targeted metabolomics with untargeted metabolomics provided a much deeper understanding of the biomolecular mechanisms related to the cytotoxic effect of SeNPs. Targeted metabolomics revealed significant alterations in energy metabolism after nanoparticle exposure (ATP, ADP, NAD^+ levels), disrupting the tricarboxylic acid cycle. Untargeted metabolomics supported previous conclusions regarding the cell cycle and revealed metabolic shifts towards

glycolysis as an alternative pathway or the induction of hypoxia due to SeNPs.

As a significant portion of the data suggested that SeNPs action was particularly focused in the cell nucleus, a SILAC experiment (proteomics) was designed for further investigation of this impact. Besides confirming the anticancer potential of SeNPs through observed metabolic pathways, new potential therapeutic targets such as PLEC, SUMO2, or RSU1 were discovered. Also, qPCR was additionally employed to validate some cell cycle-related targets.

Finally, the effectiveness of SeNPs was confirmed in an *in vivo* model (mice). Tumors treated with SeNPs showed significantly smaller sizes at the end of the experiment in comparison to untreated ones, with no signs of related side effects, confirming the potential of the nanoparticles.

However, the development of a potential chemptherapeutic drug involves not only exhibiting anticancer properties but also respecting the biological environment by avoiding or limiting harmful side effects. Therefore, the next objective of this Thesis was focused on constructing a nanomaterial that could specifically target tumors, be fully biocompatible, and have SeNPs as the pharmacological base. Mesoporous silica nanoparticles were chosen as the chemical vehicle, providing an ideal framework for functionalization with targeting ligands. Transferrin proved suitable for effective targeting in cancer cells and nuclear localization of SeNPs.

Similarly, studies were conducted to verify the ability of this nanosystem to not only enhance the chemotherapeutic action of SeNPs but also to specifically target cancer cells and understand the involved molecular mechanisms. The effectiveness of transferrin as a targeting

ligand was confirmed by comparing cells that do not express transferrin receptors on their membrane with HepG2 cells, which do express them. Additionally, studies on cell viability and the cell cycle were conducted using flow cytometry. Subsequent studies aimed to further explore the molecular mechanisms responsible for chemotherapy. Transcriptomics and senescence studies confirmed the alteration of many elements by SeNPs and allowed the discovery of others.

As the final goal of the work, the study assessed the nanosystem capacity in *in vivo* models (chicken embryos). Once again, the material showed promising behavior, reducing the growth of a highly aggressive triple-negative breast cancer tumor (MDA-MB-231) by 70%.

As secondary objectives of the research, part of the SeNPs study focused on their bactericidal capacity against tuberculosis. The prevalence, mutation capacity, and adaptation of this disease continue to grow, as does the urgency to find specific bactericidal materials. SeNPs proved highly effective in inhibiting bacterial growth, both in the Mycobacterium smegmatis and in Mycobacterium tuberculosis strains. TEM and cryo-TEM assays demonstrated significant compromise of the bacterial wall integrity and the extrusion of cytoplasmic material due to exposure to SeNPs.

Objetivos

El impacto de la nanotecnología se ha fundamentado en un redescubrimiento del comportamiento químico de elementos o materiales a través de la obtención de nuevas dimensiones físicas. A pesar de que el selenio es un elemento ampliamente estudiado en sus múltiples formas, orgánicas e inorgánicas, las propiedades de su forma nanoparticulada aún no ha sido estudiada en profundidad.

Por este motivo, el **objetivo principal** de la presente Tesis Doctoral ha sido evaluar el potencial de las nanopartículas de selenio en aplicaciones biomédicas; concretamente en su potencial como agente antitumoral y como bactericida.

Para llevar a cabo este objetivo principal, se establecieron los cuatro objetivos secundarios que se detallan a continuación:

Objetivo 1. Evaluar el efecto diferencial de las SeNPs en comparación con otras especies de selenio. Para ello se utilizó un modelo *in vitro* de células de hepatocarcinoma humano que se expuso a SeNPs y a diferentes especies de Se orgánicas e inorgánicas. El efecto de las diferentes especies fue estudiado mediante la realización de diferentes ensayos bioanalíticos basados en técnicas de microscopía, citometría de flujo, etc.

Objetivo 2. Evaluar el potencial antitumoral de las SeNPs y elucidar sus mecanismos biomoleculares de acción. Una vez demostrado el comportamiento único de las SeNPs en comparación con otras especies de Se, se emplearon técnicas bioanalíticas y las tres principales tecnologías ómicas (transcriptómica, proteómica y metabolómica) para evaluar su potencial antitumoral y descifrar las principales rutas celulares por las que las SeNPs ejercen su acción antitumoral. Asimismo, la efectividad de las SeNPs se evaluó en un modelo pre-clínico *in vivo* de melanoma.

Objetivo 3. Diseño, síntesis y caracterización funcional de un nuevo nanosistema híbrido con base Se como agente antitumoral. El tercer objetivo se basó en el diseño de un nuevo nanosistema capaz de dirigir de forma selectiva las SeNPs a células tumorales, con objeto de aumentar su efectividad y minimizar posibles efectos secundarios. Para ello se diseño una ruta sintética basada en el uso de nanopartículas de sílice mesoporosa y de transferrina como ligando de vectorización. La efectividad del nanomaterial propuesto se evaluó tanto en un modelo *in vivo* que permitió identificar igualmente los principales mecanismos de acción, como en un modelo *in vivo* que corroboró su eficacia en un ambiente más complejo.

Objetivo 4. Evaluación del potencial micobactericida de SeNPs. Como objetivo final, se exploró el potencial bactericida de las SeNPs frente a una micobacteria de especial relevancia, *Mycobacterium tuberculosis*. Para ello se emplearon ensayos bioanalíticos y técnicas de microscopía para la evaluación de posibles interacciones nanopartícula-pared bacteriana.

Objectives

The impact of nanotechnology has been grounded in a rediscovery of the chemical behavior of elements or materials through the acquisition of new physical dimensions. Despite selenium being widely studied in its various forms, both organic and inorganic, the properties of its nanoparticulate form have not been thoroughly investigated. For this reason, **the main objective** of this doctoral thesis has been to assess the potential of selenium nanoparticles in biomedical applications, specifically in their potential as an antitumoral agent and as a bactericide. To achieve this main objective, four secondary objectives were established, detailed as follows:

Objective 1: Evaluate the differential effect of SeNPs compared to other selenium species. An in vitro model of human hepatocellular carcinoma cells was exposed to SeNPs and different organic and inorganic selenium species. The effect of the different species was studied through various bioanalytical assays based on techniques such as microscopy, flow cytometry, etc.

Objective 2: Evaluate the antitumoral potential of SeNPs and elucidate their biomolecular mechanisms of action. Once the unique behavior of SeNPs compared to other selenium species was demonstrated, bioanalytical techniques and the three main omics technologies (transcriptomics, proteomics, and metabolomics) were employed to assess their antitumoral potential and decipher the main cellular pathways through which SeNPs exert their antitumoral action. Additionally, the effectiveness of SeNPs was evaluated in an in vivo pre-clinical model of melanoma.

Objective 3: Design, synthesis, and functional characterization of a new hybrid nanosystem based on selenium as an antitumoral agent. The third objective involved designing a new nanosystem capable of selectively targeting SeNPs to tumor cells to enhance their effectiveness and minimize potential side effects. This was achieved through a synthetic route using mesoporous silica nanoparticles and transferrin as a vectorization ligand. The effectiveness of the proposed nanomaterial was evaluated in both an in vitro model, allowing the identification of the main mechanisms of action, and an in vivo model that confirmed its efficacy in a more complex environment.

Objective 4: Evaluation of the mycobactericidal potential of SeNPs. As the final objective, the bactericidal potential of SeNPs against the clinically relevant Mycobacterium tuberculosis was explored. Bioanalytical assays and microscopy techniques were employed to assess possible nanoparticle-bacterial wall interactions.

I. Introducción.

I.1. Selenio

I.1.1 Características, propiedades y especies

El hallazgo del selenio (1817), como muchos de los grandes descubrimientos en ciencia, ocurrió por "accidente", fruto del trabajo de Jöns Jacob Berzelius. Durante la extracción de azufre de pirita (FeS) de la mina sueca de Falun llamada *Stora Kopparbergel* para la producción de H_2SO_4, observó que quedaba un residuo rojizo, el cual en un primer momento fue identificado como teluro. Berzelius comprobó que al ser calentado, este residuo emanaba un olor desagradable, al igual que el Te. Pronto se dio cuenta que, a pesar de poseer ciertas propiedades similares a las del Te, se trataba de un elemento nuevo. Por ello, y dado que el Te, identificado con la Tierra, fue nombrado a partir del término latino *tellus*, "tierra", Berzelius decidió llamar a este nuevo elemento selenio, a partir del término griego *selene*, que significa luna (**Figura 1**) [1].

Figura 1. Representación de Endimión y Selene, diosa griega a partir de la cual se nombra al selenio (Filippo Lauri, 1650).

El selenio, de símbolo Se y número atómico 34, pertenece a la familia de los no metales. Se clasifica dentro del grupo 16 de la tabla periódica, periodo 4 y bloque p. Su masa atómica es de 78,96 u y su

configuración electrónica es [Ar] $3d^{10}4s^{2}4p^{4}$. Tiene cuatro estados de oxidación en la naturaleza: selenio (0), seleniuro (-2), selenito (+4) y selenato (+6). Sus propiedades químicas se asemejan mucho a las del azufre en términos de tamaño atómico, energía de enlace, potencial de oxidación y principales estados de oxidación. Asimismo, tiene semejanzas con el teluro, aunque en menor medida. En la naturaleza coexisten seis isótopos con números másicos 74, 76, 77, 78, 80, y 82 [2].

El selenio es estable y no se oxida a temperatura ambiente. Puede combinarse con múltiples elementos (hidrógeno, flúor, cloro, bromo, fósforo, etc.), formando compuestos análogos a los que normalmente forma el azufre en la naturaleza. Sin embargo, el selenio tiene una menor afinidad por el oxígeno que el azufre, conociéndose solo dos óxidos principales; SeO_2 y SeO_3. El dióxido se forma por combustión del selenio en aire formando un producto estable que se solubiliza en agua produciéndose ácido selenoso (H_2SeO_3), de gran poder oxidante excepto para unos pocos metales (oro, platino y paladio). El ácido selénico (H_2SeO_4), en cambio, es un diácido fuerte e higroscópico, más oxidante que el ácido sulfúrico y que se obtiene por reacción de un agente oxidante con selenio, dióxido de selenio, o ácido selenoso en agua [3]. La combinación con hidrógeno más común es el seleniuro de hidrógeno (H_2Se), altamente reactivo, el cual se descompone en hidrógeno molecular y selenio a 160 °C.

A temperatura ambiente, el selenio es una sustancia sólida, mostrándose en diferentes formas. El selenio amorfo obtenido por precipitación a partir de una solución acuosa es semejante al polvo de ladrillo, y presenta propiedades fotoconductoras. Se torna gris al alcanzar temperaturas entre 110°C y 180°C. El selenio vítreo es marrón y se forma

por enfriamiento rápido del selenio líquido. Las formas inorgánicas de selenio se muestran en la naturaleza en forma de piritas combinadas con metales (cobre, hierro, níquel, oro, etc.), en diferentes concentraciones, normalmente en el rango entre 0,1 y 2 mg/Kg.

Gracias a la erosión de las rocas, el selenio se encuentra en suelos principalmente en forma de selenito o selenato. Estas formas aniónicas son solubles y biodisponibles y, por lo tanto, potencialmente tóxicas. La concentración media varía entre 0,1 y 0,7 mg/kg, aunque en arcilla puede llegar hasta los 2 mg/kg y en suelos tropicales hasta 4,5 mg/kg. Generalmente, el selenio tiende a concentrarse en suelos de las regiones más secas del planeta. En plantas, la incorporación y redistribución del selenio por las raíces ocurre rápidamente. Se encuentra un 85% de selenato y un 70% de selenito en tejidos aéreos (respecto al incorporado en la raíz).

El selenio se encuentra también en el agua debido a drenajes del suelo o depósitos. En agua de mar, su concentración está en torno a 0,008 g/L. En agua, el dióxido de selenio forma el ácido débil H_2SeO_3 (pKa_1=2,8, pKa_2=8,5), mientras que el trióxido produce H_2SeO_4, un ácido más fuerte (pKa_1=-3, pKa_2= 1,7). El selenato es la forma más estable de los óxidos de selenio en soluciones alcalinas y oxidantes, mientras que los compuestos alquílicos de selenio son los menos tóxicos (productos primarios de detoxificación). En condiciones de ingesta excesiva de selenio, es la forma trialquílica la que ve incrementada predominantemente su generación, la cual produce olor a ajo en la exhalación [4].

Una gran variedad de usos comerciales tiene al selenio como eje químico principal. Los principales: manufactura de cerámicas, vidrio,

células fotoeléctricas, pigmentos, semiconductores y aceros (**Figura 2**). También se emplea en fotografía o producción farmacéutica.

Figura 2. En la industria cristalera, el selenio se adiciona por su capacidad para decolorar el cristal, reduciendo las tonalidades verdes y amarillas no deseadas.

I.1.2. Selenio y salud

No es hasta 1957 cuando se subraya el carácter esencial del Se, el cual se define como un elemento traza con un carácter ambivalente, tanto de gran valor nutricional como potencialmente tóxico, antiinflamatorio, antimutagénico o antiviral, entre otros. En el cuerpo humano, forma parte de enzimas clave como la glutatión peroxidasa, la tioredoxina reductasa o las deiodinasas, las cuales juegan un papel principal en la reproducción, como antioxidantes, en funciones musculares o en prevención contra radicales libres y tumores.

Es necesario definir el impacto del selenio en la biota en relación con su concentración. Unos niveles óptimos permiten un metabolismo y crecimiento normales y, por el contrario, un exceso de selenio puede revertir sus propiedades antioxidantes, hasta convertirlo en un agente pro-oxidante. Pese a ser un elemento con potencial quimioterapéutico, puede ser tóxico, lo que compromete la supervivencia de los organismos. Su

toxicidad, además de depender de la concentración, lo hará también de la forma química en la que se presente. Por lo tanto, la relación entre el selenio y el riesgo de enfermedad dibuja una gráfica en forma de "U", en la que solo una concentración óptima permite observar beneficios asociados a este elemento [5]. Como ejemplo, una ingesta excesiva de selenio puede producir selenosis, una enfermedad que produce anomalías en el sistema nervioso, pérdida de pelo y uñas o lesiones cutáneas.

Es por eso que, desde entonces, el selenio recibe un gran foco de atención en estudios biomédicos [6,7]. Sin embargo, las investigaciones acerca de la relación selenio y salud son relativamente recientes, por lo que se han producido diferentes corrientes de opinión relativas al selenio. Una atmósfera de *selenofobia* en la década de los setenta [8], dio paso a una cultura *selenofílica* [9] en la siguiente década por sus teóricos beneficios para la salud. Actualmente, y gracias a décadas de estudio, podemos afirmar que, tanto una deficiencia como un exceso de selenio en el organismo, pueden ser el origen de diversas patologías y disfunciones.

Desregulaciones en los niveles de ingesta de selenio, tanto por exceso como por defecto pueden ocasionar por sí mismas o por lo menos contribuir a la aparición patologías cardiovasculares, metabólicas, endocrinas o neurológicas [10].

El selenio generalmente se integra dentro de los procesos moleculares de un organismo en forma de selenoproteínas. Para ser consideradas selenoproteínas, deben contener un residuo de selenocisteína en su cadena, la cual es un análogo de la cisteína en la que el átomo de azufre ha sido sustituido por uno de selenio [11]. Su función es, fundamentalmente, antagonista del estrés oxidativo, de ahí el carácter antioxidante atribuido desde siempre al selenio. La familia de las

selenoproteínas engloba no menos de veinticinco proteínas eucariotas, cuya expresión depende directamente de los niveles de selenio, y la cual se regula mediante hormonas [12], entre las que destacan la glutatión peroxidasa, la tioredoxina reductasa, o la metionina sulfóxido reductasa (**Figura 3**). La importancia de estas selenoproteínas reside en su capacidad para evitar las reacciones redox, reduciendo así el estrés oxidativo y por tanto la respuesta inflamatoria [13].

La primera de estas selenoproteínas en ser caracterizada fue la glutatión peroxidasa (GPx). Se han identificado hasta la fecha cinco enzimas de este tipo que contienen selenio: GPx1-4 y GPx6. Esta enzima es un componente indispensable del sistema antioxidante en el cuerpo humano ya que su función principal es la de proteger al organismo del efecto degradante de los hiperóxidos de forma endógena. Esta enzima

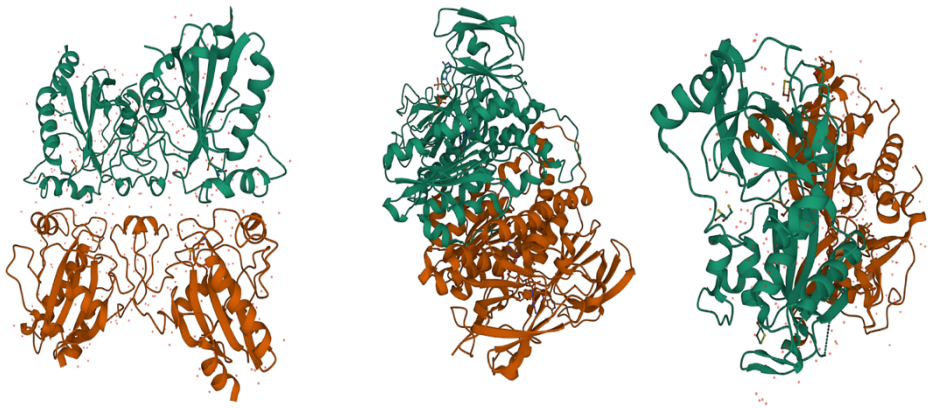

Figura 3. Selenoproteínas principales en el cuerpo humano. De izquierda a derecha: Glutatión peroxidasa (GPx), tioredoxina reductasa (TR) y metionina sulfóxido reductasa (MsrB1).

cataliza la reducción de peróxido de hidrógeno (H_2O_2) o lipoperóxido (L-OOH), mediante la acción del agente reductor glutatión reducido (GSH). Los lipoperóxidos generan especies reactivas oxígeno en tejidos animales,

como por ejemplo radicales peróxido (L-OO*). La acción de las GPx evita la oxidación de los L-OOH, reduciéndolos en presencia de GSH. Además, procesos clave como la espermatogénesis son altamente dependientes de la GPx4, ya que ésta reduce los hidroperóxidos fosfolípidos, protegiendo a los espermatozoides frente a estrés oxidativo.

Otra de las selenoproteínas clave en la regulación de procesos bioquímicos es la torredoxina (Trx), una pequeña proteína oxidorreductasa y disulfuro, globular, compacta y ubicua. La Trx tiene la capacidad de reducir grupos disulfuro (S-S) formados entre dos tioles al oxidarse. En humanos, interviene en procesos como el balance redox celular, inhibición o promoción de la muerte celular, y la modulación del proceso inflamatorio, entre otros.

Además, el selenio es parte fundamental de muchas otras selenoproteínas, las cuales participan en procesos fundamentales como la barrera antioxidante (**Figura 4**). Por ejemplo, el residuo de selenocisteína en la selenoproteína K le confiere bioactividad, y esta proteína está involucrada tanto en resistencia a estrés oxidativo como en prevenir la degradación del retículo endoplasmático, entre otros procesos. La

reducción del estrés oxidativo se da también mediante la acción de la enzima superóxido dismutasa, llevando a cabo el *quenching* del radical superóxido y convirtiéndolo en peróxido de hidrógeno; compuesto que es

A. Sistema antioxidante tiorredoxina

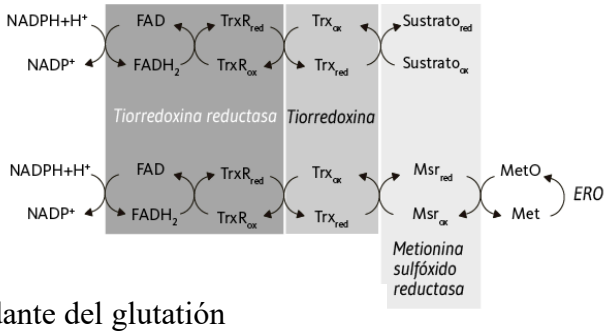

B. Sistema antioxidante del glutatión

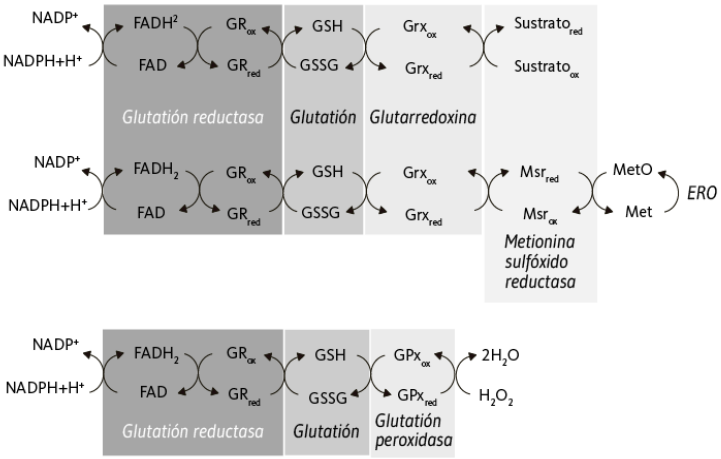

Figura 4. Selenoproteínas en sistemas antioxidantes basados en tiol.

finalmente descompuesto en agua y oxígeno mediante la enzima catalasa, previniendo así cualquier daño genético [14].

Asimismo, el selenio juega un papel fundamental en la síntesis, metabolismo y función de la hormona tiroidea, clave para el desarrollo,

crecimiento y diferenciación celular, a través de las enzimas deionidasas, encargadas de regular la función tiroidea. Además de la suplementación, la manipulación de selenoproteínas puede convertirse en una buena estrategia para mitigar la deficiencia en selenio; sin embargo, es necesario conocer en detalle el rol de cada selenoproteína así como los mecanismos moleculares en los que está involucrada [15].

Además de en procesos redox, el selenio también está implicado en la regulación del sistema inmune, el cual se define por una compleja colección de procesos que actúan conjuntamente para proteger al organismo del ataque de patógenos. El selenio adquirido a través de la dieta es esencial para una respuesta inmune óptima, influyendo tanto en la respuesta innata como en la adquirida.

La respuesta innata establece barreras contra la infección además de agentes no específicos de defensa como los macrófagos. La adquirida, por el contrario, está representada en gran medida tanto por los linfocitos T como los B. Aquellos linfocitos deficientes en selenio presentan menor capacidad proliferativa, mientras que, en macrófagos, la deficiencia de selenio afecta directamente a la síntesis de leucotrieno B4, el cual es un factor de control de la inflamación. Estos síntomas presentan mejoría con la suplementación dietética de selenio [16, 17].

La inmunidad humoral (defensa contra toxinas y microorganismos extracelulares) también se ve afectada debido a la deficiencia de selenio haciendo que los niveles de inmunoglobulinas IgM, IgG e IgA decrezcan significativamente. En células endoteliales de personas asmáticas, se comprueba que los niveles de selenio son muy bajos, resultando en una mayor adhesión a neutrófilos [18, 19].

La deficiencia en selenio está directamente relacionada con niveles altos de citokinas inflamatorias en un gran número de tejidos: tracto gastrointestinal, útero, glándulas mamarias, etc. [20, 21]. Es la administración de selenio la que consigue reducir los niveles de inflamación [22, 23].

Las funciones cerebrales están muy influidas por los niveles de selenio. Las primeras evidencias que se obtuvieron de esta relación nacieron de un estudio donde a niños que sufrían de convulsiones se les suplementaba con selenio. Estas convulsiones se atribuían a bajos niveles de glutatión peroxidasa, por lo que la suplementación conseguía atenuarlas [24]. El rol del selenio ha sido una incógnita durante décadas hasta que técnicas bioanalíticas como la genómica o la proteómica han permitido elucidarla [25, 26].

El selenio es vital para el buen funcionamiento del sistema nervioso central (SNC), sin embargo, los niveles de este elemento son inferiores en este tejido (90-110 ng $*$ mg^{-1}) si los comparamos con los presentes en otros órganos como el riñón o el hígado (400-640 ng $*$ mg^{-1} y 220-340 ng $*$ mg^{-1}) [27]. Sin embargo, algunos estudios puntualizan que el selenio se acumula preferentemente en la materia gris cerebral [28].

El selenio, gracias a sus propiedades antioxidantes, sirve de protección frente a la acción de las especies reactivas de oxígeno (ROS). La masa cerebral es especialmente sensible al estrés oxidativo debido a su alta actividad metabólica y a sus altos niveles de ácidos grasos poliinsaturados [29]. En el proceso inevitable de envejecimiento se producen desequilibrios entre fuerzas antioxidantes y las especies reactivas de oxígeno (ROS), cambios en la renovación mitocondrial y

agotamiento de células madre. Estos fenómenos están estrechamente asociados con la inflamación crónica [30]. La capacidad antioxidante de un organismo puede ser correlacionada midiendo el nivel de selenio y vitaminas A y E en sangre [31]. Normalmente, se cuantifican los niveles de actividad de glutatión peroxidasa y selenoproteína P como marcadores de selenio.

Además de su función antioxidante, también está involucrado en la señalización neuronal. Una baja actividad de selenoproteínas aumenta la probabilidad de que surjan desórdenes neurológicos o disfunciones cognitivas [32]. El selenio por medio de la selenoproteína P tiene una función protectora contra el Alzheimer, sin embargo, una dosis excesiva es neurotóxica, pudiendo inducir esclerosis lateral amiotrófica [33]. De igual manera, las formas más comunes de selenio inorgánico participan en la evolución del deterioro cognitivo en la demencia producida por el Alzheimer [34].

Aunque las propiedades inmunomoduladoras y antioxidantes son de gran interés para la biomedicina, la relación del selenio con el cáncer ha despertado un gran interés por parte de la comunidad científica en los últimos años. Hace ya 40 años del primer estudio que sugería una relación inversamente proporcional entre el selenio y el riesgo de varios tipos de cáncer [35], demostrando además que la mortalidad por cáncer era significativamente menor en áreas de Estados Unidos donde los cultivos tenían altas concentraciones de selenio. Desde entonces, se han desarrollado múltiples estudios investigando el papel del selenio en el desarrollo del cáncer.

El rol del selenio en el cuerpo humano se entiende en la misma medida que la función molecular de cada selenoproteína. Diferentes

investigaciones apuntan a que son los polimorfismos de un solo nucleótido (SNP) presentes en selenoproteínas, los responsables de modular el riesgo de cáncer [36].

Como se ha comentado previamente, el selenio es un agente antioxidante que protege a las células de las ROS. Estas especies pueden causar daños irreversibles en el material genético que deriven en la aparición de cáncer. Por ejemplo, la suplementación con selenio es capaz de reducir el daño al material genético en linfocitos humanos y de prevenir la formación de aductos de ADN [37]. Además, el selenio es responsable de la activación de rutas metabólicas que se incluyen en la patología tumoral como por ejemplo la activación de la ruta de las caspasas (inducción de apoptosis), o la inhibición de la angiogénesis, clave en la vascularización.

Sin embargo, gracias a la aparición de la nanotecnología, surgen propiedades nuevas atribuibles ya no solo al material en si mismo, sino también a la dimensión en la que se estudian. En el caso del selenio, su forma nanoparticulada es objeto de estudio en la actualidad debido a sus nuevas propiedades respecto a formas orgánicas e inorgánicas ya conocidas. Es por ello, que la presente Tesis Doctoral se ha centrado concretamente en eso, en el estudio del potencial de las nanopartículas de selenio en el ámbito biomédico.

I.2. Nanotecnología y Nanomedicina

I.2.1. Nanomateriales: clasificación y propiedades

La nanociencia se enfoca en el estudio de las propiedades de materiales, fenómenos, procesos o dispositivos en una escala de tamaños

que se encuentre entre 0,1 y 100 nm (escala nanométrica). Esta dimensión confluye con la ciencia coloidal, enfocada en la materia con un tamaño entre 1 y 1000 nm que se encuentra dispersa en otra fase [38]. Aunque 0,1-100 nm sea el rango aceptado para la escala nanométrica, no existe un consenso definido acerca del intervalo de tamaños exacto en el cual se encuentran los nanomateriales. De forma general, se considera 100 nm como el límite superior, sin embargo, aquellos destinados a fines terapéuticos tienen el límite fijado a 1000 nm por la FDA, la cual los define como *productos que involucran la aplicación de la nanotecnología* [39]. El límite inferior, de forma general también, se sitúa entre los 0,2 y 1 nm, coincidiendo en tamaño con las macromoléculas.

Por su parte, la nanotecnología se fundamenta en los mismos principios que la ciencia coloidal pero enfocándose en la caracterización, manipulación, incorporación o producción de materiales o estructuras de la escala nanométrica (al menos en una de sus direcciones). El estudio de materiales en la nanoescala revela propiedades muy distintas a las que se atribuyen a estos mismos materiales en una escala mayor. Estas diferencias se definen en aspectos tan diversos como la estabilidad, solubilidad, punto de fusión, estructura electrónica, magnetismo, etc. [40]. Son dos factores los principales responsables de este fenómeno:

-La relación entre el área superficial y la masa del material, la cual es mucho mayor, expone un mayor número de átomos a la superficie (**Figura 5**).
-Los efectos cuánticos que se producen son distintos. La energía de la densidad de estados electrónicos varía por las dimensiones del material.

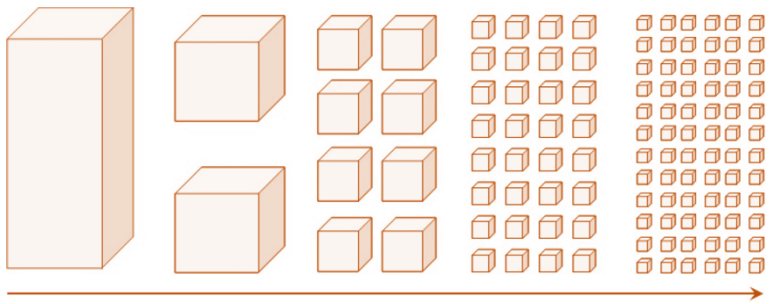

Figura 5. Aumento de la relación entre el área superficial y la masa del material según la disminución del tamaño de las partículas.

El impacto de la nanotecnología en prácticamente todos los sectores de la industria es muy notable. A menudo materiales que se emplean desde hace décadas son capaces de mejorar sus propiedades en esta escala nanométrica, convirtiéndose en materiales más duraderos, ligeros, resistentes, funcionalizables, o eficientes entre otros, aplicables en medicina, comunicaciones, agricultura, aplicaciones cotidianas y otras industrias. Además, la nanotecnología permite escalar la producción con un coste significativamente inferior en muchos casos y de forma más ecológica, lo cual tiene un impacto muy positivo tanto en la economía como en el medioambiente. El desarrollo de nanomateriales puede estar fundamentado en su mezcla o adición a un material preexistente de mayor escala o bien desarrollarse desde un inicio como un material único en forma de nanocristales o nanopartículas [41]. Atendiendo a sus dimensiones espaciales (**Figura 6**), los nanomateriales pueden clasificarse de la siguiente manera:

-Cero dimensional (0D): Las tres dimensiones son inferiores a 100 nm, estando los electrones confinados en las tres dimensiones. Ej: fullerenos, partículas coloidales, nanoclústers, quantum dots, nanopartículas metálicas, átomos, moléculas, y algunos ADN, virus y proteínas.

-Unidimensional (1D): Dos dimensiones son inferiores a los 100 nm, excediendo una el rango de la nanoescala. Ej: nanocables, nanotubos, nanofibras, nanovarillas, fibras poliméricas, o nanocampanas.

-Bidimensional (2D): Una de la dimensiones es inferior a 100 nm, mientras que las otras dos exceden el tamaño de la nanoescala. Ej: monocapas, nanorecubrimientos, películas poliméricas (nano), superficies con un espesor menor a 100 nm, o películas multicapa.

-Tridimensional (3D): Ninguna de las dimensiones es menor a 100 nm. Ej: materiales nanoestructurados, policristales, nanobolas, nanobobinas, o nanoflores entre otros.

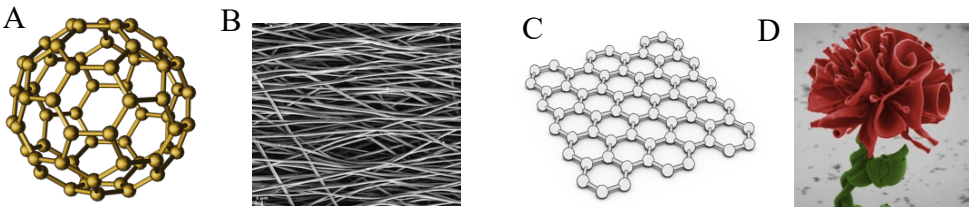

Figura 6. Ejemplos de nanomateriales según las dimensiones espaciales que ocupan. A) fullereno (cero dimensional), B) nanohilos (unidimensional), C) grafeno (bidimensional), y D) nanoflor (tridimensional).

En base a su naturaleza química, los nanomateriales pueden distinguirse según sean:

-Nanomateriales orgánicos: también conocidos como nanomateriales "blandos", la mayoría son biodegradables y no biopersistentes. Como ejemplo de nanomateriales orgánicos están los liposomas, las micelas

poliméricas, las nanopartículas poliméricas, los dendrímeros o las nanoemulsiones, entre otros.

-**Nanomateriales inorgánicos**: son fundamentalmente insolubles, lo que explica su naturaleza biopersistente y no biodegradable. Por el contrario, se les conoces como nanomateriales "duros". Ej: nanopartículas metálicas, nanopartículas de óxidos metálicos, nanomateriales de carbono, etc.

-Nanocompósitos y nanohíbridos: aquellos nanomateriales no homogéneos, anisotrópicos e integrados por al menos dos materiales diferentes [42]. Una de las fases de alguno de los multicomponentes tienen que tener una dimensión en el rango nanométrico. Los nanocompósitos se forman por mezcla o combinación física, nunca unión química. Ej: matrices cerámicas con nanopartículas metálicas, grafito intercalado con metales, etc. En los materiales nanohíbridos sí existe unión química o al menos interacciones intersticiales entre sus componentes, como por ejemplo los nanomateriales químicamente funcionalizados.

En cuanto a su origen, existen nanomateriales en la naturaleza, en forma de ceniza, minerales, coloides o fases gaseosas. Sin embargo, las actividades humanas pueden generar nanomateriales de forma intencionada (nanomateriales sintéticos) o como subproductos generalmente de actividades industriales.

El empleo de la nanotecnología en relación a la medicina y la salud se denomina nanomedicina. Esta ciencia utiliza tecnologías en la nanoescala para prevenir, diagnosticar, monitorizar o tratar enfermedades. Las grandes beneficiadas son las técnicas de imagen y diagnósticas, los sistemas *drug delivery*, el diseño de biotejidos artificiales e implantes y

las terapias farmacológicas. La nanomedicina ha supuesto una revolución en el tratamiento de enfermedades cardiovasculares, neurodegenerativas, psiquiátricas y cáncer, entre otras [43]. Hasta la fecha, se han investigado múltiples tipos de nanopartículas o nanomateriales ya aprobados para su uso clínico (**Figura 7)**:

-Micelas: moléculas anfifílicas que se agregan de forma espontánea y se estructuran en vesículas esféricas en medios acuosos. Gracias a su interior hidrófobo, pueden alojar agentes terapéuticos, mientras que mejoran su solubilidad debido a su exterior hidrófilo [44].

-Liposomas: vesículas esféricas formadas por bicapas lipídicas que pueden incorporar agentes hidrofílicos en la fase acuosa, e hidrofóbicos en la membrana liposómica. Su superficie puede ser modificada con polímeros, anticuerpos y/o proteínas [45, 46].

-Dendrímeros: estas macromoléculas con unidades ramificadas que se repiten desde su núcleo, contienen grupos funcionales a los que se pueden anclar agentes terapéuticos, haciéndolos muy biodisponibles y biodegradables [47]

-Nanotubos de carbono: consisten en una secuencia de láminas de carbono dispuestas en forma de tubo. Gracias a su alta área superficial tienen una gran capacidad como transportadores de fármacos. Además, aportan propiedades ópticas, mecánicas y electrónicas únicas [48,49].

-Nanopartículas metálicas: sirven como agente terapéutico en si mismas o como base funcionalizable para transportar otras moléculas. Se han utilizado como agentes de contraste de imagen, tratamientos de láser, biosensores ópticos y *drug delivery*, entre otros [50].

-Quantum dots: son nanocristales semiconductores fluorescentes que tienen una estructura shell-core. Principalmente se han utilizado en técnicas de imagen para diagnóstico [51].

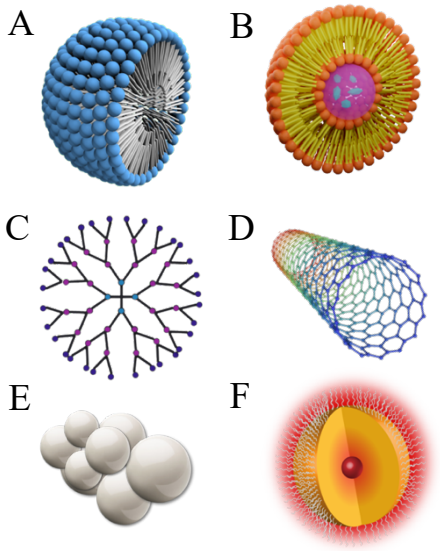

Figura 7. Tipos de nanomateriales y nanopartículas aprobados para su uso clínico. A: micelas, B: liposomas, C: dendrímeros, D: nanotubos de carbono, E: nanopartículas metálicas, F: quantum dots.

A medida que ha evolucionado el estudio de los nanomateriales, se han ido desarrollando múltiples vías para la preparación de los mismos. Sin embargo, todas ellas se distribuyen en dos estrategias básicas a seguir. La primera, "*top-down*", se fundamenta en obtener los nanomateriales a partir de materiales de mayor escala tratados mediante procedimientos térmicos, de molienda, litográficos, de alta energía, etc. Ofrece fiabilidad y complejidad aunque lleva asociados costes energéticos altos, mayor grado de imperfecciones en la superficie de la estructura y problemas de contaminación. La otra estrategia, el "*bottom-up*", es la obtención de nanomateriales a través de la síntesis química o del ensamblaje supramolecular, fundamentalmente [52]. El grado de miniaturización alcanzado por esta estrategia es significativamente superior al alcanzado

por la estrategia "*top-down*", ya que gracias a las técnicas microscópicas actuales se puede localizar con precisión una molécula o un átomo. La estrategia "*bottom-up*" suele resultar más interesante para desarrollar procedimientos con mejor rendimiento y más escalables.

I.2.2. Materiales porosos: nanomateriales mesoporosos de sílice

Los materiales porosos se clasifican atendiendo a tres aspectos básicos: tamaño de poro, composición química de la red porosa, y fortaleza de los enlaces y alcance del ordenamiento poroso (**Figura 8**).

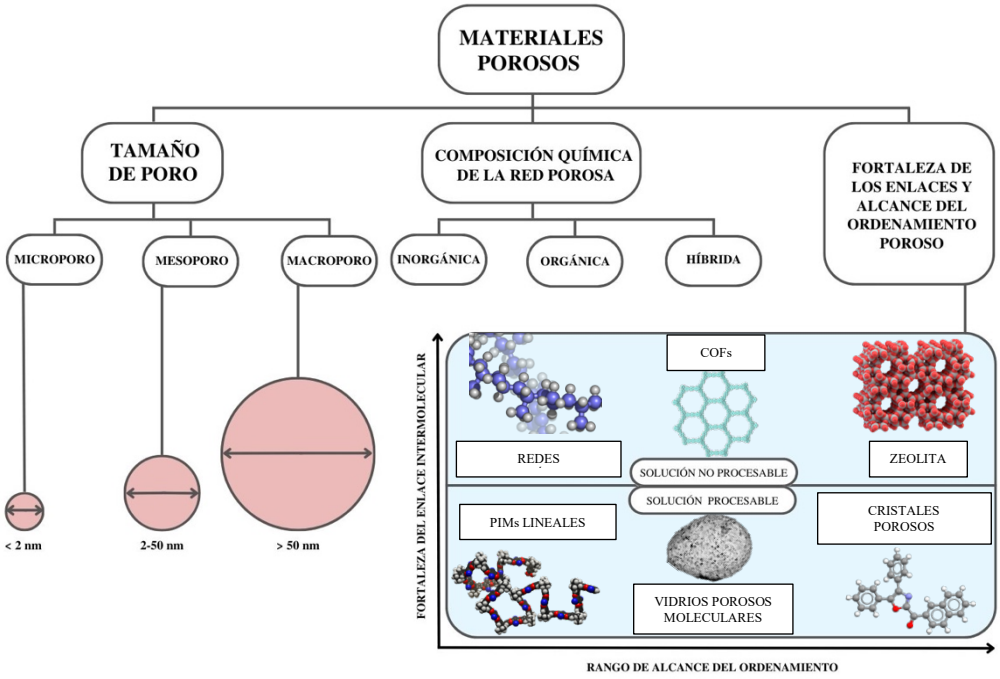

Figura 8. Clasificación de los nanomateriales porosos.

Un material mesoporoso es aquel que contiene poros en su estructura de un diámetro entre 2 y 50 nm. Dado que los materiales mesoporosos son los que engloban el rango más frecuente de la nanoescala, en la actualidad se estudian sus propiedades en relación a una

gran variedad de aplicaciones relativas a la nanotecnología. Tanto el tamaño como la propia forma de los poros pueden ser controlados seleccionando adecuadamente el método de síntesis, destacando los siguientes:

-Molde / Plantilla suave (*soft templating*): la base son moléculas orgánicas llamadas "huésped", que son co-ensambladas en la matriz del nanomaterial durante el proceso de síntesis. Estas moléculas se retiran posteriormente, dando como resultado un material mesoporoso con oquedades abiertas.

-Molde / Plantilla dura (*hard-templating / nanocasting*): La mesoestructura se obtiene a partir de plantillas preexistentes (carbón poroso, sílice mesoporosa, agregados de nanopartículas, etc). Se evita la necesidad de controlar hidrólisis y condensación de especies huésped, así como su ensamblaje con surfactantes. Además, se garantiza el llenado completo de los mesoporos, generando materiales altamente cristalinos. La principal limitación de este método es el número de plantillas duras, así como su complejidad y el tiempo requerido.

-Síntesis mixta o plantilla coloidal: Se genera *in situ* una plantilla dura a partir de especies como sales o moléculas presentes en la disolución precursora. Da lugar a materiales mesoporosos desordenados.

-Sin plantilla: los materiales mesoporosos surgen como consecuencia de la agregación de elementos nanoscópicos.

-Crecimiento reticular: se nutre de unidades moleculares (orgánicas, complejos o clústers) que generan redes orgánico-covalentes (COFs: Covalent Organic Frameworks) o metalo-orgánicas (MOFs: Metal

Organic Framework) para obtener un sólido cristalino de paredes porosas cristalinas ordenadas.

La síntesis de nanomateriales mesoporosos de sílice empieza a desarrollarse a finales de la década de los ochenta. Desde entonces, el número de publicaciones relacionadas con estos materiales no ha hecho otra cosa que crecer exponencialmente. En particular, las aplicaciones biomédicas del mismo han sido, y son, las más exploradas. En la **Figura 9** se ilustra el extraordinario interés creciente del ámbito investigador en este tipo de materiales [53].

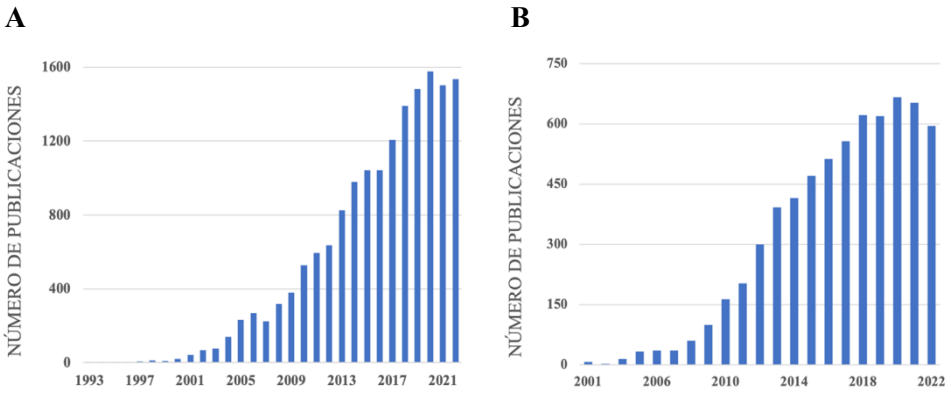

Figura 9. A: número creciente de publicaciones relativas a materiales mesoporosos por año desde el 1991 hasta el 2017. B: número de publicaciones relativas a nanopartículas de sílice mesoporosa con capacidad para transportar drogas terapéuticas (de 2001 a 2017).

El silicio se presenta en gran abundancia en la Naturaleza (20% de la corteza terrestre), normalmente en forma de redes tridimensionales poliméricas compuestas por unidades tetraédricas (un átomo de silicio unido a cuatro átomos de oxígeno). Habitualmente se combina con el oxígeno formando silicatos (SiO_4^{4-}) u óxido de silicio (SiO_2). El óxido de silicio es capaz de dar lugar a más de diez estructuras cristalinas altamente

organizadas (cuarzo, tridimita, cristobalita, etc). Asimismo, se pueden encontrar óxidos de silicio con estructura amorfa, como por ejemplo el vidrio.

Los materiales basados en silicio se han empleado desde siempre en diversas aplicaciones tecnológicas. El pedernal o sílice se usó para la fabricación de las primeras herramientas en la Edad de Piedra. De igual forma, el vidrio o la arcilla se llevan utilizando milenios como base para la alfarería o la construcción. Ya en 1940, tanto Estados Unidos como Alemania lo empleaban como sustituto del carbón negro para reforzar el caucho. Sin embargo, no es hasta la década de 1990 cuando empiezan a desarrollarse métodos para la obtención y caracterización de sólidos inorgánicos con ordenamiento poroso definido (tamiz molecular), dando lugar a zeolitas y sílice mesoporosa, entre otros [54]. El origen del ordenamiento mesoporoso en materiales de sílice está en la compañía Mobil Oil (1992), principalmente enfocado a su empleo como catalizador, aunque derivó en años posteriores hacia aplicaciones como la adsorción, eliminación selectiva de contaminantes en agua, dispersante en cosmética, ciencias biomédicas, etc. [55].

Para desarrollar sólidos con poros distribuidos en la matriz de sílice es necesario el empleo del método de plantilla suave. Una especie precursora de sílice, como el tetraoxisilano, y un surfactante, se ensamblan formando micelas formando la llamada soft template.

Los surfactantes empleados para la generación de poros se clasifican en base a la carga que presentan en su extremo polar: aniónicos, catiónicos, no iónicos o zwitteriónicos. La elección del surfactante tiene una relación directa con la naturaleza de los poros, existiendo diferentes estrategias tales como el empleo de surfactantes con distinto tamaño de

cadena (n=6-16), de copolímeros a modo de plantilla, tratamientos hidrotermales post-sintéticos, o el uso de agentes expansores (alcanos, aminas, trimetilbenceno, etc) [56].

Los materiales basados en sílice mesoporosa (MSNs), además de servir para una gran variedad de aplicaciones, son ideales para su empleo en biomedicina. Su estructura mesoporosa única facilita la incorporación efectiva de drogas y su consiguiente liberación en el sitio de interés. Asimismo, sus propiedades (tamaño de poro, capacidad de carga, porosidad, o propiedades superficiales) pueden modificarse a voluntad dependiendo del método de síntesis empleado. Las MSNs son estables frente a la temperatura, biocompatibles, y demuestran una gran capacidad para la internalización en células [57]. Estos materiales han sido ampliamente estudiados en estudios *in vivo*, demostrando no ser tóxicos para el intervalo de concentración efectivo de la mayoría de aplicaciones biomédicas. La toxicidad y el grado de internalización de estos materiales dependerá del tamaño de partícula, la forma, carga superficial y los grupos funcionales con los que hayan sido modificados [58,59].

I.2.3. Nanomedicina y cáncer

El cáncer se define mediante cambios mutagénicos en las células que producen un crecimiento descontrolado de su población, incluso su diseminación a otros tejidos u órganos distintos del de origen (metástasis) (**Figura 10**). Es la enfermedad con mayor tasa de mortalidad en todo el mundo actualmente, aproximadamente 10 millones de defunciones anuales, siendo los más mortales el cáncer de pulmón, el colorrectal, hepático, y el gástrico.

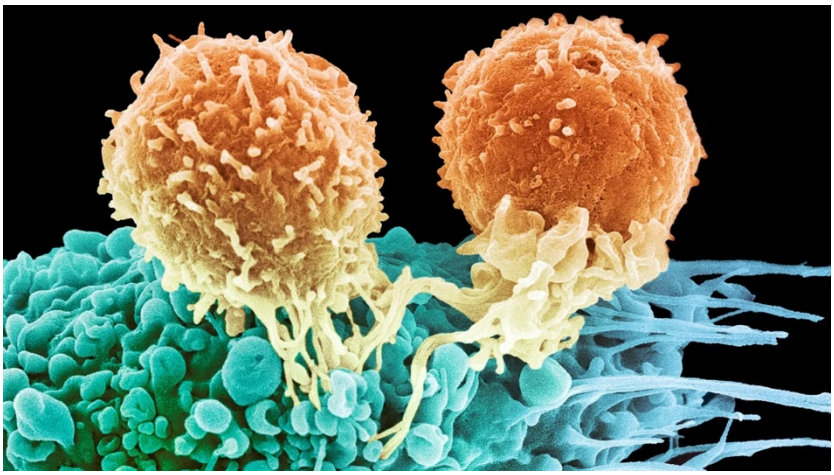

Figura 10. Micrografía electrónica de barrido coloreada de dos linfocitos T (en amarillo) señalizando a una célula cancerosa (en verde) para alertar el sistema inmune. Micrografía de Steve Gschmeissner para Science Photo Library.

Su incidencia es creciente y favorecida por nuevos hábitos de vida cada vez más comunes en la población general. Alrededor de un tercio de las muertes debidas a la enfermedad se deben al consumo de tabaco y alcohol, poca o nula actividad física, obesidad, baja ingesta de fruta y verdura, etc. La exposición a carcinógenos físicos como radiación ultravioleta e ionizante, químicos como amianto, sustancias del tabaco, o

aflatoxinas, también contribuyen a su incidencia. Además, las infecciones oncogénicas (virus de la hepatitis o del papiloma humano) son responsables de un 30% de los casos de cáncer en países subdesarollados o en vías de desarrollo.

En España, la incidencia del cáncer sigue la misma tendencia que en el resto del mundo (**Figura 11**). El envejecimiento de la población (la edad es un factor de riesgo en el desarrollo de la enfermedad) o la exposición a factores de riesgo contribuyen a aumentar el número de casos, pero también lo hace la mejora en los protocolos y tecnología para la detección precoz. A pesar de las diferencias de incidencia por sexos, estas se han reducido debido al aumento del tabaquismo entre las mujeres.

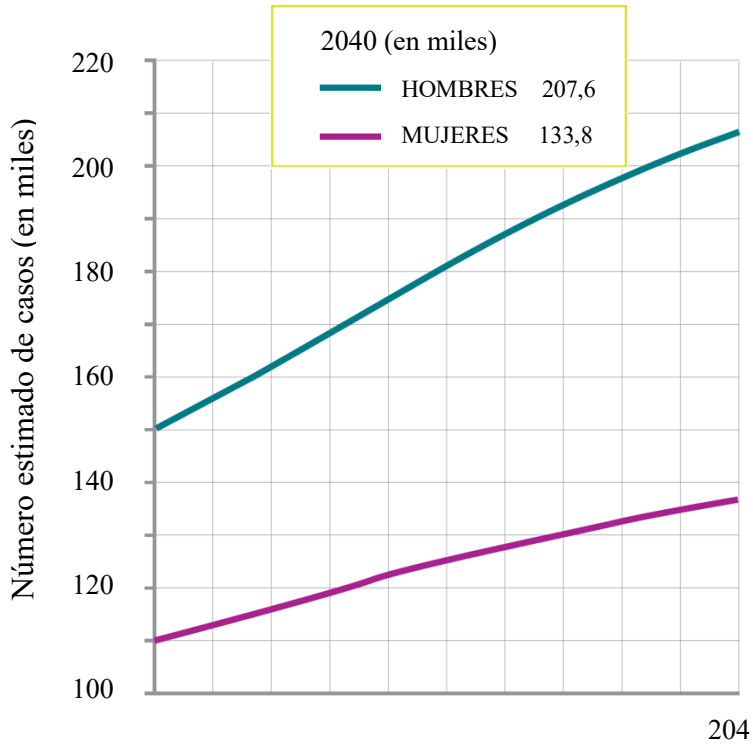

Figura 11. Incidencia estimada de tumores en España por sexos entre los años 2020 y 2040. Fuente: Global Cancer Observatory (GLOBOCAN 2020).

Debido a la gran amenaza que representa el cáncer, una gran parte de las investigaciones centradas en nanomateriales es su empleo en terapia contra el cáncer. Tradicionalmente, la intervención terapéutica frente al cáncer se limita a cirugías, radiación y quimioterapia, implicando especialmente el último, una gran cantidad de efectos secundarios, al ser tratamientos sistémicos y, por tanto, no dirigidos. Esto implica que el fármaco, al no darse una absorción específica en tejidos tumorales, también es absorbido por células sanas, lo que implica que las dosis farmacológicas tengan que ser más altas para conseguir una buena eficacia, lo que supone una prolongación del tratamiento. Además, la absorción inespecífica puede resultar tóxica para células sanas, o incluso puede derivar en el desarrollo de resistencia ante los mismos [60, 61]. Con el objetivo de evitar este tipo de inconvenientes en la terapia contra el cáncer, han surgido estrategias que permiten actuar selectivamente sobre las células tumorales, consiguiendo así reducir la cantidad de fármaco y la frecuencia de la dosis a la vez que una mayor eficacia con menores efectos adversos sobre el paciente [62]. Muchas de ellas se fundamentan en el empleo de nanosistemas.

La aplicación de la nanotecnología al *drug delivery* (estrategias para hacer llegar un agente terapéutico a una zona concreta del organismo) está cambiando por completo el paradigma de la industria farmacéutica y biotecnológica. Los primeros sistemas de *drug delivery* en nanotecnología fueron las vesículas lipídicas descubiertas en la década de 1960 y posteriormente llamadas liposomas [63]. A estos liposomas le han seguido una gran variedad de biomateriales orgánicos e inorgánicos capaces de liberar fármacos en una zona determinada [64]. Además, los nanotransportadores o *nanocarriers*, solventan los principales problemas relacionados con el desarrollo de nuevos fármacos: solubilidad y

estabilidad química, pudiendo actuar asimismo, como barrera frente a la biodegradación o la excreción, influyendo así directamente en el perfil farmacocinético del agente quimioterapéutico.

La primera estrategia en el desarrollo de *nanocarriers* se fundamentaba en el efecto de permeabilidad y retención mejoradas (EPR). El efecto EPR se define por la acumulación preferente de moléculas o materiales de ciertos tamaños en tejidos tumorales respecto de tejidos sanos. Esto se debe a que, en las zonas tumorales se produce una rápida vascularización para suplir todas las necesidades de nutrientes que tiene el tumor. La morfología de estos vasos es inusual, carecen de una capa de músculo liso, drenaje linfático insuficiente y suelen tener fugas en sus paredes. Debido a estos factores, los nanomateriales suelen quedar retenidos e incluso salen del sistema circulatorio por esas fugas y se concentran en la zona tumoral. Sin embargo, esta estrategia denominada vectorización pasiva no tiene capacidad para controlar los efectos secundarios de los fármacos en el organismo.

Las células cancerígenas, en comparación con las células sanas, tienen una demanda muy alta de nutrientes para poder sostener el crecimiento típico tumoral. Debido a esto, sobreexpresan en su membrana determinados receptores moleculares que les permitan llegar a las exigencias nutricionales que comporta el cáncer. La vectorización activa es una estrategia de anclaje o inmovilización de ligandos en la estructura del *nanocarrier,* los cuales serán reconocidos específicamente por los receptores de membrana de las células tumorales, permitiendo así discriminar células tumorales de células sanas [65,66]. Existe gran variedad de ligandos para vectorización pasiva; desde pequeñas moléculas como el ácido fólico o algunos carbohidratos, hasta moléculas de mayor

tamaño como péptidos, proteínas, anticuerpos, aptámeros, etc (**Figura 12**).

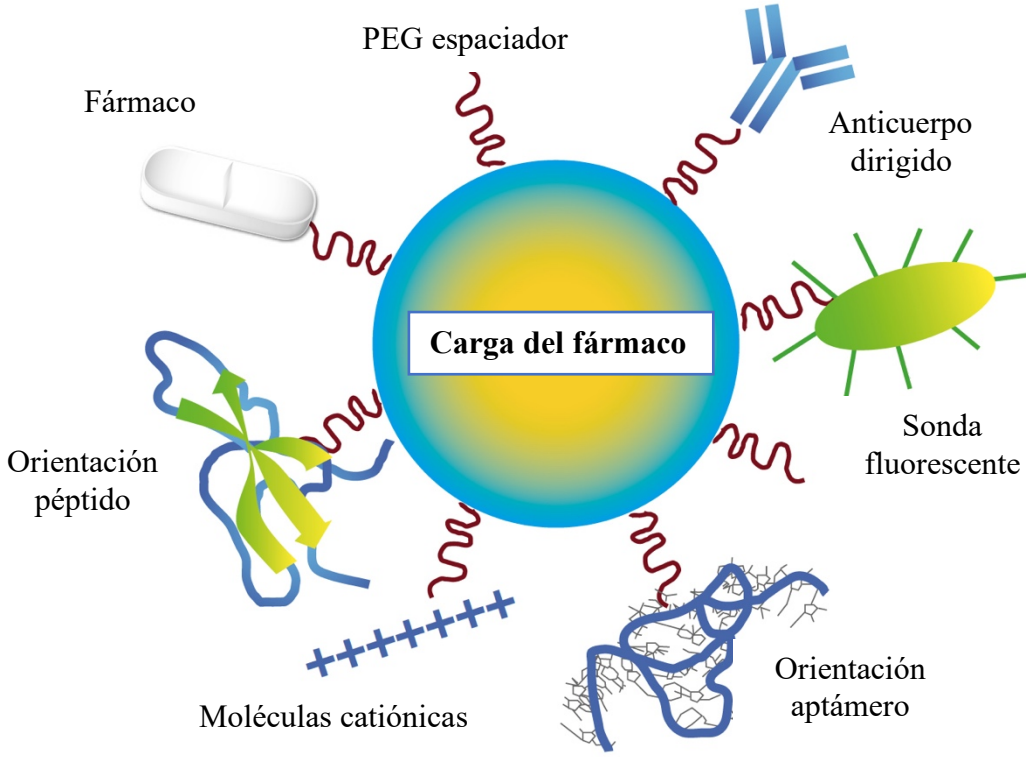

Figura 12. Principales ligandos en el vectorizado de nanoestructuras para modificar sus propiedades como nanocarriers

El receptor de transferrina es una de las dianas más relevantes para la vectorización activa en cáncer. La glicoproteína transferrina asiste la internalización de hierro hacia el interior de la célula, y puesto que participa en el metabolismo de nutrientes, no implica cascadas complejas de señalización.

Los nanocarriers deberán tener unas características muy concretas para ser considerados buenos candidatos para una vectorización pasiva. Entre ellas destaca la estabilidad, clave para evitar una liberación prematura del agente quimioterapéutico y la degradación del mismo. Es importante que no establezcan interacciones no deseadas con las proteínas del suero o con el sistema inmune, que resulten en una evacuación prematura del agente transportador. Otro factor clave es optimizar la densidad del ligando en relación al *nanocarrier* para sostener el nanosistema de forma discreta, evitando que sea reconocido por el sistema reticuloendotelial (RES) [67]. En resumen, y respecto a la vectorización pasiva, esta estrategia consigue reducir en gran medida los efectos secundarios del fármaco ya que previene su internalización en células sanas.

Dentro de todas las estructuras químicas que han sido aplicadas como base para un *nanocarrier*, las nanopartículas de sílice mesoporosa (MSNs) aportan una serie de ventajas que las hace muy atractivas para este tipo de aplicaciones. Es posible sintetizar nanopartículas de este material de al menos 50 nm sin perder carácter mesoporoso y evitando que sean excretadas por el riñón. El tamaño de partícula se puede controlar por debajo de 300 nm para facilitar su difusión hacia el tejido tumoral de forma suficiente como para ejercer su efecto terapéutico [68,69].

I.2.4. Nanomedicina y tuberculosis

La tuberculosis (TB) es una enfermedad originada por una infección bacteriana, principalmente de *Mycobacterium tuberculosis*, la cual afecta directamente a los pulmones aunque puede propagarse a otros órganos.

Aunque históricamente no ha recibido la “atención” mediática que puedan haber recibido otras enfermedades graves, es una de las principales causas de muerte a nivel mundial. En la actualidad, fallecen alrededor de 2 millones de personas, y se estima que un tercio de la población mundial está infectada (aunque no presente síntomas) [70].

Sus síntomas son tos crónica con esputo sanguinolento, fiebre y pérdida de peso principalmente. Se contagia por vía aérea, cuando las personas infectadas tose, esputan o escupen. Además, se contagia mucho más rápidamente en individuos en tratamiento con medicamentos A pesar de su prevalencia (más de 10,6 millones enfermaron por tuberculosis en 2021), es una enfermedad que se puede prevenir y curar. Desde los comienzos de milenio, se han salvado más de 74 millones de vidas gracias al diagnóstico y los tratamientos actuales contra la enfermedad. Como todas las enfermedades infecciosas la higiene es un agente de prevención clave, así como la detección temprana y la vacunación [71, 72]. Sin embargo, la tuberculosis ha evolucionado hacia la farmacorresistencia. Esto sucede cuando los medicamentos no se utilizan adecuadamente, la prescripción es inadecuada, la calidad de los fármacos es baja o el tratamiento de interrumpe de forma prematura por parte del paciente.

Actualmente, la tuberculosis multirresistente es fruto de bacterias que no responden a dos tratamientos generales: isoniacida y rifampicina. Esto hace que, en el mejor de los casos, se recurra a medicamentos de segunda línea, los cuales suelen ser caros, requieren tratamientos de mayor duración y presentan mayor toxicidad [73, 74]. Debido a esto, la tuberculosis sigue representando una amenaza a nivel mundial. Solo uno de cada tres pacientes con síntomas de infección por tuberculosis puede recibir la medicación adecuada a su caso.

El tratamiento más efectivo contra TB son las vacunas, especialmente las de ADN que producen inmunidad. Aunque la enfermedad esté presente en todo el mundo tiene más incidencia en países subdesarrollados, por lo que las condiciones en las que se transporta y conserva la vacuna se ven, en muchas ocasiones, deterioradas. Es aquí donde los nanomateriales intervienen para conseguir una conservación y transporte óptimos. Para este propósito, se han investigado nanopartículas polímericas PLGA, nanopartículas de distinta naturaleza estabilizadas con quitosano o funcionalizadas con bioliésteres, o ligandos inorgánicos y orgánicos [75, 76]. Además de para su transporte y conservación, es importante garantizar que el fármaco permanece un tiempo suficiente en el organismo. Para ello, se han desarrollado estrategias de encapsulamiento de fármacos con liposomas que son capaces de alargar la vida útil del fármaco así como de mejorar la biodistribución [77]. De igual forma, también se han empleado bionanomateriales como la albúmina como vehículo para la liberación de compuestos antimicrobianos como la benzotiazina [78].

El empleo de nanomateriales también es efectivo como tratamiento contra TB o en combinación sinérgica con otros fármacos ya existentes. Existen ya evidencias de la efectividad de nanomateriales de carbono como el óxido de grafeno o los nanotubos para el tratamiento de la TB e incluso para reducir efectos secundarios [79]. Paralelamente, se ha comprobado que las nanopartículas metálicas como las de plata o las de oro son capaces de inhibir el crecimiento bacteriano [80, 81].

Debido a la urgente necesidad de desarrollar estrategias más efectivas para paliar los efectos de la tuberculosis multirresistente en el escenario sanitario global, la investigación con nanomateriales es una

herramienta muy prometedora por si misma o en combinación con tratamientos actuales. En la presente Tesis Doctoral se muestran los resultados del estudio acerca de la aplicación de nanopartículas de selenio como agente antibacteriano, tanto para su aplicación en tratamiento como en la prevención contra la enfermedad.

I.3. Técnicas -ómicas para la elucidación de los mecanismos de acción de nanomateriales de interés biomédico

I.3.1. Transcriptómica

La transcriptómica es un campo de investigación dentro de la biología molecular que se centra en el estudio integral de la expresión genética a través del análisis del ARN. Como todas las técnicas -ómicas es una ciencia joven que nace en la década de 1990. Acompañada por el desarrollo de la tecnología, ha evolucionado muy rápidamente hasta nuestros días. La información contenida en el genoma se expresa mediante la transcripción, por eso mismo, poder obtener una "foto fija" de todos los transcritos permite conocer qué procesos celulares están activos y cuáles no. A través del análisis de estos transcritos de ARN se obtiene información muy valiosa para elucidar mecanismos moleculares responsables de procesos biológicos e incluso de enfermedades.

Dentro de las diversas aplicaciones de la transcriptómica destacan el descubrimiento y desarrollo de drogas terapéuticas, identificación de biomarcadores de enfermedades, biología embrionaria, o estudio de interacciones huésped-patógeno. Existen dos aproximaciones principales para obtener información sobre los transcritos: secuenciación individual o hibridación de una matriz ordenada de sondas de nucleótidos.

Experimentalmente, se requiere en primer lugar el aislamiento del ARN implicando la disrupción mecánica de células y tejidos, así como de la ARNasa con sales caotrópicas y otras macromoléculas que puedan interferir. Además, el ARN se concentra mediante precipitación o dilución de una matriz sólida y se genera una copia en forma de ADN complementario (ADNc), mediante acción de la transcriptasa inversa.

Una de las estrategias más utilizadas en transcriptómica son los microarrays. Consisten en un dispositivo en forma de parrilla en el cual se inmovilizan oligómeros de nucleótidos que se denominan sondas en una disposición regular y prefijada. Los transcritos marcados con fluorocromos se hibridan a estas sondas y así puede determinarse su abundancia (según la intensidad fluorescente).

Los microarrays empleados en transcriptómica pueden ser microarrays de productos de PCR o microarrays de oligonucleótidos. En los microarrays de productos de PCR (*Spotted Microarrays*), las sondas se sintetizan previamente y un robot denominado *microarray spotter* las deposita en la superficie del chip. En un experimento común de comparación de perfiles de expresión se tienen dos muestras: ARN control y ARN problema. A partir de cada ARN se obtiene los ADNc, los cuales competirán para la hibridación en el chip. Por último, el chip se escanea y se compara la intensidad de fluorescencia de cada fluorocromo para correlacionarlo con la abundancia de los transcritos. Es importante fijar una relación a partir de la cual se considera que la inducción o represión de la expresión de un gen es significativa. La principal ventaja de estos microarrays es su flexibilidad en cuanto a diseño experimental. Los microarrays de ADN pueden estar formados también por oligonucleótidos cortos (*High Density Microarrays*), los cuales se sintetizan directamente

en la superficie del vidrio. Para completar un gen, se agrupan varias sondas (*group set*). Son altamente reproducibles, y posibilitan estudiar genomas microbianos gracias al elevado número de sondas del que disponen.

Los datos obtenidos por un análisis de transcriptómica se pueden validar mediante técnicas reconocibles e independientes como la PCR cuantitativa (qPCR). La qPCR es una variante de la PCR clásica, utilizada para cuantificar copias amplificadas de una secuencia de ADN. En el caso de la qPCR, la medida de fluorescencia para evaluar la tasa de generación de productos específicos de ADN se realiza tras cada ciclo de amplificación y así construir una curva de calibrado. En investigación, la qPCR se emplea principalmente en mediciones cuantitativas de la transcripción y expresión génica [82, 83].

En los últimos años, el número de publicaciones que emplean la transcriptómica para investigaciones biomédicas se ha incrementado exponencialmente. Dentro del cuerpo de la presente Tesis Doctoral se incluye un trabajo de transcriptómica que ayuda a identificar mecanismos moleculares asociados a la acción antitumoral de nanopartículas de selenio [84], además de otros estudios centrados en estas mismas u otras nanopartículas [85, 86]. Asimismo, muchas investigaciones acerca del efecto de nanopartículas como agentes terapéuticos se sirven de esta herramienta para descubrir alteraciones genómicas [87]. La transcriptómica puede, junto con otras herramientas como la proteómica, servir para explorar nuevas dianas terapéuticas y candidatos para vacunas.[88, 89]. Concretamente, ha supuesto un gran avance en la investigación de cáncer y enfermedades degenerativas debido a el perfil metabólico y dinámico de estas [90, 91].

I.3.2. Proteómica

La proteómica cuantitativa es un conjunto de técnicas orientadas al análisis de mezclas proteicas complejas, posibilitando la identificación y cuantificación de proteínas en sistemas biológicos. El desarrollo de la espectrometría de masas (MS) es un hito central en la evolución de la proteómica ya que es una herramienta esencial en el análisis de mezclas proteicas complejas gracias a su alta sensibilidad y precisión.

La proteómica cuantitativa ofrece ventajas muy reseñables para el estudio de sistemas biológicos. Las principales son que permite la cuantificación de un gran número de proteínas en un solo experimento así como comparar la expresión de la misma proteína proveniente de diferentes muestras. También posibilita estudiar las interacciones proteína-proteína o la identificación de nuevos biomarcadores para el mejor entendimiento de múltiples patologías [92, 93]. Actualmente, la proteómica está presente en la mayoría de estudios biomédicos enfocados en el descubrimiento de dianas terapéuticas y mecanismos moleculares, muchos de ellos, con nanopartículas como droga terapéutica [94, 95].

La proteómica cuantitativa se fundamenta en el uso de estrategias de marcaje isotópico para posibilitar la cuantificación relativa de proteínas. Existe una gran variedad de métodos dentro de la proteómica cuantitativa como por ejemplo ICAT (grupo reactivo marcado isotópicamente que se une a los residuos de cisteína), iTRAQ y TMT (marcaje isobárico) o QconCATs (proteínas quiméricas), entre otros. Sin embargo, uno de los métodos más utilizados de proteómica cuantitativa es SILAC (Stable Isotopic Labeling with Amino acids in Cell culture).

Dentro de los marcajes químicos isobáricos destaca iTRAQ (isobaric tags for relative and absolute quantification), el cual se fundamenta en un grupo reactivo para la unión con los péptidos a través de los grupos amino terminal o de las lisinas, un grupo de balance, y un ion reportero. Las muestras se marcarán con diferentes proporciones de isótopos pesados entre los grupos balance y reportero, y se mezclan. Los péptidos idénticos coeluyen y se detectan como un solo ion precursor. Sus intensidades relativas son proporcionales a la abundancia relativa del péptido marcado de las diferentes muestras [96]. El marcaje químico se basa en el empleo de isotopos pesados estables para marcar proteínas o péptidos ya sintetizados. ICAT (isotope-coded affinity tags) derivatiza las cisteínas con un reactivo que contiene un grupo reactivo (tiol), un grupo de afinidad para aislar los péptidos marcados, y un grupo de unión (ligero o pesado). Ambas muestras proteicas se marcan con el reactivo ICAT (ligero o pesado), se mezclan, y se analizan. Comparando las intensidad relativa de cada uno obtiene información sobre su abundancia. No obstante, esta técnica está limitada por inespecificidad del reactivo y porque no puede marcar péptidos sin cisteína [97].

SILAC, en cambio, emplea un marcaje metabólico con isótopos estables de aminoácidos para el marcaje celular, típicamente ^{13}C y ^{15}N, posibilitando la cuantificación de los niveles de expresión de proteínas y la identificación de modificaciones post-transduccionales. El marcaje se completa tras cinco doblajes de la población inicial, asegurando la incorporación de los aminoácidos “pesados”. Después del marcaje, las proteínas se extraen, generalmente a través de una lisis celular, y las proteínas se separan por electroforesis en gel. Los péptidos extraídos, previa digestión de las proteínas, son analizados por espectrometría de masas. Las células que han sido cultivadas en medio “ligero” son

exactamente idénticas que aquellas que han incorporado los isótopos marcados salvo que sus péptidos pueden ser distinguidos de los segundos por medio de espectrometría de masas. Por ejemplo para un marcaje con arginina (seis carbonos ^{13}C) se produce una "separación" de 6-Da de su isotopómero de ^{12}C [98]. Generalmente se emplean arginina y lisina debido a la disponibilidad de tripsina como enzima proteolítica y porque virtualmente todos los péptidos estarán marcados [99].

Las células marcadas se mezclan con las no marcadas en proporción 1:1, y la mezcla resultante se procesa hasta el análisis por espectrometría de masas para cuantificar la abundancia relativa de los péptidos. SILAC proporciona un estándar interno para cada proteína. Esto minimiza la variabilidad entre muestras, lo que le confiere precisión y reproducibilidad.. Su rápida difusión como estrategia popular de proteómica cuantitativa tiene que ver con la facilidad del procedimiento experimental, la compatibilidad con la mayoría de cultivos celulares, reactivos comercialmente disponibles, y por su robustez y versatilidad entre otras. Su eficiencia de marcaje es muy eficiente, por lo que asegura una cobertura muy alta del proteoma, y se puede utilizar con varios tipos de células: cultivos primarios, células inmortalizadas, o incluso organismos enteros (empleando la variante SuperSILAC).

SILAC no es solo una estrategia útil para evaluar la abundancia relativa de proteínas de distintas poblaciones, sino que también se utiliza para estudios de dinámica de proteínas y modificaciones postransduccionales (PTMs). Además, puede combinarse con estrategias como la immunoprecipitación o la purificación por afinidad para el análisis de PTMs específicas como la fosforilación, acetilación, o la ubiquitinación.

A pesar de esto, SILAC es una estrategia que supone altos costes en reactivos (aminoácidos marcados) y supone largos tiempos experimentales para asegurar un marcaje completo o para procesar los datos. Puede estar limitada en casos donde la concentración de proteínas no sea demasiado alta (muestras clínicas o algún tipo de tejido). Actualmente, pese a ser una estrategia relativamente "joven", SILAC se emplea en muchos de los estudios de proteómica centrados en el descubrimiento de diferencias en expresión de proteínas con nanopartículas como agente central **[100, 101, 102]**

I.3.3. Metabolómica

La metabolómica es una disciplina -ómica que nace con objeto de detectar, cuantificar y elucidar la estructura de los metabolitos en un sistema biológico. Mediante la metabolómica se alcanza una gran comprensión de los procesos celulares involucrados al proporcionar una instantánea de las vías metabólicas y su regulación. Se ha convertido en una herramienta esencial en la biología de sistemas y la medicina personalizada, ya que permite la identificación de biomarcadores para el diagnóstico de enfermedades, el seguimiento de respuestas terapéuticas y la identificación de posibles objetivos de fármacos.

Esta disciplina se basa en tecnologías analíticas que permiten la detección y cuantificación de una amplia gama de moléculas pequeñas como, por ejemplo, la espectrometría de masas (MS) y la espectroscopía de resonancia magnética nuclear (NMR). Estas técnicas se complementan con herramientas de procesamiento de datos y análisis estadístico que permiten la identificación de firmas metabólicas asociadas con procesos biológicos específicos o estadios de enfermedad.

A diferencia de la genómica y la proteómica, donde la secuencia de ADN o proteína proporciona un vínculo directo con su función biológica, los metabolitos a menudo son estructuralmente complejos y químicamente diversos, lo que dificulta su identificación y cuantificación. Para abordar este desafío, se han construido bases de datos de metabolómica para facilitar la anotación de metabolitos y el intercambio de datos entre investigadores, y se han desarrollado múltiples plataformas y configuraciones analíticas [103].

Hay dos estrategias fundamentales en metabolómica: dirigida y no dirigida. La metabolómica dirigida es aquella que centra su estudio en un grupo de metabolitos de interés, la cual está normalmente condicionada por una pregunta bioquímica concreta o hipótesis. Se emplea, por ejemplo, en estudios farmacocinéticos o para la medición del efecto metabólico de modificaciones genéticas en una enzima concreta. El otro enfoque es la metabolómica no dirigida, que tiene como meta medir simultáneamente la mayor cantidad de metabolitos sin hipótesis preestablecida. Los datos obtenidos son complejos y de gran tamaño, pero proporcionan una imagen global muy detallada a partir de la cual empezar a centrar una investigación. El acoplamiento de la espectrometría de masas a la cromatografía ha supuesto un gran avance en términos de sensibilidad y reproducibilidad para la estrategia de metabolómica no dirigida. Normalmente, el análisis de compuestos orgánicos volátiles, lípidos o moléculas derivatizadas se realiza por cromatografía de gases acoplada a espectrometría de masas (GC-MS). Por otro lado, la mayoría de metabolitos semi-polares se analizan por cromatografía de líquidos acoplada a espectrometría de masas (LC-MS). Generalmente, siempre que se dispone de medios, ambas técnicas se utilizan conjuntamente para una evaluación más completa del perfil de metabolitos en un sistema

biológico. En la preparación de muestra, un análisis por GC-MS necesita volatilizar la muestra, lo cual puede requerir derivatización, mientras que por LC-MS, al realizarse en estado líquido, puede precisar de filtración o dilución. El poder de separación de metabolitos polares es mayor en el caso de GC-MS aunque necesita derivatización previa generalmente. La ionización por impacto de electrones proporciona espectros de masas más reproducibles en el caso de cromatografía de gases, lo que ha permitido la elaboración de bibliotecas de metabolitos más completas. Sin embargo, la LC-MS es la técnica que permite una evaluación más integral ya que miles de metabolitos pueden identificarse en un cromatograma LC-MS. Los errores por formación de aductos e isótopos se eliminan gracias a las bibliotecas de espectros MS/MS. La LC-MS es generalmente más lenta porque requiere más tiempo para la separación y detección de compuestos no volátiles pero no precisa de derivatización. Además, la instrumentación es más asequible y requiere menos mantenimiento, ya que un cromatógrafo de gases y el constante suminstro de gases de alta pureza requiere una mayor inversión económica [104, 105].

El rápido avance de la tecnología ha supuesto, no solo el desarrollo de la metabolómica como herramienta, sino ampliar el abanico de campos de investigación donde conocer el estado del metaboloma es de vital importancia. Actualmente, la metabolómica participa en muchas de las investigaciones relativas a cáncer [106, 107], así como en muchas acerca de enfermedades neurodegenerativas [108] o cardiovasculares [109]. De la misma forma, y debido al auge de los nanomateriales en biomedicina, se ha convertido en un recurso fundamental para la evaluación de la toxicidad o del potencial quimioterapéutico estos materiales [110, 111, 112].

II. Parte experimental.

Capítulo 1. Evaluación del potencial antitumoral de las SeNPs.

En el Capítulo 1 se establece, en primer lugar, una comparativa entre especies ya estudiadas de selenio (tanto orgánicas como inorgánicas) y las nanopartículas de selenio en relación a su efecto en células de hepatocarcinoma humano (HepG2).
Una vez probado el carácter diferencial como agente antitumoral de las SeNPs, y mediante técnicas -ómicas (transcriptómica, proteómica y metabolómica), se profundiza en los mecanismos moleculares que intervienen en su acción como agentes quimioterapéuticos. Por último, se lleva a cabo un ensayo *in vivo* que culminará su validación para la terapia contra el cáncer.

Effects of chitosan-modified selenium nanoparticles on cell proliferation, apoptosis, and cell cycle pattern: comparison with other selenospecies

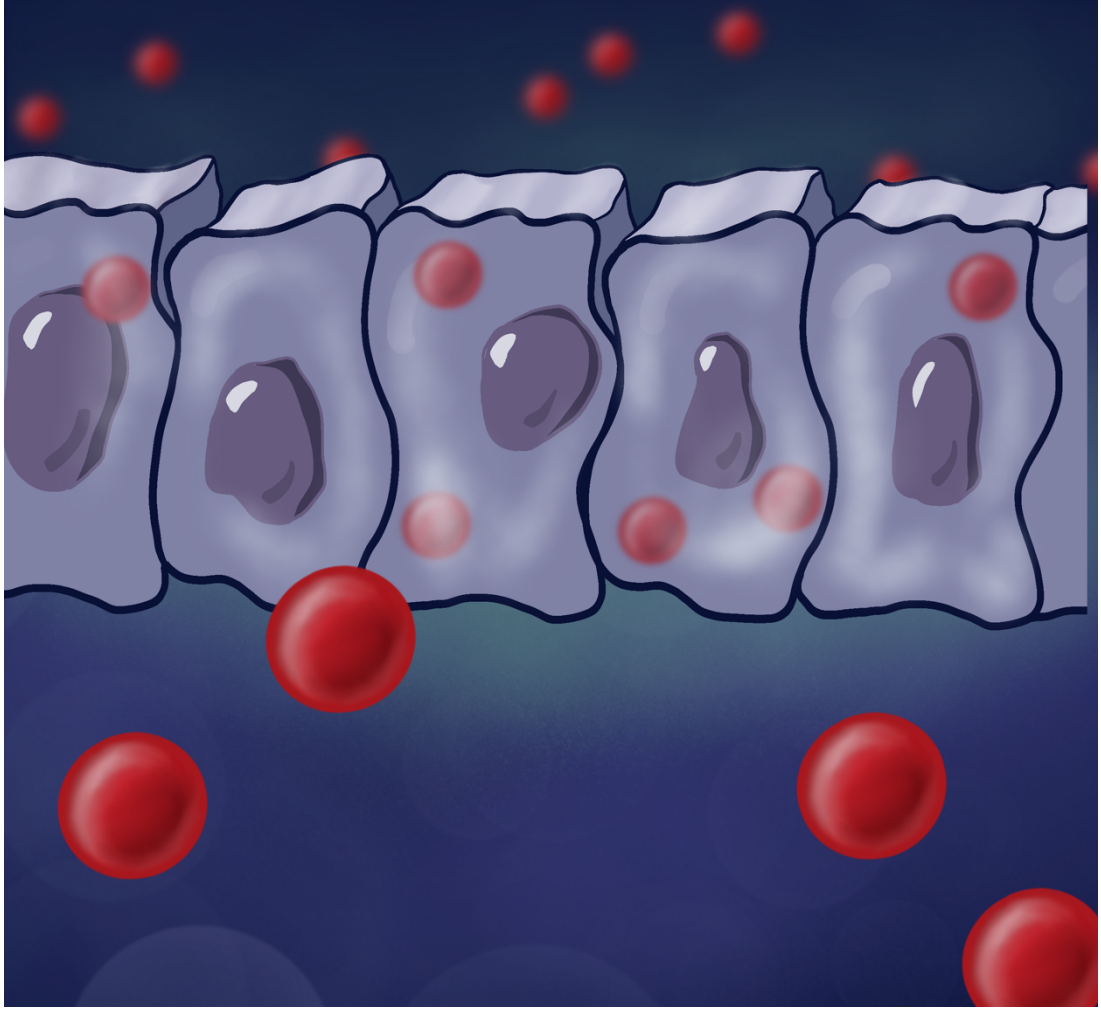

1.1. Effects of chitosan-modified selenium nanoparticles on cell proliferation, apoptosis and cell cycle pattern: comparison with other selenospecies

Hector Estevez, J. Carlos Garcia-Lidon, Jose L. Luque-Garcia, Carmen Camara

Colloids and Surfaces B Biointerfaces, 122 (2014)

Abstract

Selenium is an essential element that plays an important role in many biological functions. Many studies have reported the potential beneficial effects of Se intake for cancer therapy and prevention, which are not only dose-dependent but also closely related to the properties of specific selenospecies. Selenium nanoparticles are considered a novel selenium compound with excellent antioxidant properties; however, little is known about the properties of selenium nanoparticles in comparison to other well-studied selenospecies. Here, we combined different independent bioanalytical approaches to carry out a comparison between the effects of selenium nanoparticles and other selenocompounds (inorganic and organic selenospecies) using an *in vitro* model. The bioanalytical characterization of different parameters such as cell proliferation, apoptosis and cell cycle pattern has shown the unique properties of this relatively novel compound that support and complete prior evidences for future applications as chemotherapeutic agent.

1. Introduction

Selenium is an essential and unique micronurient that plays an important role in reglating the functions of many intracelular proteins. Fairweather-Tait et al. [1 recently reviewed the relationship between selenium intake/status and several health outcomes such as cancer, cardiovascular disease, diabetes and male fertility. Low selenium status has been associated with increased risk of mortality, poor immune function, and cognitive decline [2].

The benefits of Se as a potential chemopreventive or chemotherapeutic agent have been extensively studied [3-6]. Although the epidemiological data are somewhat controversial, it seems that both, inorganic and organic forms of Se, negatively affect cancer progression [7]. In addition, it is known that selenoproteins also play important roles in tumor development [8]. However, it is important to consider that the dose and the chemical form of selenium have a significant influence on these effects [9-13].

During the last years, attention on nanotechnology and nanomaterials has reached high relevance due to their multiple applications in several fields, including biomedical research [14]. Selenium nanoparticles (SeNPs) are considered a novel selenium compound with excellent antioxidant properties and lower toxicity than other selenospecies [15, 16]. Zhang et al [17] demonstrated that SeNPs and Se(IV) had a similar bioavailability in rats and antioxidant effect in cells. On the other hand, SeNPs have been proved to present a better selectivity between normal and cancer cells than Se(IV) at similar concentrations [18]. Moreover, SeNPs have been appointed as a potential anticancer drug [19, 20] due to its ability to inhibit the growth of cancer cells through induction of S phase arrest [21]. In fact, the relationship between nanoparticles (not only in the case of SeNPs) and cell cycle life has been recently reviewed by Kim et al. [22] and Mahmoudi et al. [23].

In the present work, we compare the effect of chitosan-modified selenium nanoparticles (Ch-SeNPs) and other inorganic and organic selenospecies including Se(IV), Se(VI), selenomethionine (SeMet), selenocystine ($SeCys_2$) and seleno methylselenocysteine (Se-MeSeCys) on hepatocarcinoma (HepG2) cells in terms of viability, proliferation and migration. We also evaluate the capacity of the different species to induce apoptosis and/or cell cycle arrest. Finally, we consider the relevance of cyclin-dependent kinase 1 (Cdk1) in governing the mitotic cell death,

which constitutes a current potential mechanism for cancer therapy. Thus, we study the inhibition degree of Cdk1 after exposing the cells to the above mentioned species in order to evaluate whether the properties exhibited by SeNPs are unique or shared by other selenocompunds.

2. Experimental

2.1. Chemicals

Materials and chemicals for electrophoresis were from BioRad (Madrid, Spain). Sodium selenite, sodium selenate, selenomethionine, selenocystine, seleno methylselenocysteine, Dulbecco´s modified Eagle´s medium (DMEM), MTT reagent, Mowiol® 4-88, chitosan, triton, paraformaldehyde (PFA), 4',6-diamidino-2-phenylindole (DAPI) and Anti-GAPDH (glyceraldehyde 3-phosphate dehydrogenase) was purchased from Sigma-Aldrich. Trypsin/EDTA and phosphate buffer saline (PBS) were purchased from Lonza (Basel, Switzerland). Anti-Cdk1 and HRP-conjugated secondary antibodies were purchased from Santa Cruz (Dallas, TX). Apo Logix sulforhodamine caspase detection kit was purchased from Cell Technology (Mountain View, CA). Hoescht 33342 was purchased from Life Technologies (Carlsbad, CA).

2.2. Synthesis of chitosan-modified SeNPs

The preparation of Ch-SeNPs was performed according to the procedure described by Bai *et al* [24]. Briefly, 10 mL of an aqueous chitosan polysaccharide solution (10 mL, 0.5% w/v) were mixed with 7.5 mL of 0.23 M ascorbic acid and 5 mL of 2.4 M acetic acid solution; then, 0.25 mL of 0.51 M sodium selenite was slowly added into the mixture. It was noted, as a proof of the formation of the Ch-SeNPs, that the color of the dispersion changed from colorless to red during the reaction process. Finally, the dispersion was diluted to 50 mL with distilled water obtaining a final concentration of 200 mg/L of Ch-SeNPs. After the synthesis, 10 mL of the dispersion were dialyzed using a 12 KDa of MWCO membrane against 2 L of distilled water for 2 h at room temperature.

2.3. Cell culture and treatment

Human hepatocarcinoma (HepG2) cells were maintained in Dulbecco´s Modified Eagle´s Medium (DMEM) supplemented with fetal bovine serum (10% v/v) and antibiotics (penicillin, 50 U/mL; streptomycin, 50 U/mL) and incubated in 5% CO_2 at 37 °C. Either Ch-SeNPs or other selenospecies including Se(IV), Se(VI), selenomethionine

(SeMet), seleno methylselenocysteine (Se-MeSeCys) and selenocystine ($SeCys_2$), were added to the cells at different concentrations ranging from 0.1 to 5 mg/L and incubated for 72 hours. Cells were then washed twice in PBS and harvested using 0.25% trypsin/0.1% EDTA.

2.4. Transmission electron microscopy analysis

For characterization of the synthesized SeNPs, droplets of the dispersion were placed onto a holey carbon film on copper grids. Micrographs were obtained using the JEOL 1010 JEM transmission electron microscope (JEOL) operating at 100 kV.

2.5. Cell viability assay

Cells were seeded in a 96-well plate at a concentration of $5x10^3$ cells per well, and incubated in complete DMEM for 24 h at 37ºC and 5% CO_2. Cells were individually exposed to each of the following selenocompounds: Ch-SeNPs, Se(IV), Se(VI), SeMet, Se-MeSeCys and $SeCys_2$ (0.1, 0.5, 1 and 5 mg/mL), or their corresponding blank media during 72 hours. Cell viability for each condition was measured by the MTT assay. Briefly, 20 μL of 5 mg/mL MTT solution were added to each well and incubated for 4 h at 37ºC. Then, the media was removed and 100 μL of dimethyl sulfoxide were added to dissolve the formazan crystals. Absorbance was measured at 595 nm in a Sunrise microplate reader (Tecan).

2.6. Cell proliferation/migration assays

Cells were seeded onto cover slips and, after incubation for 24h, exposed to 1 mg/L of the different selenocompounds for 72 h. The cells were washed with PBS on ice, fixed with paraformaldehyde **(**4% v/v) for 15 min at room temperature, and then stained with 1mg/mL 4'-6-Diamidino-2-phenylindole (DAPI). After incubation with DAPI for 10 min, cell proliferation was visually evaluated by fluorescence microscopy using a Motic AE31 epifluorescence microscope (Motic).

To examine the migration capacity of treated and non-treated cells, we carried out the wound healing assay. $3x10^6$ cells were seeded in 60 mm culture dishes and incubated for 24 h. A wound was made in the monolayer using a sterile pipette tip once the cells reached confluence and the cells were individually exposed to 1 mg/L of the different selenospecies. Using phase-contrast microscopy, photographs of cells invading the wound were taken at the indicated times (0, 36, and 72h).

2.7. Apoptosis assay

The Apo Logix sulforhodamine caspase detection kit was used following the manufacturer's instructions. Cells were seeded onto cover slips and exposed to 1 mg/L of the different selenocompounds for 72 h. After treatment, a solution containing a sulforhodamine labeled fluoromethyl ketone-peptide inhibitors of caspases was added to the cells and incubated during 1 h at 37ºC under 5% CO_2 protecting cells from light. After that time, the culture media was removed and the cells were washed twice with PBS. Cells were then fixed with paraformaldehyde **(**4% v/v) for 15 min at room temperature. Staining of nuclei was performed in a 1 mg/mL solution and finally, coverslips were mounted with Mowiol® 4-88. The activity of pre-apoptotic and apoptotic cells was visually analyzed by fluorescence microscopy in a Motic AE31 epifluorescence microscope.

2.8. Cell cycle pattern analysis

For evaluating the cell cycle arrest, around 1 x 10^6 cells were treated with 1 mg/L of either of the selenospecies tested during 72 h. Cells were resuspended in 250 μL of PBS and mixed with an equal volume of a solution containing 60% ethanol (v/v) and 20 μg/mL of Hoechst 33258 reagent. Cells were then incubated for at least 1 h at room temperature and the DNA content analyzed by flow cytometry. Collected data were analyzed using the MultiCycle AV (Phoenix Flow Systems) software.

2.9. Western blotting

Whole total lysates were separated by SDS-PAGE and transferred to nitrocellulose membranes (Bio-Rad). Membranes were blocked in PBS-tween buffer (PBST, 0.05% v/v) containing 3% skim milk and incubated at 4ºC with the corresponding primary antibodies: Cdk1 (1:100) and GAPDH (1:10000), during 1 h. After washing with PBST, membranes were incubated with HRP-conjugated secondary antibodies for 1 h at room temperature, and specific proteins were visualized by enhanced chemiluminescence (GE Healthcare).

2.10. Immunofluorescence assay

Cells were seeded onto cover slips and, after incubation for 24h, exposed to 1 mg/L of the different selenocompounds for 72 h. The cells were then washed with PBS on ice, fixed with paraformaldehyde **(**4% v/v) for 15 min at room temperature, permeabilized with 5 mL of Triton-X100 (0.1% v/v, 40mM glycine) and washed with PBS. The cells were blocked with bovine serum albumin (BSA, 2% w/v) in

PBS for 1 h followed by incubation with the primary antibody anti-Cdk1 (1:100) or anti-GAPDH (1:10000) at room temperature on humid chamber. After three washings with PBS, cells were incubated with Alexa Fluor 586-labeled anti-rabbit lgG (1:1000) (Invitrogen) for 30 minutes at room temperature. Cells were incubated with Alexa Fluor 488-labeled phalloidine (1:60) (Invitrogen) for 20 min at room temperature. Finally, staining of nuclei was performed in a 1 mg/mL solution and coverslips were mounted with Mowiol® 4-88. Fluorescence microscopy was performed in a Motic AE31 epifluorescence microscope.

3. Results and discussion

3.1. Synthesis, characterization and stability of chitosan-modified selenium nanoparticles

It has been demonstrated that monosaccharides (glucose), oligosaccharides (sucrose) and polysaccharides (chitosan) modify the size, morphology and stability of SeNPs in liquid dispersions [24]. Previous studies have shown how encapsulation of selenite into chitosan significantly improve the antioxidant properties and promote a high retention of selenium in cells [25, 26]; thus, we used chitosan to enwrappe SeNPs by forming strong hydrogen bonds between the hydroxyl groups of chitosan and the selenite. We tested concentrations of chitosan ranging from 0.01% to 0.1% in order to evaluate changes in particle size, morphology and aggregation using transmission electron microscopy (TEM). All the synthesis carried out provided Ch-SeNPs with spherical structure and a particle size between 10 and 60 nm. Among all the concentrations of chitosan tested, we observed a higher homogeneity in the NPs dispersion when using 0.1% chitosan (80-90% of Ch-SeNPs presented a particle size between 40 and 60 nm). Based on these results, we used 0.1% chitosan for further experiments.

Synthesized Ch-SeNPs were dialyzed to remove the excess of synthesis reagents. The dialysis time was optimized and 2 h was selected as optimum since longer times caused flocculation of the Ch-SeNPs dispersion. In addition, we evaluated the stability and aggregation of the synthesized Ch-SeNPs stored at 4ºC for up to two months. We did not observe significant differences in the TEM images as for changes in particle size and aggregation during this time. We also examined the potential oxidation of Ch-SeNPs to Se (IV) weekly by centrifugation of the Ch-SeNPs suspension using 10 KDa cut-off filter. The total Se present in the

liquid fraction was quantified by inductively-coupled plasma mass spectrometry (ICP-MS) and less than 0.1% of ionic Se was detected, as a proof of the good stability of the synthesized Ch-SeNPs.

3.2. Effects of Ch-SeNPs on cell viability, proliferation and migration in comparison to other selenospecies

Firstly, we evaluated the effect of Ch-SeNPs and other selenospecies on the cell viability of HepG2 cells by means of the MTT assay, which measures the reducing potential of the cells. While healthy cells can reduce the MTT to formazan (a colored compound), non-viable cells are unable to do so. Thus, cell viability can be estimated by measuring the absorbance of the MTT-treated cells. We compared the effect of the following selenospecies: Se(IV), Se(VI), SeMet, Se-MeSeCys and $SeCys_2$, with the synthesized Ch-SeNPs. We selected concentrations ranging from 0.1 to 5 mg/L and an exposure time of 72 h. We observed

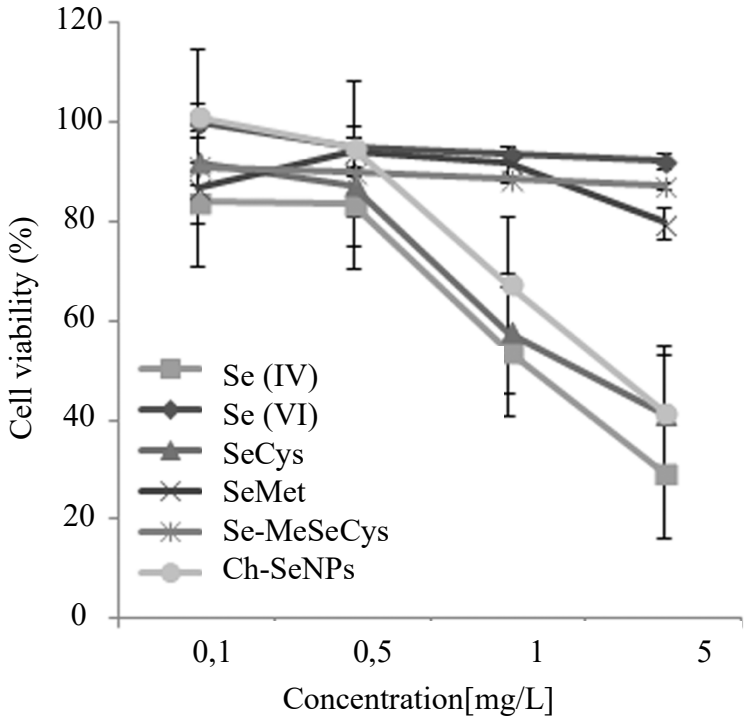

Figure 1. Cell viability of HepG2 cells exposed to different concentrations (0.1, 0.5, 1.0 and 5.0 mg/L) of Se(IV), Se(VI), Ch-SeNPs, SeMet, Se-MeSeCys and $SeCys_2$ during 72 h (n = 5). High concentrations (1 and 5 mg/L) of Ch-SeNPs, Se(IV) and $SeCys_2$ caused a significant decrease in the cell viability. Se(VI), SeMet and Se-MeSeCys did not diminish the cell viability even at the higher concentration tested.

that while Se(VI), SeMet and Se-MeSeCys barely affected cell viability in any of the tested concentrations, Se(IV), Ch-SeNPs and $SeCys_2$ significantly decreased the viability of the exposed cells at concentrations higher than 0.5 mg/L (**Figure 1**). Furthermore, Se (IV) resulted to be the most affecting species, inducing a substantial decrease in cell viability (more than 70%) at 5 mg/L. Ch-SeNPs and $SeCys_2$ caused a similar effect at 5 mg/L, while at 1 mg/L the decrease in cell viability of cells exposed to Ch-SeNPs was slightly lower as compared to cells treated with $SeCys_2$. In order to distinguish different behaviors between the species but without drastically compromising the cell viability, we chose 1 mg/L as the most suitable concentration for further experiments, since none of the species

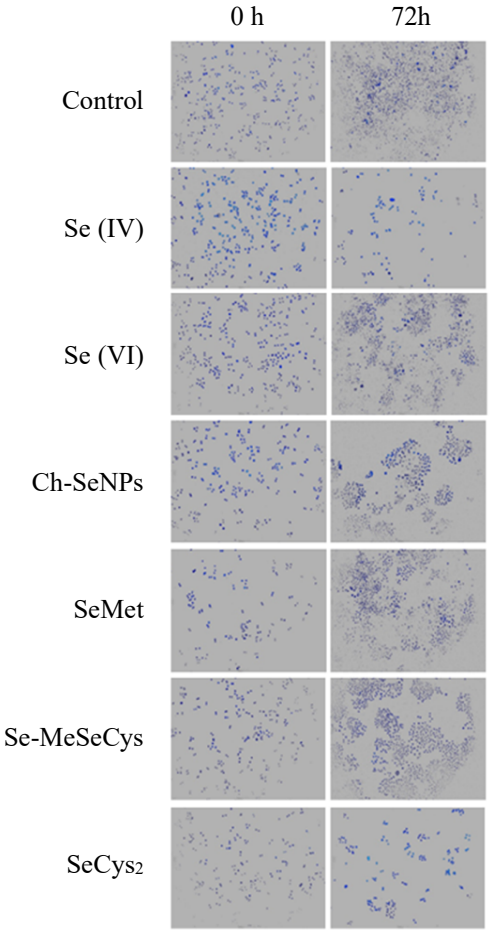

Figure 2. Cell proliferation of HepG2 cells was differently affected depending on the selenospecies tested. The nuclei of cells, before and after exposure with the different selenospecies, was stained with DAPI and visualized by fluorescence microscopy (n = 3). Cells exposed to $SeCys_2$ and Ch-SeNPs showed a lower proliferation rate in comparison to non-treated cells. Cell proliferation was drastically affected in cells exposed to Se(IV).

decreased the viability by more than 50% at that concentration. It is important to mention that neither the synthesis media nor the blank media for any of the selenospecies affected the cell viability (data not shown).

With the purpose of evaluating cell proliferation, we estimated the number of cells before and after exposure to the different selenospecies by staining the nucleus with DAPI. Stained cells were visualized by fluorescence microscopy in the UV region (**Figure 2**). As it can be observed, Se(VI), Se-MeSeCys and SeMet did not influence the cell proliferation as compared to control cells. Besides, cells exposed to $SeCys_2$ and Ch-SeNPs showed a lower proliferation rate in comparison to non-treated cells, which may indicate that these species might be either inducing a

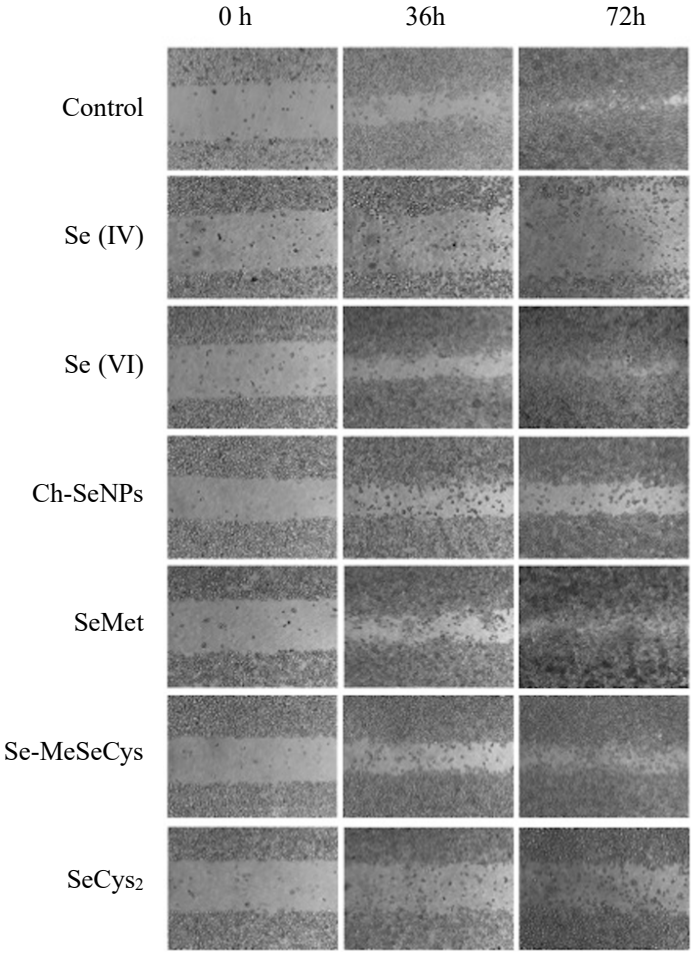

Figure 3. Cell migration was also evaluated by the wound healing assay. Cells exposed to Se(VI), SeMet and Se-MeSeCys progressively repaired the wound with the time in a similar behavior as non-treated cells. On the other hand, Ch-SeNPs and $SeCys_2$ presented a slower migration rate than control cells, whereas cells exposed to Se (IV), not only were unable to repair the wound, but also significantly diminished the number of cells at the non-wounded area.

cell cycle arrest or promoting the apoptotic pathways. In the case of cells exposed to Se(IV) cell proliferation was radically diminished. Actually, the number of cells after 72 h was even lower than before exposure, which could be related to an induction of apoptosis in Se(IV)-treated cells (**Figure 2**).

Finally, cell migration was also evaluated by the wound healing assay. This experiment allowed us to determine the ability of cells to migrate and repair the wound in presence of different selenospecies. Wound repairing was visually inspected by phase-contrast microscopy at 36 and 72 h after exposure (**Figure 3**). As in the previous experiments, we observed that cells exposed to Se(VI), SeMet and Se-MeSeCys presented a similar migratory behavior as control cells. Ch-SeNPs and $SeCys_2$ revealed a slower migration rate in comparison to control cells while cells exposed to Se (IV), as in the proliferation assay, not only were unable to repair the wound, but also the number of cells was significantly decreased (**Figure 3**).

3.3. Ch-SeNPs do not induce apoptosis in HepG2 treated-cells in contrast to Se(IV) and $SeCys_2$

Our previous results suggested that Se(IV), $SeCys_2$ and Ch-SeNPs may be inducing either cell cycle arrest or apoptosis in exposed cells. In order to clarify whether the cells were entering apoptosis and considering that the main components of the apoptotic cascade are the caspases, we detected cells with active caspases using a sulforhodamine labeled peptide fluoromethyl ketone caspase inhibitor. This inhibitor irreversibly binds to active caspases allowing detection of apoptotic cells by fluorescence microscopy.

As expected, cells treated with Se(IV) presented the highest fluorescence intensity, which proves this species to be the most toxic to HepG2 cells (**Figure 4**). This is in well agreement with previous studies showing how exposure to Se(IV) induce mitochondrial injury and apoptosis in human prostate cancer cells (LNCaP) [27] and human colon cancer cells (HCT-116 and SW620) [28, 29]. Interestingly, although in previous experiments $SeCys_2$ and Ch-SeNPs showed a similar effect in exposed cells, the degree of apoptosis was significantly higher for cells exposed to $SeCys_2$, while cells exposed to Ch-SeNPs practically did not show any caspase activity. On the other hand, although Se(VI) and Se-MeSeCys did not affect the viability, proliferation and migration of HepG2 cells, they seemed to induce a slight apoptotic effect (**Figure 4**).

3.4. Ch-SeNPs and $SeCys_2$ induce cell cycle arrest in HepG2 cells

In the results commented before, we observed how Ch-SeNPs and $SeCys_2$ inhibit cell proliferation and migration and significantly reduce the viability of exposed cells but without inducing apoptosis in the case of Ch-SeNPs. A previous study carried out by Luo *et al.* [21] showed how SeNPs induced cell cycle arrest at the S phase in HeLa and MDA-MB-231 cells. With the aim of proving whether this property is unique to elemental Se as SeNPs or other species can induce a similar cell cycle arrest, we carried out a flow cytometry analysis of cells exposed to the different selenospecies previously tested. The phase in which the cell cycle is arrested, considering that cells double the amount of their DNA during the progression through cell cycle prior entering mitosis, can be identified by

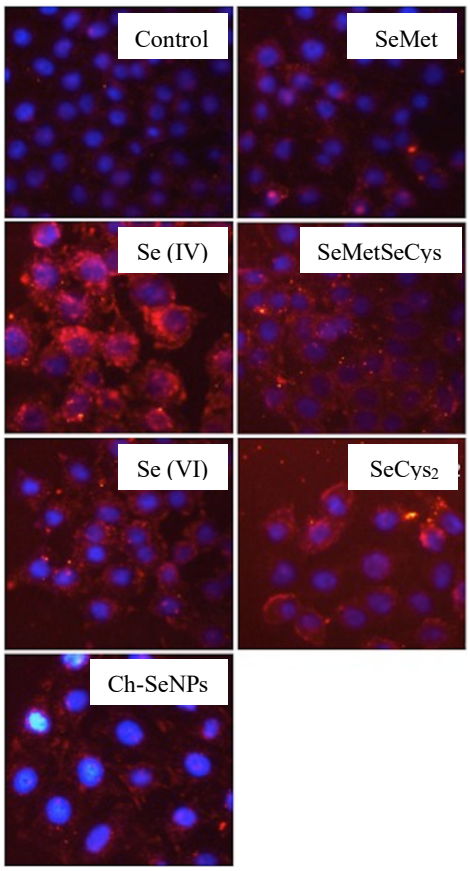

Figure 4. Induction of apoptosis by the different selenocompounds was estimated by measuring the activity of caspases (n = 3). Se(IV) was proved to be the most toxic species to HepG2 cells. The degree of apoptosis was significantly higher for cells exposed to $SeCys_2$ than in cells exposed to Ch-SeNPs, which practically did not exhibit any caspase activity. Se(VI) and Se-MeSeCys, although they did not significantly affect the viability, proliferation and migration of HepG2 cells, seemed to induce a slight apoptotic effect.

measuring the total amount of stained DNA in treated and non-treated cells.

We confirmed that cells treated with 1 mg/L of Ch-SeNPs presented a 10% increase of cell population in the S-G2/M phase as compared to controls cells. The percentage of cells treated with Ch-SeNPs in the G0/G1 phase decreased in the same way as the population in phase S-G2/M increased, thus proving that Ch-SeNPs induce cell cycle arrest at the S-G2/M phase (**Figure 5**). This result is in agreement with the data provided by Luo et al. [21]. Cells treated with $SeCys_2$ exhibited a similar behavior, whereas cells exposed to Se(IV) presented a high percentage of cells in the sub-G1 phase, meaning cells entering apoptosis. Cells treated with either Ch-SeNPs and $SeCys_2$ did not present a significant cell population in the sub-G1 phase, which is consistent with the apoptosis assay carried out before. On the other hand, Se(VI), SeMet and Se-MeSeCys did not present significant differences in cell cycle pattern as compared to control cells (**Figure 5**).

These results reinforce the proposed role of Ch-SeNPs as a potential chemotherapeutic agent. Nevertheless, $SeCys_2$ also emerged from our results to be a potential inductor of cell cycle arrest.

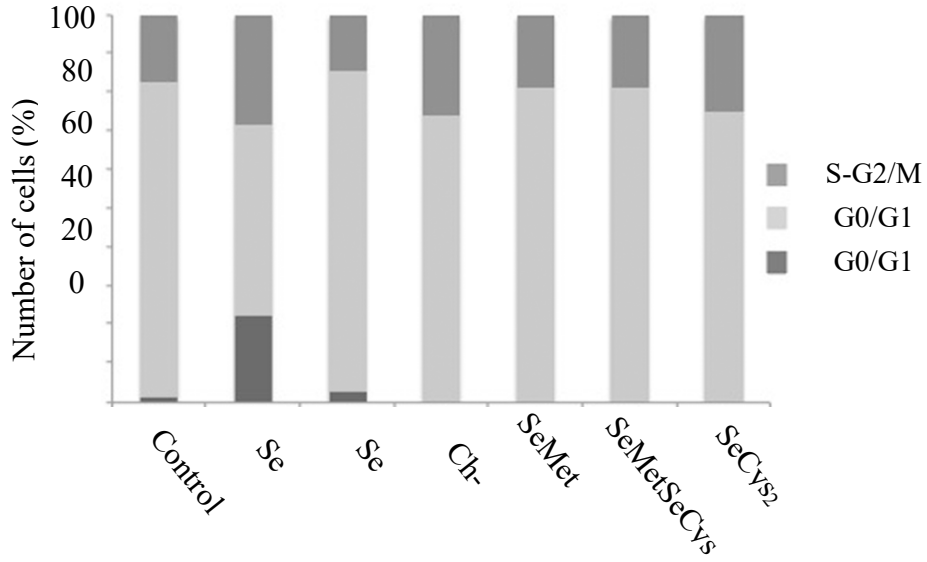

Figure 5. Cells treated with 1 mg/L of Ch-SeNPs and SeCys2 for 72 h exhibited a cell cycle arrest at the S-G2/M phase. Cells exposed to Se(IV) presented a high percentage of cells in the sub-G1 phase, meaning cells entering apoptosis. On the other hand, Se(VI), SeMet and Se-MeSeCys did not present significant differences in cell cycle pattern as compared to control cells.

3.5. Potential implications of Cdk1-targeting Ch-SeNPs in mitotic cell death for cancer therapy

One of the current trends in cancer therapy is designing chemotherapeutic drugs to impair tumor cell proliferation. Cell cycle dysfunction is a recognizable sign of cancer cells that usually implies alteration of the expression of cyclin-dependent kinases (Cdks) and inactivation of Cdks inhibitors [30]. Cdks are a family of proteins composed of a catalytic subunit (Cdk) and a regulatory subunit (Cyclins) involved in the progression of the cell cycle through the different phases [31]. While Cdk2, Cdk4 and Cdk6 trigger G1/S transition, Cdk1 promotes mitotic entry and progression (**Figure 6a**) [32]. Mechanistically, inhibition of Cdk1 prevents cells from entering mitosis and induces cell cycle arrest [33], which represents a way of precluding tumor cells progression. This fact suggests the

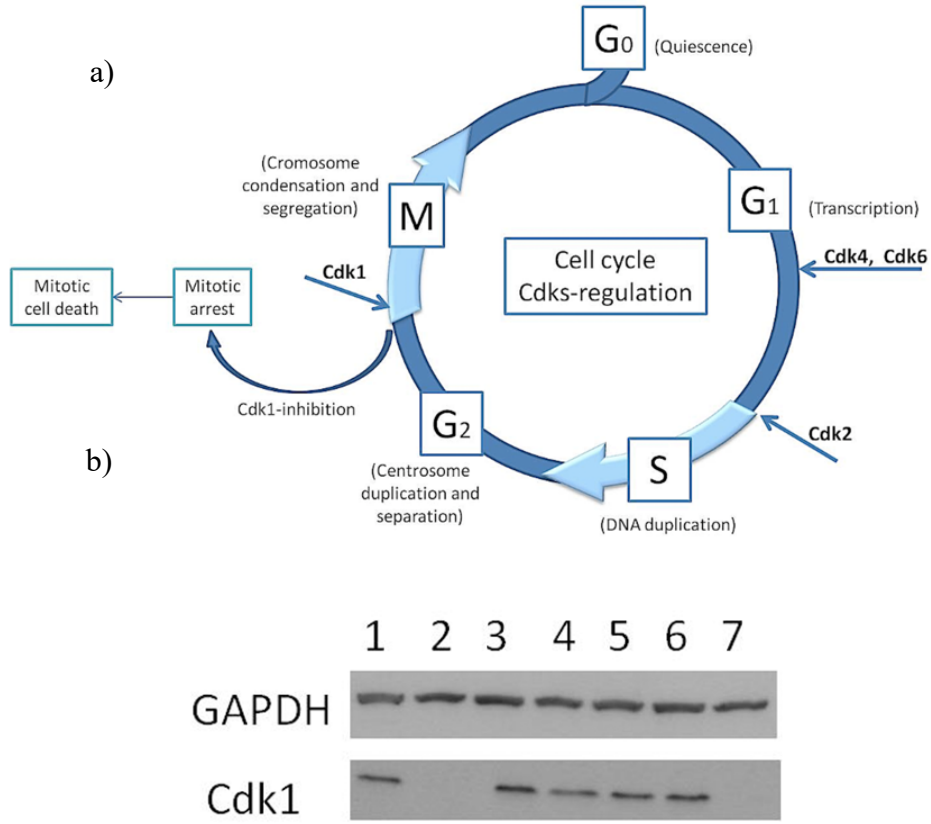

Fig. 6. Ch-SeNPs partially inhibited the expression of Cdk1. (a) Cdks play an essential role in cell cycle progression and mitosis entry. (b) The Western blot analysis showed the partial inhibition of Cdk1 induced by Ch-SeNPs whereas Se(IV) and $SeCys_2$ drastically inhibited its expression. Since strong inhibition of Cdk1 is likely to be toxic for healthy cells Se(IV) and $SeCys_2$ might not be suitable as a potential candidate for therapeutic purposes. 1, control; 2, Se(IV); 3, Se(VI); 4, Ch-SeNPs; 5, SeMet; 6, Se-MeSeCys; 7, $SeCys_2$

potential applications of Cdk1-targeting compounds in cancer therapy [34].

Previous studies have shown that Se, even without being incorporated into proteins, can modulate the activity of transcription factors and kinases [35, 36]. Based on this, and considering the ability of Ch-SeNPs to arrest the cell cycle, we performed a western blot analysis to evaluate the effect of Ch-SeNPs on the expression of Cdk1 in comparison to other selenospecies (**Figure 6b**). We observed that cells exposed to Ch-SeNPs showed a partial inhibition of Cdk1 as compared to control cells and cells treated with Se(VI), SeMet and Se-MeSeCys. In the contrary, Se(IV) and $SeCys_2$ drastically inhibited the expression of Cdk1. It is important to consider that strong inhibition of Cdk1 is likely to be toxic for healthy cells [37]; therefore, although cells exposed to $SeCys_2$ induced a similar cell cycle arrest as cells exposed to Ch-SeNPs (**Figure 5**), $SeCys_2$ might not be suitable as a potential candidate for therapeutic purposes. We further confirmed the partial inhibition of Cdk1 in cells exposed to Ch-SeNPs by immunofluorescence (**Figure 7**). These results are also consistent with the degree of apoptosis observed in cells exposed to Ch-SeNPs, Se(IV) and $SeCys_2$. Cells treated with Ch-SeNPs, in contrast to cells

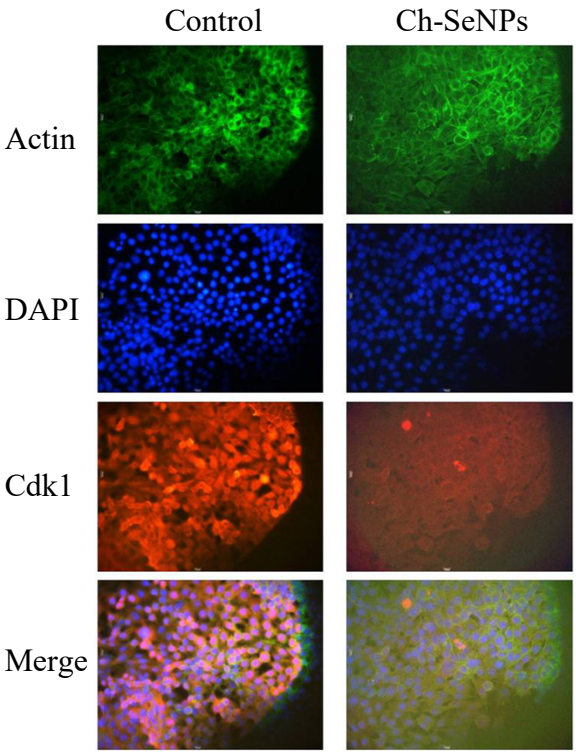

Figure 7. Immunofluorescence assay confirmed the partial inhibition of Cdk1 induced by Ch-SeNPs. Cells were stained with anti-Cdk1 (red), phalloidin (green), counterstained with DAPI (blue) and visualized by fluorescence microscopy.

exposed to $SeCys_2$ and Se(IV), did not show any activation of caspases (**Figure 4**). This is in agreement with recent data suggesting that caspases are not required for the mitotic cell death, which is governed by Cdk1 activity [38].

4. Conclusions

To the best of our knowledge, this is the first time that a systematic comparison of the effect of Ch-SeNPs with other inorganic and organic selenospecies on the behavior of cancer cells has been carried out. Our data, strongly suggest that cells exposed to Ch-SeNPs and $SeCys_2$ undergo similar alterations in terms of cell viability, proliferation, migration and cell cycle arrest at the S-G2/M phase. Cells exposed to Se(IV) showed evident signs of toxicity such as strong induction of apoptosis and a significant population of cells in the sub-G1 phase as compared to control cells. Se(VI), SeMet and Se-MeSeCys, besides a slight increase in caspase activity, did not present any other differences in comparison to non-treated cells at the tested concentrations. Whereas $SeCys_2$ induces a certain degree of apoptosis and a drastic reduction of the level of expression of Cdk1, which might involve potential toxicity of this compound for healthy cells, Ch-SeNPs only inhibited Cdk1 partially; thus supporting the potential application of Ch-SeNPs for impairing tumor progression. We have shown by different independent approaches the unique properties of Ch-SeNPs in comparison to other selenocompounds and their promising potential in cancer therapy.

Acknowledgements

Authors thank the Spanish Ministry of Economy and Competitiveness (grants CTQ2010-18644 and CTQ2011-28328C02-01), the *Comunidad de Madrid* (Spain) and the European FEDER programme (grants AS2009/AGR-1464, ANALISYC-II, Interreg European Project Orque-Sudoe). The authors thank Blanca González, Sandra Sánchez and Montserrat Colilla for their valuable help in synthesizing the Ch-SeNPs. The authors also thank Maria Luisa Garcia and Agustin Fernandez for electron microscopy services (ICTS-CNME) and the Complutense University Flow Cytometry Core.

References

[1] S.K. Fairweather-Tait, Y. Bao, M.R. Broadley, R. Collings, D. Ford, J.E. Hesketh, R. Hurst, Selenium in human health and disease, Antioxid. Redox Signal. 14 (2011) 1337–1383.

[2] M.P. Rayman, Selenium and human health, Lancet 379 (2012) 1256–1268.

[3] C. Ip, H.J. Thompson, Z. Zhu, H.E. Ganther, *In vitro* and *in vivo* studies of methylseleninic acid: evidence that a monomethylated selenium metabolite is critical for cancer chemoprevention, Cancer Res. 60 (2000) 2882–2886.

[4] G.X. Li, H.J. Lee, Z. Wang, H. Hu, J.D. Liao, J.C. Watts, G.F. Combs Jr., J. Lu, Superior in vivo inhibitory efficacy of methylseleninic acid against human prostate cancer over selenomethionine or selenite, Carcinogenesis 29 (2008) 1005–1012.

[5] P.D. Whanger, Selenium and its relationship to cancer: an update, Br. J. Nutr. 91 (2004) 11–28.

[6] J. Brozmanová, D. Mániková, V. Vlcková, M. Chovanec, Selenium: a double-edged sword for defense and offence in cancer, Arch. Toxicol. 84 (2010) 919–938.

[7] P.B. Cassidy, H.D. Fain, J.P. Cassidy Jr., S.M. Tran, P.J. Moos, K.M. Boucher, R. Gerads, S.R. Florell, D. Grossman, S.A. Leachman, Selenium for the prevention of cutaneous melanoma, Nutrients 5 (2013) 725–749.

[8] Y.C.Che, K.S.Prabhu, A.M.Mastro, Is selenium a potential treatment for cancer metastasis? Nutrients 5 (2013) 1149–1168.

[9] R. Sinha, K. El-Bayoumy, Apoptosis is a critical cellular event in cancer chemoprevention and chemotherapy by selenium compounds, Curr. Cancer Drug Targets 4 (2004) 13–28.

[10] R.Abdulah, K.Miyazaki, M.Nakazawa, H.Koyama, Chemicalf orms of selenium for cancer prevention, J. Trace Elem. Med. Biol. 19 (2005) 141–150.

[11] C.L. Shen, W. Song, B.C. Pence, Interactions of selenium compounds with other antioxidants in DNA damage and apoptosis in human normal keratinocytes, Cancer Epidemiol. Biomarkers Prevent. 10 (2001) 385–390.

[12] L.R. Ferguson, N. Karunasinghe, S. Zhu, A.H. Wang, Selenium and its' role in the maintenance of genomic stability, Mutat. Res. 733 (2012) 100–110.

[13] H.J. Jung, H.L. Kim, Y.J. Kim, J.I. Weon, Y.R. Seo, A novel chemopreventive mechanism of selenomethionine: enhancement of APE1 enzyme activity via Gadd45a, PCNA and APE1 protein complex that regulates p53-mediated base excision repair, Oncol. Rep. 30 (2013) 1581–1586.

[14] J.L. Luque-Garcia, R. Sanchez-Diaz, I. Lopez-Heras, P. Martin, C. Camara, Bioanalytical strategies for *in-vitro* and *in-vivo* evaluation of the toxicity induced by metallic nanoparticles, Trends Anal. Chem. 43 (2013) 254–268.

[15] J.Zhang, X.Wang, T.Xu, Elemental selenium at nanosize (Nano-Se) as a potential chemopreventive agent with reduced risk of selenium toxicity: comparison with se-methylselenocysteine in mice, Toxicol. Sci. 101 (2008) 22–31.

[16] H. Wang, J. Zhang, H. Yu, Elemental selenium at nano size possesses lower toxicity without compromising the fundamental effect on selenoenzymes: comparison with selenomethionine in mice, Free Radical Biol. Med. 42 (2007) 1524–1533.

[17] J.S. Zhang, X.Y. Gao, L.D. Zhang, Y.P. Bao, Biological effects of a nano red elemental selenium, Biofactors 15 (2001) 27–38.

[18] T. Chen, Y.S. Wong, W. Zheng, Y. Bai, L. Huang, Selenium nanoparticles fabricated in Undaria pinnatifida polysaccharide solutions induce mitochondria-mediated apoptosis in A375 human melanoma cells, Colloids Surf., B: Biointerfaces 67 (2008) 26–31.

[19] Y. Huang, L. He, W. Liu, C. Fan, W. Zheng, Y.S. Wong, T. Chen, Selective cellular uptake and induction of apoptosis of cancer-targeted selenium nanoparticles, Biomaterials 34 (2013) 7106–7116.

[20] H. Wu, H. Zhu, X. Li, Z. Li, W. Zheng, T. Chen, B. Yu, K.H. Wong, Induction of apoptosis and cell cycle arrest in A549 human lung adenocarcinoma cells by surface-capping selenium nanoparticles: an effect enhanced by polysaccharide-protein complexes from Polyporus rhinocerus, J. Agric. Food Chem. 61 (2013) 9859–9866,

[21] H. Luo, F. Wang, Y. Bai, T. Chen, W. Zheng, Selenium nanoparticles inhibit the growth of HeLa and MDA-MB-231 cells through induction of S phase arrest, Colloids Surf., B: Biointerfaces 94 (2012) 304–308.

[22] J.A. Kim, C. Aberg, A. Salvati, K.A. Dawson, Role of cell cycle on the cellular uptake and dilution of nanoparticles in a cell population, Nat. Nanotechnol. 7 (2011) 62–68.

[23] M. Mahmoudi, K. Azadmanesh, M.A. Shokrgozar, W.S. Journeay, S. Laurent, Effect of nanoparticles on the cell life cycle, Chem. Rev. 111 (2011) 3407–3432.

[24] Y. Bai, Y. Wang, Y. Zhou, W. Li, W. Zheng, Modification and modulation of sac- charides on elemental selenium nanoparticles in liquid phase, Mater. Lett. 62 (2008) 2311–2314.

[25] Y. Luo, B. Zhang, W.H. Cheng, Q. Wang, Preparation, characterization and evaluation of selenite-loaded chitosan/TPP nanoparticles with or without zein coating, Carbohydr. Polym. 82 (2010) 942–951.

[26] S. Zhang, Y. Luo, H. Zeng, Q. Wang, F. Tian, J. Song, W.H. Cheng, Encapsulation of selenium in chitosan nanoparticles improves selenium availability and protects cells from selenium-induced DNA damage response, J. Nutr. Biochem. 22 (2011) 1137–1142.

[27] W. Zhong, T.D. Oberley, Redox-mediated effects of selenium on apoptosis and cell cycle in the LNCaP human prostate cancer cell line, Cancer Res. 61 (2001) 7071–7078.

[28] V. Králová, S. Benesová, M. Cervinka, E. Rudolf, Selenite-induced apoptosis and autophagy in colon cancer cells, Toxicol. In Vitro 26 (2012) 258–268.

[29] Z. Li, J. Meng, T.J. Xu, X.Y. Qin, X.D. Zhou, Sodium selenite induces apoptosis in colon cancer cells via Bax-dependent mitochondrial pathway, Eur. Rev. Med. Pharmacol. Sci. 17 (2013) 2166–2171.

[30] M. Malumbres, Physiological relevance of cell cycle kinases, Physiol. Rev. 91 (2011) 973–1007.

[31] M. Malumbres, M. Barbacid, Cell cycle kinases in cancer, Curr. Opin. Genet. Dev. 17 (2007) 60–65.

[32] M. Malumbres, M. Barbacid, Mammalian cyclin-dependent kinases,

Trends Biochem. Sci. 30 (2005) 630–641.

[33] E. Manchado, M. Guillamot, M. Malumbres, Killing cells by targeting mitosis, Cell Death Differ. 19 (2012) 369–377.

[34] G.I. Shapiro, Cyclin-dependent kinase pathways as targets for cancer treatment, J. Clin. Oncol. 24 (2006) 1770–1783.

[35] H. Zeng, Selenite and selenomethionine promote HL-60 cell cycle progression, J. Nutr. 132 (2002) 674–679.

[36] H.E. Ganther, Selenium metabolims, selenoproteins and mechanisms of cancer prevention: complexities with thioredoxin reductase, Carcinogenesis 20 (1999) 1657–1666.

[37] M. Malumbres, P. Pevarello, M. Barbacid, J.R. Bischoff, CDK inhibitors in cancer therapy: what is next, Trends Pharmacol. Sci. 29 (2008) 16–21.

[38] K. Lee, A.E. Kenny, C.L. Rieder, Caspase activity is not required for the mitotic checkpoint or mitotic slippage in human cells, Mol. Biol. Cell 22 (2011) 2470–2479.

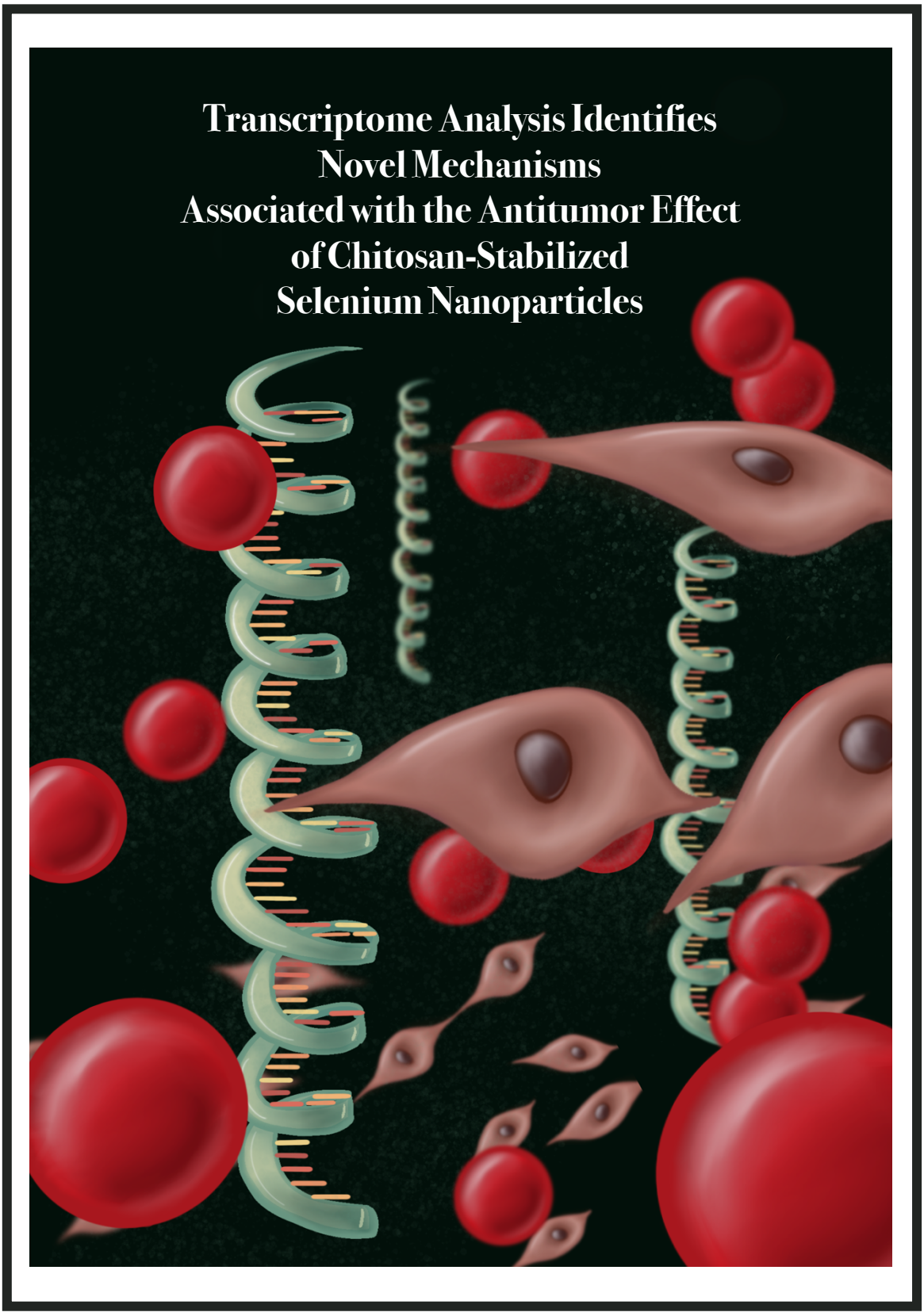
Transcriptome Analysis Identifies
Novel Mechanisms
Associated with the Antitumor Effect
of Chitosan-Stabilized
Selenium Nanoparticles

1.2. Transcriptome Analysis Identifies Novel Mechanisms Associated with the Antitumor Effect of Chitosan-Stabilized Selenium Nanoparticles

Héctor Estévez, Estefania Garcia-Calvo, Jose Rivera-Torres, María Vallet-Regí, Blanca González and Jose L. Luque-García

Pharmaceutics 2021, 13, 356

Abstract

Selenium nanoparticles (SeNPs) have been receiving special attention in recent years due to their antioxidant capacity and antitumor properties. However, the mechanisms associated with these properties remain to be elucidated. For this reason, a global transcriptome analysis has been designed in this work and it was carried out using human hepatocarcinoma cells and chitosan-stabilized SeNPs (Ch-SeNPs) to identify new targets and pathways related to the antitumor mechanisms associated with Ch-SeNPs. The results obtained confirm the alteration of the cell cycle and the effect of Ch-SeNPs on different tumor suppressors and other molecules involved in key mechanisms related to cancer progression. Furthermore, we demonstrated the antioxidant properties of these nanoparticles and their capacity to induce senescence, which was further confirmed through the measurement of β-galactosidase activity.

1. Introduction

A correct balance between ROS generation by pro-oxidants and the action of antioxidants maintains the normal cellular redox status. Loss of this balance might play a critical role in cellular signaling pathways, sometimes evolving into an uncontrolled proliferation leading to neocarcinogenesis [1, 2]. ROS are generated as a defense barrier against extracellular pathogens, including bacterial and viral infections, but an excessive production is also closely related to cancer pathologies. Cancer therapy is, in the great majority of the cases, based in chemotherapy, usually in combination with radiation therapy and immunotherapy. One of the main side effects of the cytotoxic agents used in chemotherapy is the generation of ROS, which induces DNA damage or affection of the DNA machinery [3]. To avoid this problem, many chemotherapeutic strategies are focused on using antioxidants to deplete tumor cells from ROS-induced survival signaling pathways, having such treatments also potential preventive functions.

The emerging field of nanotechnology in recent years has opened up a new field of study for the development of novel drugs in a wide variety of diseases [4, 5] and, in particular, for the development of promising nanoparticles and nanosystems with antitumoral properties [6, 7]. The anti-tumoral effect of some of these nanoparticles is based on their antioxidant properties. Such is the case of gold nanoparticles, which have been successfully tested against human breast cancer (MCF-7) cells [8].

Selenium is a well-known essential micronutrient that participates in a large number of key physiological processes. It is also considered an element with antioxidant properties and, as a matter of fact, different selenospecies have been proposed as potential anti-tumoral agents against different types of cancer [9, 10]. In a previous work, we demonstrated the unique effect of chitosan stabilized selenium nanoparticles (Ch-SeNPs), in comparison to other organic and inorganic selenospecies, to induce cell cycle arrest while preventing the formation of an uncontrolled generation of ROS that would have induced apoptosis [11]. Although additional efforts have been carried out to elucidate the action mechanisms associated to the potential anti-tumoral effect of SeNPs [11, 12, 13], further efforts are still

needed to confirm the specific targets and mechanisms responsible for the observed effects.

Transcriptomics represent a high-throughput screening tool that provides in-depth understanding of cellular functions and the genomic landscape of transcription, thanks to its capability to mirror post genomic variations. Thus, it represents an essential strategy for the study of such a dynamic pathology like cancer [14, 15].

Based on all of the above, we have synthesized and characterized selenium nanoparticles stabilized with chitosan (Ch-SeNPs), which have further been used to treat human hepatocellular carcinoma cells (HepG2 cells). The design and application of a whole transcriptome analysis on this system has provided a wide number of altered targets and pathways, thus allowing us to delve deeper into the mechanisms associated to the antitumoral effect of Ch-SeNPs.

2. Materials and Methods

2.1. Synthesis and characterization of SeNPs

Chitosan-stabilized SeNPs (Ch-SeNPs) were synthesized following the procedure described by Bai et al. [21] (**Figure 1**). An aqueous chitosan polysaccharide solution (0.5% w/v) was prepared using 0.5 M acetic acid. Then, 10 mL of this chitosan solution were mixed with 7.5 mL of ascorbic acid 0.23 M and 5 mL of acetic acid 2.4 M. To the resulting solution, 0.25 mL of sodium selenite 0.51 M were slowly added. The observed change of the solution from colorless to red was indicative of the reaction progression and the SeNPs formation. After the synthesis, the colloidal suspension was diluted to 50 mL with distilled water, resulting in final concentrations of 200 mg/L of Se and 0.1% of chitosan. Finally, the colloidal suspension was dialyzed for 2 h at room temperature in a ratio of 10 mL against 2 L of distilled water and using a 12 kDa of MWCO membrane.

Ch-SeNPs were characterized by Transmission Electron Microscopy (TEM) and energy dispersive X-ray spectroscopy (EDX) with a JEOL JEM 1400 PLUS operating at 120 kV and equipped with a CCD camera (KeenView Camera) (JEOL Ltd., Tokyo, Japan). Sample preparation was performed by placing one or two drops of the Ch-SeNPs colloidal suspension onto carbon-coated copper grids.

Electrophoretic mobility measurements for the Ch-SeNPs colloidal suspension in water were used to calculate the zeta-potential (ζ-potential) values of the nanoparticles. Measurements were performed in a Zetasizer Nano ZS (Malvem Instruments Ltd., United Kingdom) equipped with a 633 nm "red" laser. For this purpose, dilutions of the initial suspension were performed if needed. Measurements were recorded by placing ca. 1 mL of the suspension in a DTS1070 disposable folded capillary cells (Malvern Instruments). The hydrodynamic size of the nanoparticles was measured by dynamic light scattering (DLS) with the same Malvern instrument. Values presented are mean ± SD from quintuplicated measurements.

Stability of Ch-SeNPs was determined using an Agilent HP 7700x inductively coupled plasma-mass spectrometer (ICP-MS) (Agilent).

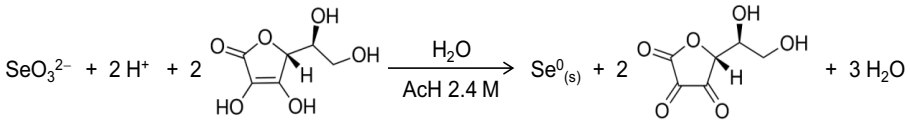

Figure 1. Redox reaction involved in the formation of SeNPs.

2.2. Cell culture

A hepatocellular carcinoma cell line (Homo sapiens), known as HepG2 cells (HEPG2, ATCC HB-8065 TM), was selected for this study. Cells were maintained in Dulbecco´s modified Eagle´s medium (DMEM) supplemented with 10% fetal bovine serum (FBS) and 1% penicillin/streptomycin at 37 °C and 5% CO_2.

2.3. Cytotoxicity assay

To evaluate the cytotoxicity induced by Ch-SeNPs, HepG2 cells were seeded into 96-well plates and incubated for 24 h. Then, cells were exposed to ranging concentrations of Ch-SeNPs (0.1 to 5 mg/L) for 72 h. After this time, 20 µL of 3-(4,5-dimethyl-thiazol-2-yl)2,5-diphenyl tetrazolium bromide (MTT, 5 mg/mL) were added to each well and incubated for 5 h at 37 °C. Then, the culture media was removed, and 100 µL of dimethyl sulfoxide were added to dissolve the insoluble purple formazan products. Absorbance was measured at 595 nm using a microplate

reader (TECAN). The final results were calculated on the basis of 5 replicates of the experiment.

2.4. Transcriptome analysis

To evaluate potential alterations in the mRNA expression levels of HepG2 cells treated with Ch-SeNPs, a transcriptome microarray analysis was performed. Cells were seeded in culture plates for 24 h, and then exposed to 1 mg/L of Ch-SeNPs for 72 h (37 °C and 5% CO_2). Control (untreated) cells were seeded in parallel and incubated at 37 °C and 5% CO_2 for 96 h (24 h + 72 h). After exposure time, mRNA was extracted and purified using a commercial kit (PureLink ®, Invitrogen). Shortly, cells were trypsinized, centrifuged and the supernatant was removed. Cells were lysed with lysis buffer containing 2-mercaptoethanol. Lysates were then centrifuged and one volume of 70% ethanol was added to the samples. 700 µL of this volume were transferred to a conical tube and centrifuged. Afterwards, samples were rinsed with washing buffer and RNase-free water was added to the spin cartridge prior to centrifugation. The purified RNA was stored at -80 °C for further analysis. Samples were processed with GeneChip® WT PLUS Reagent Kit (Applied Biosystems), hybridized with Clariom™ D Array, human (Applied Biosystems) and scanned with a GeneChip® Scanner 3000 7G (Applied Biosystems). Raw data were processed with RMA algorithm included in Transcriptome Analysis Console (Applied Biosystems) for normalization and gene level analysis. For each experimental condition, three microarray experiments corresponding to three independent RNA replicates were processed and analyzed. Fold changes between experimental conditions were calculated as a quotient between the mean of the gene expression signals. Statistical analysis was performed with e-bayes limma included in the Transcriptome Analysis Console (Applied Biosystems). Those values with an FDR (adjusted p-value) ≤ 0.05 were considered as significant.

2.5. Senescence assay

A cytochemical staining kit for the observation of β-galactosidase expression (Sigma-Aldrich) was selected to evaluate whether or not Ch-SeNPs induce senescence on HepG2 cells. Cells were seeded and exposed to either 1 mg/L of Ch-SeNPs, 10 µM of etoposide (senescence positive control) or 50 µM of etoposide (apoptosis

positive control) during 72 h at 37 °C and 5% CO2. After exposure time, cell culture solutions were removed and cells were washed with PBS. Cells were then fixed with 20% formaldehyde, 2% glutaraldehyde, 70.4 mM Na2HPO4, 14.7 mM KH_2PO_4, 1.37 M NaCl, and 26.8 mM KCl fixing buffer for 7 min at room temperature. After removing the fixing buffer, cells were washed with PBS and incubated with the staining mixture. Finally, cells were incubated at 37 °C without CO2 overnight, and then examined using a phase contrast microscope (Motic AE31).

3. Results and Discussion

3.1. Synthesis and characterization of Ch-SeNPs

Selenium nanoparticles (SeNPs) were prepared via the chemical reduction of selenite with ascorbic acid in the presence of chitosan as a soft template to control nucleation and growth of the inorganic selenium nanoparticles. Ascorbic acid acts as the reducing agent following the redox reaction in water where acid medium is provided by acetic acid in our system [22]. The role of the polysaccharide chitosan in this redox system is to act as stabilizer and capping agent, affording red elemental selenium in colloidal state [23]. Furthermore, chitosan was selected because it has been shown to increase the bioavailability of SeNPs while improving the intrinsic antioxidant properties of Se [24, 25]. A final concentration of chitosan of 0.1% was employed to prepare the SeNPs since, under these conditions, the nanoparticles are colloidally stable and possess an adequate diameter range, as we have described in previous works [11, 26]. Well-dispersed nanoparticles were obtained as shown by transmission electron microscopy images, where Ch-SeNPs exhibit spherical morphology and homogenous sizes of around 40-60 nm (**Figures 2A, 2B and 2C**). Their composition in selenium was confirmed by energy dispersive spectroscopy analysis (**Figure 2D**). Signals for C and O from chitosan and the carbon coated copper grid were also observed in the spectrum. The XRD pattern registered for Ch-SeNPs shows broad peaks and low signal-to-noise ratios that can be ascribed to a small crystalline domain size in the range of few nanometres (See Figure SI.1 in Supporting Information). The hydrodynamic diameter of the Ch-SeNPs was measured in the aqueous colloidal suspension giving a monomodal distribution in the range of ca. 25 to 100 nm, with a maximum

centered at 37.8 ± 2.7 nm (**Figure 2E**). These values are in concordance with the size of the inorganic selenium nanoparticles observed in the TEM images.

The surface stabilization of the SeNPs with chitosan was also confirmed by means of electrophoretic mobility measurements of the Ch-SeNPs colloidal suspension in water (Figure 1F). The highly positive ζ-potential value of +62.5 ± 5.2 mV falls in the zone of colloidal stability and is ascribed to the equilibrium for the protonation of the amino groups of chitosan in water. As expected, chitosan allows the SeNPs to form stable colloidal suspensions due to both electrostatic as well as steric stabilization.

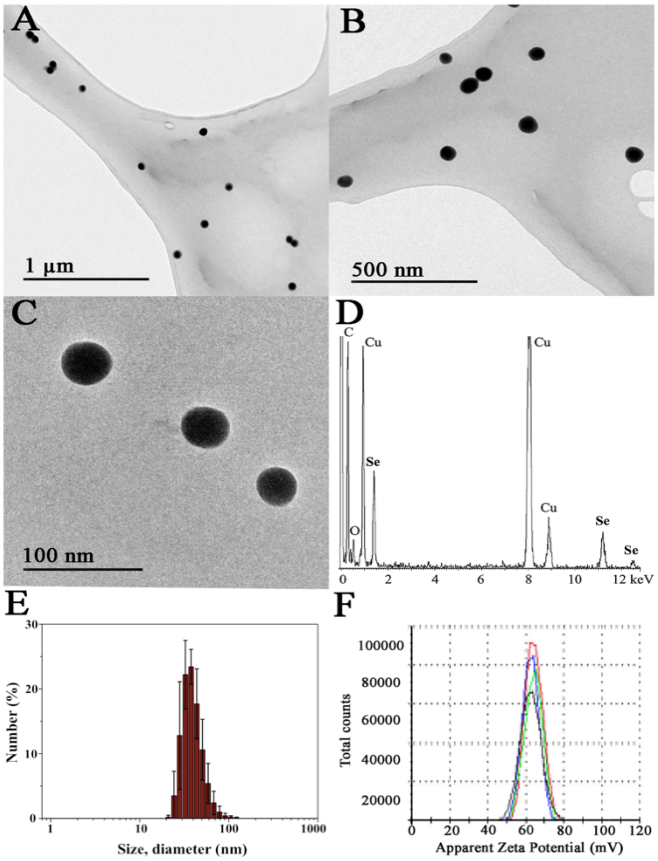

Figure 2. Characterization of the synthesized Ch-SeNPs. TEM images of a 200 mg/L suspension of Ch-SeNPs at different magnifications (A,B,C). EDS spectrum of Ch-SeNPs (D). Hydrodynamic size distribution of the Ch-SeNPs in aqueous colloidal suspension measured by dynamic light scattering (E) and ζ-potential measurements of the same sample (F).

The synthesized Ch-SeNPs were proved to be colloidally stable, with no flocculated material observed even after two months from the synthesis. No significant differences in the SeNPs size or shape were observed by TEM and the hydrodynamic size distribution does not undergo a displacement of its maximum in the DLS measurements. Moreover, the possible oxidation of Ch-SeNPs to ionic selenium was also discarded. The Ch-SeNPs suspension was centrifuged weekly using a 10 KDa MWCO filter and the liquid fraction was analyzed by ICP-MS. The amount of Se found in all cases was less than 0.1%, which also demonstrates the good stability of the synthesized Ch-SeNPs.

3.2. Cytotoxicity of Ch-SeNPs

The cytotoxicity of Ch-SeNPs was evaluated by means of the MTT assay, which correlates the reduction potential of the cells with their viability. While healthy cells are able to reduce MTT to formazan (a colored compound), non-viable cells are not able to do so. Different concentrations of Ch-SeNPs, ranging from 0.1 to 5 mg/L, were tested using an exposure time of 72 h. All measurements showed a relative standard deviation below 10% (n = 5). The exposure time (72 h) was selected as optimal based on previously published studies [11, 17]. As expected, cell viability decreased with increasing concentrations of Ch-SeNPs (**Figure 3**). The cell viability of HepG2 was significantly compromised after

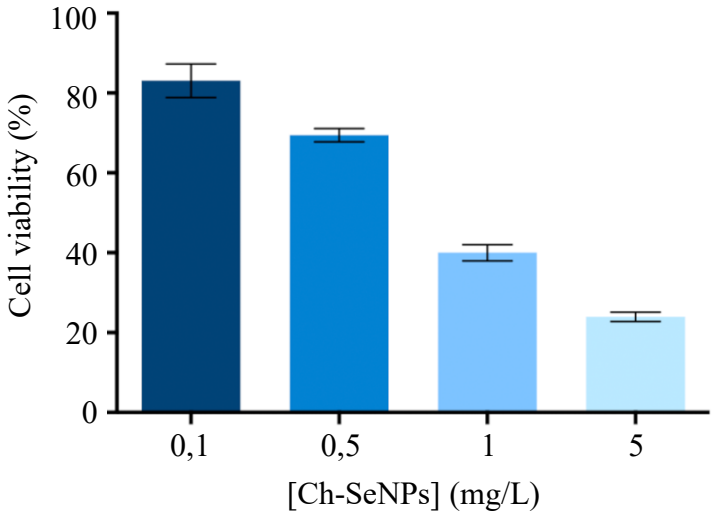

Figure 3. Viability of HepG2 cells exposed to Ch-SeNPs (n = 5).

exposure to Ch-SeNPs above 1.0 mg/L, falling below 30% at the higher concentration tested (5 mg/L). In order to investigate the molecular mechanisms involved in the potential antitumoral effect exerted by Ch-SeNPs but without drastically compromising the cell viability, 1 mg/L was selected for further experiments.

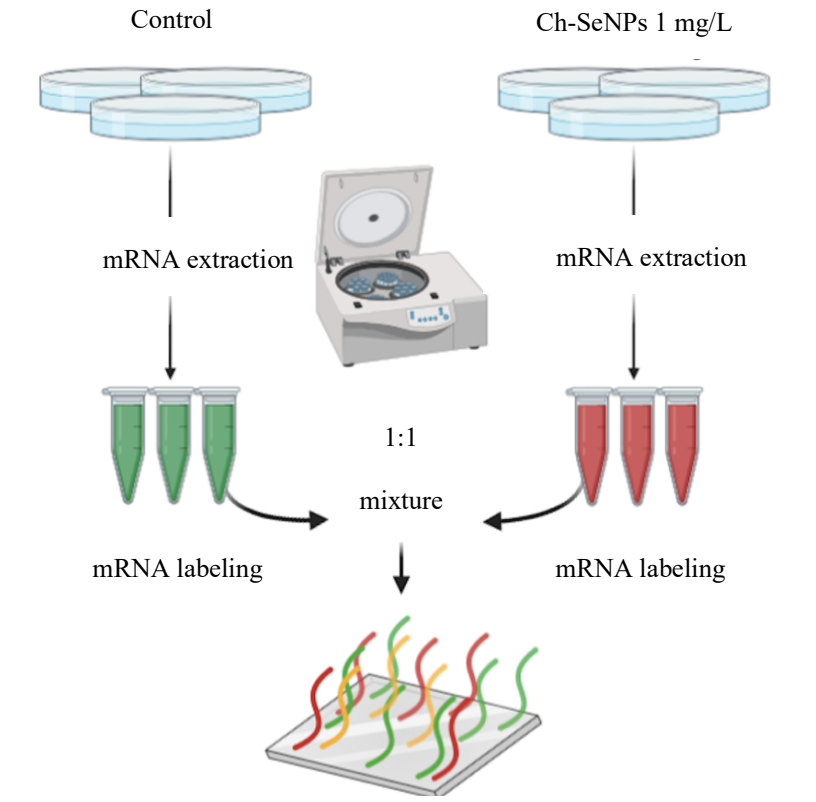

Figure 4. General scheme of the transcriptome analysis.

3.3. Revealing the mechanisms associated with the antitumoral effect of Ch-SeNPs by transcriptomic analysis

In a previous study, we confirmed the ability of Ch-SeNPs to inhibit proliferation and migration of HepG2 cells and demonstrated that Ch-SeNPs do not induce apoptosis but cell cycle arrest by partially inhibiting the expression of CDK1, which regulates the promotion of the cell cycle from S/G2 phase to mitosis [11]. This effect was unique for Ch-SeNPs as compared to other selenospecies including Se (IV), Se (VI), SeCys2, SeMet and Se-MeSeCys [11]. Furthermore, we demonstrated that the observed effect was due exclusively

to SeNPs, as cells treated with chitosan (Ch) alone did not experience any effect compared to control cells [17]. Since partial inhibition of CDK1 represent a way for precluding tumor cells progression, we carried out a pairwise differential gene expression analysis to compare control cells versus cells exposed to Ch-SeNPs (**Figure 4**), to get a deeper insight into the molecular mechanisms underlying the potential antitumoral effect of Ch-SeNPs.

Among the more than 20,000 well-annotated human genes analyzed, 279 genes were found differentially expressed with a log2 fold change of 2.0 and 0.5 (with a P-value < 0.05) (Table A1). From those differentially expressed genes, 221 were found up-regulated (ratios above 2.0) while 58 were found down-regulated (ratios below 0.5).

Supporting the inhibition of CDK1 found in the previous work [11], overexpression of CDKN1A (FC = 2.67), also known as p21, was observed after Ch-SeNPs exposure. This up-regulation correlated with reduced expression levels of other cell cycle participant genes such as cyclin CDK1 (FC = 0.80) and CDC25 (FC = 0.47) and CDCA2 (FC = 0.50) [27, 28]. While CDC25 is essential for the G1-S transition associated with the activation of the cell cycle kinase cyclin E-CDK2 [27, 29], knockdown of CDCA2 significantly inhibits cellular proliferation by arresting cell-cycle progression at the G1 phase, effect that has also been observed when using a well-known antitumoral compound such as cisplatin [30, 31]. The activation of p21 upon Ch-SeNPs exposure is supported by the fact that this gene, together with p15 and p27, is directly activated by the MXD1, which was overexpressed in our experiment (FC = 2.42). Tumor suppressor MXD family encompasses a group of transcriptional repressors that antagonize the activation of genes mediated by oncogenic MYC [32]. Diminishing expression of angiopoietin-like 3 protein (ANGPTL3) has been correlated with reduced cellular growth and cell cycle arrest at the G1 phase [33]. Interestingly, ANGPTL3, a target downstream of p21, showed strong down-regulation (FC = 0.49) upon Ch-SeNPs exposure. Moreover, FAM111B, a gene silencing which induces cell cycle arrest at the G2/M phase through the p53-signaling pathway [34], was also found down-regulated (FC = 0.50) in our analysis. Taking together and as expected, alteration of genes involved in cell cycle

regulation were confirmed upon Ch-SeNPs, thus supporting our previous studies and suggesting cell cycle as an interesting target on which the Ch-SeNPs exert their anti-tumoral action (**Figure 5**).

Since senescence plays a key role in cell cycle arrest, we investigated the pattern expression of key senescence targets after exposure to Ch-SeNPs. Senescence consists on a stable cell cycle arrest in which cells become resistant to any growth stimuli, generally in response to DNA damage. This state implies several morphological and metabolic changes, chromatin reorganization, de-regulations in gene expression and even the production of an inflammatory phenotype known as the senescence-associated secretory phenotype (SASP) [35]. Expression pattern for some of those genes were indeed found inhibited in cells exposed to Ch-SeNPs, such was the case of HIST1H2BM (FC = 0.43), HIST2H3A (FC = 0.44), ADHFE1 (FC = 0.49) and SGO1 (FC = 0.42) [36-38]. In addition, previous studies have also demonstrated that inhibition of C5AR1 can attenuate the acquisition of the senescent phenotype [39]. Remarkably, C5AR1 (FC = 5.64) was found highly overexpressed in our study. This result, together with the fact that overexpression of C5AR1 has been related with the overexpression of p21 and other genes associated with the appearance of a senescent phenotype [40] such as IL-6 (FC = 2.83) and PAI-1 (FC = 7.03), also found overexpressed after Ch-SeNPs treatment, support the

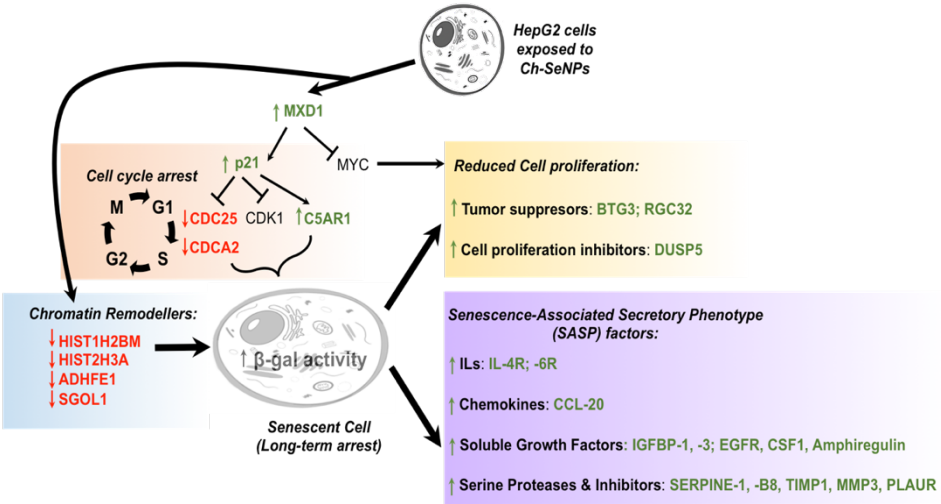

Figure 5. Proposed mechanism leading to cell cycle arrest and senescence in HepG2 cells exposed to Ch-SeNPs

potential of Ch-SeNPs to induce senescence in HepG2 cells. Particularly interesting is the overexpression of PAI-1, also known as SERPINE 1, a serine protease inhibitor that functions as the main inhibitor of the tissue plasminogen activator (tPA) (**Figure 5**).

Besides the effect of Ch-SeNPs on cell cycle arrest and their potential to induce senescence in HepG2 cells, well-known tumor suppressors were also found altered. That is the case of RASD1 (FC = 3.42), a key inhibitory player in glioma tumor progression [41]. Similarly, EGR1, which controls a network of suppressor gene products and is even considered a tumor suppressor itself [42], was also found significantly overexpressed (FC = 4.22). In addition, it has been described that EGR1 induces the expression of PAI-1 that, as stated above, was clearly found up-regulated in cells exposed to Ch-SeNPs [43]. Another tumor suppressor that was found overexpressed in the transcriptome analysis was CSTA (FC = 4.4), which is considered a potential biomarker for lung cancer and tumor differentiation. Although the role of CSTA in cancer has not yet been fully elucidated, Ma et al. [44] confirmed that CSTA exerts tumor suppressive function by inhibiting the MAPK and the AKT pathways. CSTA has been found down-regulated in several lung cancers and its restoration after chemotherapy is considered a sign a good prognosis [44]. DUSP5 (FC = 14.23), which is also considered a tumor suppressor, was highly overexpressed in cells treated with Ch-SeNPs. DUSP5 has also been related with the inhibition of the ERK2/MAPK pathways. Loss of DUSP5 expression has been detected in advanced gastric and prostate cancer; furthermore, the re-expression of DUSP5 in gastric cancer cell lines have been demonstrated to reduce both cell proliferation and colony forming ability *in vitro* [45]. Additional tumor suppressors that were found up-regulated upon Ch-SeNPs treatment were GPRC5A (FC = 5.90) and AKAP12 (FC = 8.11). Deletion of these transcripts has been demonstrated to promote tumor initiation and progression [46, 47]. In addition to these overexpressed tumor suppressors, other interesting transcripts that are currently being considered as therapeutic targets of special interest against cancer, and that were found down-regulated after exposing HepG2 cells to Ch-SeNPs were: ROR1 (FC = 0.50), PRLR (FC = 0.44), HMMR (FC = 0.40) and CENPI (FC = 0.29). While ROR1-knockdown resulted in decrease proliferation and

migration but enhanced resistance to apoptosis and anoikis [48], PRLR overexpression has been linked with increased proliferation, viability, clonogenicity, chemoresistance, and matrix metalloproteinase activity [49]. As for HMMR, its overexpression promotes germline stem cell self-renewal and intracranial tumor propagation [50], while up-regulation of CENPI has been associated to tumorigenesis and drug resistance through chromosome instability [51]. Considering other potential therapeutic targets that have been found to be altered after exposure of HepG2 cells to Ch-SeNPs, the inhibition observed in the ALDOB transcript (FC = 0.20) is noteworthy. Metabolic reprogramming has been proposed as an alternative mechanism used by metastatic cells to obtain the high levels of energy they need. In particular, it has been described that metastatic cells from the liver up-regulate the enzyme ALDOB, which provides fuel for several pathways of the central carbon metabolism, thus promoting the fructose metabolism. Based on this, targeting the expression of ALDOB could represent a powerful chemotherapeutic strategy against metastatic cells [52]. Interestingly, treatment with Ch-SeNPs was able to drastically inhibit the expression of ALDOB in HepG2 cells.

Oxidative stress is defined by the difference between the production of reactive oxygen species (ROS) and their elimination through metabolism. Hypoxia and oxidative stress are involved in cell cycle progression and proliferation, cell survival and apoptosis, energy metabolism, cell morphology, cell-cell adhesion, cell motility, angiogenesis, and thereby can promote tumorigenesis [53, 54]. Many chemotherapeutic strategies focused on the use of antioxidants to deplete tumor cells from ROS-induced survival signaling pathways. Such treatment may also have preventive functions. Since selenium has been considered as an antioxidant element, we sought to investigate the potential role of Ch-SeNPs as promising candidate to be used in this type of chemotherapeutic strategy; thus, expression of transcripts potentially involved in these mechanisms were also investigated. Our analysis showed down-regulation of ANGPTL8 (FC = 0.30) and CD24 (FC = 0.48) in cells exposed to Ch-SeNPs. While ANGPTL8 is considered as an inflammatory marker [55], CD24 is also a much-highlighted marker for some types of cancers (eg. breast cancer).

Interestingly, it has been demonstrated that their suppression correlates with lower cell proliferation rates and reduced ROS production [56]. In addition, the several transcripts from the p450 cytochrome (CYPs) family, one of the main enzymatic sources of ROS production [57, 58] were found down-regulated in our assay at different levels: CYP7A1 (FC = 0.5), CYP4F2 (FC = 0.5), CYP3A7 (FC = 0.46), CYP3A5 (FC = 0.44) and CYPA43 (FC = 0.41). Furthermore, ADHFE1 (FC = 0.49) was also found inhibited. ADHFE1 is considered an oncoprotein associated with disease survival and known for promoting a reduction of the glutamine metabolism while increasing formation of D-2-hydroxyglutarate and mitochondrial reactive oxygen species (ROS) [59]. The fact that Ch-SeNPs exposure inhibited the expression of ADHFE1 also supports the antioxidant role of Ch-SeNPs. Similarly, the transcription factor SOX6 (FC = 0.48), which also promotes elevated levels of oxidative stress and it is normally overexpressed in tumors such as the Ewing sarcoma, was found inhibited in HepG2 cells treated with Ch-SeNPs [60].

3.4. Ch-SeNPs induce senescence in a preclinical human cell model

One of the aspects considered most relevant after studying the results of the transcriptomic analysis was the ability of Ch-SeNPs to induce senescence. In order to validate such interesting results, we performed an experiment to measure the activity of β-galactosidase, a well-known marker of senescence, in HepG2 cells after exposure to Ch-SeNPs (**Figure 6**). The results demonstrated that HepG2 mock cells showed background levels of senescence (**Figure 6A**), whilst the Ch-SeNPs-exposed cells did show a significant expression of β-galactosidase staining (**Figure 6B**). These levels were similar to those observed in cells treated with 10 μM etoposide (**Figure 6C**), a bona fide inducer of senescence in HepG2 cells. On the contrary, cells treated with 50 μM etoposide (**Figure 6D**), which is a positive control for apoptosis, showed an stronger staining compared to cells treated with Ch-SeNPs, thus suggesting that Ch-SeNPs induce senescence in human hepatocarcinoma cells rather than apoptosis.

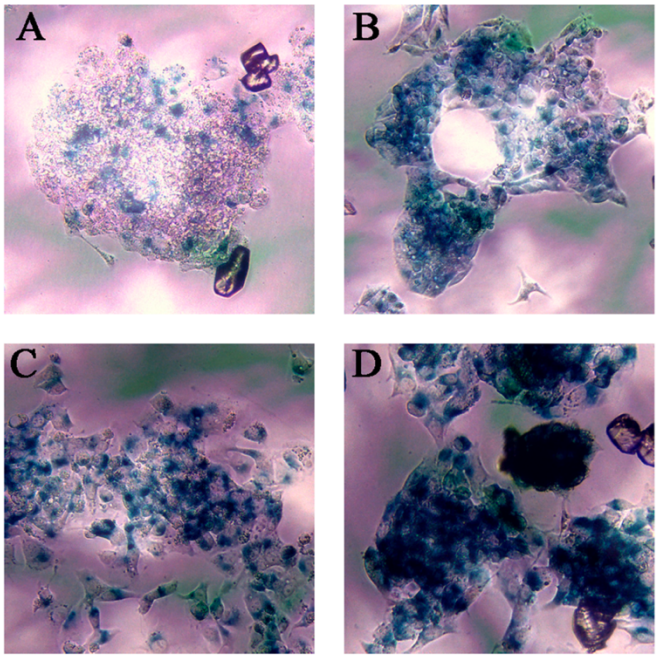

Figure 6. Senescence assay. Blue staining shows ß-galactosidase activity. Control cells (A), cells exposed to 1 mg/L of Ch-SeNPs (B), cells exposed to 10 µM of etoposide – senescence positive control (C), and cells exposed to 50 µM of etoposide – apoptosis positive control (D)

4. Conclusions

This study has been carried out with the aim of identifying new mechanisms associated with the anti-tumor potential associated with the use of Ch-SeNPs. For this purpose, a model of human hepatocellular carcinoma cells (HepG2 cells) has been selected and a whole transcriptome analysis has been carried out. This analysis has shown the alteration of different groups of transcripts involved in the arrest of the cell cycle and in the induction of senescence. Likewise, it has been proven that exposure to Ch-SeNPs induces the alteration of tumor suppressors, which supports the capacity of Ch-SeNPs to inhibit tumor proliferation. In addition, several transcripts related to ROS generation and the induction of oxidative stress has also been found altered, demonstrating the antioxidant capacity of Ch-SeNPs. Overall, the set of altered transcripts has allowed confirmation of the anti-tumor potential of Ch-SeNPs through their effect on several key mechanisms related to cancer progression. Especially relevant has been the discovery of the capacity of Ch-

SeNPs to induce senescence, which has been confirmed by measuring of β-galactosidase activity. Based on the promising results obtained and the proven capability of Ch-SeNPs as potential anti-tumor agents, the focus of future work will be on the evaluation of the effect of Ch-SeNPs in other cell lines and in pre-clinical animal models. Additionally, efforts will be made for designing novel hybrid nanosystems for cancer cell targeting and selective delivery of SeNPs.

Author contributions: J.L.L.G and J.R.T contributed to the conception and the design of the study. H.E., B.G. and M.V.R. were involved in the synthesis and characterization of the nanoparticles H.E. carried out all the experiments and was involved in the acquisition of data. H.E., E.G.C., and J.L.L.G. contributed to the analysis and interpretation of data. All authors were involved in drafting the manuscript and gave final approval for the submission of the manuscript. All authors have read and agreed to the published version of the manuscript.

Funding: This work was supported by Ministerio de Ciencia e Innovación grants: CTQ2017-85673-R and the European Research Council ERC-2015-AdG (VERDI) Proposal No. 694160. CIBER is a public research consortium created by ISCIII whose actions are co-funded by the European Regional Development Fund.

Conflicts of Interest: Authors declare there is no conflict of interest.

Acknowledgements: H.E. thanks the Ministerio de Ciencia e Innovación for a pre-doctoral fellowship (PRE2018-084196). We would also like to thank Arancha Rivera Pedrosa for editing Figure 4.

References

[1] Sreevalsan, S.; Safe, S. Reactive oxygen species and colorectal cancer. Curr. Colorectal Cancer Rep. 2013, 9(4), 350–357.

[2] Marinescu, S.; Anghel, R.; Gruia, M. I.; Beuran, M. Involvement of reactive oxygen species in the mechanisms associated with cervical cancer specific treatment. Chirurgia 2014, 109(6), 806–811.

[3] Thyagarajan, A.; Sahu, R. P. Potential contributions of antioxidants to cancer therapy: Immunomodulation and radiosensitization. Integr. Cancer Ther. 2018, 17(2), 210–216.

[4] Nunes, R.; Neves, J. D.; Sarmento, B. Nanoparticles for the regulation of intestinal inflammation: opportunities and challenges. Nanomedicine 2019, 14, 2631-2644.

[5] Tapeinos, C.; Battaglini, M.; Ciofani, G. Advances in the design of solid lipid nanoparticles and nanostructured lipid carriers for targeting brain diseases. J. Control Release. 2017, 264, 306-332.

[6] Machuca, A.; Garcia-Calvo, E.; Anunciacao, D. S.; Luque-Garcia, J. L. Rhodium nanoparticles as a novel photosensitizing agent in photodynamic therapy against cancer. Chem. Eur. J. 2020, 26, 7685-7691.

[7] Montalvo-Quirós, S.; Aragoneses-Cazorla, G.; Garcia-Alcalde, L.; Vallet-Regí, M.; Gonzalez, B.; Luque-Garcia, J. L. Cancer cell targeting and therapeutic delivery of silver nanoparticles by mesoporous silica nanocarriers: insights into the action mechanisms using quantitative proteomics. Nanoscale 2019, 11, 4531-4545.

[8] Oueslati, H. M.; Tahar, B. L.; Harrath, H. A. Catalytic, antioxidant and anticancer activities of gold nanoparticles synthesized by kaempferol glucoside from Lotus leguminosae. Arab. J. Chem. 2020, 13, 3112-3122.

[9] Vinceti, M.; Filippini, T.; Del Giovane, C.; Dennert, G.; Zwahlen, M.; Brinkman, M.; Zeegers, M.P.; Horneber, M.; D'Amico, R.; Crespi, C.M. Selenium for preventing cancer. Cochrane Database System. Rev. 2011, 11, CD005195.

[10] Aboul-Fadl, T. Selenium derivatives as cancer preventing agents. Curr. Med. Chem. Anticancer Agents. 2005, 5, 637-652.

[11] Geoffrion, L. D., Hesabizadeh, T., Medina-Cruz, D., Kusper, M., Taylor, P., Vernet-Crua, A., Chen, J., Ajo, A., Webster, T. J., & Guisbiers, G. (2020). Naked Selenium Nanoparticles for Antibacterial and Anticancer Treatments. ACS omega, 5(6), 2660–2669.

[12] Estevez, H.; Garcia-Lidon, J. C.; Luque-Garcia, J. L.; Camara, C. Effects of chitosan-stabilized selenium nanoparticles on cell proliferation, apoptosis and cell cycle pattern in HepG2 cells: comparison with other selenospecies. Colloid. Surface. B. 2014, 122, 184-193.

[13] Malekifard, F.; Tavassoli, M.; Vaziri, K. In vitro assessment antiparasitic effect of selenium and copper nanoparticles on Giardia deodenalis Cyst. Iran J. Parasitol. 2020, 15, 411-417.

[14] Wang, H.; He, Y.; Liu, L.; Tao, W.; Wang, G.; Sun, W.; Pei, X.; Xiao, Z.; Jin, Y.; Wang, M. Prooxidation and cytotoxicity of selenium nanoparticles at nonlethal level in Sprague-dawley rats and buffalo rat liver cells. Oxid. Med. Cell Longev. 2020, 7680276.

[15] Toubhans, B.; Gazze, S.A.; Bissardon, C.; Bohic, S.; Gourlan, A.T.; Gonzalez, D.; Charlet, L.; Conlan, R.S.; Francis, L.W. Selenium nanoparticles trigger alterations in ovarian cancer cell biomechanics. Nanomedicine 2020, 29, 102258.

[16] Zhao, G.; Dong, R.; Teng, J.; Yang, L.; Liu, T.; Wu, X.; He, Y.; Wang, Z.; Pu, H.; Wang, Y. N-acetyl-l-cysteine enhances the effect of selenium nanoparticles on cancer cytotoxicity by increasing the production of selenium-induced reactive oxygen species. ACS Omega, 2020, 5, 11710-11720.

[17] Hussein, H.A.; Darwesh, O.M.; Mekki, B.B.; El-Hallouty, S.M. Evaluation of cytotoxicity, biochemical profile and yield components of gloundnut plants treated with nano-selenium. Biotechnol. Rep. 2019, 24, e00377.

[18] Lopez-Heras, I.; Sanchez-Diaz, R.; Anunciacao, D.S.; Madrid, Y.; Luque-Garcia, J. L.; Camara, C. Effect of chitosan-stabilized selenium nanoparticles on cell cycle arrest and invasiveness in hepatocarcinoma cells revealed by quantitative proteomics. J. Nanomed. Nanotechnol. 2014, 5, 1000226.

[19] Neagu, M.; Boda, D. Transcriptomics in Cancer - Stages Toward Patents in Biomarkers. Recent Pat. Biomark. 2012, 2, 75 82.

[20] Alkhateeb, A.; Rezaeian, I.; Singireddy, S.; Cavallo-Medved, D.; Porter, L. A.; Rueda, L. Transcriptomics signature from next-generation sequencing data reveals new transcriptomic biomarkers related to prostate cancer. Cancer Inform. 2019, 18, 1176935119835522.

[21] Bai, Y.; Wang, Y.; Zhou, Y.; Li, W.; Zheng, W. Modification and modulation of sacharides on elemental selenium nanoparticles in liquid phase. Mater. Lett. 2008, 62, 2311-2314.

[22] Mees, D.R.; Pysto, W.; Tarcha, P.J. Formation of selenium colloids using sodium ascorbate as the reducing agent. J. Colloid Interface Sci. 1995, 170, 254-260.

[23] Zhang, Y.; Wang, J.; Zhang, L. Creation of highly stable selenium nanoparticles capped with hyperbranched polysaccharide in water. Langmuir 2010, 26, 17617-17623.

[24] Zhang, S.; Luo, Y.; Zeng, H.; Wang, Q.; Tian, F.; Song, J.; Cheng, W. H. Encapsulation of selenium in chitosan nanoparticles improves selenium availability and protects cells from selenium-induced DNA damage response. J. Nutr. Biochem. 2011, 22(12), 1137–1142.

[25] Zhai, X.; Zhang, C.; Zhao, G.; Stoll, S.; Ren, F.; Leng, X. Antioxidant capacities of the selenium nanoparticles stabilized by chitosan. J. Nanobiotechnology. 2017, 15(1), 4.

[26] Estevez, H.; Palacios, A.; Gil, D.; Anguita, J.; Vallet-Regí, M.; Gonzalez, B.; Prados-Rosales, R.; Luque-Garcia, J. L. Antimycobacterial effect of selenium nanoparticles on mycobacterium tuberculosis. Frontiers Microbiol. 2020, 11, 800.

[27] Charrier-Savournin, F. B.; Château, M. T.; Gire, V.; Sedivy, J.; Piette, J.; Dulic, V. p21-Mediated nuclear retention of cyclin B1-Cdk1 in response to genotoxic stress. Mol. Biol. Cell. 2004, 15(9), 3965–3976.

[28] Abbas, T.; Dutta, A. p21 in cancer: intricate networks and multiple activities. Nat. Rev. Cancer 2009, 9(6), 400–414.

[29] Saha, P.; Eichbaum, Q.; Silberman, E. D.; Mayer, B. J.; Dutta, A. p21CIP1 and Cdc25A: competition between an

inhibitor and an activator of cyclin-dependent kinases. Mol. Cell. Biol. 1997, 17(8), 4338–4345.

[30] Feng, Y.; Qian, W.; Zhang, Y.; Peng, W.; Li, J.; Gu, Q.; Ji, D.; Zhang, Z.; Wang, Q.; Zhang, D.; Sun, Y. CDCA2 promotes the proliferation of colorectal cancer cells by activating the AKT/CCND1 pathway in vitro and in vivo. BMC cancer 2019, 19(1), 576.

[31] Uchida, F.; Uzawa, K.; Kasamatsu, A.; Takatori, H.; Sakamoto, Y.; Ogawara, K.; Shiiba, M.; Bukawa, H.; Tanzawa, H. Overexpression of CDCA2 in human squamous cell carcinoma: correlation with prevention of G1 phase arrest and apoptosis. PloS one 2013, 8(2), e56381.

[32] Wiese, K. E.; Walz, S.; von Eyss, B.; Wolf, E.; Athineos, D.; Sansom, O.; Eilers, M. The role of MIZ-1 in MYC-dependent tumorigenesis. CSH. Perspect. Med. 2013, 3(12), a014290.

[33] Koyama, T.; Ogawara, K.; Kasamatsu, A.; Okamoto, A.; Kasama, H.; Minakawa, Y.; Shimada, K.; Yokoe, H.; Shiiba, M.; Tanzawa, H.; Uzawa, K. ANGPTL3 is a novel biomarker as it activates ERK/MAPK pathway in oral cancer. Cancer Med. 2015, 4(5), 759–769.

[34] H. Sun.; K. Liu.; J. Huang.; Q. Sun.; C. Shao.; J. Luo.; L. Xu.; Y. Shen.; B. Ren. FAM111B, a direct target of p53, promotes the malignant process of lung adenocarcinoma. Onco. Targets. Ther. 2019, 12, 2829–2842.

[35] Regulski M. J. Cellular Senescence: What, Why, and How. Wounds 2017, 29(6), 168–174.

[36] Cruickshanks, H. A.; McBryan, T.; Nelson, D. M.; Vanderkraats, N. D.; Shah, P. P.; van Tuyn, J.; Singh Rai, T.; Brock, C.; Donahue, G.; Dunican, D. S.; Drotar, M. E.; Meehan, R. R.; Edwards, J. R.; Berger, S. L.; Adams, P. D. Senescent cells harbor features of the cancer epigenome. Nat. Cell. Mol. 2013, 15(12), 1495–1506.

[37] Moon, J. W.; Lee, S. K; Lee, Y. W.; Lee, J. O.; Kim, N.; Lee, H. J.; Seo, J. S.; Kim, J.; Kim, H. S.; Park, S. H. Alcohol induces cell proliferation via hypermethylation of ADHFE1 in colorectal cancer cells. BMC cancer 2014, 14, 377.

[38] Murakami-Tonami, Y.; Ikeda, H.; Yamagishi, R.; Inayoshi, M.; Inagaki, S.; Kishida, S.; Komata, Y.; Koster, J.;

Takeuchi, I.; Kondo, Y.; Maeda, T.; Sekido, Y.; Murakami, H.; Kadomatsu, K. SGO1 is involved in the DNA damage response in MYCN-amplified neuroblastoma cells. Sci. Rep. 2016, 6, 31615.

[39] Hernandez, M. X.; Jiang, S.; Cole, T. A.; Chu, S. H.; Fonseca, M. I.; Fang, M. J.; Hohsfield, L. A.; Torres, M. D.; Green, K. N.; Wetsel, R. A.; Mortazavi, A.; Tenner, A. J. Prevention of C5aR1 signaling delays microglial inflammatory polarization, favors clearance pathways and suppresses cognitive loss. Mol. Neurodegener. 2017, 12, 1-19.

[40] Castellano, G.; Franzin, R.; Sallustio, F.; Stasi, A.; Banelli, B.; Romani, M.; De Palma, G.; Lucarelli, G.; Divella, C.; Battaglia, M.; Crovace, A.; Staffieri, F.; Grandaliano, G.; Stallone, G.; Ditonno, P.; Cravedi, P.; Cantaluppi, V.; Gesualdo, L. Complement component C5a induces aberrant epigenetic modifications in renal tubular epithelial cells accelerating senescence by Wnt4/βcatenin signaling after ischemia/reperfusion injury. Aging 2019, 11(13), 4382-4406.

[41] Gao, S.; Jin, L.; Liu, G.; Wang, P.; Sun, Z.; Cao, Y.; Shi, H.; Liu, X.; Shi, Q.; Zhou, X.; Yu, R. Overexpression of RASD1 inhibits glioma cell migration/invasion and inactivates the AKT/mTOR signaling pathway. Sci. Rep. 2017, 7(1), 3202.

[42] Krones-Herzig, A.; Mittal, S.; Yule, K.; Liang, H.; English, C.; Urcis, R.; Soni, T.; Adamson, E. D.; Mercola, D. Early growth response 1 acts as a tumor suppressor in vivo and in vitro via regulation of p53. Cancer Res. 2005, 65(12), 5133–5143.

[43] Ruoslahti, E. Fibronectin and its integrin receptors in cancer. Adv. Cancer Res. 1999, 76, 1–20.

[44] Ma, Y.; Chen, Y.; Li, Y.; Grün, K.; Berndt, A.; Zhou, Z.; Petersen, I. Cystatin A suppresses tumor cell growth through inhibiting epithelial to mesenchymal transition in human lung cancer. Oncotarget 2017, 9(18), 14084–14098.

[45] Kidger, A.M.; Keyse, S.M. The regulation of oncogenic Ras/ERK signalling by dual-specificity mitogen activated protein kinase phosphatases (MKPs). Semin. Cell Dev. Biol. 2016, 50, 125–132.

[46] Goeppert, B.; Schmezer, P.; Dutruel, C.; Oakes, C.; Renner, M.;

Breinig, M.; Warth, A.; Vogel, M. N.; Mittelbronn, M.; Mehrabi, A.; Gdynia, G.; Penzel, R.; Longerich, T.; Breuhahn, K.; Popanda, O.; Plass, C.; Schirmacher, P.; Kern, M. A. Down-regulation of tumor suppressor A kinase anchor protein 12 in human hepatocarcinogenesis by epigenetic mechanisms. Hepatology 2010, 52(6), 2023–2033.

[47] Jiang, X.; Xu, X.; Wu, M.; Guan, Z.; Su, X.; Chen, S.; Wang, H.; Teng, L. GPRC5A: An Emerging Biomarker in Human Cancer. BioMed Res. Int. 2018, 2018, 1823726.

[48] Cetin, M.; Odabas, G.; Douglas, L.; Duriez, P.; Balcik-Ercin, P.; Yalim-Camci, I.; Sayan, A.; Yagci, T. ROR1 Expression and Its Functional Significance in Hepatocellular Carcinoma Cells. Cells 2019, 8, 1-18.

[49] Asad, A. S.; Nicola Candia, A. J.; Gonzalez, N.; Zuccato, C. F.; Abt, A.; Orrillo, S. J.; Lastra, Y.; De Simone, E.; Boutillon, F.; Goffin, V.; Seilicovich, A.; Pisera, D. A.; Ferraris, M. J.; Candolfi, M. Prolactin and its receptor as therapeutic targets in glioblastoma multiforme. Sci. Rep. 2019, 9(1), 19578.

[50] Tilghman, J.; Wu, H.; Sang, Y.; Shi, X.; Guerrero-Cazares, H.; Quinones-Hinojosa, A.; Eberhart, C.G.; Laterra, J.; Ying, M. HMMR Maintains the Stemness and Tumorigenicity of Glioblastoma. Cancer Res. 2014, 74, 3168–3179.

[51] Thangavelu, P.U.; Lin, C.Y.; Vaidyanathan, S.; Nguyen, T.H.M.; Dray, E.; Duijf, P.H.G. Overexpression of the E2F target gene CENPI promotes chromosome instability and predicts poor prognosis in estrogen receptor-positive breast cancer. Oncotarget 2017, 8, 62167–62182.

[52] Bu, P.; Chen, K. Y.; Xiang, K.; Johnson, C.; Crown, S. B.; Rakhilin, N.; Ai, Y.; Wang, L.; Xi, R.; Astapova, I.; Han, Y.; Li, J.; Barth, B. B.; Lu, M.; Gao, Z.; Mines, R.; Zhang, L.; Herman, M.; Hsu, D.; Zhang, G. F.; Shen, X. Aldolase B-Mediated Fructose Metabolism Drives Metabolic Reprogramming of Colon Cancer Liver Metastasis. Cell Metab. 2018, 27(6), 1249–1262.

[53] Liou, G.Y.; Storz, P. Reactive oxygen species in cancer. Free Radic. Res. 2010, 5, 479-496.

[54] Paardekooper, L.M.; Vos, W.; Van Den Bogaart, G. Oxygen in the tumor

microenvironment: effects on dendritic cell function. Oncotarget 2019, 10, 883–896.

[55] Holmannova, D.; Borska, L.; Andrys, C.; Borsky, P.; Kremlacek, J.; Hamakova, K.; Rehacek, V.; Malkova, A.; Svadlakova, T.; Palicka, V.; Krejsek, J.; Fiala, Z. The Impact of Psoriasis and Metabolic Syndrome on the Systemic Inflammation and Oxidative Damage to Nucleic Acids. J. Imunnol. Res. 2020, 2020, 7352637.

[56] Bensimon, J.; Biard, D.; Paget, V.; Goislard, M.; Morel-Altmeyer, S.; Konge, J.; Chevillard, S.; Lebeau, J. Forced extinction of CD24 stem-like breast cancer marker alone promotes radiation resistance through the control of oxidative stress. Molecular carcinogenesis 2016, 55(3), 245–254.

[57] Hrycay, E. G.; Bandiera, S. M. Involvement of Cytochrome P450 in Reactive Oxygen Species Formation and Cancer. Advances in pharmacology (San Diego, Calif.). 2015, 74, 35–84.

[58] Veith, A.; Moorthy, B. Role of cytochrome p450 in the generation and metabolism of reactive oxygen species. Curr. Opin. Toxicol. 2018, 7, 44–51.

[59] Mishra, P.; Tang, W.; Ambs, S. ADHFE1 is a MYC-linked oncogene that induces metabolic reprogramming and cellular de-differentiation in breast cancer. Mol. Cell. Oncol. 2018, 5, 1–3.

[60] Marchetto, A.; Ohmura, S.; Orth, M. F.; Knott, M.; Colombo, M. V.; Arrigoni, C.; Bardinet, V.; Saucier, D.; Wehweck, F. S.; Li, J.; Stein, S.; Gerke, J. S.; Baldauf, M. C.; Musa, J.; Dallmayer, M.; Romero-Pérez, L.; Hölting, T.; Amatruda, J. F.; Cossarizza, A.; Henssen, A. G.; Grünewald, T. Oncogenic hijacking of a developmental transcription factor evokes vulnerability toward oxidative stress in Ewing sarcoma. Nat. Comm. 2020, 11(1), 2423.

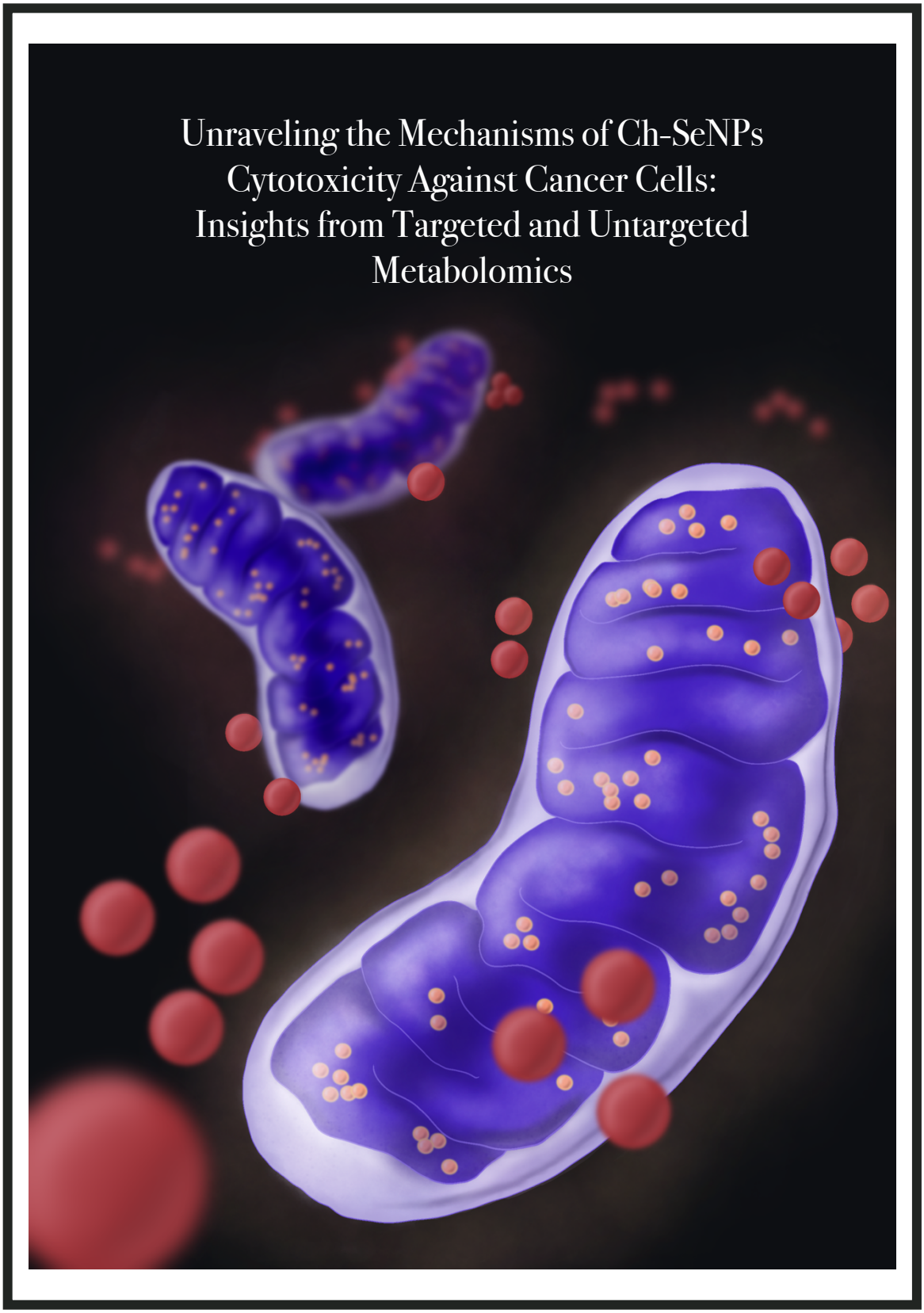
Unraveling the Mechanisms of Ch-SeNPs
Cytotoxicity Against Cancer Cells:
Insights from Targeted and Untargeted
Metabolomics

1.3. Unraveling the Mechanisms of Ch-SeNPs Cytotoxicity Against Cancer Cells: Insights from Targeted and Untargeted Metabolomics

Hector Estevez, Estefania Garcia-Calvo, Maria L. Mena,
Roberto Alvarez-Fernandez Garcia and Jose L. Luque-Garcia*

Nanomaterials 2023, 13, 2204.

Abstract

Despite chitosan-stabilized selenium nanoparticles (Ch-SeNPs) have emerged as a promising chemical form of selenium for anticancer purposes, gathering more profound knowledge related to molecular dysfunctions contributes significantly to promote their evolution as a chemotherapeutic drug. In this sense, metabolites are the end products in the flow of gene expression and, thus, the most sensitive to changes in the physiological state of a biological system. Therefore, metabolomics provides a functional readout of the biochemical activity and cell state. In the present study, we have evaluated alterations in the metabolome of HepG2 cells after the exposure to Ch-SeNPs, to elucidate the biomolecular mechanisms involved in their therapeutic effect. A targeted metabolomics approach was conducted to evaluate the levels of four of the main energy-related metabolites (adenosine triphosphate, ATP; adenosine diphosphate, ADP; nicotinamide adenine dinucleotide, NAD^+ and 1,4-dihydronicotinamide adenine dinucleotide, NADH), revealing alterations as a result of exposure to Ch-SeNPs related to a shortage in the energy supply system in the cell. Besides, an untargeted metabolomics experiment was performed, which allowed the study of alterations in the global metabolic profile as a consequence of Ch-SeNPs exposure. The results indicate that the TCA cycle and glycolytic pathways were impaired, while alternative pathways such as glutaminolysis and cysteine metabolism were upregulated. Additionally, increased fructose levels suggested the induction of hypoxia-like conditions. These findings highlight the potential of Ch-SeNPs to disrupt cancer cell metabolism and provide insights into the mechanisms underlying their antitumor effects.

1. Introduction

Metabolites are not only energy bricks for the cell but also signaling molecules, immune modulators, endogenous toxins, and environmental sensors, among others. All together, these chemical entities constitute the metabolome, which has had a relatively recent entry into the "multi-omics" tools. Metabolites are entwined in the metabolism machinery by the activity of genes and proteins. Thus, metabolomics is widely accepted as one of the most sensitive approaches for the discovery of key biomarkers and mechanisms for the understanding of pathophysiological processes.

Metabolomics, through analytical chemistry, enables the high throughput characterization of metabolites from cells, organs, tissues or biofluids. As technology improves, metabolomics is gaining more interest for unraveling the role that small molecules play in a great variety of biological processes. Consequently, metabolomics has been reconsidered as not only a biomarker identification tool, but also as an instrument that allows the discovery of active biological processes operators [1].

There is a crucial awareness about the role of metabolites that has changed the perception of how these small molecules can participate in the evolution of pathologies. Metabolites, far from being just a downstream product of genes or proteins activity, actually show a wide-range of regulatory activities related to other "omics" levels. Studies investigating seminal discoveries of relationships between glucose, fatty acids, and other lipids with insulin secretion, the lac operon in bacteria, and nutrient sensing by the mammalian target of rapamycin (mTOR) kinase confirm the impact of metabolites over biological systems [2-4].

Generally, targeted metabolomics is focused on the identification and quantification of a small and defined chemically characterized group of known metabolites, providing information of a specific metabolic process. The use of internal standards allows a quantitative or semi-quantitative analysis of the selected metabolites, and the dominance of abundant molecules as well as analytical artifacts can be avoided by the isolation of the target metabolites during sample preparation [5]. Here, our focal point was energy metabolism, due to its

significance in cancer development. Therefore, we selected four key metabolites to dig into potential dysfunctions in the energy production machinery.

As a complementary approach, untargeted metabolomics is a major tool for global metabolite discovery, when there is no prior specific metabolic hypothesis, comparing groups of samples and underlining perturbations between them. Therefore, these studies generate large quantities of data, which is not only characterized by its volume but also for its complexity [6,7].

Parallel to the evolution of metabolomics, nanomaterials have gathered a great deal of attention for its novel properties in comparison to larger scale materials. Besides from a large number of applications, the integration of nanomaterials in chemotherapy is one of the most encouraging advances in nanomedicine (drug delivery, imaging, killing cancer cells, etc.) [8,9]. In previous studies in our group, selenium nanoparticles (SeNPs) have proven their chemotherapeutic abilities in comparison to other selenospecies [10]. When hepatocarcinoma cells (HepG2) are exposed to Ch-SeNPs, they experience a drastic decrease in their normal proliferation. Based on their promising therapeutic effect, there is an urgent need for a deeper understanding of the molecular mechanisms through which these nanoparticles are capable of inhibiting cancer development. Metabolic signaling has a central role in malignant transformation, cell proliferation, and cancer stemness, among others. Likewise, intercellular metabolite signaling modulates inflammatory response in the tumor microenvironment. Discerning how SeNPs are responsible for metabolic alterations outcomes is crucial for building a chemotherapeutic strategy based on this novel nanomaterial.

In the present work, in house-synthesized chitosan-estabilized selenium nanoparticles (Ch-SeNPs) were characterized and their cytotoxic effect in hepatocarcinoma cancer cells (HepG2) was investigated. Furthermore, the combination of both targeted and untargeted metabolomic experiments is proposed for an in-depth evaluation of changes in the metabolic profile of the cancer cells due to exposure to Ch-SeNPs. The complementary results obtained by both approaches were in good agreement and have been exhaustively discussed, providing a

deeper insight into the biomolecular mechanisms of action of these nanoparticles.

2. Materials and Methods

2.1. Synthesis and Characterization of Ch-SeNPs

Synthesis reagents such as chitosan, ascorbic acid, acetic acid and sodium selenite were purchased from Sigma-Aldrich (St. Louis, MI, USA). Chitosan-stabilized selenium nanoparticles (Ch-SeNPs) were synthesized following the procedure described by Bai et al. [11]. Summarily, chitosan polysaccharide solution (0.5% w/v) was prepared using 0.5 M acetic acid. 0.25 mL of sodium selenite 0.51 M were slowly added to a mixture of 10 mL of this chitosan solution, 7.5 mL of ascorbic acid (0.23 M) and 5 mL of acetic acid (2.4 M). A change in the solution from colorless to intense red was observed as a proof of the formation of the Ch-SeNPs. Then, the resulting colloidal suspension was diluted to 50 mL with deionized water (Millipore Corporation, Burlington, MA, USA), resulting in a final concentration of 200 mg/L of SeNPs and 0.1% of chitosan. 10 mL of the suspension were finally dialyzed for 2 h against 2 L of water, using a 12-kDa molecular weight cut-off (MWCO) membrane (Merck, Darmstadt, Germany).

Ch-SeNPs were analytically characterized by transmission electron microscopy (TEM) and energy dispersive X-ray spectroscopy (EDX) using a JEOL JEM 1400 PLUS operating at 120 kV and equipped with a charge-coupled device CCD camera (KeenView Camera) (JEOL Ltd., Tokyo, Japan).

2.2. Cell Culture and Exposure Conditions

For the *in vitro* study, the HepG2 cell line (ATCC HB-8065 TM, Manassas, VA, USA) was selected. The cells were grown at 37 °C and 5% CO_2 in a Dulbecco's modified Eagle´s medium (DMEM) supplemented with 10% fetal bovine serum (FBS) and antibiotics (penicillin, 50 U/mL; streptomycin 50 U/mL). Cells were exposed to different concentrations of Ch-SeNPs. The appropriate concentration of Ch-SeNPs were suspended in DMEM and added to the cell culture. Cells were then incubated for 72 h at 37 ºC and 5% CO_2.

2.3. Cell Viability

The 3-(4,5-dimethylthiazol-2-yl)-2,5-diphenyltetrazolium bromide (MTT) assay was chosen for the evaluation of

the effects on the cellular viability after Ch-SeNP exposure. The MTT assay measures the metabolic activity of viable cells, which are able to reduce the MTT to formazan (a purple-colored compound). Cells were seeded in 96-well plates at a concentration of 9 × 103 cells per well. After cell attachment, they were exposed to 0.1, 0.5, 1, and 5 mg/L of Ch-SeNPs for 72 h. Then, 20 µL of MTT solution (5 mg/mL) was added to each well and incubated for 4 h at 37 ◦C. The formed formazan crystals were dissolved in 100 µL of dimethyl sulfoxide, and the absorbance of the resulting solution was measured at 595 nm in a microplate reader (Sunrise, Tecan, Männedorf, Switzerland).

2.4. Targeted Metabolomic Analysis

2.4.1. Extraction of Energy-Related Metabolites

HepG2 cells were cultured in 100 mm Petri dishes and exposed to Ch-SeNPs at a concentration of 1 mg/L for 72 h. Following the treatment, both the exposed and control cells underwent a washing step using 0.9% (w/v) sodium chloride (Fisher Scientific, Waltham, MA, USA) and were then placed on ice. To extract metabolites, 100 µL of methanol at −20 ◦C and 400 µL of water containing 2% (v/v) formic acid (Fisher Scientific, Waltham, MA, USA) were added to the cells before harvesting. The cells were transferred to EppendorfTM tubes and vortexed for 1 min. After 3 min of incubation on ice, 45 µL of 15% ammonium bicarbonate (w/v) was added to neutralize the pH of the samples. The samples were vortexed for 1 min, incubated for 20 min on ice, and then centrifuged at 16,000× g and 4 ◦C for 10 min. The supernatant was collected and filtered through a Whatman® PTFE membrane filter (pore size: 0.22 µm; Merck, Darmstadt, Germany). The total protein concentration of each sample was determined using the Bradford assay, allowing for the normalization of the concentration of each metabolite to account for variations in the initial cell content. Ten replicates were used for each studied condition, including samples treated with Ch-SeNPs and untreated controls.

2.4.2. Mass Spectrometry (LC-QqQ-MS) Analysis

The investigation was performed using an LC-QqQ-MS instrument (LC/MS-8030 Shimadzu, Kyoto, Japan) that was equipped with an electrospray ionization source (ESI) operating in the negative-ionization mode. The quantification of four metabolites related

to energy: ATP, ADP, NADH, and NAD+, was carried out using the Multiple-Reaction- Monitoring (MRM) mode, following the method described by García-Calvo et al. [12]. The MRM chromatograms for each analyte in both the control and Ch-SeNPs-exposed samples can be observed in Figure S1.

2.4.3. Statistical Analysis

Variances in ATP, ADP, NADH, and NAD+ levels between the control group and cells exposed to Ch-SeNPs were evaluated using ANOVA statistical tests with a confidence level of 95% (p-value < 0.05). Subsequently, a Bonferroni test was conducted for further analysis.

2.5. Untargeted Metabolomics

2.5.1. Sample Preparation

HepG2 cells were cultured in 100 mm Petri dishes and exposed to Ch-SeNPs at a concentration of 1 mg/L for 72 h. Following the exposure, the cell culture medium was removed, and the cells were washed with 10 mL of 0.9% NaCl. To halt cell metabolism, a mixture of 400 µL of methanol at -20 °C and 400 µL of ice-cold water was added to the cells. The cells were then scraped and transferred into 1.5 mL tubes.

For metabolite extraction, an ultrasound-assisted method was employed. This involved adding 400 µL of chloroform at -20 °C to the tubes, followed by subjecting them to 20 sonication pulses (2 s pulse and 5 s rest) using a cell disruptor (FB50, Thermo Fischer Scientific, USA). The samples were kept on ice during the extraction process. Subsequently, the tubes were centrifuged at 13,000 rpm and 4 °C for 5 min, resulting in the separation of two distinct phases (polar and non-polar). From each phase, 300 µL was transferred to separate glass vials.

For further analysis, the protein interphase was isolated and quantified using the Bradford method. In each of the phases, 20 mg/L of 4-phenylbutyric acid (Sigma-Aldrich, St. Louis, MI, USA) was added as an internal standard. The extracts were then evaporated under a nitrogen stream at 4 °C. To prepare the samples for gas chromatography-mass spectrometry (GC-MS) analysis, metabolites were chemically derivatized. The samples were reconstituted in 30 µL of 40 mg/L methoxyamine hydrochloride in pyridine (Sigma Aldrich, St. Louis, MI, USA) and mixed

at 500 rpm for 90 min at 37 °C. Afterward, 60 µL of N,O-Bis(trimethylsilyl) trifluoroacetamide (BSTFA) (Sigma Aldrich, St. Louis, MI, USA) containing 1% trimethylsilyl chloride (TMCS) (Sigma Aldrich, St. Louis, MI, USA) were added and incubated at 60 °C with mixing at 500 rpm for 1 h [13].

To ensure the reliability and stability of the metabolomics approach, quality control (QC) samples were prepared. The residual supernatants from all samples were pooled and divided into 200 µL aliquots. These QC samples underwent the same treatment as the analytical samples during vacuum drying, resuspension, instrumental analysis, and data processing. For every 5 analytical samples, one QC sample was inserted and analyzed.

2.5.2. High Resolution Mass spectrometry (GC-TOF-MS) Analysis

Ten replicates of each experimental condition, including samples exposed to Ch-SeNPs and untreated controls, were subjected to analysis using a gas chromatograph (7890A Agilent, Santa Clara, CA, USA) coupled to a high-resolution time-of-flight mass spectrometer (GCT Premier Micromass Waters, Waters Corporation, Milford, MA, USA).

During the analysis, a 2 µL volume of the samples was injected in split mode at a 1:3 ratio. Metabolite separation was achieved using a ZB-5MS plus column (30 m, 0.25 mm × 0.25 µm, Phenomenex, Alcobendas, Spain) at a flow rate of 1 mL/min, with He serving as the carrier gas. The column temperature was initially set at 60 °C for 3 min, and then it was gradually increased at a rate of 6 °C/min until reaching 325 °C, where it was held for 3 min. The inlet temperature was maintained at 270 ºC, and a solvent delay of 2.5 min was employed.

The mass spectrometer was equipped with an electron ionization (EI) ion source, and it recorded spectra within a mass range of 50 to 800 m/z. To monitor the performance of the analysis, a GC column test standard (Phenomenex, Alcobendas, Spain) was included and analyzed every 5 samples as a quality control measure.

2.5.3. Data Treatment and Statistical Analysis

The chromatographic data obtained from the analysis were processed using Mass Lynx software.

For each metabolite, the peak area was determined and then normalized based on the internal standard. Metabolites were identified by analyzing their mass spectra and accurate masses using the NIST MS search 2.0 library.

For multivariate statistical analysis, the data was auto-scaled using the mean and standard deviation of the entire dataset [14]. Pearson's correlation analysis was performed using Microsoft Excel software. Additionally, Principal Component Analysis (PCA) was conducted using Unscrambler software (version 9.7) as an unsupervised technique to reduce the dataset's dimensionality and identify patterns. The data matrix was established with metabolites as columns and HepG2 cells exposed to Ch-SeNPs and control cells as rows. To compare the normalized peak areas of metabolites between the two experimental conditions, a two-tailed Student's t-test was employed at a 95% confidence level (p-value < 0.05 considered statistically significant). Metabolites that showed statistically significant differences in levels after Ch-SeNPs exposure (p-values < 0.05) were used to construct a network using STITCH software (version 4.0). The network was created with a medium stringency of 0.40 and allowed the inclusion of some proteins as predicted functional partners with a score of up to 0.99. Finally, the network was visualized using Cytoscape software (version 3.7.0) to gain insights into the interactions and

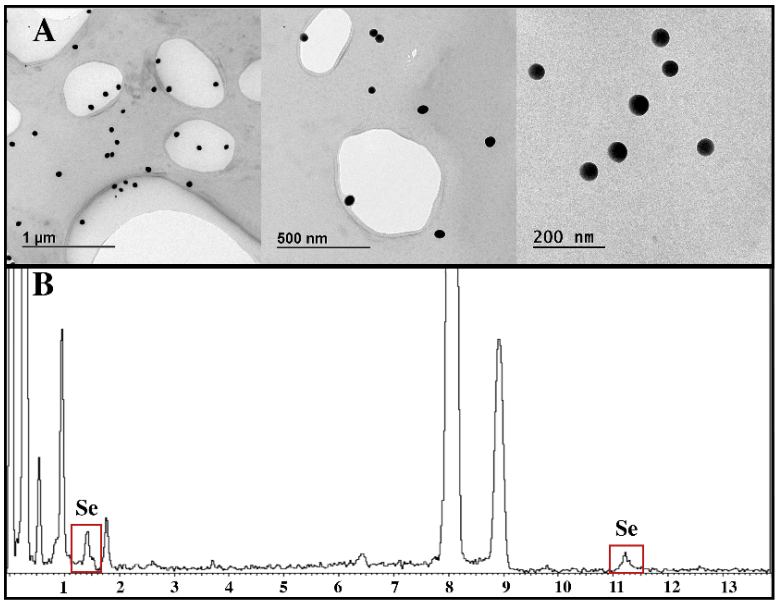

Figure 1. (A) TEM micrographs of well dispersed Ch-SeNPs with ranging sizes from 40 to 50 nm; (B) EDS analysis.

relationships among the identified metabolites and proteins, shedding light on the effects of Ch-SeNPs exposure on the cellular metabolic pathways.

Before carrying out the metabolomic approach and in order to confirm previous results, the viability of HepG2 was evaluated after exposure to Ch-SeNPs for 72 h. As expected, cell viability decreased in a concentration-dependent manner (**Figure 2**). A decrease in cell viability close to 70 % was obtained for the highest concentration of particles assayed (5 mg/L). However, for targeted and untargeted metabolomic experiments, a concentration of 1 mg/L was chosen in order to further investigate the antitumor effect of the particles without drastically compromising cell viability.

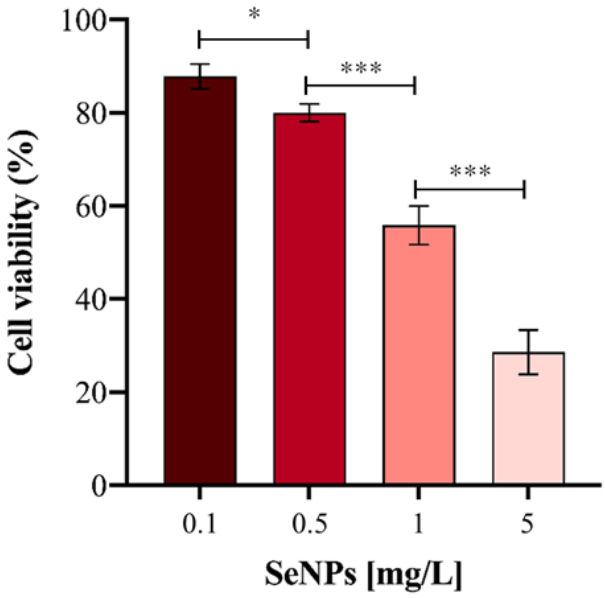

Figure 2. Cell viability (%) of HepG2 cells exposed to different concentrations of Ch-SeNPs. Results are plotted as the mean ± relative standard deviation (n = 5, statistical significance: *p < 0.05, ***p < 0.001).

3. Results

3.1. Characterization of Ch-SeNPs

As shown in **Figure 1A**, the followed Ch-SeNPs synthesis strategy provided spherical and well dispersed nanoparticles, with sizes ranging between 40 and 50 nm. These features makes them ideal for their internalization by HepG2 cells in culture. EDS analysis (**Figure 1B**) assured the presence of selenium in the samples.

3.2. Citotoxicity of Ch-SeNPs

3.3. Evaluation of the levels of enery-related metabolites

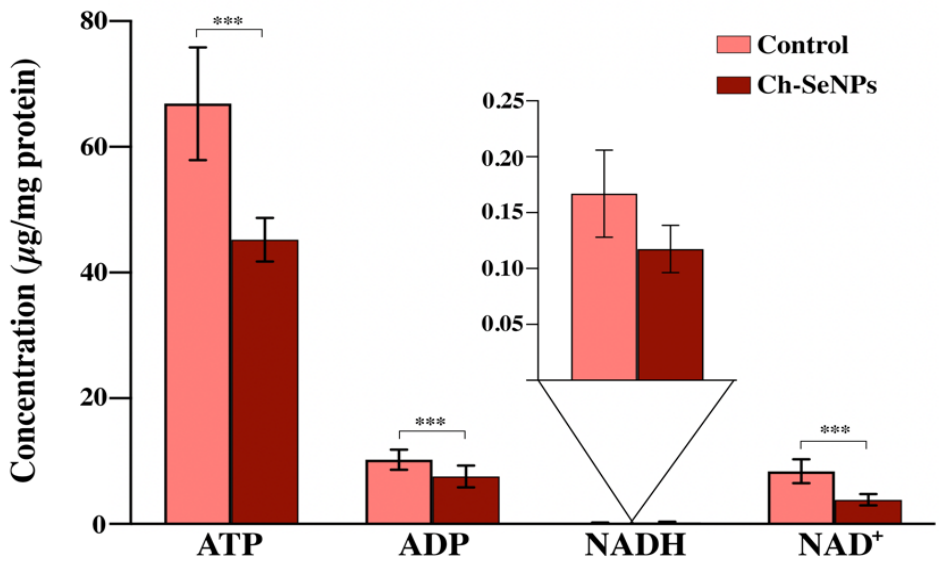

Figure 3. Concentration levels for ATP, ADP, NADH, and NAD^+ in HepG2 cells exposed to Ch-SeNPs Figure 3. Concentration levels for ATP, ADP, NADH, and NAD^+ in HepG2 cells exposed to Ch-SeNPs (1 mg/L). Results are plotted as the mean ± relative standard deviation (n = 10). The data were evaluated via ANOVA and subsequent Bonferroni test (* $p < 0.001$; ns: non-significant).**

Analysis by LC-QqQ-MS working in MRM mode allowed the quantification of the selected metabolites (ATP, ADP, NADH, NAD^+) in control and treated samples, in order to unravel energy metabolism alterations as a consequence of Ch-SeNPs exposure.

As **Figure 3** illustrates, significant differences (with a 95% confidence level, p-value < 0.05) in the concentration of ATP, ADP and NAD^+ were found. The levels of these metabolites were found significantly diminished in Ch-SeNPs exposed cells in comparison with control cells. On the contrary, no significant differences were found in the analysis of NADH levels of non-exposed cells in comparison to Ch-SeNPs exposed cultures.

3.4. Identification of metabolic alterations in cells exposed to Ch-SeNPs

GC-TOF-MS analysis allowed the identification (minimum NIST Rmatch of 700) of 26 commom metabolites, from a wide range of biochemical natures, between treated and control cells. Multivariant analysis, by means of Principal Component Analysis (PCA)

was required to analyze the data. [22]. The projection of the obtained data for each sample in the first two principal components allowed visualization of the groups and interrelations between them. As shown in **Figure 4**, PC1 and PC2 represented the 94.9 % of the explained variance. A clear separation could be appreciated between control and Ch-SeNPs treated samples, which reflects a different metabotype between both experimental conditions.

Posterior statistical analysis based on the Student t test detected significant differences (p-values < 0.05) in the average normalized areas and, thus, in the concentration levels of metabolites from exposed and control cells. Among the 26 identified metabolites, 13 where shown upregulated in Ch-SeNPs exposed cells, while 13 metabolites where in significantly lower concentration. **Table 1** gathers retention times and the "NIST Rmatch" parameter for each metabolite, besides from the ratio between average normalized areas. As a tool for interrelations comparison, hierarchical clustering and heat map graphical representation is represented in **Figure 5** in accordance with the results described.

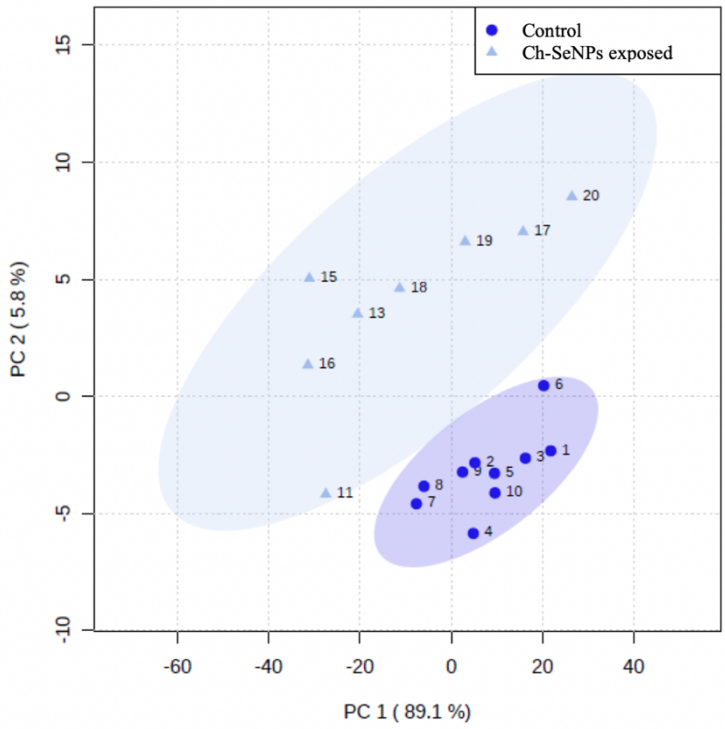

Figure 4. Principal component analysis for control and Ch-SeNPs exposed

Table 1. ***Significantly altered metabolites in HepG2 cells after exposure to 1 mg/L of Ch-SeNPs for 72 h.***

Metabolite	Retention time (min)	NIST Rmatch	R_M*
Glycine	**9.56**	**844**	**0.25**
Butanoic acid	**9.64**	**783**	**1.84**
Benzoic acid	**10.14**	**718**	**1.50**
L-Valine	**11.55**	**848**	**0.18**
Serine	**12.47**	**798**	**0.61**
Urea	**12.63**	**825**	**1.35**
Glycerol	**12.91**	**896**	**3.18**
L-Proline	**13.33**	**729**	**0.47**
Pyrimidine	**14.17**	**816**	**1.50**
2-butenoic acid	**14.55**	**869**	**0.21**
Aminomalonic acid	**17.00**	**850**	**1.81**
Malic acid	**17.48**	**828**	**0.15**
L-Cisteine	**18.71**	**905**	**3.69**
Glutamine	**20.06**	**844**	**0.25**
L-Isoleucine	**20.74**	**747**	**0.16**
Alpha-aminoadipic acid	**21.79**	**732**	**0.01**
Hydracrylic acid	**23.39**	**863**	**1.97**
2-desoxigalactopiranose	**23.75**	**777**	**0.74**
Adenine	**24.25**	**824**	**1.20**
D-Fructose	**24.47**	**881**	**2.16**
D-Glucose	**24.89**	**817**	**1.64**
Pantothenic acid	**26.38**	**908**	**0.11**
Inositol	**26.95**	**854**	**0.22**
N-acetylglucosamine	**27.63**	**714**	**1.24**
PET-cGMP	**33.60**	**963**	**3.22**
2-(1H)-pyrimidinone	**38.15**	**805**	**0.66**

**Ratio exposed/control cells*

improves significantly their antioxidant properties and their retention in the cells. Here, chitosan enwraps selenium

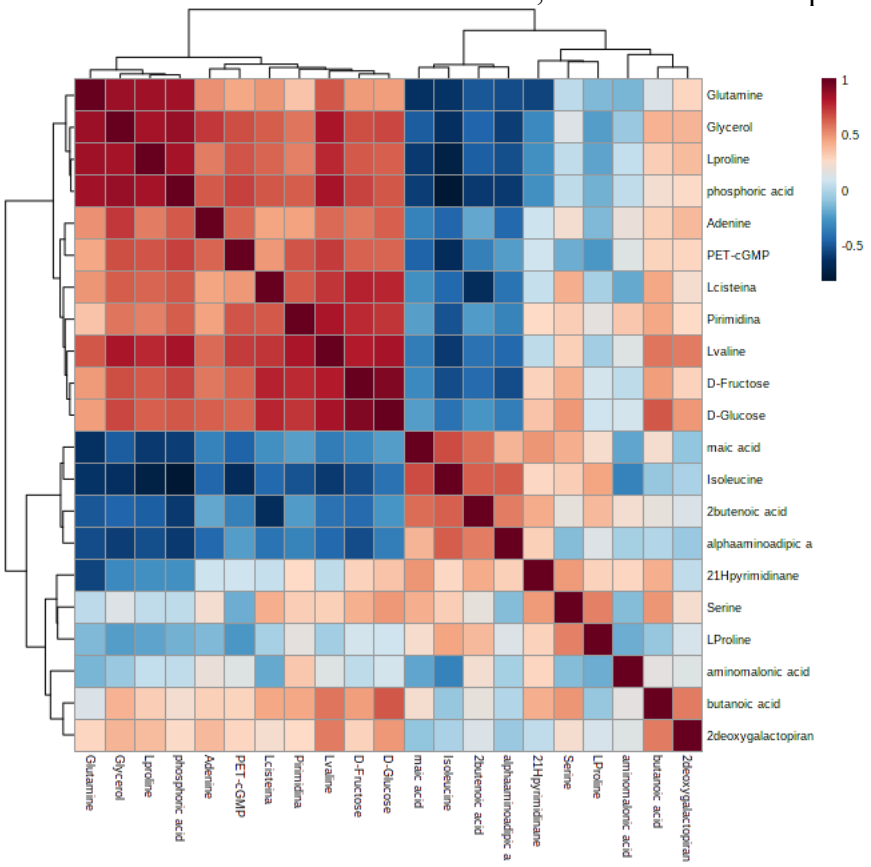

Figure 5. Hierarchically clustered analysis and heat map of metabolites found at different levels (represented by colors) in control v.s treated samples ($p < 0.05$).

4. Discussion

Commonly synthesized bare selenium nanoparticles are prone to aggregate in aqueous solution, hindering their uptake by cells and reducing their bioavailability. As previously shown by Luo et al. and Zhang et al. [15,16], encapsulation of selenium nanoparticles into a polysaccharide like chitosan nanoparticles by means of hydrogen bonds between the hydroxyl groups of chitosan and selenite. The use of chitosan under the synthesis conditions allowed to control size and morphology of the particles, obtaining well dispersed spherical Ch-SeNPs with sizes ranging from 40 to 50 nm as seen in **Figure 1**. A dialysis was performed to remove all the reagent excess from the final Ch-SeNPs suspension, as a guarantee that the observed effects in metabolism

alterations are only related to Ch-SeNPs exposure.

The synthesized Ch-SeNPs were able to significantly reduced the viability of HepG2 cells after 72 h, thus showing their antitumoral potential (**Figure 2**). Based on these results, 1 mg/mL of Ch-SeNPs was selected as the optimum concentration for carrying out the metabolomics approaches, since the cells were affected but not drastically compromised.

To evaluate alterations in energy metabolism after Ch-SeNPs exposure, four energy-related metabolites were analyzed: ATP, ADP, NADH, and NAD^+. Energy within cells is obtained from the oxidation of carbohydrates, lipids, or proteins, among others. Free energy derived from oxidation processes is stored in phosphoanhydrine "high energy bonds" within molecules such as adenosine 5`diphosphate and adenosine 5`triphosphate (ADP and ATP respectively). The four measured metabolites participate in the three main steps of cellular respiration: glycolysis, the TCA cycle and the mitochondrial electron transport chain.

LC-QqQ-MS working in MRM mode presents high sensitivity and selectivity, thus, it was the analytical platform selected for quantifying these metabolites. Analytical features of the LC-QqQ-MS method employed were previously optimized by García-Calvo et al. [12]. The four metabolites were quantified both in control and in cells exposed to Ch-SeNPs. Each concentration was normalized based on the total protein concentration of each sample, previously determined by a Bradford assay. Statistical ANOVA assays were conducted with a 95% confidence level (p-value < 0.05) and Bonferroni's post-test was performed. Significant differences in the concentration of ATP, ADP and NAD^+ between control and Ch-SeNPs exposed cells were observed (**Figure 3**). The concentration of these three energy-related metabolites were significantly lower as a result of the Ch-SeNPs effect. However, no significant differences were observed for the NADH levels.

Anabolic pathways will consume ATP and generate NADH, while catabolic pathways will generate ATP from ADP + Pi and oxidize NADH into NAD^+. Therefore, ATP and NAD^+ are key molecules in growth processes, depending on ATP synthesis and NADH turnover [17]. Cancer cells, in order to sustain the abnormal proliferation, require a more significant amount of energy production than healthy cells.

Mostly, metabolic reprogramming in cancer is characterized by enhanced glucose uptake and glycolysis, thus generating larger amounts of ATP in the cytosol. In sufficient oxygen concentration conditions, the rate of oxidative phosphorylation is governed by the mitochondrial ATP synthase, which catalyzes the synthesis of ATP through the proton motive force generated by the respiratory chain [18,19]. ATP, as the central energy storing molecule in the cell, is responsible for fueling the majority of biological processes. In our experiment, one of the most significant results on HepG2 cells after Ch-SeNPs exposure was the drastic reduction in the ATP levels. As commented above, energy supplies depend directly on this molecule; therefore, in cancer cells is even more critical to prevent uncontrolled proliferation.

In addition, in order to complete aerobic glycolysis, NAD^+ has to be regenerated from NADH in the pyruvate to lactate step. NADH, produced by glyceraldehyde phosphate dehydrogenase (GAPDH), is consumed regenerating NAD^+ and keeping glycolysis active. Higher glycolysis conversions yield in biomolecule production lines activity, such as the conversion of siphon 3-phosphoglycerate to serine for one-carbon metabolism-mediated production of nucleotides [20,21]. After Ch-SeNPs exposure, NAD^+ levels were reduced approximately by a 50%, which is directly related to the glycolytic activity and, thus, to a metabolic situation which prevents cancer cells to meet their biosynthetic requirements for uncontrolled proliferation.

To get a deeper insight into the metabolic alterations experienced by cells exposed to Ch-SeNPs, an untargeted metabolomic approach based on GC-MS was carried out. 36 metabolites were identified, including fatty acids, amino acids, organic acids, sugars and other small molecules. As shown in **Figure 4**, while samples within the same experimental condition presented a similar metabolic profile and were grouped together, a clear separation between control and Ch-SeNPs exposed cells was obtained, reflecting metabolic differences between the two conditions (**Figure 5**).

The statistical analysis revealed significant alterations in 26 metabolites (**Table 1)**, from which 13 were at a significantly higher concentration in exposed cells, while the other 13 were at

a lower level as compared to control cells.

The promising potential of Ch-SeNPs in cancer therapy through the cell cycle arrest has been observed in previous studies [8]. The inhibition of tyrosine (R_M = 0.18), in our study, supports these results, as it is involved in the activation of protein tyrosine phosphatase signaling events. The downregulation of this protein activity decreases cell proliferation, as well as expression of cyclins E and B1, PCNA, PTTG1 and phospho-histone H3 proteins and, consequently, causes cell cycle arrest [23]. On the other hand, high levels of palmitic acid, also known as hexadecanoic acid, (R_M = 2.87), have been reported to induce cell cycle arrest and to promote apoptosis in human neuroblastoma, prostate cancer and breast cancer cells; which is in accordance with the effects observed in cells exposed to Ch-SeNPs [24].

Cancer metabolism is constantly reprogrammed to enable abnormal proliferation and to ensure survival under insufficient nutrient environments. Given that proline (R_M = 0.47), serine (R_M = 0.18) and glycine (R_M = 0.25) are essential for tumor growth and survival, they are considered oncogenesis-supportive metabolites; all of them were found downregulated in cells exposed to Ch-SeNPs [25,26]. Some studies have directly linked proline biosynthesis to tumor growth capacity [27]. The other two amino acids are closely related, as serine interconversion provides glycine, generating a large number of one-carbon units. These units induce one-carbon metabolism, key in cancer metabolism for methylation pathways and biosynthesis of both purine and pyrimide nucleotides, among others [28]. These one-carbon units fuel two different pathways: the folate cycle [29,30] and the methionine cycle [31]. Therefore, Ch-SeNPs appear to be responsible of draining serine and glycine and prevent HepG2 cells from using them as a molecular base for synthesis of organic molecules or as energetic agents [32-35]. Consequently, alterations in serine and glycine metabolism result in profound dysregulations in cancer normal progression. Following on from this idea, the downregulation of alpha-aminoadipic acid (R_M = 0.01) is also related to tumor shrinkage through activation of a tumor suppressor known as KLF4 [36]. In addition to all this, in cancer cells, lipids are essential for maintaining the integrity of biological membranes and for providing energy for

malignant biological behavior. The accumulation of glycerol (R_M = 3.18), as a decrease in its transformation to glycerol-3-phosphate, the main intermediate for generating lipids and ATP, also hinders the proliferation of cancer cells [37].

The bioenergetic profile of tumors can provide crucial prognostic information, thus, raising the need for targeted therapies against primary pathways of energy production. The energy imbalance produced by Ch-SeNPs was reflected in decreased levels of ATP, ADP and NAD^+ as shown in the targeted metabolomics results. In fact, ATP, together with adenosine (R_M = 0.11), fuel signaling pathways that are thought to promote cancer growth and malignancy. The inhibition of both metabolites is in agreement with the paralysis of cancer cell growth [38]. One of the metabolic pathways that provides energy and intermediates for biosynthesis is the tricarboxylic acid (TCA) cycle. Glucose is, in a first step, oxidized into pyruvate in the cytoplasm, and the complete metabolism of glucose takes place through the TCA cycle. The ATP production in the TCA cycle occurs via NADH and FADH2 as intermediates after oxidative phosphorilation (OXPHOS) [21,39]. The downregulation of both, ATP and NAD^+, seems to reflect the inhibition of both pathways. The alteration of different metabolites, following the study of untargeted metabolomics results, confirmed this hypothesis. For example, 2-hydroxybutanedioic acid or malic acid, which is an intermediate of TCA cycle necessary for energy production through the consumption of pyruvic acid [40-43], was found at lower levels in cells exposed to Ch-SeNPs (R_M = 0.15). Another metabolite that revealed the impairment of the TCA cycle progression was the pantothenic acid (R_M = 0.11), an essential vitamin (B5) that plays a central role in the synthesis of CoA and, therefore, in the TCA cycle and fatty acid metabolism. Also, CoA serves as precursor for acylation reactions. CoA catabolism generates pantotheine that is acted upon vanins (pantotheinases), which generate pantothenate and cysteamine [44]. After Ch-SeNPs exposure, HepG2 cells showed drastic lower levels of pantothenic acid in comparison with non-treated cells, which leads to the conclusion that the exposure to Ch-SeNPs impairs the TCA cycle and, therefore, reduces the production of

energy in the cell, essential for the survival of cancer cells.

Although being a relevant route in terms of oxidative phosphorylation, it has been observed that under certain circumstances, cancer cells bypass the TCA cycle, and predominantly use aerobic glycolysis for fulfilling their bioenergetic, biosynthetic and redox balance requirements. Recent evidence suggests that tumor cells are able to uncouple glycolysis from the TCA cycle, allowing the use of glutamine (R_M = 4.85) to meet their needs [45]. Specifically, cancer cells are normally characterized by significantly promoting glutaminolyis in comparison to healthy cells, giving glutamine a central role in cancer proliferation [46,47]. Kamphorst et al. [48] demonstrated that KRAS-driven pancreatic cells scavenge proteins from the extracellular space for their lysosomal degradation in amino acids, such as glutamine, used to fuel the TCA cycle. In a similar way to what is happening with glutamine, after Ch-SeNPs exposure, HepG2 cells produce higher quantities of cysteine (R_M = 3.69) as compared to untreated cells. Cysteine is a proteinogenic amino acid with a free thiol group that confers particular properties on functional sites of proteins. This amino acid has key roles in the metabolic rewiring of cancer cells to withstand the poor-nutrient and oxygen-deficient conditions. These are, for example, being a precursor of glutathione, regulating oxidative stress and serving as a carbon source for biomass and energy production. In particular, cysteine is metabolized and converted into 3-mercaptopyruvate (3-MP), releasing one amino group that reacts with α-ketoglutarate, generating glutamate and pyruvate, and fueling, in an alternative way, the TCA cycle [49]. Higher levels of cysteine show that cells are rewiring their metabolism in order to provide alternative ways of maintaining the normal functioning of the pathway, thus confirming that the main sources are altered due to Ch-SeNPs exposure. Finally, fructose (R_M = 2.16) has been revealed as a strong modulator of the metabolic syndrome, preferentially promoting the glycolytic pathway, and also capable of inducing mitochondrial dysfunction and oxidative stress (suppressing aconitase in the TCA cycle) [50]. In addition to glucose, it has been suggested that fructose could also serve as an alternative nutrient for cancer cells to grow. A scheme of the alteration of energy metabolism, previously described, is shown in Figure 6. It shows

the main metabolites and metabolic pathways affected as a consequence of exposure to Ch-SeNPs, as well as the main proteins involved in them.

Increased fructose *(R_M = 2.16)* levels are also associated with other effects in the cell, specifically fructose metabolism is enhanced in response to low oxygen or anoxia conditions, and it promotes the production of uric acid and lactate as the main metabolic products. Particularly, uric acid induces the Warburg effect by downregulating the mitochondrial respiration and inducing aerobic glycolysis [51]. As observed by Park et al. [52], naked mole rats under hypoxia/anoxia endogenously produced substantial quantities of fructose in several organs like the kidney and liver. In our experiment, fructose production appeared to be at significantly higher levels in cells treated with Ch-SeNPs as compared to control cells, which is a predictable fact in terms of cancer metabolism and energy sources. In addition, these higher levels of fructose observed in treated cells correlate well with the fact that Ch-SeNPs exposure has been previously demonstrated to induce hypoxia in cancer cells [53]. Furthermore, these results are in agreement with the targeted metabolomics results, because fructose induces ATP depletion in a transient phenomenon, therefore, reducing intracellular ATP levels, and impairing cellular growth. Another indicator of the hypoxia state in cells exposed to Ch-SeNPs, might be the increased levels of cysteine (R_M = 3.69). Cysteine is an

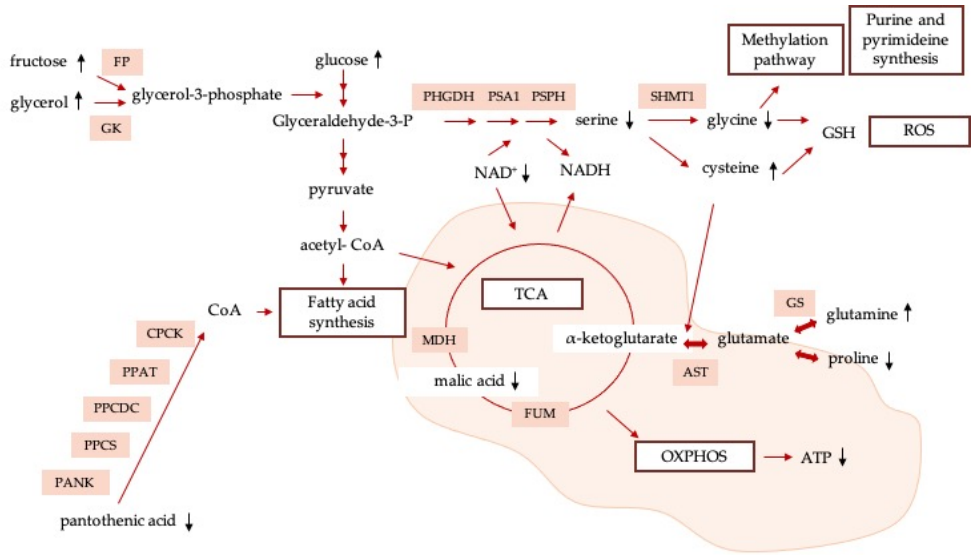

Figure 6. Network map containing the main metabolic pathways involved in the antitumoral effect of Ch-SeNPs.

scavenger of free radicals, it can abrogate most of the oxidative or alkylating drugs used in cancer therapy [54]; thus, it makes perfect sense the high levels of cysteine found as a cellular defense mechanism to help cancer cells to survive drug exposure and other Ch-SeNPs-mediated stress conditions such as hypoxia.

5. Conclusions

In this study, the combination of targeted and untargeted metabolomics has provided valuable insights into the biomolecular mechanisms underlying the cytotoxic effects of Ch-SeNPs against cancer cells. The results confirm that Ch-SeNPs can disrupt cell cycle modulators, reinforcing their potential for arresting cell growth and inhibiting cancer development. Several key metabolites crucial for cancer growth were found at lower levels in treated cells compared to controls, indicating the ability of Ch-SeNPs to restrict oncogenesis-supportive metabolites, such as proline, serine, and glycine.

Moreover, the targeted metabolomics experiment revealed significant alterations in energy metabolism following Ch-SeNPs exposure. These nanoparticles were found to disrupt the TCA cycle, a primary source of cellular energy, leading to decreased levels of important energy-related metabolites, like pantothenic acid and malic acid. The cells adapted by shifting to glycolysis as an alternative pathway, as evidenced by higher cysteine levels in Ch-SeNPs exposed cells. Additionally, the study demonstrated the ability of Ch-SeNPs to induce hypoxia in cancer cells, as evidenced by the promotion of specific metabolites like fructose and cysteine, associated with this stress condition.

Compared to previous findings, this study offers new insights into the specific metabolic pathways targeted by Ch-SeNPs in cancer cells. The results reinforce the potential of Ch-SeNPs as an effective antitumor agent and shed light on the mechanisms underlying their therapeutic efficacy.

In conclusion, this research has advanced our understanding of the therapeutic potential of Ch-SeNPs and their mode of action against cancer cells. The findings suggest that Ch-SeNPs have a multifaceted impact on cancer metabolism, disrupting key pathways and restricting essential metabolites,

which collectively contribute to their antitumor effects. These insights have implications for the development of targeted nanoparticle-based therapies in cancer treatment.

Supplementary Materials: The following supporting information can be downloaded at: www.mdpi.com/xxx/s1, **Figure S1**: MRM chromatograms of each analyte from both, control and Ch-SeNPs exposed samples.

Author Contributions: Héctor Estévez: Methodology, Formal analysis, Investigation, Writing, Original draft. Estefanía García-Calvo: Methodology, Formal analysis, Investigation, Writing, Original draft. María L. Mena: Writing – review and editing. Roberto Alvarez-Fernandez Garcia: Formal analysis, Writing – review and editing. José L. Luque García: Conceptualization, Writing – review and editing, Funding acquisition, Supervision, Project administration. All authors have read and agreed to the published version of the manuscript.

Funding: This research was funded by the Ministerio de Ciencia e Innovación through grant PID2020-114529RB-I00.

Acknowledgments: H.E. thanks the Ministerio de Ciencia e Innovación for a pre-doctoral fellowship (PRE2018-084196).

Conflicts of Interest: The authors declare no conflict of interest.

References

[1] Johnson, C. H.; Ivanisevic, J.; Siuzdak, G. Metabolomics: beyond biomarkers and towards mechanisms. Nat. Rev. Mol. Cell Biol. 2016, 17(7), 451–459.

[2] Yang, Q.; Vijayakumar, A.; Kahn, B. B. Metabolites as regulators of insulin sensitivity and metabolism. Nat. Rev. Mol. Cell Biol. 2018, 19(10), 654–672.

[3] Jacob, F.; Monod, J. Genetic regulatory mechanisms in the synthesis of proteins. JMB 1961, 3, 318–356.

[4] Rinschen, M. M.; Ivanisevic, J.; Giera, M.; Siuzdak, G. Identification of bioactive metabolites using activity metabolomics. Nat. Rev. Mol. Cell Biol. 2019, 20(6), 353–367.

[5] Roberts, L. D.; Souza, A. L.; Gerszten, R. E.; Clish, C. B. Targeted metabolomics. Current protocols in molecular biology, 2012, Chapter 30, Unit 30.2–30.2.24.

[6] Di Minno, A.; Gelzo, M.; Stornaiuolo, M.; Ruoppolo, M.; Castaldo, G. The evolving landscape of untargeted metabolomics. NMCD, 2021, 31(6), 1645–1652.

[7] Schrimpe-Rutledge, A. C.; Codreanu, S. G.; Sherrod, S. D.; McLean, J. A. Untargeted Metabolomics Strategies-Challenges and Emerging Directions. J. Am. Soc. Mass Spectrom. 2016, 27(12), 1897–1905.

[8] Dai, X.; Yu, L.; Zhao, X.; Ostrikov, K. K. Nanomaterials for oncotherapies targeting the hallmarks of cancer. Nanotechnology, 2020, 31(39), 392001.

[9] Yu, H.; Tang, Z.; Zhang, D.; Song, W.; Zhang, Y.; Yang, Y.; Ahmad, Z.; Chen, X. Pharmacokinetics, biodistribution and in vivo efficacy of cisplatin loaded poly(L-glutamic acid)-g-methoxy poly(ethylene glycol) complex nanoparticles for tumor therapy. J. Control Release 2015, 205, 89–97.

[10] Estevez H.; Garcia-Lidon J. C.; Luque-Garcia J. L.; Camara C. Effects of chitosan-stabilized selenium nanoparticles on cell proliferation, apoptosis and cell cycle pattern in HepG2 cells: comparison with other selenospecies. Colloids Surf. B 2014, 122:184-193.

[11] Bai, Y.; Wang, Y.; Zhou, Y.; Li, W.; Zheng, W. Modification and modulation of saccharides on elemental selenium

nanoparticles in liquid phase. Mater. Lett. 2008, 62(15), 2311-2314.

[12] Garcia-Calvo, E.; Machuca, A.; Nerín, C.; Rosales-Conrado, N.; Anunciação, D. S.; Luque-Garcia, J. L. Integration of untargeted and targeted mass spectrometry-based metabolomics provides novel insights into the potential toxicity associated to surfynol. Food Chem. Toxicol. 2020, 146, 111849.

[13] Sapcariu, S. C.; Kanashova, T.; Weindl, D.; Ghelfi, J.; Dittmar, G.; Hiller, K. Simultaneous extraction of proteins and metabolites from cells in culture. MethodsX 2014, 1, 74–80.

[14] Papadimitropoulos, M. P.; Vasilopoulou, C. G.; Maga-Nteve, C.; Klapa, M. I. Untargeted GC-MS Metabolomics. Methods Mol. Biol. 2018, 1738, 133–147.

[15] Luo, Y.; Zhang, B.; Cheng, W.H.; Wang, Q. Preparation, characterization and evaluation of selenite-loaded chitosan/TPP nanoparticles with or without zein coating. Carbohydrates Polymers. 2010, 82, 942–951.

[16] Zhang, S.; Luo, Y.; Zeng, H.; Wang, Q.; Tian, F.; Song, J.; Cheng, W. H. Encapsulation of selenium in chitosan nanoparticles improves selenium availability and protects cells from selenium-induced DNA damage response. J. Nutr. Biochem. 2011, 22(12), 1137–1142.

[17] Rigoulet, M.; Bouchez, C. L.; Paumard, P.; Ransac, S.; Cuvellier, S.; Duvezin-Caubet, S.; Mazat, J. P.; Devin, A. Cell energy metabolism: An update. Biochim. Biophys. Acta Bioenerg. 2020, 1861(11), 148276.

[18] Bonora, M.; Patergnani, S.; Rimessi, A.; De Marchi, E.; Suski, J. M.; Bononi, A.; Giorgi, C.; Marchi, S.; Missiroli, S.; Poletti, F.; Wieckowski, M. R.; Pinton, P. ATP synthesis and storage. Purinergic Signal. 2012, 8(3), 343–357.

[19] Galber, C.; Acosta, M. J.; Minervini, G.; Giorgio, V. The role of mitochondrial ATP synthase in cancer. Biol. Chem. 2020, 401(11), 1199–1214.

[20] Lunt, S. Y.; Vander Heiden, M. G. Aerobic glycolysis: meeting the metabolic requirements of cell proliferation. Annu. Rev. Cell Dev. Biol. 2011, 27, 441–464.

[21] Liberti, M. V.; Locasale, J. W. The Warburg Effect: How Does it Benefit Cancer Cells?. Trends Biochem. Sci. 2016, 41(3), 211–218.

[22] Steuer, R.; Morgenthal, K.; Weckwerth, W.; Selbig, J. A gentle guide to the analysis of metabolomic data. Methods Mol. Biol. 2007, 358, 105–126.

[23] Castilla, C.; Flores, M. L.; Conde, J. M.; Medina, R.; Torrubia, F. J.; Japón, M. A.; Sáez, C. Downregulation of protein tyrosine phosphatase PTPL1 alters cell cycle and upregulates invasion-related genes in prostate cancer cells. Clin. Exp. Metastasis 2012, 29(4), 349–358.

[24] Zhu, S.; Jiao, W.; Xu, Y.; Hou, L.; Li, H.; Shao, J.; Zhang, X.; Wang, R.; Kong, D. Palmitic acid inhibits prostate cancer cell proliferation and metastasis by suppressing the PI3K/Akt pathway. Life Sci. 2021, 286, 120046.

[25] DeBerardinis, R. J.; Chandel, N. S. Fundamentals of cancer metabolism. Sci. Adv. 2016, 2(5), e1600200.

[26] DeBerardinis R. J. Serine metabolism: some tumors take the road less traveled. Cell Metab. 2011, 14(3), 285–286.

[27] Liu, W.; Hancock, C. N.; Fischer, J. W.; Harman, M.; Phang, J. M. Proline biosynthesis augments tumor cell growth and aerobic glycolysis: involvement of pyridine nucleotides. Sci. Rep. 2015, 5, 17206.

[28] Geeraerts, S. L.; Heylen, E.; De Keersmaecker, K.; Kampen, K. R. The ins and outs of serine and glycine metabolism in cancer. Nat. Metab. 2021, 3(2), 131–141.

[29] Tibbetts, A. S.; Appling, D. R. Compartmentalization of Mammalian folate-mediated one-carbon metabolism. Annu. Rev. Nutr. 2010, 30, 57–81.

[30] Pasternack, L. B.; Laude, D. A. Jr; Appling, D. R. 13C NMR detection of folate-mediated serine and glycine synthesis in vivo in Saccharomyces cerevisiae. Biochemistry. 1992, 31(37), 8713–8719.

[31] Maddocks, O. D.; Labuschagne, C. F.; Adams, P. D.; Vousden, K. H. Serine Metabolism Supports the Methionine Cycle and DNA/RNA Methylation through De Novo ATP Synthesis in Cancer Cells. Mol. Cell 2016, 61(2), 210–221.

[32] Yang, M.; Vousden, K. H. Serine and one-carbon metabolism in cancer. Nat. Rev. Cancer 2016, 16(10), 650–662.

[33] Kampen, K. R.; Fancello, L.; Girardi, T.; Rinaldi, G.; Planque, M.; Sulima, S. O.; Loayza-Puch, F.; Verbelen, B.; Vereecke, S.; Verbeeck, J.; Op de Beeck, J.; Royaert, J.; Vermeersch, P.; Cassiman, D.; Cools, J.; Agami, R.; Fiers, M.; Fendt, S. M.; De Keersmaecker, K. Translatome analysis reveals altered serine and glycine metabolism in T-cell acute lymphoblastic leukemia cells. Nat. Commun. 2019, 10(1), 2542.

[34] Schwartz, N. U.; Linzer, R. W.; Truman, J. P.; Gurevich, M.; Hannun, Y. A.; Senkal, C. E.; Obeid, L. M. Decreased ceramide underlies mitochondrial dysfunction in Charcot-Marie-Tooth 2F. FASEB J. 2018, 32(3), 1716–1728.

[35] Muthusamy, T.; Cordes, T.; Handzlik, M. K.; You, L.; Lim, E. W.; Gengatharan, J.; Pinto, A.; Badur, M. G.; Kolar, M. J.; Wallace, M.; Saghatelian, A.; Metallo, C. M. Serine restriction alters sphingolipid diversity to constrain tumour growth. Nature 2020, 586(7831), 790–795.

[36] Jung, K.; Reszka, R.; Kamlage, B.; Bethan, B.; Stephan, C.; Lein, M.; Kristiansen, G. Tissue metabolite profiling identifies differentiating and prognostic biomarkers for prostate carcinoma. Int. J. Cancer 2013, 133(12), 2914–2924.

[37] Chen, L.; Li, Z.; Zhang, Q.; Wei, S.; Li, B.; Zhang, X.; Zhang, L.; Li, Q.; Xu, H.; Xu, Z. Silencing of AQP3 induces apoptosis of gastric cancer cells via downregulation of glycerol intake and downstream inhibition of lipogenesis and autophagy. Onco Targets Ther. 2017, 10, 2791–2804.

[38] Boison, D.; Yegutkin, G. G. Adenosine Metabolism: Emerging Concepts for Cancer Therapy. Cancer Cell. 2019, 36(6), 582–596.

[39] Eniafe, J.; Jiang, S. The functional roles of TCA cycle metabolites in cancer. Oncogene 2021, 40(19), 3351–3363.

[40] Zhang, B.; Tornmalm, J.; Widengren, J.; Vakifahmetoglu-Norberg, H.; Norberg, E. Characterization of the Role of the Malate Dehydrogenases to Lung Tumor Cell Survival. J. Cancer. 2017, 8(11), 2088–2096.

[41] Lim, J.K.M.; Leprivier, G. The impact of oncogenic RAS on redox balance and implications for cancer

development. Cell Death Dis. 2019, 10, 955.

[42] Ren, J. G.; Seth, P.; Everett, P.; Clish, C. B.; Sukhatme, V. P. Induction of erythroid differentiation in human erythroleukemia cells by depletion of malic enzyme 2. PloS ONE 2010, 5(9), e12520.

[43] Ren, J. G.; Seth, P.; Clish, C. B.; Lorkiewicz, P. K.; Higashi, R. M.; Lane, A. N.; Fan, T. W.; Sukhatme, V. P. Knockdown of malic enzyme 2 suppresses lung tumor growth, induces differentiation and impacts PI3K/AKT signaling. Sci. Rep. 2014, 24(4), 5414.

[44] Peterson, C. T.; Rodionov, D. A.; Osterman, A. L.; Peterson, S. N. B Vitamins and Their Role in Immune Regulation and Cancer. Nutrients 2020, 12(11), 3380.

[45] Pavlova, N. N.; Thompson, C. B. The Emerging Hallmarks of Cancer Metabolism. Cell Metab. 2016, 23(1), 27–47.

[46] Fung, M.; Chan, G. C. Drug-induced amino acid deprivation as strategy for cancer therapy. Hematol. Oncol. 2017, 10(1), 144.

[47] Anderson, N. M.; Mucka, P.; Kern, J. G.; Feng, H. The emerging role and targetability of the TCA cycle in cancer metabolism. Protein Cell 2018, 9(2), 216–237.

[48] Kamphorst, J. J.; Nofal, M.; Commisso, C.; Hackett, S. R.; Lu, W.; Grabocka, E.; Vander Heiden, M. G.; Miller, G.; Drebin, J. A.; Bar-Sagi, D.; Thompson, C. B.; Rabinowitz, J. D. Human pancreatic cancer tumors are nutrient poor and tumor cells actively scavenge extracellular protein. Cancer Res. 2015, 75(3), 544–553.

[49] Bonifácio, V.; Pereira, S. A.; Serpa, J.; Vicente, J. B. Cysteine metabolic circuitries: druggable targets in cancer. Br. J. Cancer 2021, 124(5), 862–879.

[50] Nakagawa, T.; Johnson, R. J.; Andres-Hernando, A.; Roncal-Jimenez, C.; Sanchez-Lozada, L. G.; Tolan, D. R.; Lanaspa, M. A. Fructose Production and Metabolism in the Kidney. JASN 2020, 31(5), 898–906.

[51] Nakagawa, T.; Lanaspa, M. A.; Millan, I. S.; Fini, M.; Rivard, C. J.; Sanchez-Lozada, L. G.; Andres-Hernando, A.; Tolan, D. R.; Johnson, R. J. Fructose contributes to the Warburg

effect for cancer growth. Cancer Metab. 2020, 8, 16.

[52] Park, T. J.; Reznick, J.; Peterson, B. L.; Blass, G.; Omerbašić, D.; Bennett, N. C.; Kuich, P.; Zasada, C.; Browe, B. M.; Hamann, W.; Applegate, D. T.; Radke, M. H.; Kosten, T.; Lutermann, H.; Gavaghan, V.; Eigenbrod, O.; Bégay, V.; Amoroso, V. G.; Govind, V.; Minshall, R. D.; Smith, E.St.J.; Larson, J.; Gotthardt, M.; Kempa, S.; Lewin, G. R. Fructose-driven glycolysis supports anoxia resistance in the naked mole-rat. Science 2017, 356(6335), 307–311.

[53] Estevez, H.; Garcia-Calvo, E.; Rivera-Torres, J.; Vallet-Regí, M.; González, B.; Luque-Garcia, J. L. Transcriptome Analysis Identifies Novel Mechanisms Associated with the Antitumor Effect of Chitosan-Stabilized Selenium Nanoparticles. Pharmaceutics 2021, 13(3), 356.

[54] Bonifácio, V.; Pereira, S. A.; Serpa, J.; Vicente, J. B. Cysteine metabolic circuitries: druggable targets in cancer. Br. J. Cancer 2021, 124(5), 862–879.

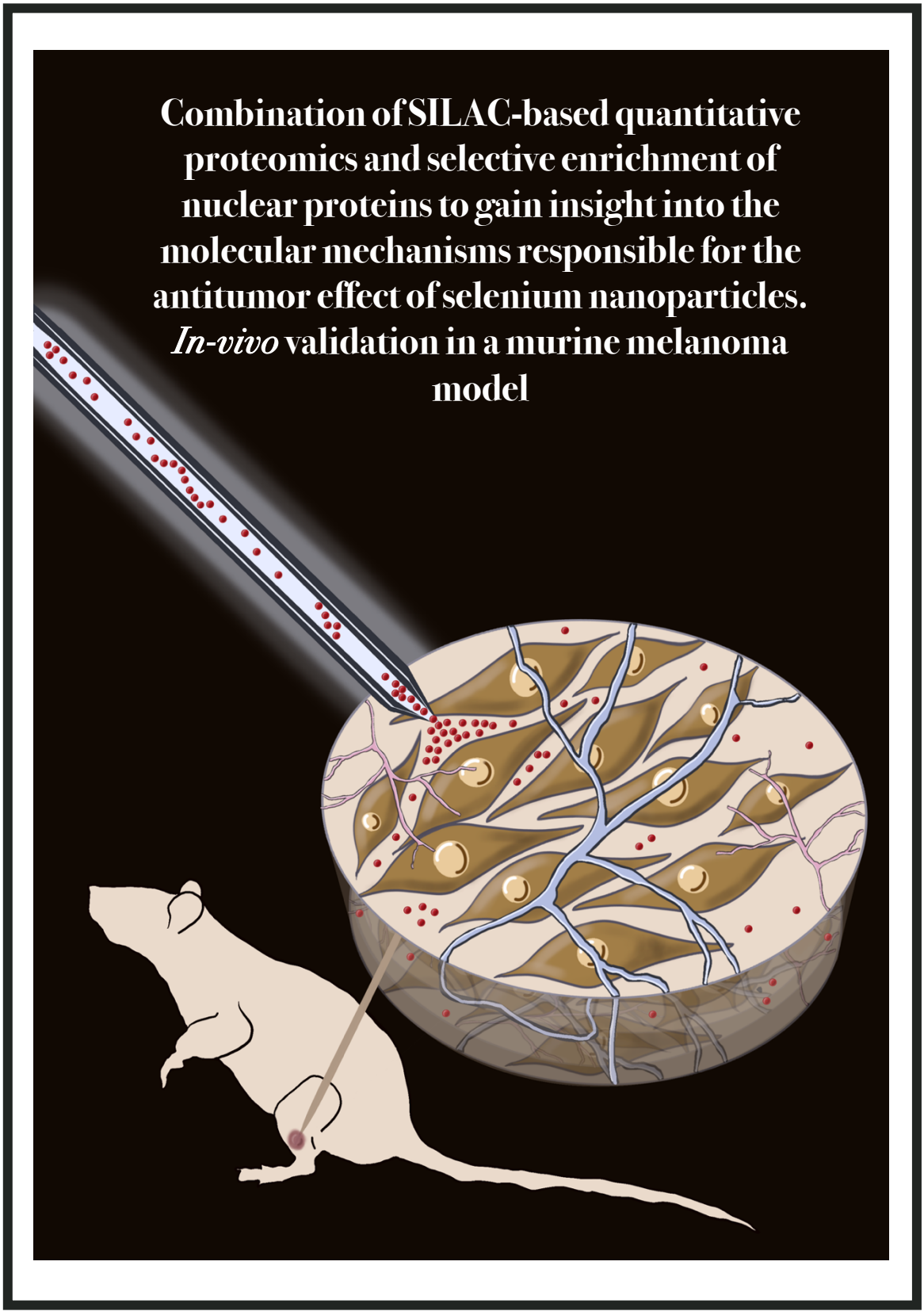
Combination of SILAC-based quantitative proteomics and selective enrichment of nuclear proteins to gain insight into the molecular mechanisms responsible for the antitumor effect of selenium nanoparticles. *In-vivo* validation in a murine melanoma model

1.4. Combination of SILAC-based quantitative proteomics and selective enrichment of nuclear proteins to gain insight into the molecular mechanisms responsible for the antitumor effect of selenium nanoparticles. *In-vivo* validation in a murine melanoma model

Hector Estevez, Estefania Garcia-Calvo, Raquel Sanchez, Juan José Lazcano, Pilar Martin, and Jose L. Luque-Garcia

Enviado a la revista Small

Abstract

Nanoparticles have emerged as promising candidates for innovative cancer treatments. Among these, chitosan-stabilized selenium nanoparticles (Ch-SeNPs) have exhibited unique physico-chemical properties, including a spherical morphology and homogenous size distribution. Building on prior studies highlighting the antitumoral potential of Ch-SeNPs, this research delves into their
molecular mechanisms, focusing on the nuclear proteome. We conducted an extensive quantitative proteomics analysis, identifying 343 proteins with 47 exhibiting significant alterations upon Ch-SeNPs exposure. Key proteins, such as CDK1 and CDC5, shed light on the intricate molecular pathways contributing to cell cycle arrest and tumor suppression. Furthermore, the impact of Ch-SeNPs extends to diverse cellular functions, with mRNA metabolism and cytoskeleton organization among the affected processes. *In vivo* experiments utilizing a murine melanoma model validate the therapeutic potential of Ch-SeNPs, demonstrating a substantial suppression of tumor growth without adverse effects on overall health.

1. Introduction

In the current landscape of cancer therapeutics, nanotechnology has emerged as a pivotal player, offering innovative approaches to combat tumors with enhanced precision and efficacy (Chaturvedi et al., 2019). Nanoparticles play a crucial role in cancer treatment by enabling targeted drug delivery, minimizing side effects, and enhancing therapeutic efficacy (Sun et al., 2014). Their ability to navigate biological barriers and specifically target cancer cells holds immense promise in revolutionizing oncological interventions (Tang et al., 2019).

Among the different types of nanoparticles that are currently being under study for tumor treatments, selenium nanoparticles (SeNPs) are particularly promising, since they have already shown their ability to induce cell cycle arrest and to induce senescence, thus impairing tumoral growth (Estevez et al., 2021; Estevez et al. 2023). However, although some of the biomolecular mechanisms by which SeNPs exert their action have already been studied, there is still a need for a better understanding of such mechanisms, specially at the nuclear level where these SeNPs seems to play a crucial role.

Proteomics, particularly quantitative proteomics, plays a crucial role in unraveling the mechanisms of action of novel antitumor agents (Tan et al, 2012). By identifying and quantifying protein changes, quantitative proteomics approaches offer a comprehensive understanding of the molecular processes underlying the effects of new antitumor compounds (Chen et al., 2007). Among the different strategies, stable isotopic labeling by amino acids in cell culture (SILAC), remains the most widely employed strategy, due to its high accuracy and versatility (Zhang et al, 2014; Guo et al., 2023).

Based on the above, in this work we have used the SILAC strategy in combination with a nuclear protein purification method to gain insight into the mechanisms of action of SeNPs at the nuclear level. Furthermore, in addition to finding important targets responsible for the cytotoxic action of SeNPs in tumor cells, an *in vivo* experiment using a murine model of melanoma has been carried out, which has allowed us to evaluate the efficacy of SeNPs treatment in a more complex environment. The results obtained have contrasted previous studies and have supported the

therapeutic potential of SeNPs as an antitumor agent.

2. Materials and Methods

2.1.Synthesis and characterization of Ch-SeNPs

Chitosan-stabilized selenium nanoparticles (Ch-SeNPs) were synthesized following a previously published procedure [Bai et al., 2008]. Briefly, 7.5 mL of 0.23 M ascorbic acid and 5 mL of 2.4 M acetic acid were mixed with 10 mL of an aqueous chitosan polysaccharide solution (0.5% w/v). Afterwards, 0.51 M sodium selenite was slowly added to the mixture. The formation of Ch-SeNPs was noted through the change of the dispersion from colorless to red. Then, 10 mL of the dispersion were dialyzed against 2 L of distilled water using a 12 kDa MWCO membrane for 2 h at room temperature. Synthesized Ch-SeNPs were stored at 4 ºC up to two months.

Synthesized Ch-SeNPs were observed by Transmission Electron Microscopy (TEM). Droplets of the dispersion were placed onto a holey carbon film on copper grids. Micrographs were obtained with a JEOL JEM 1400 PLUS operating at 120 kV.

2.2.Cell culture

Two cell types were employed in this work: HepG2, used in the *in vitro* experiments, and B16 cells, used in the *in vivo* experiments. HepG2 cells were maintained in Dulbecco´s modified Eagle´s medium (DMEM) supplemented with 10% fetal bovine serum (FBS) and 1% penicillin/streptomycin at 37 ºC and 5% CO_2. B16 cells were cultured in DMEM, supplemented with 10% FBS, L-glutamine and penicillin and streptomycin at 37 ºC in a humidified 5% CO_2 atmosphere. Cells were harvested under exponential growth, centrifuged and placed in $1x10^6$/50 µl of PBS before injection.

2.3.Quantitative proteomics

Metabolic labeling

HepG2 cells were maintained in DMEM supplemented with 10% dialyzed FBS, 100 units per 100 mL of penicillin/streptomycin and either naturally occurring isotopes (“light”) or stable isotope-labeled (“heavy”) $^{13}C_6$ arginine and lysine amino acids. Culture media were refreshed when 80% (8×10^6 cells) plate confluence was reached and the cells were grown for at least 6 doublings to allow full incorporation of the labeled amino acids. Two large-scale SILAC replicates were performed. To verify the complete incorporation of

$^{13}C_6$-Lys and $^{13}C_6$-Arg in isotopically heavy medium after eight cell divisions, an MS analysis of a protein digest was performed (data not shown).

2.4. Exposure to Ch-SeNPs and isolation of nuclear proteins.

HepG2 cells labeled with "heavy" (direct SILAC) or "light" (reverse SILAC) amino acids were exposed to 1 mg/L of Ch-SeNPs for 72 h. Cells grown in either "light" or "heavy" media were harvested, counted and mixed in a 1:1 ratio. Then, isolation of nuclear proteins was carried out with the Qproteome Nuclear Protein kit (Qiagen). Briefly, cells were washed with PBS and centrifuged 5 min at 450 x g (4 ºC). Once cells were resuspended in 500 µL of lysis buffer, 25 µL of detergent solution were added and vortex mixed for 10 s. Cells were centrifuged 5 min at 10000 x g (4 ºC). Afterwards, the pellet (which contains cell nuclei) was re-suspended in nuclear protein lysis buffer. After 5 min centrifugation at 10000 x g, the nuclear pellet was re-suspended in 50 µL of extraction buffer NX1. The mixture was then incubated for 30 min at 4 ºC and centrifuged at 12000 x g for 10 min. The nucleic-acid binding proteins were isolated in the supernatant. For the extraction of "insoluble" nuclear proteins, the pellet was re-suspended in 100 µL of extraction buffer NX2 and incubated for 1 h. Finally, the suspension was centrifuged at 12000 x g for 10 min to obtain the "insoluble" nuclear proteins fraction.

2.5. SDS-page and in-gel digestion.

Proteins were separated by means of SDS-PAGE on 10% SDS-polyacrylamide gels. After electrophoresis and Coomassie Brilliant Blue staining, gel lanes were cut into approximately 20 sections. Gel bands were de-stained in 25 mM ammonium bicarbonate/ 50% acetonitrile, cut into smaller pieces, dehydrated with acetonitrile and dried. Gel pieces were incubated with a 12.5 ng/µL trypsin solution in 25 mM ammonium bicarbonate overnight at 37 ºC. To extract the peptides, gel pieces were incubated with acetonitrile and 5% formic acid, dried using vacuum centrifugation and reconstituted in 12 µL of and aqueous solution containing 2% acetonitrile and 0.1 % formic acid.

2.6. Mass spectrometry analysis.

Analysis was performed with a nanoflow LC-MS/MS. Peptides fractions were loaded onto a C18 trap column (0.3 x 10mm, SGE) and then separated on a reverse-phase column (75

µm x 25 cm fused silica capillary C18 HPLC PepMap column, 3 µm, 100 A, Thermo) selecting a linear gradient of 5-95% acetonitrile in 0.1% aqueous solution of formic acid. A nano LC ultra 1D plus system (Eksigent) delivered the mentioned gradient at a flow-rate of 200 nL/min through the analytical column up to a stainless nano-bore emitter (Proxeon). An LTQ XL linear ion trap mass spectrometer (Thermo Scientific) scanned and fragmented the peptides operating in data-dependent Zoom Scan and MS/MS switching mode using the three most intensive precursor ions detected in a survey scan from 400 to 1600 u (three scans). In order to monitor the entire $^{12}C/^{13}C$ isotopic envelope of most doubly and triply charged peptides, the ZoomScan mass window was set to 12 Da. Singly charged ions were excluded for MS/MS analysis. Resulting .raw files were converted to .mgf files to enable MASCOT database search. The Uniprot A database containing the Uniprot *Homo Sapiens* sequences containing 20416 entries (19/10/20) was searched using the MASCOT protein identification software (v2.3 MatrixScience). Search restrictions were set: trypsin specificity with one missed cleavage allowed, methionine oxidation and $^{13}C_6$-Arg and $^{12}C_6$-Lys as variable modifications. Minimum precursor and fragment-ion mass accuracies for 1.2 and 0.3 Da were used. At least one unique peptide (bold-red peptides meaning highest scoring peptide matching to protein with highest total score) was required for protein identification and at least two unique peptides were required for quantification. The cut-off values for MASCOT scores of peptides and proteins were set to 40 ($p < 0.05$) and 46 ($p < 0.01$), respectively. The false positive rate was estimated by searching the same spectra against the Uniprot *Homo Sapiens* decoy database. QuiXoT open-source software (version 1.3.26) was used to calculate the relative quantification ratios (R_{SILAC}) of identified proteins based on peak area. Verification of all protein ratios obtained by QuiXoT was carried out by manually inspecting all quantified peptides.

2.7. Gene expression analysis

Trizol reagent (Invitrogen) was employed to isolate total RNA from HepG2 cells exposed to Ch-SeNPs (1 mg/L and 72 h). The quantity of extracted RNA was measured using a NanoDrop One (Thermo Fisher Scientific). A Quantitec reverse transcription kit (Qiagen) was used for the synthesis of cDNAs and for the

integrated removal of genomic DNA contamination. For the RT-qPCR analysis, TaqMan gene expression assays and TaqMan Fast advance master mix (Thermo Fischer Scientific) were used according to manufacturer´s instructions. The references of Taqman gene expression assays used are listed in Table 1. The relative expression of genes was normalized using GAPDH as the endogenous control. Gene expression in each sample was calculated as $2^{-\Delta\Delta Ct}$.

for Cardiovascular Research) animal facility. All animal procedures were approved by the ethics committee of the *Comunidad Autónoma de Madrid* and conducted in accordance with the institutional guidelines that comply with the European Institutes of Health´s; *Directive 2010/63/EU of the European Parliament and the Council on the Protection of Animals Used for Scientific Purposes (Official Journal of the European Union. Vol. 53:33-79, 2010).*

Table 1 References of TaqMan gene expression assays used for the RT-PCR analysis.

Gene	RefSeq	Assay ID
CDK1	NM_001170406	Hs00938777_m1
CCNB1	NM_031966.3	Hs01030099_m1
CCNA2	NM_001237.3	Hs00996788_m1
CDKN1A	NM_000389.4	Hs00355782_m1
GAPDH	NM_001256799.2	Hs03929097_g1

2.8. *In-vivo* inhibition of melanoma tumor growth

12 weeks old females in the C57BL/6J background, weighting ~20-25 g, were injected intradermally (ID) in both sides of the back with $1x10^6$ B16 cells. Animals were housed and used in specific pathogen-free (SPF) conditions at the CNIC (Spanish National Center

5 days after intradermal B16 injections, tumors became established (~50 mm^3) into the mice at the minimum size to begin the treatment with the NPs. A control group of non-treated mice was analyzed in parallel. Ch-SeNPs were prepared at a final concentration of 200 mg/L. 50µl of vehicle (synthesis media) alone or containing Ch-SeNPs were

injected intra tumor with a 25G needle in the right and left back sides, respectively. Treatment as described was performed on alternate days. The mice body weights and tumor sizes were recorded on alternate days after treatment. The tumor size was determined by *Ratio* (Ref. 6369H15) digital caliper measurements and calculated as length x width x height. After 10-15 days, mice with tumors > 1.5 cm in diameter were sacrificed.

3. Results and Discussion

3.1. Characterization of Ch-SeNPs

Although the synthesis of Ch-SeNPs has been previously carried out with an extensive fisico-chemical characterization TEM micrographs were acquired in order to verify the size and morphology of the newly synthesized Ch-SeNPs. As shown in **Figure 1**, well-dispersed Ch-SeNPs were obtained, with nanoparticles exhibiting spherical morphology and homogeneous sizes of around 40-60 nm.

3.2. Mechanisms of action of Ch-SeNPs at the nuclear level

In previous studies [Estevez et al., 2021; Estevez et al., 2023], we identified some of the biomolecular mechanisms of action related to the antitumoral potential of Ch-SeNPs. Since some of these findings were directly related with the action of Ch-SeNPs over nuclear proteins, we designed a SILAC-based assay focused on the nuclear proteome, in order to gain deeper insights into these mechanisms. Thus, we conducted an extensive SILAC experiment (**Figure 2**) that included purification of the nuclear proteome.343 proteins were identified, with 236 meeting the criteria for protein quantitation. These criteria include the identification of at least two unique peptides with a MASCOT score >46 (p

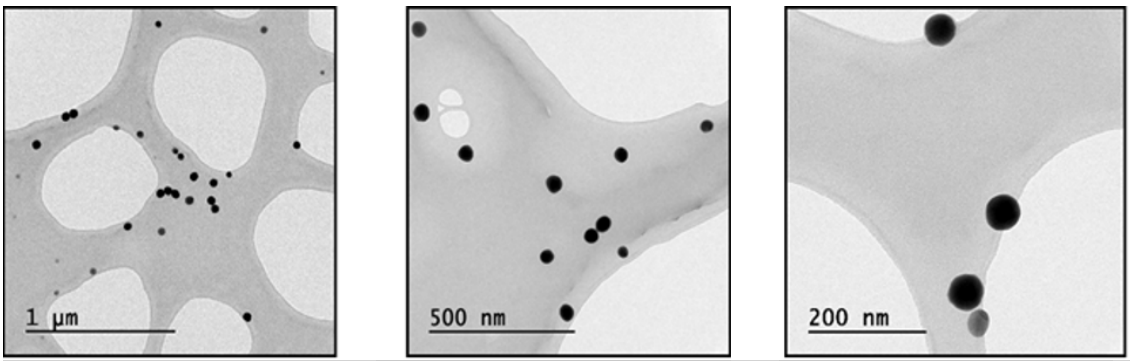

Figure 1. TEM micrographs of synthesized Ch-SeNPs.

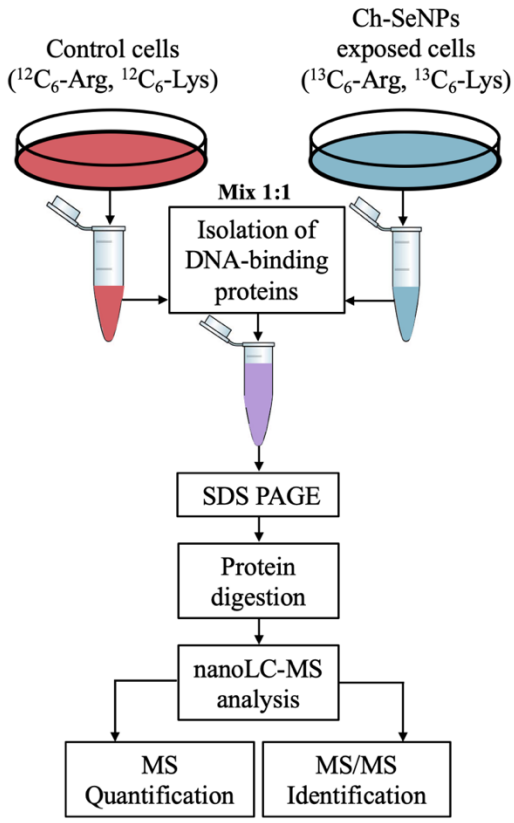

Figure 2. SILAC quantitative MS approach scheme.

< 0.01). The majority of these proteins exhibited a SILAC ratio close to 1, as expected for a 1:1 mixture. Applying a threshold ratio of 1.30, we identified 47 altered proteins, with 22 upregulated and 25 downregulated upon Ch-SeNPs exposure (Table 2).

A false discovery rate of 0.3% was estimated by the number of hits against the reverse sequence/total hits (p < 0.01). The mean relative standard deviation (RSD) of ratios obtained from biological replicates was lower than 20%, indicating good agreement between experiments. Subcellular localization of each protein was checked in Gene Ontonlogy (GO) database and confirmed that more than 62% of identified proteins came from the nucleus, 31% from cytoplasm, 3% from endoplasmic reticulum, 2% from mitochondria and 2% from plasma membrane, thus showing the usefulness of the purification protocol followed to isolate nuclear proteins. We also categorized the proteins based on their molecular and cellular functions using GO database, and the results pointed out that exposure to Ch-SeNPs mainly

Table 2. Differentially expressed proteins in HepG2 cells exposed to 1 mg/L of Ch-SeNPs

Accession number (gi)	*Protein Name*	*Common Name*	R_{SILAC}	*RSD (%)*
41322923	plectin isoform 1a	PLEC	-4,07	13,81
4506687	40S ribosomal protein S15	RPS15	-2,71	0,86
5453740	myosin regulatory light chain 12A	MYLA12	-1,82	14,59
54792069	small ubiquitin-related modifier 2 isoform a precursor	SUMO2	-1,78	0,89
4504257	histone H2B type 1-C/E/F/G/I	H2BC4	-1,74	19,97
7330335	chloride intracellular channel protein 4	CLIC4	-1,58	18,46
4502709	cyclin-dependent kinase 1 isoform 1	CDK1	-1,46	7,28
30581135	structural maintenance of chromosomes protein 1A	SMC1A	-1,45	12,10
4504445	heterogeneous nuclear ribonucleoprotein A1 isoform a	HNRNPA1	-1,45	16,43
15431288	60S ribosomal protein L10a	RPL10a	-1,44	19,40
4557469	AP-2 complex subunit beta isoform b	AP2B1	-1,44	17,89
4885379	histone H1.4	H14	-1,41	16,00
4758012	clathrin heavy chain 1	CHC1	-1,41	12,69
4758302	enhancer of rudimentary homolog	ERH	-1,40	13,45
4506753	ruvB-like 1	RUVB1	-1,40	3,85
6912638	ras suppressor protein 1 isoform 1	RSU1	-1,40	3,75
11067747	cell division cycle 5-like protein	CDC5	-1,39	9,69
5902076	serine/arginine-rich splicing factor 1 isoform 1	SRSF10	-1,37	14,14
42734325	wings apart-like protein homolog	WAPL	-1,37	14,99
4506697	40S ribosomal protein S20 isoform 2	RPS20	-1,36	11,27
110611218	ribosome-binding protein 1	RBP1	-1,34	14,83
188536047	SWI/SNF complex subunit SMARCC1	SMARCC1	-1,34	7,42
7657269	sister chromatid cohesion protein PDS5 homolog B	PDS5B	-1,33	15,08
21361114	mitochondrial 2-oxoglutarate/malate carrier protein	M2OM	-1,32	4,83
51477708	heterogeneous nuclear ribonucleoprotein D0 isoform d	HNRNPD	-1,31	2,54
21464101	14-3-3 protein gamma	YWHAG	1,31	2,49
4503477	elongation factor 1-beta	EFB1	1,32	3,98
5031653	pre-mRNA-splicing factor SPF27	SPF27	1,32	5,30
7706326	pre-mRNA branch site protein p14	SF3B6	1,33	16,12
24234747	interleukin enhancer-binding factor 2 isoform 1	ILF3	1,36	20,00
4505591	peroxiredoxin-1	PRDX1	1,38	18,46
47271443	serine/arginine-rich splicing factor 2	SRSF2	1,38	0,17
5031875	lamin isoform C	LMNC	1,38	19,27
62414289	vimentin	VIM	1,39	17,73
304555581	elongation factor 1-delta isoform 1	EFD1	1,41	13,73
11024700	mitochondrial import inner membrane translocase subunit	TIMM13	1,42	7,95
4503249	protein DEK isoform 1	DEK	1,48	17,58
31543164	THO complex subunit 6 homolog isoform 1	THOC5	1,57	19,66
4503507	eukaryotic translation initiation factor 2 subunit 3	EIF2I	1,69	3,81
5803165	protein transport protein Sec61 subunit beta	SEC61B	1,72	19,92
11545813	UPF0428 protein CXorf56 isoform 1	CXorf56	1,79	14,14
148596949	nucleolar and coiled-body phosphoprotein 1	NOLC1	1,92	8,70
4505087	protein mago nashi homolog	MAGOH	1,95	19,75
4505773	prohibitin	PHB	2,02	13,66
7657381	pre-mRNA-processing factor 19	PRPF19	2,03	9,58
16507237	78 kDa glucose-regulated protein precursor	HSPA5	3,57	19,56
12025678	alpha-actinin-4	ACTN4	9,58	3,30

affected the mRNA metabolism, the cell cycle and the transcription process.

The antitumor potential of Ch-SeNPs, demonstrated in previous studies (Estevez et al., 2014; Lopez Heras, 2014), involves the arrest of the cell cycle in the S-G2/M phase. The protein CDK1 (R_{SILAC} = -1.46), known for promoting replicative DNA synthesis, was identified as the primary factor responsible for the G2/M phase cell cycle arrest (Liao et al., 2017). Our quantitative proteomics findings further support this cell cycle arrest by confirming the inhibition of CDK1 and other affected proteins. Since no other crucial proteins directly involved in the cell cycle were detected, we conducted gene expression analysis using the qPCR technique (**Figure 3**). This experiment validated the inhibition of CDK1 and revealed alterations in other genes that corroborate the cell cycle arrest. P21 upregulation (CDKN1A), known to inhibit the kinase activity of CDK1 (Abbas and Dutta, 2010), along with the inhibition of CCNB1 and CCNA1, which form a complex with CDK1 and are essential for cell progression into mitosis (Jang et al., 2016; Yang et al., 1999), were among the confirmed effects.

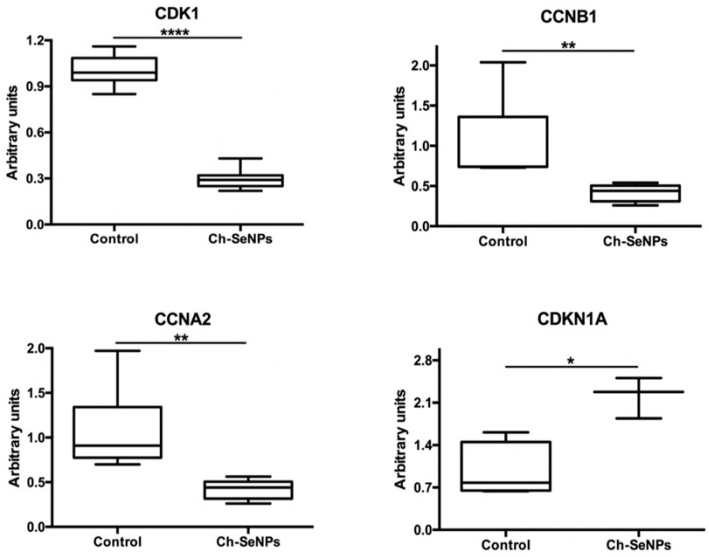

Figure 3. Relative expression of cell cycle-related genes qPCR.

Among the proteins experiencing deregulation, CDC5 (RSILAC = -1.39)

stands out as a vital component of the pre-mRNA splicing complex, crucial for cell cycle progression in yeast, plants, and mammals. There is evidence suggesting CDC5L overexpression in various tumors, including glioma and hepatocellular carcinoma. Knockdown of CDC5L has been shown to significantly impede tumor cell proliferation in glioma and hepatocellular carcinoma by inducing cell cycle arrest at the G2/M phase. In osteosarcoma, CDC5L overexpression has been linked to poor prognosis, making its inhibition a potential therapeutic strategy (Gräub et al., 2008; Wang et al., 2016). Other deregulated proteins play key roles in sister chromatids cohesion and condensation during the mitosis process, essential for proper chromosome segregation from the S phase to metaphase. SMC1 (RSILAC = -1.45) is instrumental in establishing linkages between duplicated DNAs during the S phase, contributing to DNA damage repair and maintaining genomic stability. Inhibiting SMC1 has been associated with growth suppression in various cancer cells through G1/S cell cycle phase arrest (Gandhi et al., 2006; Yi et al., 2017; Zhang et al., 2013). WAPL (RSILAC = -1.37) and its interaction with PDS5B (RSILAC = -1.33), both inhibited by Ch-SeNPs, are crucial in the cohesion process. Human WAPL expression has been linked to tumor progression, and inhibiting this protein arrests cells at the S phase (Oikawa et al., 2004). Another protein required for chromosome segregation during mitosis is ERH (RSILAC = -1.30), essential for recovering from cell cycle arrest induced by compounds like Ch-SeNPs. RNAi-mediated ERH knockdown leads to G2/M arrest (Kavanaugh et al., 2015; Pang et al., 2017; Weng and Luo, 2013). Related to cell cycle arrest, CHC1 (RSILAC = -1.41) and AP2B1 (RSILAC = -1.44), both downregulated by Ch-SeNPs, play roles in membrane trafficking and mitosis. Altered CHC function could contribute to oncogenesis, as CHC inhibition results in growth arrest, cessation of DNA synthesis, overduplication of centrosomes, and senescence (Blixt and Royle, 2011; Olszewski et al., 2014; Raman et al., 2015; Royle et al., 2005). On a different note, NOLC1 (RSILAC = 1.92), a phosphoprotein essential for rRNA synthesis and ribosome biosynthesis, induces a DNA damage response at telomeres when overexpressed, promoting apoptosis and cell cycle arrest (Duan et al., 2013; Yuan et al., 2017).

Certain deregulated proteins, despite not having a direct association with the cell cycle, exemplify the notable ability of Ch-SeNPs to significantly diminish tumors, making their expression modifications a subject of clinical interest. PLEC (RSILAC = -4.07), for instance; while it plays a critical role in organizing the cytoskeleton network in normal cells, its expression and mislocalization in tumor cells contribute to tumor progression. Silencing PLEC expression in pancreatic cancer cells has been demonstrated to negatively impact proliferation, invasion, and migration (Shin et al., 2013). Another intriguing protein is SUMO2 (RSILAC = -1.78), involved in reversible post-translational modification known as sumoylation. This modification is crucial for maintaining genomic integrity, regulating gene expression, and intracellular signaling. Numerous studies have established SUMO-regulated mechanisms in various cancers, and the inhibition of this protein has shown promise in reducing tumors. Consequently, compounds inhibiting SUMO are undergoing clinical trials for cancer treatment (Seeler and Dejean, 2017; Zhou et al., 2018). RSU1 (RSILAC = -1.40), an oncoprotein influencing cellular proliferation, differentiation, survival, and gene expression, has been associated with cancer development. Approximately 30% of human tumors harbor RSU1 mutations, with certain cancers, such as pancreatic cancer, exhibiting RSU1 mutations in nearly 100% of cases. Similar to SUMO, RSU1 inhibition constitutes a primary objective in numerous anticancer therapies (Gkretsi et al., 2017; Gurung and Bhattacharjee, 2015; O'Bryan, 2019). A parallel situation is observed with SMARCC1 (RSILAC = -1.34), a complex contributing to gene expression regulation by altering chromatin structure and enhancing the androgen receptor's transactivation. This protein is upregulated in prostate cancer, and its mutations are present in 20% of all human cancers (Heebøll et al., 2008; Helming et al., 2014). Additionally, H1.4 (RSILAC = -1.41), participating in nucleosome spacing and higher-order chromatin structure formation, specifically induces cell proliferation arrest upon depletion (Sancho et al., 2008). Lastly, PHB (RSILAC = 2.02) regulates mitochondrial respiration activity, and its overexpression represses AR-induced gene activation and suppresses tumor growth, particularly in

the context of aging (Koushyar et al., 2015).

On another hand, Ch-SeNPs trigger mechanisms that safeguard the cell. Notably, the protein PRDX1 (RSILAC = 1.38) takes center stage in this group. As an antioxidant protein, PRDX1 mitigates the adverse effects of reactive oxygen species (ROS) and exhibits the potential to enhance natural killer cell cytotoxicity while suppressing oncogenic proteins such as c-Myc (Ding et al., 2017). Furthermore, there is evidence of activated translation and transcription, reflected in the upregulation of numerous proteins involved in these processes, including SPF27 (RSILAC = 1.32), SF3B6 (RSILAC = 1.33), ILF3 (RSILAC = 1.36), EFB1 (RSILAC = 1.32), EFD1 (RSILAC = 1.41), THOC5 (RSILAC = 1.57), and EIF2I (RSILAC = 1.69) (Elgamal et al., 2016; Larochelle et al., 2012; Singh, 2018; Wu et al., 2018).

Nevertheless, the overexpression of specific proteins indicates that the progression of cancer has not been entirely curtailed. A notable example is YWHAG (RSILAC = 1.31), a protein that plays a crucial role in coordinating cell cycle progression, regulating responses to DNA damage, and is upregulated in melanoma cells resistant to cisplatin, etoposide, fotemustine, or vindesine (Gardinoa and Yaffe, 2011; Pennington et al., 2018). Another protein showing increased expression is VIM (RSILAC = 1.39), whose overexpression impedes apoptosis and enhances invasion (Chakraborty et al., 2019). Lastly, DEK (RSILAC = 1.48), HSPA5 (RSILAC = 3.57), and ACTN4 (RSILAC = 9.58) are upregulated proteins whose depletion results in slower tumor growth, making them potential biomarkers associated with malignant phenotypes (Cerezo and Rocchi, 2017; Chakraborty et al., 2019; Lee et al., 2019; Liu and Chu, 2017; Yang et al., 2015).

3.3. *In-vivo* inhibition of melanoma tumor growth after Ch-SeNPs exposure

To study the potential of Ch-SeNPs to suppress tumor growth, we challenge the mice ID with a poorly immunogenic tumor cells of melanoma origin in syngeneic C57BL/6J mice. The B16 cell line is widely used as a mouse model for melanoma induction that mimics human melanoma (Overwijk and Restifo, 2001). This subcutaneous model allows the development of ~1x1 cm tumors in approximately two weeks, becoming necrotic when they exceed

this size. B16 –induced melanoma aggressively progresses within a dynamic microenvironment allowing the study of anti-tumor effect of several molecules. The mice were then ID injected with $1x10^6$ B16 cells in

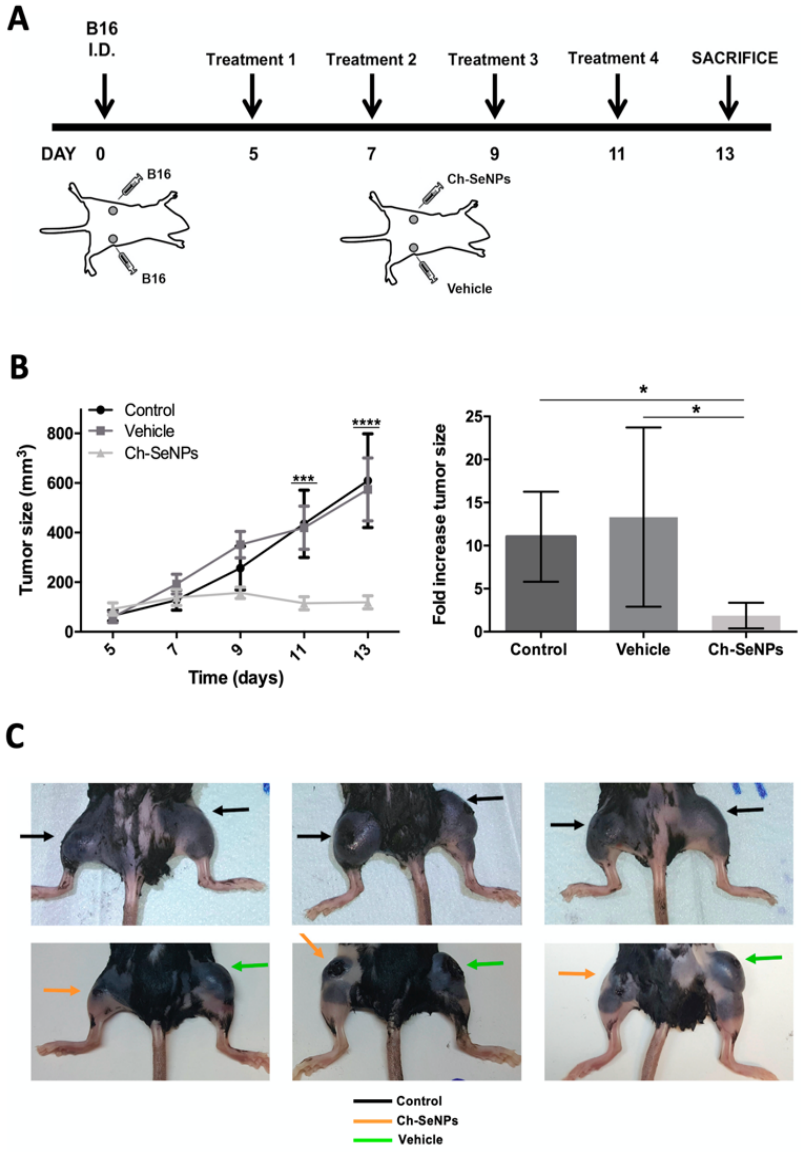

Figure 4. *In vivo* experiment. (A) Timeline, (B) tumor growth evaluation, (C) tumor photographs after 13 days.

(200 mg/L) in the right and left flank, respectively, on alternate days. The treatment least until the control tumors reach > 1.5 cm in diameter, approximately 2 weeks. After treatment the mice were sacrificed, and the tumors volume calculated (**Figure 4A**).

The average volume of the tumor growth was monitored every two days (Figure 4A). At the beginning of the

treatment, on day 5, the average tumor volume of the control mice was 65.234 $mm^3 \pm 20.998$, likely the average volume of the vehicle-treated tumour and the Ch-SeNPs treated tumours was 58.576 mm^3 ± 21.932 and 92.206 mm^3 ± 25.126 respectively, in the same period (Figure 4B). After 13 days, the average tumor volume of the control increased to 609.078 mm^3 ± 189.431 (8.6-fold increase), the vehicle treated tumors volumen increased to 574.420 mm^3 ± 127.301 (13.2-fold increase) whereas the Ch-SeNPs treated tumors volume barely increased to 119.170 mm^3 ± 26.604, meaning only 1.8-fold increase of the tumor volume in the same period (**Figure 4B**). Therefore, i.t. administration of 200mg/l Ch-SeNPs substantially suppressed tumor growth. Furthermore, we also monitored the weight and general health parameters of mice, and we do not observe a significant body weight changes or worsening of general health of the mice derived of the treatment with Ch-SeNPs.

4. Conclusions

In this study, we characterized chitosan-stabilized selenium nanoparticles (Ch-SeNPs) by acquiring TEM micrographs, confirming their spherical morphology and homogeneous sizes in the range of 40-60 nm. These results support previous synthesis efforts and provide a detailed assessment of the physical and chemical properties of Ch-SeNPs. At the nuclear level, we explored the mechanisms of action of Ch-SeNPs using a SILAC-based approach on the nuclear proteome. We identified 343 proteins, of which 236 met the criteria for protein quantitation. These findings unveiled alterations in 47 proteins, with 22 increased and 25 decreased following exposure to Ch-SeNPs. The majority of these proteins belonged to the cellular nucleus, underscoring the efficacy of the employed purification protocol. Functional assessment highlighted the influence of Ch-SeNPs on key processes such as mRNA metabolism, the cell cycle, and transcription. We confirmed the anti-tumor potential of Ch-SeNPs by inducing cell cycle arrest in the S-G2/M phase. CDK1 was identified as a key player in this arrest, supporting previous studies and providing a deeper understanding of the molecular mechanisms involved. Additionally, we observed the ability of Ch-SeNPs to modulate proteins not directly related to the cell cycle, emphasizing their multifaceted impact on tumor inhibition. Proteins such as PLEC, SUMO2, RSU1,

and SMARCC1 exhibited significant alterations, highlighting their clinical relevance and suggesting new therapeutic avenues. In an *in vivo* context, we demonstrated the effectiveness of Ch-SeNPs in suppressing tumor growth in a murine melanoma model. Intra-tumoral administration of Ch-SeNPs resulted in a significant reduction in tumor volume, underscoring their promising therapeutic application. Importantly, Ch-SeNPs administration showed no adverse impact on body weight or general health in mice, supporting the safety of this therapeutic approach. In summary, this study provides a comprehensive characterization of Ch-SeNPs, reveals their effects at the molecular and cellular levels, and validates their *in vivo* efficacy as an anti-tumor agent. These findings support the biomedical potential of Ch-SeNPs and open new perspectives for their clinical application in cancer treatment.

Acknowledgements

This work was supported by Ministerio de Ciencia e Innovación (MINECO) grant PID2020-114529RB-I00. Hector Estevez acknowledges Ministry of Science, Innovation and Universities from the Spanish Government for a pre-doctoral fellowship (PRE2018-084196)

References

Abbas, T., Dutta, A., 2010. P21 in Cancer: intricate networks and multiple activities Tarek. Nat. Rev. Cancer 9, 400–414.

Bai, Y., Wang, Y., Zhou, Y., Li, W., Zheng, W., 2008. Modification and modulation of saccharides on elemental selenium nanoparticles in liquid phase. Materials Letters 62, 2311-2314.

Blixt, M.K.E., Royle, S.J., 2011. Clathrin Heavy Chain Gene Fusions Expressed in Human Cancers: Analysis of Cellular Functions. Traffic 12, 754–761.

Cerezo, M., Rocchi, S., 2017. New anti-cancer molecules targeting HSPA5/BIP to induce endoplasmic reticulum stress, autophagy and apoptosis. Autophagy 13, 216–217.

Chakraborty, S., Kumar, Aviral, Faheem, M.M., Katoch, A., Kumar, Anmol, Jamwal, V.L., Nayak, D., Golani, A., Rasool, R.U., Ahmad, S.M., Jose, J., Kumar, R., Gandhi, S.G., Dinesh Kumar, L., Goswami, A., 2019. Vimentin activation in early apoptotic cancer cells errands survival pathways during DNA damage inducer CPT treatment in colon carcinoma model. Cell Death Dis. 10, 1–16.

Chaturvedi, V.K., Singh, A., Singh, V.K., Singh, M.P. 2019. Cancer nanotecnology: a new revolution for cancer diagnosis and therapy. Curr. Drug Metab. 20, 416-429.

Chen, E., Yates 3rd, J.R., 2007. Cancer proteomics by quantitative shotgun proteomics. Mol. Oncol. 1, 144-159.

Ding, C., Fan, X., Wu, G., 2017. Peroxiredoxin 1 – an antioxidant enzyme in cancer. J. Cell. Mol. Med. 21, 193–202.

Duan, X., Zhang, J., Liu, S., Zhang, M., Wang, Q., Cheng, J., 2013. Methylation of nucleolar and coiled-body phosphoprotein 1 is associated with the mechanism of tumorigenesis in hepatocellular carcinoma. Oncol. Rep. 30, 2220–2228.

Elgamal, S., Artsimovitch, I., Ibba, M., 2016. Maintenance of transcription-translation coupling by elongation factor P. MBio 7, 1–11.

Estevez, H., Garcia-Lidon, J.C., Camara, C., Luque-Garcia, J.L., 2014. Effects of chitosan-modified selenium nanoparticles on cell proliferation,

apoptosis and cell cycle pattern in HepG2 cells: Comparison with other selenospecies. Colloids Surfaces B Biointerfaces 122, 184–193.

Estevez, H., Garcia-Calvo, E., Rivera-Torres, J., Vallet-Regi, M., Gonzalez, B., Luque-Garcia, J.L., 2021. Transcriptome analysis identifies novel mechanisms associated with the antitumor effect of chitosan-stabilized selenium nanoparticles. Pharmaceutics 13, 356.

Estevez, H., Garcia-Calvo, E., Mena, M.L., Alvarez-Fernandez Garcia, R., Luque-Garcia, J.L., 2023. Unraveling the mechanisms of Ch-SeNPs cytotoxicity against cancer cells: insights from targeted and untargeted metabolomics. Nanomaterials 13, 2204.

Gandhi, R., Gillespie, P.J., Hirano, T., 2006. Human Wapl Is a Cohesin-Binding Protein that Promotes Sister-Chromatid Resolution in Mitotic Prophase. Curr. Biol. 16,

Gardinoa, A.K., Yaffe, M.B., 2011. 14-3-3 Proteins As Signaling Integration Points for Cell Cycle Control and Apoptosis. Semin Cell Dev Biol. 22, 688–695.

Gkretsi, V., Stylianou, A., Louca, M., Stylianopoulos, T., 2017. Identification of Ras suppressor-1 (RSU-1) as a potential breast cancer metastasis biomarker using a three-dimensional in vitro approach. Oncotarget 8, 27364–27379.

Goto, Y., Yamagishi, Y., Shintomi-Kawamura, M., Abe, M., Tanno, Y., Watanabe, Y., 2017. Pds5 Regulates Sister-Chromatid Cohesion and Chromosome Bi-orientation through a Conserved Protein Interaction Module. Curr. Biol. 27, 1005–1012.

Gräub, R., Lancero, H., Pedersen, A., Chu, M., Padmanabhan, K., Xu, X.Q., Spitz, P., Chalkley, R., Burlingame, A.L., Stokoe, D., Bernstein, H.S., 2008. Cell cycle-dependent phosphorylation of human CDC5 regulates RNA processing. Cell Cycle 7, 1795–1803.

Guo, Y., Deng, X., Wang, S., Yuan, Y., Guo, Z., Hao, H., Jiao, Y., Li, P., Han, S., 2023. SILAC proteomics based on 3D cell spheroids unveils the role of RAC2 in regulating the crosstalk between triple-negative breast cancer cells and tumor-associated macrophages. Int. J. Biol. Macromol. 254, 127639.

Gurung, A.B., Bhattacharjee, A., 2015. Significance of Ras Signaling in Cancer

and Strategies for its Control. Oncol. Hematol. Rev. 11, 147–152.

Hartman, T., Stead, K., Koshland, D., Guacci, V., 2000. Pds5p is an essential chromosomal protein required for both sister chromatid cohesion and condensation in Saccharomyces cerevisiae. J. Cell Biol. 151, 613–626.

Heebøll, S., Borre, M., Ottosen, P.D., Andersen, C.L., Mansilla, F., Dyrskjøt, L., Ørntoft, T.F., Tørring, N., 2008. SMARCC1 expression is upregulated in prostate cancer and positively correlated with tumour recurrence and dedifferentiation. Histol. Histopathol. 23, 1069–1076.

Helming, K.C., Wang, X., Roberts, C.W.M., 2014. Vulnerabilities of mutant SWI/SNF complexes in cancer. Cancer Cell 26, 309–317.

Jang, S.H., Kim, A.R., Park, N.H., Park, J.W., Han, I.S., 2016. DRG2 regulates G2/M progression via the cyclin B1-Cdk1 complex. Mol. Cells 39, 699–704.

Kavanaugh, G., Zhao, R., Guo, Y., Mohni, K.N., Glick, G., Lacy, M.E., Hutson, M.S., Ascano, M., Cortez, D., 2015. Enhancer of Rudimentary Homolog Affects the Replication Stress Response through Regulation of RNA Processing. Mol. Cell. Biol. 35, 2979–2990.

Koushyar, S., Jiang, W.G., Dart, D.A., 2015. Unveiling the potential of prohibitin in cancer. Cancer Lett. 369, 316–322.

Larochelle, M., Lemay, J.F., Bachand, F., 2012. The THO complex cooperates with the nuclear RNA surveillance machinery to control small nucleolar RNA expression. Nucleic Acids Res. 40, 10240–10253.

Lee, K.F., Tsai, M.M., Tsai, C.Y., Huang, C.G., Ou, Y.H., Hsieh, C.C., Hsieh, H.L., Wang, C.S., Lin, K.H., 2019. DEK is a potential biomarker associated with malignant phenotype in gastric cancer tissues and plasma. Int. J. Mol. Sci. 20, 1–19.

Liao, H., Ji, F., Ying, S., 2017. CDK1: Beyond cell cycle regulation. Aging (Albany. NY). 9, 2465–2466.

Liu, X., Chu, K.M., 2017. α-Actinin-4 promotes metastasis in gastric cancer. Lab. Investig. 97, 1084–1094.

Lopez Heras, I., 2014. Effect of Chitosan-Stabilized Selenium Nanoparticles on Cell Cycle Arrest and Invasiveness in Hepatocarcinoma Cells

Revealed by Quantitative Proteomics. J. Nanomed. Nanotechnol. 05.

O'Bryan, J.P., 2019. Pharmacological Targeting of RAS: Recent Success with Direct Inhibitors. Pharmacol. Res. 139, 503–511.

Oikawa, K., Ohbayashi, T., Kiyono, T., Nishi, H., Isaka, K., Umezawa, A., Kuroda, M., Mukai, K., 2004. Expression of a novel human gene, human wings apart-like (hWAPL), is associated with cervical carcinogenesis and tumor progression. Cancer Res. 64, 3545–3549.

Olszewski, M.B., Chandris, P., Park, B.C., Eisenberg, E., Greene, L.E., 2014. Disruption of Clathrin-Mediated Trafficking Causes Centrosome Overduplication and Senescence. Traffic 15, 60–77.

Overwijk, W.W., Restifo, N.P., 2001. B16 as a mouse model for human melanoma. Curr. Protoc. Immunol. Chapter 20:Unit 20.1.

Pang, K., Lv, Q., Ning, S., Hao, L., Shi, Z., Zang, G., Shen, K., Zhu, X., Zhu, G., Wang, X., Han, C., 2017. ERH is up-regulated in bladder cancer and regulates the proliferation and apoptosis of T24 bladder cancer cells. Int. J. Clin. Exp. Med. 10, 15269–15277.

Pennington, K., Chan, T., Torres, M., Andersen, J., 2018. The dynamic and stress-adaptive signaling hub of 14-3-3: emerging mechanisms of regulation and context-dependent protein–protein interactions. Oncogene 37, 5587–5604.

Raman, D., Sai, J., Hawkins, O., Richmond, A., 2015. Adaptor Protein2 (AP2) orchestrates CXCR2-mediated cell migration. Traffic 15, 451–469.

Royle, S.J., Bright, N.A., Lagnado, L., 2005. Clathrin is required for the function of the mitotic spindle. Nature 434, 1152–1157.

Sancho, M., Diani, E., Beato, M., Jordan, A., 2008. Depletion of human histone H1 variants uncovers specific roles in gene expression and cell growth. PLoS Genet. 4, 1–17.

Seeler, J.S., Dejean, A., 2017. SUMO and the robustness of cancer. Nat. Rev. Cancer 17, 184–197.

Shin, S.J., Smith, J.A., Rezniczek, G.A., Pan, S., Chen, R., Brentnall, T.A., Wiche, G., Kelly, K.A., 2013. Unexpected gain of function for the scaffolding protein plectin due to

mislocalization in pancreatic cancer. Proc. Natl. Acad. Sci. U. S. A. 110, 19414–19419.

Singh, R., 2018. RNA – Protein Interactions That Regulate Pre-mRNA Splicing. Gene Expr. 10, 79–92.

Sun, T., Zhang, Y.S., Pang, B., Hyun, D.C., Yang, M., Xia, Y., 2014. Engineered nanoparticles for drug delivery in cancer therapy. Angew Chem. Int. Ed. Engl. 53, 12320-12364.

Tan, H.T., Lee, Y.H., Ching, M.C.M., 2012. Cancer proteomics. Mass Spectrom. Rev. 31, 583-605.

Tang, W., Fan, W., Lau, J., Deng, L., Shen, Z., Chen, X., 2019. Emerging blood-brain-barrier-crossing nanotechnology for brain cancer theranostics. Chem. Soc. Rev. 48, 2967-3014.

Wang, Y., Chang, H., Gao, D., Wang, L., Jiang, N., Yu, B., 2016. CDC5L contributes to malignant cell proliferation in human osteosarcoma via cell cycle regulation. Int. J. Clin. Exp. Pathol. 9, 10451–10457.

Weng, M.T., Luo, J., 2013. The enigmatic ERH protein: Its role in cell cycle, RNA splicing and cancer. Protein Cell 4, 807–812.

Wu, T.H., Shi, L., Adrian, J., Shi, M., Nair, R. V., Snyder, M.P., Kao, P.N., 2018. NF90/ILF3 is a transcription factor that promotes proliferation over differentiation by hierarchical regulation in K562 erythroleukemia cells. PLoS One 13, 1–21.

Yang, R., Müller, C., Huynh, V., Fung, Y.K., Yee, A.S., Koeffler, H.P., 1999. Functions of Cyclin A1 in the Cell Cycle and Its Interactions with Transcription Factor E2F-1 and the Rb Family of Proteins. Mol. Cell. Biol. 19, 2400–2407.

Yang, Z., Zhuang, L., Szatmary, P., Wen, L., Sun, H., Lu, Y., Xu, Q., Chen, X., 2015. Upregulation of heat shock proteins (HSPA12A, HSP90B1, HSPA4, HSPA5 and HSPA6) in tumour tissues is associated with poor outcomes from HBV-related early-stage hepatocellular carcinoma. Int. J. Med. Sci. 12, 256–263.

Yi, F., Wang, Zhuo, Liu, J., Zhang, Y., Wang, Zhijun, Xu, H., Li, X., Bai, N., Cao, L., Song, X., 2017. Structural maintenance of chromosomes protein 1: Role in genome stability and

tumorigenesis. Int. J. Biol. Sci. 13, 1092–1099.

Yuan, F., Li, G., Tong, T., 2017. Nucleolar and coiled-body phosphoprotein 1 (NOLC1) regulates the nucleolar retention of TRF2. Cell Death Discov. 3, 1–9.

Zhang, H., Xu, Y., Papanastasopoulos, P., Stebbing, J., Giamas, G., 2014. Broader implications of SILAC-based proteomics for dissecting signaling dynamics in cancer. 11, 713-731.

Zhang, Y.F., Jiang, R., Li, J.D., Zhang, X.Y., Zhao, P., He, M., Zhang, H.Z., Sun, L.P., Shi, D.L., Zhang, G.X., Sun, M., 2013. SMC1A knockdown induces growth suppression of human lung adenocarcinoma cells through G1/S cell cycle phase arrest and apoptosis pathways in vitro. Oncol. Lett. 5, 749–755.

Zhou, Y., Ji, C., Cao, M., Guo, M., Huang, W., Ni, W., Meng, L., Yang, H., Wei, J.F., 2018. Inhibitors targeting the SUMOylation pathway: A patent review 2012-2015 (Review). Int. J. Mol. Med. 41, 3–12.

Capítulo 2. Diseño y síntesis de un nuevo nanosistema híbrido con base de SeNPs con potencial antitumoral

El **Capítulo 2** recoge la investigación que pretende diseñar, sintetizar, caracterizar y evaluar un nanosistema que tiene como objetivo conducir específicamente la acción antitumoral de las SeNPs hacia las células cancerígenas. Dicho nanosistema se construye en una base de nanopartículas de sílice mesoporosa a las que se ancla la proteína de targeting, en este caso transferrina, la cual tiene la capacidad para nuclear en su estructura nanopartículas de selenio.

Se llevaron a cabo múltiples ensayos bioanalíticos para evaluar la efectividad del targeting, la viabilidad o el ciclo celular. Asimismo, se realizó un ensayo de transcriptómica para obtener una información más detallada del proceso quimioterapéutico. Por último, se comprobó la efectividad del nanosistema en un *modelo in vivo*.

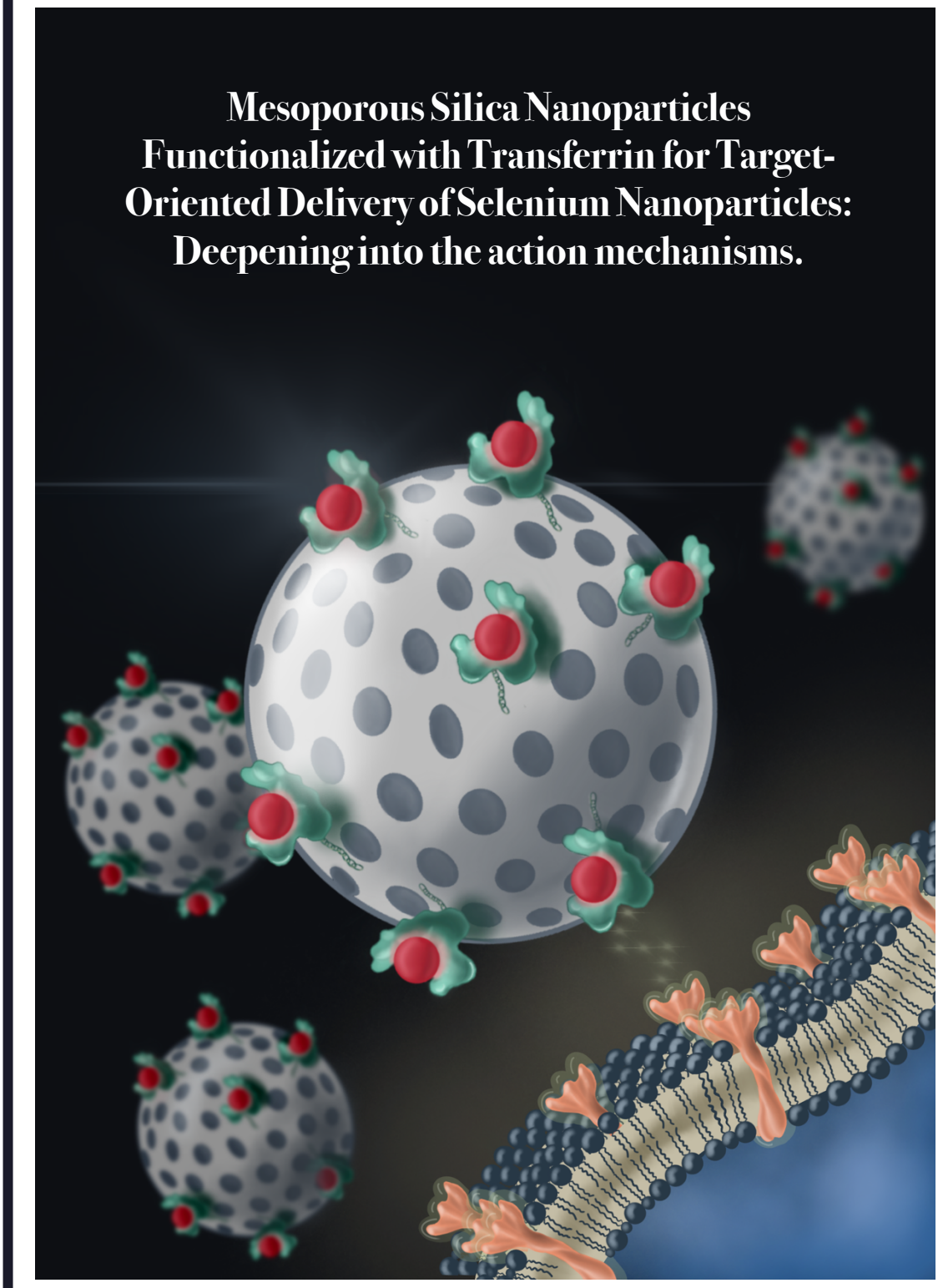
Mesoporous Silica Nanoparticles
Functionalized with Transferrin for Target-
Oriented Delivery of Selenium Nanoparticles:
Deepening into the action mechanisms.

2.1. Mesoporous Silica Nanoparticles Functionalized with Transferrin for Target-Oriented Delivery of Selenium Nanoparticles: Deepening into the action mechanisms

Hector Estevez, Sandra Montalvo-Quiros, Maria Vallet-Regí, Jose Rivera-Torres.
Blanca Gonzalez, Jose L. Luque-Garcia.

Enviado a Acta Biomaterialia (2023)

Abstract

The integration of nanotechnology in the development of novel anti-tumor drugs holds immense promise for enhancing targeted delivery, precision, and efficacy. In this context, this research presents the synthesis and characterization of a novel hybrid material, MSNs-Tf-SeNPs, designed for potential applications in cancer therapy. The material was synthesized through multi-step processes, involving the functionalization of mesoporous silica nanoparticles (MSNs) with transferrin protein to facilitate targeted delivery. Comprehensive analyses confirmed the successful incorporation of the protein and the uniform dispersion of selenium nanoparticles (SeNPs) on the MSNs surface. The material demonstrated selective internalization in cancer cells overexpressing transferrin receptors, establishing its suitability as a targeted therapeutic agent. Furthermore, MSNs-Tf-SeNPs exhibited dose-dependent cytotoxicity and induced cell cycle arrest at S-G2/M phases, indicative of its potential impact on cancer cell growth. Transcriptome analysis revealed significant alterations in gene expression associated with diverse cellular processes, emphasizing the multifaceted anti-tumor effects of the nanosystem. Additionally, the nanosystem was shown to induce a senescence-related pathway in hepatocarcinoma cells, triggering immune responses and a senescence-associated secretory phenotype. Finally, *in vivo* experiments using a chicken embryo model not only confirmed the anti-tumoral ability of the nanosystem, but also demonstrated its effectiveness in reducing cellular proliferation.

1. Introduction

In the recent years, potential of nanoparticles for a wide range of applications have been explored. In comparison with bulk materials, nanoparticles present novel physical-chemical properties (high surface area, nanoscale size, optical and magnetic properties, reactivity, etc) that can significantly improve challenges of a great variety of domestic and commercial tasks. Specifically, nanoparticles have rapidly gained special relevance for the research of therapeutic applications because of their cytotoxic effect on cancer cells or even for their value as nanocarriers of anticancer drugs (Pugazhendhi et al., 2018). Moreover, one of the most urgent matters in nanotechnology is the development of nanosystems able to transport and specifically deliver drugs to the affected tissue.

Both, organic and inorganic nanoparticles have earned a central role in many biomedical investigations because of their bioavailability, low toxicity and biological activity. In addition, they can also be employed as diagnosis tools (Bayda et al., 2018). Among a great variety of elements, selenium has always received attention as a supplement for major chronic metabolic diseases due to its antioxidant properties. Also, the lack of selenium impairs the synthesis of selenoproteins, leading to various disorders such as Keshan disease, thyroid dysfunction, arthrophyma or cognitive limitation (Guan et al., 2018). Moreover, selenium nanoparticles (SeNPs) have been proposed for a large number of purposes; they can be used as chemopreventive or chemotherapeutic agent, also they have been tested as antimicrobials and antifungals, drug delivery carriers, and even protective agents against metal intoxication (Hosnedlova et al., 2018). We previously described how SeNPs in comparison to other inorganic and organic selenospecies, are able to impair HepG2 cell cycle proliferation by partially inhibiting the expression of Cdk1, key in controlling the progression from S/G2 to M phase, and therefore impairing normal cell proliferation (Estevez et al., 2014). Similarly, it was found by means of quantitative proteomics that SeNPs appear to deregulate the eIF3 complex, which also lead to a cell cycle arrest (Lopez-Heras et al., 2014).

Although SeNPs are able to interfere with tumor development by inducing cell cycle arrest, they should be effectively delivered to the tumor in

order to prevent any off-target effects. In this sense, several strategies have been proposed to specifically target the tumor cells. Those approaches are based on building drug complexes with improved safety, solubility, pharmacokinetic profiles, and therapeutic efficacy, while accomplishing optimal drug delivery in cancerous tissues (Kumari et al., 2016). Hence, the aim of the study is the synthesis and characterization of a hybrid nanosystem that consists on a biocompatible matrix of mesoporous silica nanoparticles decorated with a targeting protein, transferrin, that also allows for the nucleation of selenium nanoparticles onto the surface of the nanoparticle (MSNs-Tf-SeNPs). The ability of the synthesized nanosystem, together with its capacity to induce cytotoxicity and alterations in the cell cycle profile, has been evaluated. In addition, the mechanisms of action of the proposed nanosystem have been evaluated by transcriptomics analysis, allowing the identification of key pathways involved in the therapeutic effect of MSNs-Tf-SeNPs, that reinforce the potential of the designed nanosystem as potential antitumoral drug.

At last, the potential of the nanosystem has also been effectively assessed using an *in vivo* chicken embryo model.

2. Materials and methods

2.1. Material Synthesis.

The starting materials denoted MSNs, MSNs-$COOH_{ext}$ and MSNs-Tf were synthesized as previously described (Montalvo-Quiros et al., 2019). Briefly, under N_2 atmosphere, 3-Aminopropyltriethoxysilane (APTS) (5 μL, 0.023 mmol) was added over a stirred fluorescein isothiocyanate (FITC) (2 mg, 0.005 mmol) solution in ethanol (0.5 mL); the mixture was stirred for 2 h in the dark and then added to a mixture of ethanol (1 mL) and tetraethylorthosilicate (TEOS) (5 mL, 23 mmol). The cationic surfactant cetyltrimethylammonium bromide (CTAB) (1 g, 2.74 mmol) was dissolved in 480 mL of water with 3.75 mL of NaOH 2 M and the solution was heated to 80 °C. Then, the solution containing TEOS and the silane-modified fluorescein was slowly added at a constant rate of 0.43 mL/min under vigorous stirring. The reaction was stirred for 1 h at 80 °C in the dark, centrifuged, and the particles were subsequently washed. CTAB-containing MSNs (40% wt) were dehydrated at 80

°C, under vacuum for 3 h in the dark, and then re-dispersed under an inert atmosphere in dry toluene (58 mL). A solution of 3-(triethoxysilyl)propylsuccinic anhydride (TESPSA) (145 mg, 10% exc.) in 15 mL of dry toluene was added to the vigorously stirred suspension of the CTAB-containing MSNs and the mixture was heated to 110 °C overnight in the dark. The reaction mixture was centrifuged and the obtained solid was exhaustively washed and finally dried. The surfactant was removed from the functionalized material by heating a well-dispersed suspension of the obtained solid in ethanol (360 mL), water (40 mL) and HCl (10 mL) overnight at 60 °C; the solid was then washed with water and ethanol. Before conjugation of the transferrin protein, the –COOH groups on the surface of MSNs-$COOH_{ext}$ were activated. N-(3-dimethylaminopropyl)-N′-ethylcarbodiimide hydrochloride (EDC·HCl) (820 mg, 10 equiv. per nominal –COOH group) was dissolved in water and added to a vigorously stirred suspension of MSNs-$COOH_{ext}$ (0.4 g) well dispersed in water (150 mL, HPLC grade). The mixture was stirred at RT for 3 h in the dark, centrifuged and rinsed with water. Then, activated MSNs-$COOH_{ext}$ was re-dispersed in 2-morpholinoethanesulfonic acid (MES) monohydrate (50 mM, pH depending on the protein) under gentle stirring. After that, transferrin was dissolved in 50 mM MES monohydrate (pH 6) and added over the material suspension. The mixture was stirred overnight in the dark, centrifuged and the solid was exhaustively washed. The resulting material was denoted as MSNs-Tf.

For the synthesis of MSNs-Tf-SeNPs, 50 mg of MSNs-Tf were dispersed in 8.45 mL of water under controlled agitation. 2.4 M (1.132 mL) acetic acid was added to this dispersion, followed by 37.5 µL of 0.54 M Na_2SeO_3. Finally, drop by drop under controlled stirring, 1.698 mL of 0.23 M ascorbic acid were added to the previous mixture to allow reduction of Se^{4+} and the formation of Se nanoparticles (SeNPs) during 16 h under vigorous stirring. The synthesis of the material used as control and containing bovine serum albumin (BSA) instead of transferrin (MSNs-BSA-SeNPs) was carried out under the same procedure with the exception of the pH used for anchoring the BSA to the MSNs, which was fixed at 4.8, below the isoelectric point of the protein.

2.2.Materials Characterization.

Mesoporous materials were characterized by means of the following techniques: transmission electron microscopy (TEM), energy dispersive X-ray spectroscopy (EDS), thermogravimetric and differential thermal analysis (TGA), chemical microanalysis, electrophoretic mobility measurements to calculate the values of the zeta-potential (ζ) and dynamic light scattering (DLS).

TEM and EDS characterizations were carried out with a JEOL JEM 1400 instrument operating at 120 kV (JEOL Ltd., Tokyo, Japan). Samples were first dispersed in water and then sonicated in a low power sonicator bath (Selecta, Sapin) during 5 min. Finally, one drop per sample was deposited onto carbon-coated copper grids.

TGA was performed with a Perkin Elmer Pyris Diamond TG/DTA analyser (Perkin Elmer, California, USA) by placing approximately 5 mg of sample in a platinum crucible applying 5 ºC/min heating ramps up to 800 ºC under a flow rate of 100 mL/min of air.

Zeta-potential (ζ) values of the nanosystems were calculated using electrophoretic mobility measurements of the materials suspended in water. The measurements were carried out with a Zetasizer Nano Zs (Malvem Instruments LTD., United Kingdom) equipped with a 633 nm "red" laser. Samples were added to water, then vortex and ultrasonicated to obtain a homogeneous suspension. Suspensions were placed in DTS1070 disposable folded capillary cells (Malvern Instruments). The hydrodynamic size of the nanoparticles was measured by dynamic light scattering (DLS) with the same Malvern instrument. Values presented are mean ± SD from quintuplicate measurements.

2.3. Cell Culture.

Two cell types were employed in this study: HepG2 and MC3T3 cells. While HepG2 cells (human hepatocellular carcinoma cell line, ATCC HB-8065 TM) overexpress transferrin receptor, MC3T3-E1 cells (mouse osteoblast-like cell line, ATCC CRL-2593 TM) show low expression of transferrin receptors. Both cell lines were maintained in Dulbecco´s modified Eagle´s medium (DMEM) supplemented with 10% fetal bovine serum (FBS) and 1% penicillin/streptomycin at 37 ºC and 5% CO_2.

2.4. Selective Internalization Assay.

HepG2 and MC3T3-E1 cells were seeded into 6-well plates and

exposed to 10 μg/mL of MSNs, MSNs-BSA-SeNPs and MSNs-Tf-SeNPs materials for 24 h. After this time, cell culture media was removed and cells were washed with phosphate buffer saline (PBS). A 0.25% trypsin-EDTA solution was added to the cells and after 5 min, trypsin reaction was stopped by adding culture media. At that time, 0,4% Trypan Blue solution was added in order to quench the fluorescence of the MSNs adsorbed on the outside of the cell membrane. Cells were then centrifuged at 300 g for 5 min and resuspended in PBS for analysis by flow cytometry.

2.5. Cytotoxicity Assay.

Cells were seeded in 96-well plates and incubated at 37 ºC under 5% CO_2 for 24 h prior to the experiment. Then, cells were exposed to ranging concentrations of MSNs-Tf-SeNPs (10, 50 and 100 μg/mL) and incubated for 72 h. After this time, 20 μL of 3-(4,5-dimethyl-thiazol-2-yl)2,5- diphenyl tetrazolium bromide (MTT, 5 mg/mL) were added to each well. After incubation for 5 h, the MTT solution was removed and 100 μL of dimethyl sulfoxide (DMSO) were added to each well to dissolve the purple formazan crystals formed by mitochondrial reduction of the MTT reagent. The absorbance at 595 nm was measured using a microplate reader (TECAN). The relation between the absorbance of treated vs. control cells was used to determine the cell viability.

2.6. Transcriptome Array Analysis.

To evaluate potential alterations in the mRNA expression levels of HepG2 cells treated with MSNs-Tf-SeNPs, a transcriptome microarray analysis was performed. HepG2 cells were exposed to either MSNs-Tf-SeNPs (10 μg/mL) or MSNs-Tf (as control) and incubated at 37 ºC under 5% CO_2 for 72 h. After the exposure time, extraction and purification of the mRNAs were carried out using a commercial kit following the manufacturer instructions (PureLink ®, Invitrogen). Briefly, cells were trypsinized, centrifuged and the supernatant was removed. Cells were lysed with lysis buffer containing 2-mercaptoethanol. Lysates were then centrifuged and one volume of 70 % ethanol was added to the samples. 700 μL of this volume were transferred to a conical tube and centrifuged. Afterwards, samples were rinsed with washing buffer and RNase-free water was added to the spin cartridge prior to centrifugation. The purified RNA was stored at -80 ºC for further analysis.

RNA integrity was assessed and only samples showing enough quality on RNA and 28S/18S ratios were used for further analyses.

The samples were processed with GeneChip® WT PLUS Reagent Kit (Applied Biosystems), hybridized with Clariom™ D Array, human (Applied Biosystems) and scanned with a GeneChip® Scanner 3000 7G (Applied Biosystems). Raw data were processed with RMA algorithm included in Transcriptome Analysis Console (Applied Biosystems) for normalization and gene level analysis. For each experimental condition, three microarray experiments corresponding to three independent RNA replicates were processed and analyzed. Fold changes between experimental conditions were calculated as a quotient between the mean of the gene expression signals. Statistical analysis was performed with e-bayes limma included in the Transcriptome Analysis Console (Applied Biosystems). Those values with an FDR (adjusted p-value) ≤ 0.05 were considered as significant.

2.7. Senescence Assay.

Since many senescence-associated transcripts were found de-regulated upon MSNs-Tf-SeNPs treatment, evaluation of the activity of β-galactosidase (only detectable in senescent cells, not in quiescent, immortal or tumorous cells) was conducted by cytochemical staining (Sigma-Aldrich senescence cells histochemical staining kit). Cells were exposed to MSNs-Tf (10 μg/mL), MSNs-Tf-SeNPs (10 μg/mL) or etoposide (10 and 50 μg/mL) and incubated at 37 ºC under 5% CO_2 for 72 h. After the exposure time, cell culture solutions were removed and cells were washed with PBS. Cells were fixed with a 20 % formaldehyde, 2% glutaraldehyde, 70.4 mM Na_2HPO_4, 14,7 mM KH_2PO_4, 1.37 M NaCl, and 26.8 mM KCl fixing buffer for 7 min at room temperature. After removing the fixing buffer, the cells were washed with PBS and incubated with the staining mixture. Cells were incubated overnight at 37 ºC without any additional CO_2, sealing plated to prevent from dryness. Cells were examined using a phase contrast microscope (Motic AE31) to reveal blue-stained senescent cells.

2.8. *In vivo* evaluation.

Experiments conducted *in vivo* using chicken embryos do not

necessitate special permits, provided the embryos are sacrificed prior to hatching, as was the case in this study. Premium specific pathogen-free (SPF) fertile chicken eggs at day 11 of fertilization were employed for chicken chorioallantoic membrane (CAM) xenografts. Triple negative breast cancer MDA-MB-231 cells were utilized for the experiment. Chicken eggs were initially incubated for 10 days at 37 ºC and 55% humidity, with regular rotation. A small window was opened over the air sac of fertilized eggs, and incubation continued until tumor inoculation. MDA-MB-231 cells, pre-treated with 10 μg/mL MSNs-Tf-SeNPs 24 h before the experiment, were inoculated into each egg. A cell suspension containing $2x10^6$ cells mixed with matrigel was deposited over a vein of the chicken embryo, and eggs were incubated for 24 h. Tumors were treated by adding 30 μL of a 10 μg/mL MSNs-Tf-SeNPs suspension, followed by a repeat treatment after 72 h. After an additional 72 h incubation, tumors were resected, weighed, and measured. Control eggs received culture medium over tumors.

3. Results and discussion

3.1. Material synthesis and characterization.

The final material was obtained with a synthesis in several steps (**Figure 1**). Initially, the MSNs were functionalized with carboxylic acid groups to facilitate the anchorage of the transferrin protein by amide bonds formation. This step of synthesis requires adequate pH conditions in order to avoid repulsions between the COOH groups, negatively charged on the surface of the MSNs, and the negatively charged protein groups. For this reason, the pH of the reaction was fixed below the isoelectric point of the protein (Luo et al., 2013). In addition, the functionalization was carried out with the optimal amount of protein that was evaluated in a previous study (Montalvo-Quiros et al., 2019). The modification of the initial MSNs material (4.5% wt) with carboxylic acids and the protein was evaluated by chemical analysis and TGA (**Table 1**, **shown in the end**) The increase in organic content (MSNs-Tf, 13.67% wt) after functionalization, as well as the percentage of sulfur and nitrogen, around 3% N and 0.3% S, confirms the incorporation of the protein (**Table 1**, **shown in the end**). Organic content (wt %) was determined from the TGA weight losses, excluding the weight loss due to the water desorption (up to 125 °C) and further corrected by

the weight loss of the remaining alkoxysilanes after the sol–gel reaction (surfactant extracted from the unmodified MSNs). Finally, nucleation of SeNPs to obtain the hybrid material involved the reduction of sodium selenite, the metallic ion precursor, using ascorbic acid. TEM micrographs of the material (MSNs-Tf-SeNPs) show a good dispersion of SeNPs onto the surface of the MSNs (**Figure 2**) with a homogeneous size of around 60 nm. The atomic percentages for Se and Si were measured by EDS analysis registered at low magnifications, showing 7.05% Se and 92.95% Si, which represent a 0.075 Se/Si molar ratio.

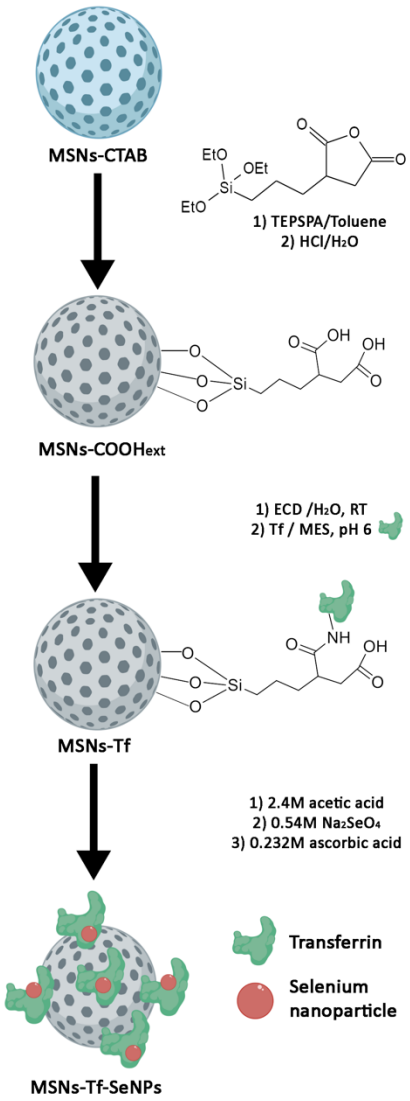

Figure 1. Synthesis steps for obtaining MSNs-Tf-SeNPs

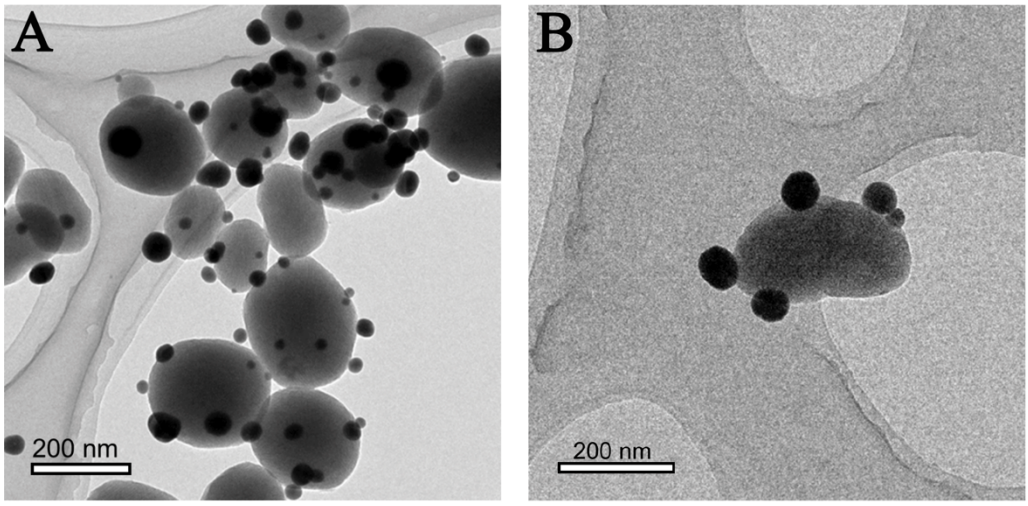

Figure 2. TEM micrographs of the synthesized MSNs-Tf-SeNPs

MSNs-Tf-SeNPs exhibit a ζ-potential value of 26 ± 8 mV (**Table 2**, **shown in the end**), what makes it be in the colloidal stability zone (Rosenholm et al., 2010). Dynamic light scattering (DLS) measurement shows a monomodal hydrodynamic size distribution of 164 ± 38 nm (**Table 2**, **shown in the end**). It also showed well-dispersed and homogeneous SeNPs with an average size of 50 nm and a 0.069 molar ratio of Se/Si. These characteristics show its resemblance to the MSNs-Tf-SeNPs material, apart from the anchored protein, thus demonstrating its suitability as a control.

3.2. MSNs-Tf-SeNPs selectively internalize in cells overexpressing TfR.

To prove the role of transferrin (Tf) as a suitable targeting ligand, two cell lines with significantly different expression levels of transferrin receptor (TfR) were used: HepG2 and MC3T3-E1 cells (Tang et al., 2019; Kawabata et al., 1999). Cells were exposed to 10 μg/mL of MSNs, MSNs-BSA-SeNPs and MSNs-Tf-SeNPs for 24 h. Next, flow cytometry was employed for evaluating the degree of internalization by the quantification of the intensity of fluorescent cells (**Figure 3**). While there were no significant differences in the degree of internalization of MSNs or MSNs-BSA-SeNPs in both cell lines, functionalization with transferrin resulted in a significant increase in the internalization of MSNs-Tf-SeNPs in HepG2 (high expression of TfR in their outer membranes) in comparison to

MC3T3-E1 cells (low TfR expression levels). Therefore, these results confirmed the selectivity of the transferrin mediated targeting towards cancer cells with high levels of TfR receptors.

3.3. Cytotoxicity of MSNs-Tf-SeNPs.

As evidences of successful transferrin-mediated targeting were obtained, the cytotoxic effect of the designed nanosystem was evaluated. Upon exposure of HepG2 cells to increasing amounts of MSNs-Tf-SeNPs (10, 50, and 100 µg/mL) for 72 h, cell viability was assessed by using the MTT assay, which correlates the reducing potential of cellular mitochondria with cell. Cells able to reduce the MTT compound to formazan (an insoluble purple colored compound) are considered viable. **Figure 4** shows that cell viability was significantly reduced in a dose-dependent manner, therefore proving the cytotoxic effect of the nanosystem at all the tested concentrations. Exposure to 10 µg/mL of MSNs-Tf-SeNPs was selected for further experiments in order to evaluate the functionality of the designed nanosystem at different levels without drastically compromising cell viability.

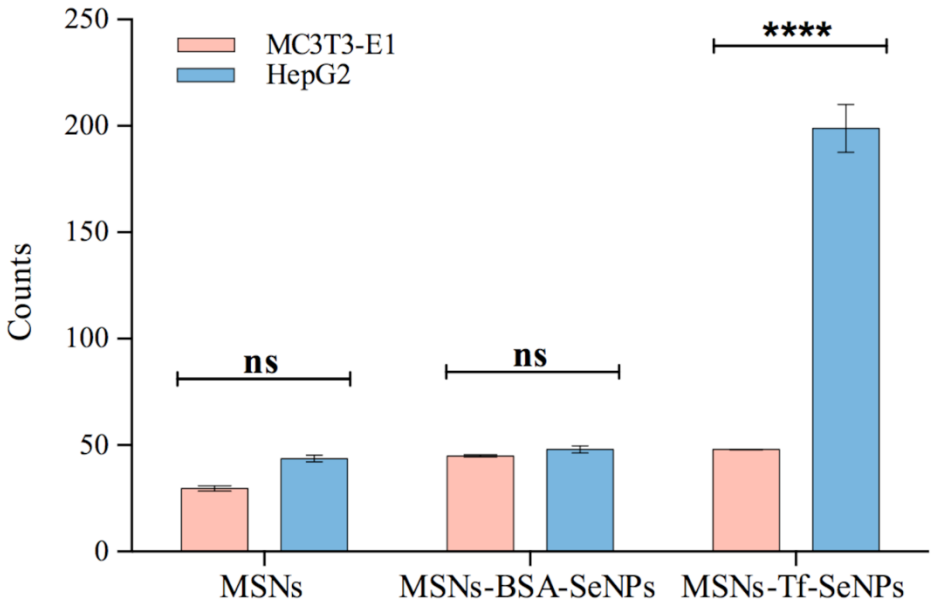

Figure 3. Cellular uptake of MSN materials evaluated on HepG2 and MC3T3 cells exposed to 10 µg/mL of MSNs, MSNs-BSA-SeNPs and MSNs-Tf-SeNPs for 24 h. Statistical significance: ****p < 0.0001.

3.4. MSNs-Tf-SeNPs induces cell cycle arrest at the S-G2/M phases.

One of the main features of SeNPs is their ability to induce cell cycle arrest by inhibiting Cdk1(Estevez et al., 2014; Estevez et al., 2021; Luo et al., 2012) rendering them particularly promising in cancer therapy. To demonstrate its functionality in the designed nanosystem (MSNs-Tf-SeNPs) we performed cell cycle analyses in a preclinical model by flow cytometry. Exposure to the nanosystem resulted in a clear decline of the cell population in G0/G1 phase in comparison to control cells (**Figure 5**). On the contrary, the population of cells undergoing S-G2/M phases was significantly higher after exposure to MSNs-Tf-SeNPs as compared to control cells and cells exposed to MSNs-Tf (**Figure 5**), thus demonstrating that the observed effect is unequivocally due to the presence of SeNPs in the nanosystem. These results are in agreement to previous experiments with SeNPs alone (Estevez et al., 2021; Estevez et al., 2023), and demonstrate the ability of the designed nanosystem to arrest the cell cycle in the S-G2/M phases, thus suggesting that mitotic damage and therefore

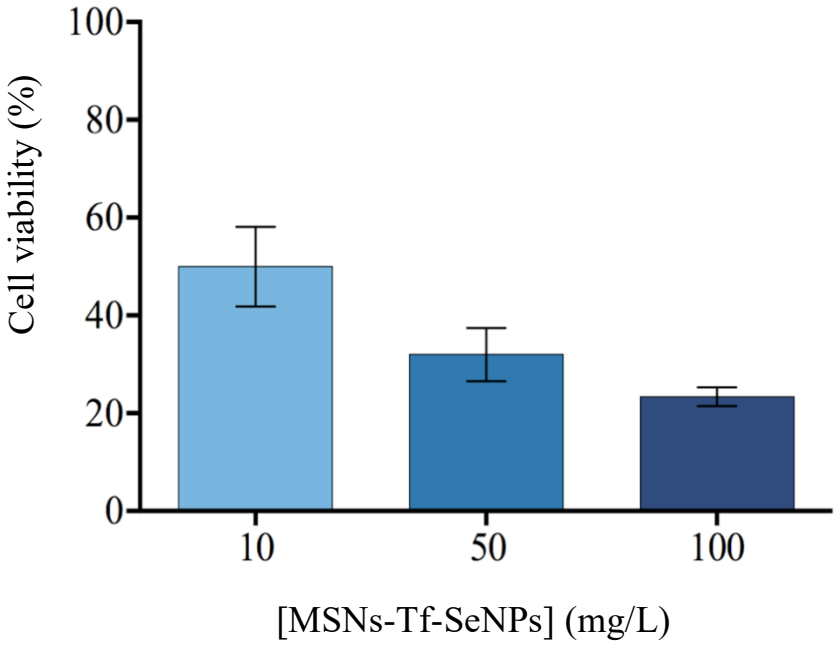

Figure 4. Viability of HepG2 cells exposed to different concentrations of MSNs-Tf-SeNPs.

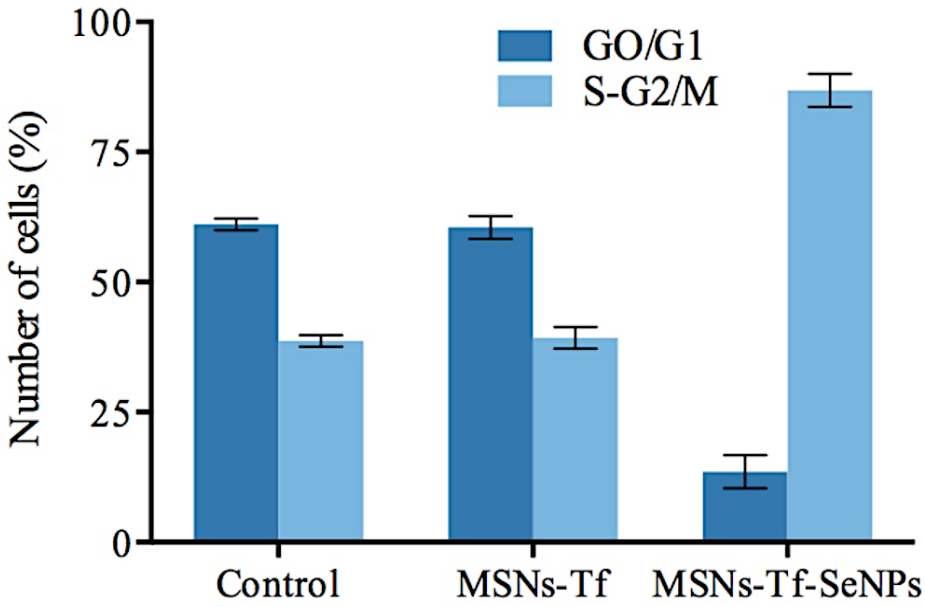

Figure 5. Cell cycle profile of HepG2 cells exposed to 10 µg/mL of MSNs-Tf-SeNPs

impairment of the cellular growth process is occurring.

3.5. Transcriptome analyses reveal the antitumor molecular mechanisms of action of MSNs-Tf-SeNPs.

Previous experiments revealed growth impairment of hepatocarcinoma cells upon exposure to our engineered nanosystem. To unravel the molecular mechanisms underlying its potentially therapeutic antitumor effect we aimed to investigate the gene expression signature from HepG2-treated cells by using whole transcriptomic data. Therefore, we performed pairwise differential expression to identify the pathways altered upon MSNs-Tf-SeNPs treatment.

Whole transcriptome comparisons of control versus MSNs-Tf-SeNPs treated cells to identify the differentially expressed genes with a $\log_2$ fold change of 1,5 and 0,5 (with a P-value < 0.05), demonstrated differential expression of a large number (278) of genes among the more than 20.000 well-annotated human genes analyzed. From those altered genes, 224 demonstrated up-regulation (ratios above 1,5) while the 54 remaining were down-regulated (ratios below 0.5) (**Table 3**, **shown in the end**). When comparing non-treated versus mock-treated cells, non-statistically significant genes profiles were identified (data not shown) suggesting that neither MSNs nor

MSNs-Tf explained the antitumoral effect demonstrated by our nanosystem, thus reinforcing previous data that indicated that SeNPs are the sole therapeutic active elements of the hybrid nanosystem.

MSNs-Tf-SeNPs demonstrated a wide effect on the expression of genes involved in a large variety of cellular processes such as cellular metabolism and energy, cell growth and maintenance, protein metabolism and enzyme activity, among others (**Table 3, shown in the end**). In addition, most of the genes found to be altered are directly related to molecular mechanisms involved in cancer-related processes; thus, their up- or down-regulation confirms the anti-tumor potential of the designed nanosystem. In this way, several genes that are considered as useful biomarkers in cancer appeared de-regulated after treatment with MSNPs-Tf-SeNPs. For example, aldolase B (ALDOB) was significantly inhibited in our results and its over-expression has been correlated to poor prognosis in several types of cancer including colorectal cancer (Tian et al., 2017) and hepatocellular carcinoma (Tao et al., 2015). In the same vein, a great number of evidences has supported the correlation between carcinogenesis and over-expression of protein members of the angiopoietin-like protein (ANGPTL) family, though their precise role has not been fully elucidated. If confirmed, they would represent new promising targets for therapeutic strategies (Carbone et al., 2018). Interestingly, the treatment of hepatocarcinoma cells with MSNPs-Tf-SeNPs revealed a strong down-regulation of some members of the family such as ANGPTL3 (0,28), ANGPTL7 (0,65) and. ANGPTL8 (0,32) suggesting the potential of our nanosystem to affect these promising therapeutic targets.

Cytochrome P450 genes encodes a family of enzymes that play a key role in the etiology of a great variety of cancers due to their implication in detoxification of potential carcinogens (involved in phase I metabolism of more than 80% of anticancer drugs). CYP450 inhibitors are being evaluated for their ability to improve pharmacokinetics and oral formulation of several chemotherapy agents (Mittal et al., 2015).

After exposing HepG2 cells to our nanosystem (MSNPs-Tf-SeNPs) we found a significant inhibition of the expression of several CYP450 genes, such as CYP2, CYP3A (0,34), CYP4 (0,43), CYP7 (0,45), and CYP17 (0,42).

CYP3A has already been confirmed as reliable prognostic marker for hepatocellular carcinoma (Yu et al., 2018), CYP17 inhibition is a potential targeting strategy for prostate cancer (Vasaitis et al., 2011), and up-regulated genes encoding CYP4 enzymes expression, is related to be a prognostic phenomenon in hepatocellular, breast, colon and ovarian cancers (Murray et al., 2010; Alexanian et al., 2012).

Inhibitors of DNA binding proteins are transcription regulatory factors that play critical roles in a wide range of cancerous metabolic processes, generally associated with poor prognosis and advanced clinical stages.

To date, only four members of ID proteins have been identified. ID1 (3,81) and ID2 (0,67) are the most intensively studied, sharing a similar helix-loop-helix motif with 79% homology and high conservation. ID3 (1,85) is closely related to ID1, exhibiting overlapping expression patterns, suggesting they could have similar functions. After nanosystem exposition, we found actively overexpressed ID1 and ID3, while ID2 is slightly down-regulated. Although ID proteins are rarely found in adult tissues, they have been reported to be altered in several human cancers. Specifically, ID1, ID2, ID3 are considered potential oncogenes (Ke et al., 2018). ID proteins expression is strongly influenced by many growth factors. For example, TGF-β (1,76), overexpressed in our experiment, induces transcription of ID1, which leads to tumor angiogenesis in pancreas cancers, and, therefore, inhibits cell proliferation (Lee et al., 2004). ID1 expression can also be promoted by early growth response gene (EGR, 2,60), clearly up-regulated also in our results.

The MAPK/ERK pathway, communicate signals from receptors in the surface of the cell to the DNA in the nucleus. The communication is mediated by phosphorylation, so, when protein expression is altered, signaling might be interrupted. Thus, new drugs that find targets to repair pathway dysfunctions are urgently needed for disease therapies. One of the key members of the mitogen-activated protein kinase family, ERK1/2, is responsible for delivering extracellular signals to the nucleus, and its role with aging processes depends on its target proteins/regulators, negative feedback loops, phosphorylation or translocation to the nucleus. Generally, it is accepted that ERK1/2 promotes senescence, while the key point for activation is the successful transmission of a signal from tyrosine receptors,

including epidermal growth factor receptor (EGFR, 1,43) that is significantly up-regulated in our results. ERK1/2 requires the phosphorylation of its threonine and tyrosine residues to develop its kinase function. Dual-specificity Thr/Tyr phosphatases (DUSPs) regulate the activity of MAPKs dephosphorylating these residues, therefore modulating the biologically active form of ERK1/2 in the nucleus. We found significantly overexpressed DUSP5 (5,31) after treatment with MSNs-Tf-SeNPs, which means deprivation of the phosphate group from ERK1/2 in the nucleus, potentially leading to a cellular senescent state (Zou et al., 2018).

One of the most important trigger molecules in the ERK/MAPK pathway is transforming growth factor-β1, showing abnormally high expression in situations of premature or replicative senescence. Transforming growth factor β1 (TGFB1, 1,76) is known to activate the $p38^{MAPK}$ pathway by triggering an increase in the concentration of H_2O_2, generating an oxidative stress, which will lead to senescence. Also, TGF-β1 leads to the appearance of senescent markers such as senescence-like morphology, β-gal activity (GLB1, 1,14), overexpression of osteonectin (SPOCK2, 1,14) and transgelin (TAGLN, 1,37), all of them up-regulated in our experiment. Another aspect of TGF-β1 increased levels is the overexpression of insulin-like growth factor binding proteins (Debacq-Chainiaux et al., 2010) [19].

3.6. MSNs-Tf-SeNPs induces senescence-related pathway in human hepatocarcinoma cells.

Interestingly, a deeper analysis of altered genes demonstrated that a considerable number of genes participated in pathways involving the immune function and the interferon response. Upregulation of these pathways, have been previously related to senescence, a cellular mechanism identified as a chemotherapy response (Kuilman et al., 2010).

Senescence is defined as an irreversible state in which cells stop dividing, generally triggered by a great variety of physiologic stress stimuli such as oncogene activity, among others (Porath et al., 2005). Thus, senescence development might represent an antitumor state at the time of representing a promising strategy as cancer therapy.

Since senescent cells frequently show activation of specific gene targets and pathways such as those belonging to the Rb and p53 tumor suppressor pathways (Sherr et al., 2002) at the time of producing a senescence-associated secretory phenotype (SASP) (Kuilman et al., 2010), we performed a detailed search to identify altered genes involved in those pathways.

One of the genes exhibiting greater than threefold increase in expression levels in SeNP treated cells versus control cells was the RNA helicase p68 (DDX5), a well-established co-activator of the p53 tumor suppressor activated in genotoxic stress situations, favoring cell survival instead of inducing pro-apoptotic genes (Nicol et al., 2013). In agreement, and though tumor suppressor p53 was moderately upregulated (1,23), two of the best characterized p53 senescence-associated genes p21/CDKN1A and p16/CDKN2A were upregulated. Similarly, we also detected expression differences of LGFBP3 and ATF3 downstream targets of the tumor suppressor. Thus, MSNs-Tf-SeNP-HepG2 treated cells consistently elicits a stress signaling pathway that is evidenced by a marked upregulation of p53 target genes.

In addition, we identified upregulation of E2F1, a transcription factor that plays a crucial role in the control of cell cycle that function as a tumor suppressor. This protein binds preferentially to retinoblastoma protein pRB in a cell-cycle dependent manner and to plasminogen activator inhibitor 1 (PAI-1), an activator of p53 phosphorylation at the time of being a p53 downstream target (3,29). The latter also prevents the proteolytic degradation of IGF-binding protein-3 (LGFBP3), senescence activator (Deelen et al., 2013) overexpressed in our experiment.
In addition to growth arrest, senescence is associated with a series of distinctive molecular and morphological alterations. Accordingly, we also observed a marked upregulation of secretory factors including TIMP metallopeptidase inhibitor 1 (TIMP1; higher than twofold), protease cathepsin B (CTSB, 1,4), macrophage colony stimulating factor 1 (CSF1; 1,4), growth factors (Amphiregulin, EGF and EGFR) as well as antiapoptotic factors (ITPR3 and ITPRIP).

To confirm the activation of genes associated with the SASP we sought the signature of Interleukin 1 (IL1), a prominently activated pathway in senescence. Although, IL1 ligands

(IL1α/β) and its receptor (IL1R) did not show changes upon treatment, essential downstream targets in the pathway (ICAM1; MyD88) did show, thus confirming that changes in the IL1 pathway appears during senescence independently of the cell type used. Altogether, our results demonstrates that our engineered nanosystem triggers a senescence phenotype which might be considered as a novel therapeutic agent.

To conclude, our results also reinforce the importance of centromere integrity in cellular senescence development. As telomere shorten, centromere defects led to a senescence of human primary fibroblasts (Maehara et al., 2010). Accordingly, after MSNPs-Tf-SeNPs exposure, hepatocarcinoma cells members of the centromere complex (CENP) were downregulated in our RNA-seq assay, thus suggesting the crucial role of CENP depletion as a "self-defense mechanism" to prevent centromere-defective cells from undergoing mitotic proliferation, and the consequent generation of aneuploid cells.

To validate our transcriptomic results, we evaluated the extent of senescence induced by the treatment of HepG2 cells with MSNs-Tf-SeNPs. Since one of the best characterized biological biomarkers of senescent cells is the increased activity of the lysosomal senescence-associated β-galactosidase (SA-β-GAL), we assessed senescence-associated β-galactosidase by a histochemical staining (**Figure 6**). Assessment of features characteristic of senescence in hepatocarcinoma cells treated with MSNs-Tf-SeNPs showed that 10 μg/mL of the nanosystem for 3 days (**Figure 6B**), were enough to induced flattening and enlargement of HepG2 cell morphology. Similarly, treated cells were positively stained for β-galactosidase at pH 6.0 at similar extent as etoposide-treated HepG2, used as β-galactosidase staining control (**Figures 6C and 6D**). On the contrary, HepG2 cells treated with the mesoporous system lacking selenium showed background levels (**Figure 6A**). These results confirms that senescence is actively induced in HepG2 hepatocarcinoma upon treatment with MSNs-Tf-SeNPs.

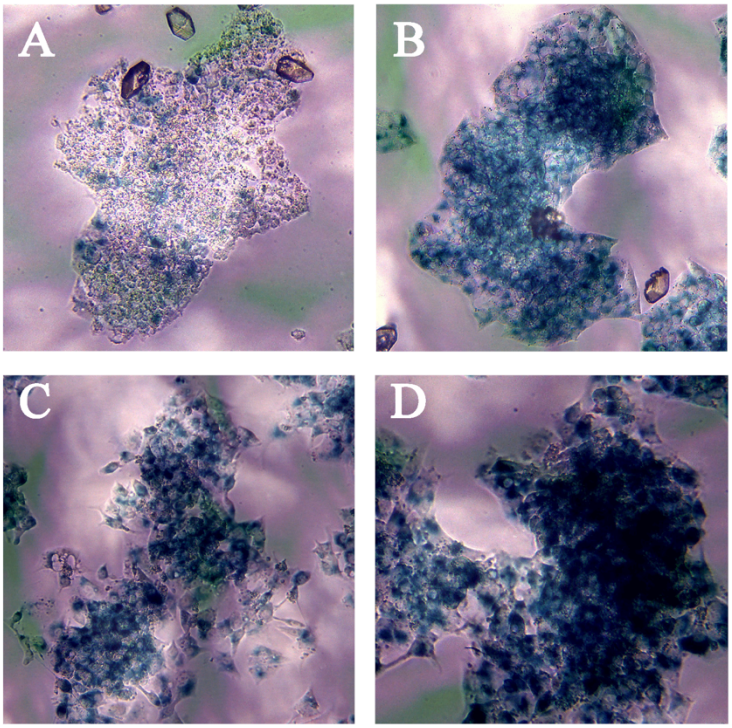

Figure 6. Cytochemical staining of senescence-associated β-galactosidase. HepG2 cells exposed to (A) 10 µg/mL of MSNs-Tf, (B) 10 µg/mL of MSNs-Tf-SeNPs, (C) 10 µg/mL of etoposide, and (D) 50 µg/mL of etoposide.

3.7. MSNs-Tf-SeNPs inhibits *in vivo* triple negative breast tumor growth.

Given the promising outcomes observed *in vitro*, we proceeded to assess the antiproliferative efficacy of the MSNs-Tf-SeNPs nanosystem in a more complex biological environment, employing an *in vivo* assay based on a chicken embryo model. As shown in **Figure 7**, treatment of the generated CAM xenografts with MSNs-Tf-SeNPs, demonstrate the ability of the nanosystem to significantly reduce the size of the tumors as compared to controls, thus demonstrating the ability of the proposed nanosystem to significantly inhibit the proliferative capacity of a triple negative breast tumor in an *in vivo* environment.

4. Conclusions

This study explores the synthesis and characterization of a hybrid nanomaterial (MSNs-Tf-SeNPs) with potential applications in cancer therapy. The successful synthesis involved multi-step processes, including functionalizing MSNs with carboxylic acid groups and anchoring transferrin protein to facilitate specific targeting. Analysis confirmed the incorporation of the protein, and

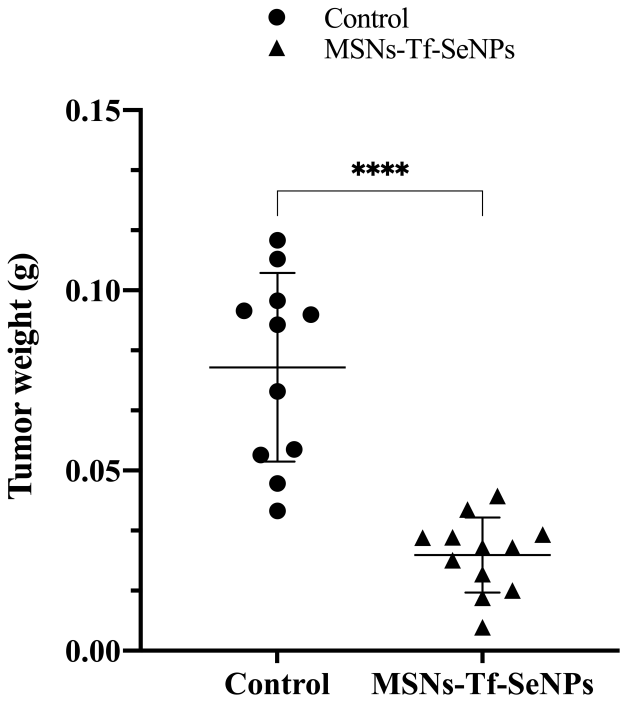

Figure 7. Weight of control tumors and tumors treated with 10 µg/mL of MSNs-Tf-SeNPs using a chicken embryo *in vivo* model.

TEM micrographs illustrated a uniform dispersion of selenium nanoparticles (SeNPs) on the MSNs surface. The material demonstrated selective internalization in cancer cells overexpressing transferrin receptors, validating the role of transferrin as a selective targeting ligand. Moreover, MSNs-Tf-SeNPs exhibited dose-dependent cytotoxicity and induced cell cycle arrest at S-G2/M phases, suggesting a potential mechanism for cancer therapy. Transcriptome analysis revealed significant alterations in gene expression related to various cellular processes, emphasizing the anti-tumor potential of the designed nanosystem. Notably, MSNs-Tf-SeNPs induced a senescence-related pathway in hepatocarcinoma cells, triggering immune responses and a senescence-associated secretory phenotype. Experimental validation confirmed senescence induction in HepG2 cells treated with MSNs-Tf-SeNPs. Finally, the efficacy of the proposed nanosystem to inhibit the proliferative capacity of a triple negative breast cancer tumor, was demonstrated in an *in vivo* chicken embryo model. In summary, this study highlights the multifaceted therapeutic potential of MSNs-Tf-SeNPs,

combining targeted delivery, cytotoxicity, cell cycle modulation, and induction of senescence as promising strategies in cancer treatment.

Acknowledgements

This work was supported by Ministerio de Ciencia e Innovación (MINECO) grant PID2020-114529RB-I00. Hector Estevez acknowledges Ministry of Science, Innovation and Universities from the Spanish Government for a pre-doctoral fellowship (PRE2018-084196).

Table 1. Organic content and elemental composition form thermogravimetric and chemical analysis of MSNs and functionalized MSNs materials.

Material	Theor. Org. (wt%)	Org. Content (wt%)	%C	%N	%S
MSNs	-	4.53	3.64	0.05	0.03
MSNs-$COOH_{ext}$ (with CTAB)	-	36.27 [b]	30.86	1.85	0.02
MSNs-$COOH_{ext}$	9.73	7.81 [b]	10.11	0.10	0.01
MSNs-Tf	19.55 [a]	13.67 [b]	13.94	2.86	0.26

[a] Theorical organic content (wt%) is calculated without taking into account the losses of water molecules which are produced in the reaction of condensation for the protein anchorage.
[b] Organic content (wt%) is determined from the TGA weight losses, excluding the weight loss due to the desorption of water (up to 125 °C) and further corrected by the weight loss of the remaining alcoxysilanes after the sol-gel reaction without condensation.

Table 2. ζ-Potential values and hydrodynamic particle size in water medium of MSN materials

Material	Z-potential (mV)	Hydrodynamic size [a] (nm)
MSNs	-25 ± 8	199 ± 8
MSNs-COOH$_{ext}$	-29 ± 5	209 ± 15
MSNs-Tf	-20 ± 4	166 ± 16
MSNs-Tf- SeNPs	26 ± 8	164 ± 38

Table 3. Expression values of significantly altered transcripts after exposure to MSNs-Tf-SeNPs in comparison to control cells. (CUT-OFF: 0,67-1,5)

MSNs-Tf-SeNPs *vs.* Control	Gene code	Gene name
0,11	ALDOB	aldolase B, fructose-bisphosphate
0,21	G6PC	glucose-6-phosphatase, catalytic subunit
0,28	ANGPTL3	angiopoietin like 3
0,30	POTEE	POTE ankyrin domain family, member E
0,32	ANGPTL8	angiopoietin like 8
0,34	POTEF	POTE ankyrin domain family, member F
0,34	CYP3A7; CYP3A7-CYP3A51P	cytochrome P450, family 3, subfamily A, polypeptide 7; CYP3A7-CYP3A51P readthrough
0,36	CYP3A5	cytochrome P450, family 3, subfamily A, polypeptide 5
0,38	KNG1	kininogen 1
0,39	HRG	histidine-rich glycoprotein
0,39	FSD1L	fibronectin type III and SPRY domain containing 1-like
0,40	DGKD	diacylglycerol kinase, delta 130kDa
0,42	CYP17A1	cytochrome P450, family 17, subfamily A, polypeptide 1
0,42	CENPI	centromere protein I
0,42	DEPDC4	DEP domain containing 4
0,43	ERV3-1; ZNF117	endogenous retrovirus group 3, member 1; zinc finger protein 117
0,43	POTEI	POTE ankyrin domain family, member I
0,43	TNFSF10	tumor necrosis factor (ligand) superfamily, member 10
0,43	PRLR	prolactin receptor
0,43	CYP4F2	cytochrome P450, family 4, subfamily F, polypeptide 2
0,43	TAT	tyrosine aminotransferase
0,44	LINC00612	long intergenic non-protein coding RNA 612
0,45	HMGCS2	3-hydroxy-3-methylglutaryl-CoA synthase 2 (mitochondrial)
0,45	PRPF19	Memczak2013 ALT_ACCEPTOR, ALT_DONOR, coding, INTERNAL, intronic best transcript NM_014502
0,45	PLGLB1; PLGLB2	plasminogen-like B1; plasminogen-like B2
0,45	ABCC11	ATP binding cassette subfamily C member 11
0,45	CYP7A1	cytochrome P450, family 7, subfamily A, polypeptide 1
0,45	PPAP2B	Transcript Identified by AceView, Entrez Gene ID(s) 8613
0,46	GOLGA8O	golgin A8 family, member O
0,47	HAL	histidine ammonia-lyase
0,47	CHGB	chromogranin B
0,47	ADHFE1; C8orf46	alcohol dehydrogenase, iron containing 1; chromosome 8 open reading frame 46
0,47	SPATA25	spermatogenesis associated 25
0,47	GOLGA8A; GOLGA8B	golgin A8 family, member A; golgin A8 family, member B
0,47	FAR2P1	fatty acyl-CoA reductase 2 pseudogene 1
0,48	LOC389834; AL354822.1	ankyrin repeat domain 57 pseudogene
0,48	FRY	FRY microtubule binding protein

MSNs-Tf-SeNPs *vs.* Control	Gene code	Gene name
0,48	SLC17A1	solute carrier family 17 (organic anion transporter), member 1
0,48	AQP8	aquaporin 8
0,48	CAPN3	calpain 3
0,49	SNX33	sorting nexin 33
0,49	KSR1	Zhang2013 ALT_ACCEPTOR, ALT_DONOR, coding, INTERNAL, intronic best transcript NM_014238
0,49	GOLGA8B	golgin A8 family, member B
0,49	ZNF841	zinc finger protein 841
0,50	ZGRF1	zinc finger, GRF-type containing 1
0,50	TSGA10	testis specific 10
0,50	TTC6	tetratricopeptide repeat domain 6
0,50	AFM	afamin
0,50	PER3	period circadian clock 3
0,50	ABCA7	ATP binding cassette subfamily A member 7
0,50	THRSP	thyroid hormone responsive
0,50	CYB561D2	cytochrome b561 family, member D2
0,50	DEPDC5	DEP domain containing 5
0,50	LEAP2	liver expressed antimicrobial peptide 2
0,51	SLC22A7	solute carrier family 22 (organic anion transporter), member 7
0,51	ACSS3	acyl-CoA synthetase short-chain family member 3
0,51	SLC16A7	solute carrier family 16 (monocarboxylate transporter), member 7
0,51	SPDL1	spindle apparatus coiled-coil protein 1
0,51	HIBCH	Transcript Identified by AceView, Entrez Gene ID(s) 26275
0,52	LOC730183; RP11-146F11.1; hitema	uncharacterized LOC730183; Transcript Identified by AceView; novel transcript, antisense to SRCAP
0,52	TCERG1	Transcript Identified by AceView, Entrez Gene ID(s) 10915
0,52	GPR75	G protein-coupled receptor 75
0,52	MTHFR	methylenetetrahydrofolate reductase (NAD(P)H)
0,52	SLC10A5	solute carrier family 10, member 5
0,52	EPPK1	epiplakin 1
0,53	C1QTNF9B-AS1	C1QTNF9B antisense RNA 1
0,53	ATG4A	autophagy related 4A, cysteine peptidase
0,53	SLC26A6; MIR6824	solute carrier family 26 (anion exchanger), member 6; microRNA 6824
0,54	ARRDC3	arrestin domain containing 3
0,54	CYP4F3	cytochrome P450, family 4, subfamily F, polypeptide 3
0,54	DDX12P; DDX11	DEAD/H (Asp-Glu-Ala-Asp/His) box polypeptide 12, pseudogene; DEAD/H (Asp-Glu-Ala-Asp/His) box helicase 11
0,54	STARD4	StAR-related lipid transfer domain containing 4
0,54	BBOF1	basal body orientation factor 1
0,55	KLKB1	kallikrein B1
0,55	SYNGAP1; MIR5004	synaptic Ras GTPase activating protein 1; microRNA 5004
0,55	STARD5	StAR-related lipid transfer domain containing 5
0,55	SLC22A25	solute carrier family 22, member 25
0,55	SLC2A6	solute carrier family 2 (facilitated glucose transporter), member 6 [Source:HGNC Symbol;Acc:HGNC:11011]

MSNs-Tf-SeNPs *vs.* Control	Gene code	Gene name
0,55	PLG	plasminogen
0,55	ANKRD36C	ankyrin repeat domain 36C
0,55	IRAK4	interleukin 1 receptor associated kinase 4
0,55	ABCC3	ATP binding cassette subfamily C member 3
0,55	HACE1	HECT domain and ankyrin repeat containing E3 ubiquitin protein ligase 1
0,55	CCDC142; MRPL53	coiled-coil domain containing 142; mitochondrial ribosomal protein L53
0,55	CCDC64	coiled-coil domain containing 64
0,55	SWT1	SWT1 RNA endoribonuclease homolog
0,55	DZIP3	DAZ interacting zinc finger protein 3
0,55	INO80	INO80 complex subunit
0,55	SPIRE2	spire-type actin nucleation factor 2
0,55	SLC22A9	solute carrier family 22 (organic anion transporter), member 9
0,55	LTB4R; LTB4R2	leukotriene B4 receptor; leukotriene B4 receptor 2
0,55	FKBP2	FK506 binding protein 2
0,56	KIAA1217	KIAA1217
0,56	SOX5	Transcript Identified by AceView, Entrez Gene ID(s) 6660
0,56	PLGLB2	plasminogen-like B2
0,56	LINC01588	long intergenic non-protein coding RNA 1588
0,56	COL27A1	collagen, type XXVII, alpha 1
0,56	ZNF221	zinc finger protein 221
0,56	DNAJC27	DnaJ (Hsp40) homolog, subfamily C, member 27
0,56	APEX2	Transcript Identified by AceView, Entrez Gene ID(s) 27301
0,56	HOOK2	hook microtubule-tethering protein 2
0,56	ZNF483	zinc finger protein 483
0,56	DMXL1	Dmx-like 1
0,57	ANKRD27	ankyrin repeat domain 27 (VPS9 domain)
0,57	ZNF565	zinc finger protein 565
0,57	PARD3B	par-3 family cell polarity regulator beta
0,57	ACSM1	acyl-CoA synthetase medium-chain family member 1
0,57	MFSD11	major facilitator superfamily domain containing 11
0,57	DMGDH	dimethylglycine dehydrogenase
0,57	IQCH	IQ motif containing H
0,57	MST1L	macrophage stimulating 1-like
0,57	ACSM5	acyl-CoA synthetase medium-chain family member 5
0,57	TECTB	tectorin beta
0,57	MID1	midline 1
0,57	TOMM40L; MIR5187	translocase of outer mitochondrial membrane 40 homolog (yeast)-like; microRNA 5187
0,57	GPD1	glycerol-3-phosphate dehydrogenase 1
0,57	NPC1L1	NPC1-like 1
0,57	SLX4	SLX4 structure-specific endonuclease subunit
0,57	EPG5	ectopic P-granules autophagy protein 5 homolog (C. elegans)
0,58	DCAF11	DDB1 and CUL4 associated factor 11

MSNs-Tf-SeNPs *vs.* Control	Gene code	Gene name
0,58	CHD6	chromodomain helicase DNA binding protein 6
0,58	YPEL2	yippee like 2
0,58	PRKCA	Jeck2013 ALT_ACCEPTOR, ALT_DONOR, coding, INTERNAL, intronic best transcript NM_002737
0,58	POC5	POC5 centriolar protein
0,58	NKTR	natural killer cell triggering receptor
0,58	ZNF682	zinc finger protein 682
0,58	ZNF189	zinc finger protein 189
0,58	ABCA5	ATP binding cassette subfamily A member 5
0,58	ERVK13-1	endogenous retrovirus group K13, member 1
0,58	DGKD	diacylglycerol kinase, delta 130kDa
0,58	SH3YL1	SH3 and SYLF domain containing 1
0,58	CA13	carbonic anhydrase XIII
0,58	SP100	SP100 nuclear antigen
0,58	TUBGCP6	tubulin, gamma complex associated protein 6
0,58	NGEF	neuronal guanine nucleotide exchange factor
0,58	STAT2	signal transducer and activator of transcription 2
0,58	GCA	grancalcin, EF-hand calcium binding protein
0,58	ITIH1	inter-alpha-trypsin inhibitor heavy chain 1
0,58	MIS12	MIS12 kinetochore complex component
0,58	POLI	polymerase (DNA directed) iota
0,58	NSUN6	NOP2/Sun domain family, member 6
0,58	MAPK8IP3	mitogen-activated protein kinase 8 interacting protein 3
0,58	ATP9B	ATPase, class II, type 9B
0,59	BTAF1	BTAF1 RNA polymerase II, B-TFIID transcription factor-associated, 170kDa
0,59	XRCC4	X-ray repair complementing defective repair in Chinese hamster cells 4
0,59	BCAT2	branched chain amino-acid transaminase 2, mitochondrial
0,59	SYNJ1	synaptojanin 1
0,59	HELZ	helicase with zinc finger
0,59	PDE4C	phosphodiesterase 4C, cAMP-specific
0,59	ARL5A	ADP-ribosylation factor like GTPase 5A
0,59	AHSA2	AHA1, activator of heat shock 90kDa protein ATPase homolog 2 (yeast)
0,59	NXT2	nuclear transport factor 2-like export factor 2
0,59	UGT1A1; UGT1A6; UGT1A4; UGT1A10; UGT1A8; UGT1A7; UGT1A5; UGT1A3; UGT1A9	UDP glucuronosyltransferase 1 family, polypeptide A1; UDP glucuronosyltransferase 1 family, polypeptide A6; UDP glucuronosyltransferase 1 family, polypeptide A4; UDP glucuronosyltransferase 1 family, polypeptide A10; UDP glucuronosyltransferase 1 family, polypeptide A8; UDP glucuronosyltransferase 1 family, polypeptide A7; UDP glucuronosyltransferase 1 family, polypeptide A5; UDP glucuronosyltransferase 1 family, polypeptide A3; UDP glucuronosyltransferase 1 family, polypeptide A9
0,59	ALLC	allantoicase
0,59	NOTCH2NL	notch 2 N-terminal like
0,59	SLC2A6	solute carrier family 2 (facilitated glucose transporter), member 6 [Source:HGNC Symbol;Acc:HGNC:11011]
0,59	SLC2A6	solute carrier family 2 (facilitated glucose transporter), member 6 [Source:HGNC Symbol;Acc:HGNC:11011]
0,59	SPG7	spastic paraplegia 7 (pure and complicated autosomal recessive)

MSNs-Tf-SeNPs *vs.* Control	Gene code	Gene name
0,59	KMT2D	lysine (K)-specific methyltransferase 2D
0,59	STAG3L3; STAG3L2	stromal antigen 3-like 3 (pseudogene); stromal antigen 3-like 2 (pseudogene)
0,59	MTFR1	mitochondrial fission regulator 1
0,59	ZNF546	zinc finger protein 546
0,59	POTEJ	POTE ankyrin domain family, member J
0,59	KCTD18	potassium channel tetramerization domain containing 18
0,60	TBX15	T-box 15
0,60	CAPN12	calpain 12
0,60	PIH1D2	PIH1 domain containing 2
0,60	CCDC84	coiled-coil domain containing 84
0,60	SENP7	SUMO1/sentrin specific peptidase 7
0,60	ETFDH	electron-transferring-flavoprotein dehydrogenase
0,60	FAM161B	family with sequence similarity 161, member B
0,60	GATM	glycine amidinotransferase (L-arginine:glycine amidinotransferase)
0,60	PRELID3A	PRELI domain containing 3A
0,60	HTRA2	HtrA serine peptidase 2
0,60	SLC2A2	solute carrier family 2 (facilitated glucose transporter), member 2
0,60	RSRP1	arginine/serine-rich protein 1
0,60	STAG3L1	stromal antigen 3-like 1 (pseudogene)
0,60	NR2C2	Transcript Identified by AceView, Entrez Gene ID(s) 7182
0,60	DDX58	DEAD (Asp-Glu-Ala-Asp) box polypeptide 58
0,60	PRIMPOL	primase and DNA directed polymerase
0,60	TMEM178A	transmembrane protein 178A
0,60	CDCA2	cell division cycle associated 2
0,60	ANKRD36	ankyrin repeat domain 36
0,60	TIGD3	tigger transposable element derived 3
0,60	ABCA1	ATP binding cassette subfamily A member 1
0,60	GSTA2	glutathione S-transferase alpha 2
0,60	F11	coagulation factor XI
0,60	AC208162.1	
0,61	NBPF9	neuroblastoma breakpoint family, member 9
0,61	CCBL1	cysteine conjugate-beta lyase, cytoplasmic
0,61	GPCPD1	glycerophosphocholine phosphodiesterase 1
0,61	CNTF	ciliary neurotrophic factor
0,61	CDON	cell adhesion associated, oncogene regulated
0,61	CKMT2	creatine kinase, mitochondrial 2 (sarcomeric)
0,61	PPARGC1B	peroxisome proliferator-activated receptor gamma, coactivator 1 beta
0,61	GABRE; MIR224; MIR452	gamma-aminobutyric acid (GABA) A receptor, epsilon; microRNA 224; microRNA 452
0,61	FST	follistatin
0,61	C1orf112	chromosome 1 open reading frame 112
0,61	ZNF75D	zinc finger protein 75D
0,61	MAFTRR	MAF transcriptional regulator RNA

MSNs-Tf-SeNPs *vs.* Control	Gene code	Gene name
0,61	MDN1	midasin AAA ATPase 1
0,61	PANK1	pantothenate kinase 1
0,61	KIF16B	kinesin family member 16B
0,61	ONECUT2	one cut homeobox 2
0,61	SARM1	sterile alpha and TIR motif containing 1
0,61	SLC25A36	solute carrier family 25 (pyrimidine nucleotide carrier), member 36
0,61	SBF2	SET binding factor 2
0,61	LOC100129924; C1orf50; RP5-994D16.11	uncharacterized LOC100129924; Transcript Identified by AceView, Entrez Gene ID(s) 79078; novel transcript
0,61	EFCAB12	EF-hand calcium binding domain 12
0,61	PCNXL3	pecanex-like 3 (Drosophila)
0,61	KCNIP2	Kv channel interacting protein 2
0,61	AKR1C4	aldo-keto reductase family 1, member C4
0,61	FNIP2	folliculin interacting protein 2
0,61	RNF213	ring finger protein 213
0,61	C2orf15	chromosome 2 open reading frame 15
0,61	ERI1	exoribonuclease 1
0,61	STK36	serine/threonine kinase 36
0,61	RDH16	retinol dehydrogenase 16 (all-trans)
0,62	ADAMTS6	ADAM metallopeptidase with thrombospondin type 1 motif 6
0,62	SLC25A52	solute carrier family 25, member 52
0,62	GCC2	Jeck2013 ANTISENSE, CDS, coding, INTERNAL, intronic, OVCODE, OVEXON best transcript NM_181453
0,62	SERINC4	serine incorporator 4
0,62	TRPV1	transient receptor potential cation channel, subfamily V, member 1
0,62	FLJ45513; RP11-304F15.3	uncharacterized LOC729220; novel transcript antisense to TAC4
0,62	MVD	mevalonate (diphospho) decarboxylase
0,62	FLVCR1	feline leukemia virus subgroup C cellular receptor 1
0,62	MCM3AP-AS1	MCM3AP antisense RNA 1
0,62	SLC38A4	solute carrier family 38, member 4
0,62	KIAA1524	KIAA1524
0,62	NUDT12	nudix hydrolase 12
0,62	FSTL4	follistatin-like 4
0,62	MYSM1	Myb-like, SWIRM and MPN domains 1
0,62	DDX11	DEAD/H (Asp-Glu-Ala-Asp/His) box helicase 11
0,62	HYKK	hydroxylysine kinase
0,62	LRP1	LDL receptor related protein 1
0,62	FAM20A	family with sequence similarity 20, member A
0,62	IFIT3	interferon-induced protein with tetratricopeptide repeats 3
0,62	SAMD4A	Jeck2013 ALT_ACCEPTOR, ALT_DONOR, coding, INTERNAL, intronic best transcript NM_015589
0,62	HDAC6	histone deacetylase 6
0,62	CXorf23	chromosome X open reading frame 23

MSNs-Tf-SeNPs *vs.* Control	Gene code	Gene name
0,62	AGBL2	ATP/GTP binding protein-like 2
0,62	C5orf51	chromosome 5 open reading frame 51
0,62	ZNF211	zinc finger protein 211
0,62	RNF111	ring finger protein 111
0,62	EPHA1	EPH receptor A1
0,62	TDRKH	tudor and KH domain containing
0,62	ERI2	ERI1 exoribonuclease family member 2
0,62	ANKRD36	Transcript Identified by AceView, Entrez Gene ID(s) 375248
0,62	AMICA1	adhesion molecule, interacts with CXADR antigen 1
0,62	SEC16B	SEC16 homolog B, endoplasmic reticulum export factor
0,62	LRRC17	leucine rich repeat containing 17
0,63	SORBS1	Transcript Identified by AceView, Entrez Gene ID(s) 10580
0,63	COBLL1	cordon-bleu WH2 repeat protein like 1
0,63	KATNA1	katanin p60 (ATPase containing) subunit A 1
0,63	MCOLN1	mucolipin 1
0,63	RCHY1	ring finger and CHY zinc finger domain containing 1, E3 ubiquitin protein ligase
0,63	MYOM1	myomesin 1
0,63	C19orf44	chromosome 19 open reading frame 44
0,63	IL17RB	interleukin 17 receptor B
0,63	HIP1	huntingtin interacting protein 1
0,63	PLA2G6	phospholipase A2, group VI (cytosolic, calcium-independent)
0,63	PHF14	PHD finger protein 14
0,63	SECTM1	secreted and transmembrane 1
0,63	SUSD2	sushi domain containing 2
0,63	DCUN1D2	DCN1, defective in cullin neddylation 1, domain containing 2
0,63	POLR2J4	polymerase (RNA) II (DNA directed) polypeptide J4, pseudogene
0,63	PSTK	phosphoseryl-tRNA kinase
0,63	CNBD2	cyclic nucleotide binding domain containing 2
0,63	FGF17	fibroblast growth factor 17
0,63	LINS1	lines homolog 1
0,63	TMEM234	transmembrane protein 234
0,63	YLPM1	YLP motif containing 1
0,63	STIM2	stromal interaction molecule 2
0,63	SLC7A9	solute carrier family 7 (amino acid transporter light chain, bo,+ system), member 9
0,63	DNAJC28	DnaJ (Hsp40) homolog, subfamily C, member 28
0,63	NDUFA10	NADH dehydrogenase (ubiquinone) 1 alpha subcomplex, 10, 42kDa
0,63	STAG3L2	stromal antigen 3-like 2 (pseudogene)
0,63	ELMO1	engulfment and cell motility 1
0,63	GPATCH2	G-patch domain containing 2
0,63	CYB5A	cytochrome b5 type A (microsomal)
0,63	SASS6	SAS-6 centriolar assembly protein
0,63	PTGR2	prostaglandin reductase 2

MSNs-Tf-SeNPs *vs.* Control	Gene code	Gene name
0,63	SLC2A6	solute carrier family 2 (facilitated glucose transporter), member 6
0,63	ABHD17B	abhydrolase domain containing 17B
0,64	FAM161A	family with sequence similarity 161, member A
0,64	CCDC93	coiled-coil domain containing 93
0,64	NEDD1	neural precursor cell expressed, developmentally down-regulated 1
0,64	C3orf35	chromosome 3 open reading frame 35
0,64	C17orf53	chromosome 17 open reading frame 53
0,64	CIB3	calcium and integrin binding family member 3
0,64	TMEM91	transmembrane protein 91
0,64	CCDC84	coiled-coil domain containing 84
0,64	AP3D1	adaptor-related protein complex 3, delta 1 subunit
0,64	ZBTB40	zinc finger and BTB domain containing 40
0,64	SWI5	SWI5 homologous recombination repair protein
0,64	MVK	mevalonate kinase
0,64	MICAL3	microtubule associated monooxygenase, calponin and LIM domain containing 3
0,64	ZNF138	zinc finger protein 138
0,64	RNF8	ring finger protein 8, E3 ubiquitin protein ligase
0,64	SCAF11	SR-related CTD-associated factor 11
0,64	ZBED9	zinc finger, BED-type containing 9
0,64	PLAC8	placenta specific 8
0,64	C1orf101	chromosome 1 open reading frame 101
0,64	OXNAD1	oxidoreductase NAD-binding domain containing 1
0,64	PECR	peroxisomal trans-2-enoyl-CoA reductase
0,64	MTOR	mechanistic target of rapamycin (serine/threonine kinase)
0,64	TCF19	transcription factor 19
0,64	CTSK	cathepsin K
0,64	STIL	SCL/TAL1 interrupting locus
0,64	CLCN6	chloride channel, voltage-sensitive 6
0,64	LYPD1	LY6/PLAUR domain containing 1
0,64	CDH11	cadherin 11, type 2, OB-cadherin (osteoblast)
0,64	CNBD2	cyclic nucleotide binding domain containing 2
0,64	ZNF594	zinc finger protein 594
0,64	TACR1	tachykinin receptor 1
0,64	CRIP1	cysteine-rich protein 1 (intestinal)
0,64	FEM1C	Jeck2013 ALT_ACCEPTOR, ALT_DONOR, coding, INTERNAL, intronic best transcript NM_020177
0,64	C5orf42	chromosome 5 open reading frame 42
0,64	SP140L	SP140 nuclear body protein-like
0,64	PLEKHA6	Transcript Identified by AceView, Entrez Gene ID(s) 22874
0,64	SAR1B	Transcript Identified by AceView, Entrez Gene ID(s) 51128
0,65	THRAP3	Jeck2013 ALT_ACCEPTOR, ALT_DONOR, coding, INTERNAL, intronic best transcript NM_005119
0,65	RALGPS1	Ral GEF with PH domain and SH3 binding motif 1
0,65	PFKFB4; MIR6823	6-phosphofructo-2-kinase/fructose-2,6-biphosphatase 4; microRNA 6823

MSNs-Tf-SeNPs *vs.* Control	Gene code	Gene name
0,65	ACAD11	acyl-CoA dehydrogenase family, member 11
0,65	UPRT	uracil phosphoribosyltransferase (FUR1) homolog (S. cerevisiae)
0,65	CREBBP	CREB binding protein
0,65	NMNAT1	nicotinamide nucleotide adenylyltransferase 1
0,65	SLC12A6	solute carrier family 12 (potassium/chloride transporter), member 6
0,65	HSD17B7	hydroxysteroid (17-beta) dehydrogenase 7
0,65	RASA4	RAS p21 protein activator 4
0,65	SLC22A18	solute carrier family 22, member 18
0,65	KAT6B	K(lysine) acetyltransferase 6B
0,65	SREBF1	sterol regulatory element binding transcription factor 1
0,65	TIAM2	T-cell lymphoma invasion and metastasis 2
0,65	KIF24	kinesin family member 24
0,65	SNAI2	snail family zinc finger 2
0,65	NPHP3-ACAD11	NPHP3-ACAD11 readthrough (NMD candidate)
0,65	TRIM39	tripartite motif containing 39
0,65	ARID4A	AT rich interactive domain 4A (RBP1-like)
0,65	RPL5	Memczak2013 ALT_ACCEPTOR, ALT_DONOR, coding, INTERNAL, intronic best transcript NM_000969
0,65	UBN1	ubinuclein 1
0,65	FCGR1A	Fc fragment of IgG, high affinity Ia, receptor (CD64)
0,65	UBE3B	ubiquitin protein ligase E3B
0,65	SGK3; C8orf44-SGK3	serum/glucocorticoid regulated kinase family, member 3; C8orf44-SGK3 readthrough
0,65	C6orf203	chromosome 6 open reading frame 203
0,65	ZNF436	zinc finger protein 436
0,65	SON; MIR6501	SON DNA binding protein; microRNA 6501
0,65	SCRN3	secernin 3
0,65	MUC20; SDHAP2; MIR570; LINC00969	mucin 20, cell surface associated; succinate dehydrogenase complex subunit A, flavoprotein pseudogene 2; microRNA 570; long intergenic non-protein coding RNA 969
0,65	CDH1	cadherin 1, type 1
0,65	XKR9	X-linked Kx blood group related 9
0,65	ETNPPL	ethanolamine-phosphate phospho-lyase
0,65	CREB3	cAMP responsive element binding protein 3
0,65	NBPF19	neuroblastoma breakpoint family, member 19
0,65	STX17	syntaxin 17
0,65	SF1	Memczak2013 ALT_ACCEPTOR, ALT_DONOR, coding, INTERNAL, intronic best transcript NM_201998
0,65	RCN3	reticulocalbin 3, EF-hand calcium binding domain
0,65	C12orf60	chromosome 12 open reading frame 60
0,65	GSAP	gamma-secretase activating protein
0,65	CCDC7	coiled-coil domain containing 7
0,65	OTC	ornithine carbamoyltransferase
0,65	ZSCAN26	zinc finger and SCAN domain containing 26
0,65	NISCH	nischarin
0,65	GPR52	G protein-coupled receptor 52

MSNs-Tf-SeNPs *vs.* Control	Gene code	Gene name
0,65	FIGNL1	fidgetin-like 1
0,65	IFT172	intraflagellar transport 172
0,65	KIF27	kinesin family member 27
0,65	NDUFB3	NADH dehydrogenase (ubiquinone) 1 beta subcomplex, 3, 12kDa
0,65	MOB3C	MOB kinase activator 3C
0,65	MST1	macrophage stimulating 1
0,65	EZH1	enhancer of zeste 1 polycomb repressive complex 2 subunit
0,65	DNAJC11	Zhang2013 ALT_ACCEPTOR, ALT_DONOR, coding, INTERNAL, intronic best transcript NM_018198
0,65	KANSL1L	KAT8 regulatory NSL complex subunit 1 like
0,65	KNTC1	kinetochore associated 1
0,65	HIBCH	3-hydroxyisobutyryl-CoA hydrolase
0,65	CPEB3	cytoplasmic polyadenylation element binding protein 3
0,65	ADH4	alcohol dehydrogenase 4 (class II), pi polypeptide
0,65	SERPINA6	serpin peptidase inhibitor, clade A (alpha-1 antiproteinase, antitrypsin), member 6
0,65	ANGPTL7	angiopoietin like 7
0,65	DCLRE1C	DNA cross-link repair 1C
0,66	BTBD9	BTB (POZ) domain containing 9
0,66	ZBTB1	zinc finger and BTB domain containing 1
0,66	CREBRF	CREB3 regulatory factor
0,66	SYT11	synaptotagmin XI
0,66	BAAT	bile acid-CoA:amino acid N-acyltransferase
0,66	PDPR	pyruvate dehydrogenase phosphatase regulatory subunit
0,66	ANKRD26	ankyrin repeat domain 26
0,66	PPP1R12B	protein phosphatase 1, regulatory subunit 12B
0,66	GBP2	guanylate binding protein 2, interferon-inducible
0,66	PNPLA3	patatin-like phospholipase domain containing 3
0,66	PIK3C2B	phosphatidylinositol-4-phosphate 3-kinase, catalytic subunit type 2 beta
0,66	PBLD	phenazine biosynthesis-like protein domain containing
0,66	FBRSL1	fibrosin-like 1
0,66	FBXW11	F-box and WD repeat domain containing 11
0,66	YLPM1	YLP motif containing 1
0,66	CWF19L2	CWF19-like 2, cell cycle control (S. pombe)
0,66	RNPC3	RNA binding region (RNP1, RRM) containing 3
0,66	APOL2	apolipoprotein L, 2
0,66	GS1-259H13.2; TCONS_l2_00026125; TCONS_l2_00026126; ZNF655	transmembrane protein 225-like; Jeck2013 ALT_ACCEPTOR, ALT_DONOR, ncRNA, OVCODE, OVEXON, upstream_start best transcript TCONS_l2_00026125; Salzman2013 ANNOTATED, INTERNAL, ncRNA, OVCODE, OVEXON best transcript TCONS_l2_00026126; novel transcript; Transcript Identified by AceView, Entrez Gene ID(s) 79027
0,66	PTCD2	pentatricopeptide repeat domain 2
0,66	RD3	retinal degeneration 3
0,66	CYP3A43	cytochrome P450, family 3, subfamily A, polypeptide 43
0,66	FAM188A	family with sequence similarity 188, member A
0,66	TMEM99	transmembrane protein 99

MSNs-Tf-SeNPs *vs.* Control	Gene code	Gene name
0,66	ZBTB26	zinc finger and BTB domain containing 26
0,66	LYN	LYN proto-oncogene, Src family tyrosine kinase
0,66	RASSF4	Ras association (RalGDS/AF-6) domain family member 4
0,66	NUP107	nucleoporin 107kDa
0,66	CYP2D6	cytochrome P450, family 2, subfamily D, polypeptide 6
0,66	EBP	emopamil binding protein (sterol isomerase)
0,66	OCLM	Transcript Identified by AceView, Entrez Gene ID(s) 10896
0,66	TINAG	tubulointerstitial nephritis antigen
0,66	AP4E1	adaptor-related protein complex 4, epsilon 1 subunit
0,66	SH2D1B	SH2 domain containing 1B
0,66	DIS3L2	DIS3 like 3-5 exoribonuclease 2
0,66	ZFR	Transcript Identified by AceView, Entrez Gene ID(s) 51663
0,66	MCCC1	methylcrotonoyl-CoA carboxylase 1
0,66	DDRGK1	DDRGK domain containing 1
0,66	SPTLC3	serine palmitoyltransferase, long chain base subunit 3
0,66	CHST9	carbohydrate (N-acetylgalactosamine 4-0) sulfotransferase 9
0,66	ZNF638	Transcript Identified by AceView, Entrez Gene ID(s) 27332
0,66	RUNDC3B	RUN domain containing 3B
0,66	RANBP2	RAN binding protein 2
0,66	CLSTN2	calsyntenin 2
0,66	DQX1	DEAQ box RNA-dependent ATPase 1
0,66	ERMARD	ER membrane-associated RNA degradation
0,66	DHRS12	dehydrogenase/reductase (SDR family) member 12
0,66	CYP19A1	cytochrome P450, family 19, subfamily A, polypeptide 1
0,67	UBR4	ubiquitin protein ligase E3 component n-recognin 4
0,67	GBA	glucosidase, beta, acid
0,67	ZNF587	zinc finger protein 587
0,67	IFT140	intraflagellar transport 140
0,67	SCLT1	sodium channel and clathrin linker 1
0,67	SULT1B1	sulfotransferase family 1B member 1
0,67	CHST11	Transcript Identified by AceView, Entrez Gene ID(s) 50515
0,67	NBPF12	neuroblastoma breakpoint family, member 12
0,67	ZDHHC11	zinc finger, DHHC-type containing 11
0,67	NBEAL1	neurobeachin like 1
0,67	ZNF165	zinc finger protein 165
0,67	LSS	lanosterol synthase (2,3-oxidosqualene-lanosterol cyclase)
0,67	FAM160A1	family with sequence similarity 160, member A1
0,67	LOC81691; AC004381.6; U4atac	exonuclease NEF-sp; Putative RNA exonuclease NEF-sp [Source:UniProtKB/Swiss-Prot;Acc:Q96IC2]; Salzman2013 ANNOTATED, CDS, coding, OVCODE, OVERLAPTX, OVEXON, UTR3, UTR5 best transcript NM_001199053; Salzman2013 ANNOTATED, CDS, coding, INTERNAL, OVCODE, OVERLAPTX, OVEXON best transcript NM_001199053; Salzman2013 ANNOTATED, CDS, coding, OVCODE, OVERLAPTX, OVEXON, UTR3 best transcript NM_001199053; Transcript Identified by AceView, Entrez Gene ID(s) 81691; U4atac minor spliceosomal RNA [Source:RFAM;Acc:RF00618]
0,67	TM7SF2	transmembrane 7 superfamily member 2

MSNs-Tf-SeNPs *vs.* Control	Gene code	Gene name
0,67	C5orf34	chromosome 5 open reading frame 34
0,67	MFAP3	microfibrillar associated protein 3
0,67	PLXNA3	plexin A3
0,67	DPY19L3	dpy-19-like 3 (C. elegans)
0,67	AC010894.3; SCRN3	novel transcript; Transcript Identified by AceView, Entrez Gene ID(s) 79634
0,67	STKLD1	serine/threonine kinase-like domain containing 1 [Source:HGNC Symbol;Acc:HGNC:28669]
0,67	VPRBP	Vpr (HIV-1) binding protein
0,67	LRRC28	Transcript Identified by AceView, Entrez Gene ID(s) 123355
0,67	POLR2A	polymerase (RNA) II (DNA directed) polypeptide A, 220kDa
0,67	RPGRIP1L	RPGRIP1-like
0,67	CENPL	centromere protein L
0,67	SNRNP25	small nuclear ribonucleoprotein, U11/U12 25kDa subunit
0,67	OTUD7B	OTU deubiquitinase 7B
0,67	dorsnarby; IGF2BP2	Transcript Identified by AceView; Zhang2013 ALT_ACCEPTOR, ALT_DONOR, coding, INTERNAL, intronic best transcript NM_006548
0,67	ANKHD1; EIF4EBP3; ANKHD1-EIF4EBP3	ankyrin repeat and KH domain containing 1; eukaryotic translation initiation factor 4E binding protein 3; ANKHD1-EIF4EBP3 readthrough
0,67	PIGN	phosphatidylinositol glycan anchor biosynthesis class N
0,67	THAP2	THAP domain containing, apoptosis associated protein 2
0,67	TSSK3	testis-specific serine kinase 3
0,67	ID2	inhibitor of DNA binding 2, dominant negative helix-loop-helix protein
0,67	GINS2	GINS complex subunit 2 (Psf2 homolog)
0,67	NAPEPLD	N-acyl phosphatidylethanolamine phospholipase D
0,67	TMF1	TATA element modulatory factor 1
0,67	PIEZO2	piezo-type mechanosensitive ion channel component 2
0,67	CENPC	centromere protein C
0,67	MYBPH	myosin binding protein H
0,67	KLHL13	kelch-like family member 13
0,67	TMEM141	transmembrane protein 141
0,67	PDP2	pyruvate dehyrogenase phosphatase catalytic subunit 2
0,67	MICALCL	MICAL C-terminal like
0,67	ACOT2	acyl-CoA thioesterase 2
0,67	STARD13	StAR-related lipid transfer domain containing 13
0,67	KIAA1107	KIAA1107
0,67	APC	adenomatous polyposis coli
0,67	BCAS3	breast carcinoma amplified sequence 3
0,67	CEP135	centrosomal protein 135kDa
0,67	MAF	v-maf avian musculoaponeurotic fibrosarcoma oncogene homolog
0,67	SMC4	structural maintenance of chromosomes 4
0,67	AP1B1	Zhang2013 ALT_ACCEPTOR, ALT_DONOR, coding, INTERNAL, intronic best transcript NM_001127
0,67	CDK12	Transcript Identified by AceView, Entrez Gene ID(s) 51755
0,67	ZFX	zinc finger protein, X-linked
0,67	C2orf27A	chromosome 2 open reading frame 27A

MSNs-Tf-SeNPs *vs.* Control	Gene code	Gene name
0,67	ELOVL7	ELOVL fatty acid elongase 7
0,67	GPX3	glutathione peroxidase 3
0,67	CHMP2A	charged multivesicular body protein 2A
0,67	ACYP2	acylphosphatase 2, muscle type
0,67	DEPDC7	DEP domain containing 7
0,67	SLC12A4	solute carrier family 12 (potassium/chloride transporter), member 4
0,67	C22orf46	chromosome 22 open reading frame 46
0,67	DCDC5; DCDC1	doublecortin domain containing 5; doublecortin domain containing 1
0,67	L3HYPDH	L-3-hydroxyproline dehydratase (trans-)
0,67	ATP6V1D	ATPase, H+ transporting, lysosomal 34kDa, V1 subunit D
0,67	ZNF318	zinc finger protein 318
1,50	STK39	serine threonine kinase 39
1,50	SORBS1	Transcript Identified by AceView, Entrez Gene ID(s) 10580
1,50	ACTA2	actin, alpha 2, smooth muscle, aorta
1,50	LMLN	leishmanolysin-like (metallopeptidase M8 family)
1,50	PCBP4	poly(rC) binding protein 4
1,50	NRP2	neuropilin 2
1,50	ANKUB1	ankyrin repeat and ubiquitin domain containing 1
1,50	RCVRN	recoverin
1,50	MRPL39	mitochondrial ribosomal protein L39
1,50	NR4A1	nuclear receptor subfamily 4, group A, member 1
1,50	RDM1	RAD52 motif containing 1
1,50	GPR3	G protein-coupled receptor 3
1,50	ITPKA	inositol-trisphosphate 3-kinase A
1,50	SLC35F3	solute carrier family 35, member F3
1,51	PFDN2	prefoldin subunit 2
1,51	NOTUM	notum pectinacetylesterase homolog (Drosophila)
1,51	TRIM55	tripartite motif containing 55
1,51	PTEN	phosphatase and tensin homolog
1,51	PADI6	peptidyl arginine deiminase, type VI
1,51	CCPG1; MIR628	cell cycle progression 1; microRNA 628
1,51	SMIM8	small integral membrane protein 8
1,51	PRMT6	protein arginine methyltransferase 6
1,51	HKDC1	hexokinase domain containing 1
1,51	ZNF703	zinc finger protein 703
1,51	ACTL6B	actin-like 6B
1,51	SLC24A3	solute carrier family 24 (sodium/potassium/calcium exchanger), member 3
1,51	SOX8	SRY box 8
1,51	KCNJ10	potassium channel, inwardly rectifying subfamily J, member 10
1,52	C16orf72	Memczak2013 ANTISENSE, coding, INTERNAL, intronic best transcript NM_014117
1,52	GNAQ; skeyplorbu	Memczak2013 ANTISENSE, coding, INTERNAL, intronic best transcript NM_002072; Transcript Identified by AceView
1,52	LRRC58	Memczak2013 ANTISENSE, CDS, coding, INTERNAL, intronic, UTR3 best transcript NM_001099678

MSNs-Tf-SeNPs *vs.* Control	Gene code	Gene name
1,52	CRLF3	cytokine receptor-like factor 3
1,52	LETM2	leucine zipper-EF-hand containing transmembrane protein 2
1,52	C1orf158	Transcript Identified by AceView, Entrez Gene ID(s) 93190
1,53	PLEKHG4	pleckstrin homology domain containing, family G (with RhoGef domain) member 4
1,53	AFF4	Memczak2013 ANTISENSE, CDS, coding, INTERNAL best transcript NM_014423
1,53	DBNDD2	dysbindin (dystrobrevin binding protein 1) domain containing 2
1,53	PHLDA2	pleckstrin homology-like domain, family A, member 2
1,53	SDK1	sidekick cell adhesion molecule 1
1,53	IFITM3	interferon induced transmembrane protein 3
1,53	TCF4	Memczak2013 ANTISENSE, coding, INTERNAL, intronic best transcript NM_001243234
1,53	FAM168A	family with sequence similarity 168, member A
1,53	TCF23	transcription factor 23
1,54	UBASH3B	ubiquitin associated and SH3 domain containing B
1,54	GPX2	glutathione peroxidase 2
1,54	ACSL5	acyl-CoA synthetase long-chain family member 5
1,54	OOEP	oocyte expressed protein
1,54	NQO1	NAD(P)H dehydrogenase, quinone 1
1,54	C5AR1	complement component 5a receptor 1
1,54	CSGALNACT1	chondroitin sulfate N-acetylgalactosaminyltransferase 1
1,54	MYC	v-myc avian myelocytomatosis viral oncogene homolog
1,55	APOPT1	apoptogenic 1, mitochondrial
1,55	PRAMEF2	PRAME family member 2
1,55	ICAM1	intercellular adhesion molecule 1
1,55	TAGLN3	transgelin 3
1,55	FKBP11; ARF3	FK506 binding protein 11; ADP-ribosylation factor 3
1,55	MMRN1	multimerin 1
1,56	ERBB2	erb-b2 receptor tyrosine kinase 2
1,56	BCAN	brevican
1,56	NTSR1	neurotensin receptor 1 (high affinity)
1,56	DEFB113	defensin, beta 113
1,56	SCAP	Memczak2013 ANTISENSE, CDS, coding, INTERNAL best transcript NM_012235
1,56	TNFRSF21	tumor necrosis factor receptor superfamily, member 21
1,56	TMSB10	thymosin beta 10
1,57	SOX2	SRY box 2
1,57	VAMP2	vesicle associated membrane protein 2
1,57	WDPCP	WD repeat containing planar cell polarity effector
1,57	CDKN2A	cyclin-dependent kinase inhibitor 2A
1,57	ZFP36L1	ZFP36 ring finger protein-like 1
1,57	PDCD2L	programmed cell death 2-like
1,57	VASP	vasodilator-stimulated phosphoprotein
1,57	CCNI	cyclin I
1,57	TEKT1	tektin 1

MSNs-Tf-SeNPs *vs.* Control	Gene code	Gene name
1,58	LURAP1L	leucine rich adaptor protein 1-like
1,58	CEACAM5	carcinoembryonic antigen-related cell adhesion molecule 5
1,58	OR2M7	olfactory receptor, family 2, subfamily M, member 7
1,58	FHL3	four and a half LIM domains 3
1,58	SMYD1	SET and MYND domain containing 1
1,58	CYGB; RP11-666A8.8	Transcript Identified by AceView, Entrez Gene ID(s) 114757; novel transcript, antisense to PRCD
1,58	HEPHL1	hephaestin-like 1
1,58	ZNF133	zinc finger protein 133
1,59	METTL18	methyltransferase like 18
1,59	FCAR	Fc fragment of IgA receptor
1,59	C6orf48; SNORD52; SNORD48	chromosome 6 open reading frame 48; small nucleolar RNA, C/D box 52; small nucleolar RNA, C/D box 48
1,59	YBX3	Y box binding protein 3
1,60	PPP6R1	Memczak2013 ANTISENSE, CDS, coding, INTERNAL best transcript NM_014931
1,60	IFITM2	interferon induced transmembrane protein 2
1,60	ORAOV1	oral cancer overexpressed 1
1,60	LPAR6	lysophosphatidic acid receptor 6
1,60	TIMM22	translocase of inner mitochondrial membrane 22 homolog (yeast)
1,60	CCNJL	cyclin J-like
1,61	KCNQ5	potassium channel, voltage gated KQT-like subfamily Q, member 5
1,61	ATP1A2	ATPase, Na+/K+ transporting, alpha 2 polypeptide
1,61	TRIB1	tribbles pseudokinase 1
1,61	GTPBP2	GTP binding protein 2
1,61	WDR6	Memczak2013 ANTISENSE, CDS, coding, INTERNAL best transcript NM_018031
1,62	SGCB	sarcoglycan beta
1,62	CLDN12	claudin 12
1,62	HPCAL1	hippocalcin-like 1
1,62	ABR	active BCR-related
1,62	DLX1	distal-less homeobox 1
1,62	TGM2	transglutaminase 2
1,62	SH3BP2	SH3-domain binding protein 2
1,62	CD44	Memczak2013 ALT_ACCEPTOR, ALT_DONOR, coding, INTERNAL, intronic best transcript NM_001202557
1,63	TM4SF19	transmembrane 4 L six family member 19
1,63	ABCC8	ATP binding cassette subfamily C member 8
1,63	ITPR3	inositol 1,4,5-trisphosphate receptor, type 3
1,64	FAM89A; MIR1182	family with sequence similarity 89, member A; microRNA 1182
1,64	SLC51B	solute carrier family 51, beta subunit
1,64	EMC1	ER membrane protein complex subunit 1
1,64	FABP4	fatty acid binding protein 4, adipocyte
1,64	MRGPRX4	MAS-related GPR, member X4
1,65	SPIRE1	spire-type actin nucleation factor 1
1,65	PAX8	paired box 8

MSNs-Tf-SeNPs *vs.* Control	Gene code	Gene name
1,65	PRAMEF2	PRAME family member 2
1,65	MT1B; MT1CP	metallothionein 1B; metallothionein 1C, pseudogene
1,66	NOS1	nitric oxide synthase 1 (neuronal)
1,66	PHF21A	PHD finger protein 21A
1,66	CDCA5	Memczak2013 ANTISENSE, CDS, coding, INTERNAL, UTR3 best transcript NM_080668
1,66	RBM24	RNA binding motif protein 24
1,67	ARG2	arginase 2
1,67	ANXA3	annexin A3
1,67	PPP1R18	protein phosphatase 1, regulatory subunit 18
1,67	SNORA17A; SNORA17B; SNHG7	small nucleolar RNA, H/ACA box 17A; small nucleolar RNA, H/ACA box 17B; small nucleolar RNA host gene 7
1,68	SPP1	secreted phosphoprotein 1
1,68	CYP2S1	cytochrome P450, family 2, subfamily S, polypeptide 1
1,69	HES1	hes family bHLH transcription factor 1
1,69	IL4R	interleukin 4 receptor
1,69	KRT20	keratin 20, type I
1,69	SLC51A	solute carrier family 51, alpha subunit
1,69	CCDC86	coiled-coil domain containing 86
1,69	MAP4K2	Memczak2013 ANTISENSE, CDS, coding, INTERNAL, intronic best transcript NM_004579
1,69	SLC29A3	solute carrier family 29 (equilibrative nucleoside transporter), member 3
1,69	CCL20	chemokine (C-C motif) ligand 20
1,70	NEK3	NIMA-related kinase 3
1,70	DGKK	diacylglycerol kinase, kappa
1,71	FAM102A	Memczak2013 ANTISENSE, CDS, coding, INTERNAL, intronic, UTR3 best transcript NM_203305
1,71	EPDR1	ependymin related 1
1,71	FAM213B	Memczak2013 ANTISENSE, coding, INTERNAL, UTR3 best transcript NM_001195737
1,71	SGK1	serum/glucocorticoid regulated kinase 1
1,71	LOC105371242; AC243756.1	peptidyl-prolyl cis-trans isomerase A-like 4G; Peptidyl-prolyl cis-trans isomerase [Source:UniProtKB/TrEMBL;Acc:A0A075B767]
1,72	MSH2	mutS homolog 2
1,72	SFN	stratifin
1,72	SPRY4	sprouty RTK signaling antagonist 4
1,72	CD55	CD55 molecule, decay accelerating factor for complement (Cromer blood group)
1,73	SERPINB8	serpin peptidase inhibitor, clade B (ovalbumin), member 8
1,74	PEBP1	Memczak2013 ANTISENSE, coding, INTERNAL, UTR3 best transcript NM_002567
1,75	ZC3H13	Memczak2013 ANTISENSE, CDS, coding, INTERNAL best transcript NM_015070
1,75	MAVS	Jeck2013 ANTISENSE, coding, INTERNAL, OVEXON, UTR3 best transcript NM_020746
1,75	MBL2	mannose-binding lectin (protein C) 2, soluble
1,75	TTC39B	tetratricopeptide repeat domain 39B
1,75	ADORA2B	adenosine A2b receptor
1,76	SCAF11	Memczak2013 ANTISENSE, CDS, coding, INTERNAL best transcript NM_004719
1,76	GNAZ	guanine nucleotide binding protein (G protein), alpha z polypeptide

MSNs-Tf-SeNPs *vs.* Control	Gene code	Gene name
1,76	TGFB1	transforming growth factor beta 1
1,77	CCR7	chemokine (C-C motif) receptor 7
1,77	EIF2A	eukaryotic translation initiation factor 2A, 65kDa
1,78	CEMIP	cell migration inducing protein, hyaluronan binding
1,78	CYGB	cytoglobin
1,78	DMRTA1	DMRT-like family A1
1,79	MANSC1	MANSC domain containing 1
1,80	SERPINE2	serpin peptidase inhibitor, clade E (nexin, plasminogen activator inhibitor type 1), member 2
1,80	RASD1	RAS, dexamethasone-induced 1
1,80	TCP11L1	t-complex 11, testis-specific-like 1
1,80	APOBEC3C	apolipoprotein B mRNA editing enzyme, catalytic polypeptide-like 3C
1,81	EDA2R	ectodysplasin A2 receptor
1,81	CD22; MIR5196	CD22 molecule; microRNA 5196
1,83	IL11	interleukin 11
1,84	LAPTM5	lysosomal protein transmembrane 5
1,84	GDF15	growth differentiation factor 15
1,84	PXK	PX domain containing serine/threonine kinase
1,84	AXL	AXL receptor tyrosine kinase
1,84	JAG1	jagged 1
1,85	CREB5	cAMP responsive element binding protein 5
1,85	ID3	inhibitor of DNA binding 3, dominant negative helix-loop-helix protein
1,86	GPAT3	glycerol-3-phosphate acyltransferase 3
1,86	ITGA2	integrin, alpha 2 (CD49B, alpha 2 subunit of VLA-2 receptor)
1,87	ENO1	Memczak2013 ANTISENSE, coding, INTERNAL, UTR3 best transcript NM_001428
1,89	HIST1H1C	Memczak2013 ANTISENSE, CDS, coding, INTERNAL best transcript NM_005319
1,89	NKIRAS2	Memczak2013 ANTISENSE, coding, INTERNAL, UTR3 best transcript NM_001001349
1,90	DYNLL2	Memczak2013 ANTISENSE, coding, INTERNAL, UTR3 best transcript NM_080677
1,91	ERRFI1	ERBB receptor feedback inhibitor 1
1,91	SLC6A14	solute carrier family 6 (amino acid transporter), member 14
1,92	HMGA1	high mobility group AT-hook 1
1,93	SMAD6	SMAD family member 6
1,95	FOSL1	FOS-like antigen 1
1,95	CDKN1A	cyclin-dependent kinase inhibitor 1A (p21, Cip1)
1,96	CORO2B	coronin, actin binding protein, 2B
1,96	CSGALNACT2	chondroitin sulfate N-acetylgalactosaminyltransferase 2
1,98	HEY1	hes-related family bHLH transcription factor with YRPW motif 1
2,00	TM4SF19-TCTEX1D2	TM4SF19-TCTEX1D2 readthrough (NMD candidate)
2,01	CAPN2	calpain 2, (m/II) large subunit
2,01	CACNA2D4	calcium channel, voltage-dependent, alpha 2/delta subunit 4
2,02	APOBEC3D	apolipoprotein B mRNA editing enzyme, catalytic polypeptide-like 3D
2,03	SERPINA3	serpin peptidase inhibitor, clade A (alpha-1 antiproteinase, antitrypsin), member 3
2,06	PLA2G2A	phospholipase A2, group IIA (platelets, synovial fluid)

MSNs-Tf-SeNPs *vs.* Control	Gene code	Gene name
2,09	ARHGAP1	Memczak2013 ANTISENSE, CDS, coding, INTERNAL, UTR3 best transcript NM_004308
2,09	PAEP	progestagen-associated endometrial protein
2,09	SLC16A6	solute carrier family 16, member 6
2,11	SETBP1	Memczak2013 ALT_ACCEPTOR, ALT_DONOR, coding, INTERNAL, intronic best transcript NM_001130110
2,11	MATN3	matrilin 3
2,12	CSTA	cystatin A (stefin A)
2,14	CRKL	Memczak2013 ANTISENSE, CDS, coding, INTERNAL best transcript NM_005207
2,17	F2RL1	coagulation factor II (thrombin) receptor-like 1
2,25	HIST1H4C	Jeck2013 ANTISENSE, CDS, coding, INTERNAL, OVCODE, OVEXON, UTR3 best transcript NM_003542
2,25	HSD17B1	hydroxysteroid (17-beta) dehydrogenase 1
2,30	HKR1	Memczak2013 ANTISENSE, CDS, coding, INTERNAL best transcript NM_181786
2,34	IGFBP3	insulin like growth factor binding protein 3
2,35	EMP3	epithelial membrane protein 3
2,39	MYADM	Memczak2013 ANTISENSE, CDS, coding, INTERNAL best transcript NM_001020819
2,39	GRN	Memczak2013 ANTISENSE, CDS, coding, INTERNAL best transcript NM_002087
2,40	ESAM	endothelial cell adhesion molecule
2,51	TIMP1	TIMP metallopeptidase inhibitor 1
2,56	AQP3	aquaporin 3 (Gill blood group)
2,57	PDGFA	platelet-derived growth factor alpha polypeptide
2,60	EGR1	early growth response 1
2,60	MYO9B	Memczak2013 ANTISENSE, CDS, coding, INTERNAL best transcript NM_004145
2,67	FLNA	Jeck2013 ANTISENSE, CDS, coding, INTERNAL, OVCODE, OVEXON best transcript NM_001110556
2,71	GPRC5A; MIR614	G protein-coupled receptor, class C, group 5, member A; microRNA 614
2,71	PLLP	plasmolipin
2,79	PALLD	palladin, cytoskeletal associated protein
2,84	AKAP12	A kinase (PRKA) anchor protein 12
2,94	IER3	immediate early response 3
3,11	S100A11	S100 calcium binding protein A11
3,18	PAQR5	progestin and adipoQ receptor family member V
3,29	SERPINE1	serpin peptidase inhibitor, clade E (nexin, plasminogen activator inhibitor type 1), member 1
3,54	RGCC	regulator of cell cycle
3,81	DDX5	Memczak2013 ANTISENSE, CDS, coding, INTERNAL best transcript NM_004396
3,81	ID1	inhibitor of DNA binding 1, dominant negative helix-loop-helix protein
3,89	TMC7	transmembrane channel like 7
5,31	DUSP5	dual specificity phosphatase 5

References

Alexanian, A.; Miller, B.; Roman, R. J.; Sorokin, A. 20-HETE-producing enzymes are up-regulated in human cancers. Cancer Genomics Proteomics. 2012, 9(4), 163–169.

Bayda, S.; Hadla, M.; Palazzolo, S.; Riello, P.; Corona, G.; Toffoli, G.; Rizzolio, F. Inorganic nanoparticles for cancer therapy: a transition from lab to clinic. Curr Med Chem. 2018, 25(34), 4269–4303.

Carbone, C.; Piro, G.; Merz, V.; Simionato, F.; Santoro, R.; Zecchetto, C.; Tortora, G.; Melisi, D. Angiopoietin-Like Proteins in Angiogenesis, Inflammation and Cancer. Int J Mol Sci. 2018, 19(2), 1-22.

Debacq-Chainiaux F.; Boilan E.; Le Moutier J.D.; Weemaels G.; Toussaint O. p38MAPK in the Senescence of Human and Murine Fibroblasts. Protein Metabolism and Homeostasis in Aging. 2010, 694, 126-137.

Deelen, J.; Uh, H.; Monajemi, R.; Van Heemst, D.; Thijssen, P. E.; Böhringer, S.; Van den Akker, E.; De Craen, A.; Rivadeneira, F.; Uitterlinden, A. G.; Westendorp, R. G. J.; Goeman, J. J.; Slagboom, P. E.; Houwing-Duistermaat, J. J.; Beekman, M. Gene set analysis of GWAS data for human longevity highlights the relevance of the insulin/IGF-1 signalling and telomere maintenance pathways. Age. 2013, 35, 235-249.

Estevez, H.; Garcia-Lidon, J. C.; Luque-Garcia, J. L.; Camara, C. Effects of chitosan-stabilized selenium nanoparticles on cell proliferation, apoptosis and cell cycle pattern in HepG2 cells: comparison with other selenospecies. Colloid. Surface. B 2014, 122, 184-193.

Estevez, H.; Garcia-Calvo, E.; Rivera-Torres, J.; Vallet-Regi, M.; Gonzalez, B.; Luque-Garcia, J.L. Transcriptome analysis identifies novel mechanisms associated with antitumor effect of chitosan-stabilized selenium nanoparticles. Pharmaceutics 2021, 13, 356.

Estevez, H.; Garcia-Calvo, E.; Mena, M.L.; Alvarez-Fernandez Garcia, R.; Luque-Garcia, J.L. Unraveling the mechanisms of Ch-SeNPs cytotoxicity against cancer cells: insights from targeted and untargeted metabolomics. Nanomaterials 2023, 13, 2204.

Guan, B.; Yan, R.; Li, R.; Zhang, X. Selenium as a pleiotropic agent for medical discovery and drug delivery. Int J Nanomedicine. 2018, 13, 7473–7490.

Hosnedlova, B.; Kepinska, M.; Skalickova, S.; Fernandez, C.; Ruttkay-Nedecky, B.; Peng, Q.; Baron, M.; Melcova, M.; Opatrilova, R.; Zidkova, J.; Bjørklund, G.; Sochor, J.; Kizek, R. Nano-selenium and its nanomedicine applications: a critical review. Int J Nanomedicine. 2018, 13, 2107–2128.

Kawabata, H.; Yang, R.; Hirama, T.; Vuong, P. T.; Kawano, S.; Gombart, A. F.; Koeffler, H.P. Molecular cloning of transferrin receptor 2. A new member of the transferrin receptor-like family. J. Biol. Chem. 1999, 274, 20826-20832.

Ke, J.; Wu, R.; Chen, Y.; Abba, M. L. Inhibitor of DNA binding proteins: implications in human cancer progression and metastasis. Am J Trans Res. 2018, 10(12), 3887–3910.

Kuilman, T.; Michaloglou, C.; Mooi, W.J.; Peeper, D.S. The essence of senescence. Genes Dev 2010, 24, 2463-79

Kumari, P.; Ghosh, B.; Biswas, S. Nanocarriers for cancer-targeted drug delivery. . Dru. Target. 2016, 24(3), 179-191.

Lee, K. T.; Lee, Y. W.; Lee, J. K.; Choi, S. H.; Rhee, J. C.; Paik, S. S.; & Kong, G. Overexpression of Id-1 is significantly associated with tumour angiogenesis in human pancreas cancers. Br J Cancer. 2004, 90(6), 1198–1203.

Lopez-Heras, I.; Sanchez-Diaz, R.; Anunciacao, D. S.; Madrid, Y.; Luque-Garcia, J. L.; Camara, C. Effect of chitosan-stabilized selenium nanoparticles on cell cycle arrest and invasiveness in hepatocarcinoma cells revelead by quantitative proteomics. J. Nanomed. Nanotechnol. 2014, 5, 1000226.

Luo, H.; Wang, F.; Bai, Y.; Chen, T.; Zheng, W. Selenium nanoparticles inhibit the growth of HeLa and MDA-MB-231 cells through induction of S phase arrest. Colloid. Surface. B. 2012, 94, 304-308.

Luo, Z.; Hu,Y.; Xin, R.; Zhang, B.; Li, J.; Ding, X.; Hou, Y.; Yang, L.; Cai, K. Surface functionalized mesoporous silica nanoparticles with natural proteins

for reduced immunotoxicity. J. Biomed. Mater. Res. 2013, 102, 3781-3794.

Maehara, K.; Takahashi, K.; Saitoh, S. CENP-A reduction induces a p53-dependent cellular senescence response to protect cells from executing detective mitoses. Mol Cell Biol. 2010, 9, 2090-2104.

Mittal, B.; Tulsyan, S.; Kumar, S.; Mittal, R. D.; Agarwal, G. Cytochrome P450 in Cancer Susceptibility and Treatment. Adv Clin Chem. 2015, 71, 77–139.

Montalvo-Quiros, S.; Aragoneses-Cazorla, G.; Garcia-Alcalde, L.; Vallet-Regi, M.; Gonzalez, B.; Luque-Garcia, J.L. Cancer cell targeting and therapeutic delivery of silver nanoparticles by mesoporous silica nanocarriers: insights into the action mechamisms using quantitative proteomics. Nanoscale 2019, 11, 4531.

Murray, G. I.; Patimalla, S.; Stewart; K. N.; Miller, I. D.; Heys, S. D. Profiling the expression of cytochrome P450 in breast cancer. Histopathology. 2010, 57(2), 202-211.

Nicol, S.M.; Bray, S.E.; Black, H.; Lorimore, S.A.; Wright, E.G.; Lane, D.P.; Meek, D.W.; Coates, P.J.; Fuller-Pace, F.V. The RNA helicase p68 (DDX5) is selectively required for the induction of p53-dependent p21 expression and cell cycle arrest after DNA damage. Oncogene. 2013, 32, 3461 - 3469.

Porath, B.; R.A. Weinberg. The signals and pathways activating cellular senescence. Int J Biochem Cell Biol. 2005, 37, 961-976.

Pugazhendhi, A.; Edison, T.; Karuppusamy, I.; Kathirvel, B. Inorganic nanoparticles: A potential cancer therapy for human welfare. Int J Pharm. 2018, 539(1-2), 104–111.

Rosenholm, J. M.; Sahlgren, C.; Lindén, M. Towards multifunctional, targeted drug delivery systems using mesoporous silicananoparticles – opportunities & challenges. Nanoscale, 2010, 2, 1870-1883.

Sherr, C.J.; McCormick, F. The RB and p53 pathways in cancer. Cancer Cell 2002, 2, 103-12.

Tang, J.; Wang, Q.; Yu, Q.; Qiu, Y.; Mei, L.; Wan, D.; Wang, X.; Li, M.; He, Q. A stabilized retro-inverso peptide ligando

of transferrin receptor for enhanced liposome-based hepatocellular carcinoma-targeted drug delivery. Acta Biomater. 2019, 83, 379-389.

Tao, Q. F.; Yuan, S. X.; Yang, F.; Yang, S.; Yang, Y.; Yuan, J. H.; Wang, Z. G.; Xu, Q. G.; Lin, K. Y.; Cai, J., Yu, J.; Huang, W. L.; Teng, X. L.; Zhou, C. C.; Wang, F.; Sun, S. H.; Zhou, W. P. Aldolase B inhibits metastasis through Ten-Eleven Translocation 1 and serves as a prognostic biomarker in hepatocellular carcinoma. Mol Cancer. 2015, 14, 170.

Tian, Y. F.; Hsieh, P. L.; Lin, C. Y.; Sun, D. P.; Sheu, M. J.; Yang, C. C.; Lin, L. C.; He, H. L.; Solórzano, J.; Li, C. F.; Chang, I. W. High Expression of Aldolase B Confers a Poor Prognosis for Rectal Cancer Patients Receiving Neoadjuvant Chemoradiotherapy. J Cancer. 2017, 8(7), 1197–1204.

Vasaitis, T. S.; Bruno, R. D.; Njar, V. C. CYP17 inhibitors for prostate cancer therapy. J Steroid Biochem Mol Biol. 2011, 125(1-2), 23–31.

Yu, T.; Wang, X.; Zhu, G.; Han, C.; Su, H.; Liao, X.; Yang, C.; Qin, W.; Huang, K.; Peng, T. The prognostic value of differentially expressed CYP3A subfamily members for hepatocellular carcinoma. Cancer Manag Res. 2018, 10, 1713–1726.

Zou, J.; Lei, T.; Guo, P.; Yu, J.; Xu, Q.; Luo, Y.; Ke, R.; Huang, D. Mechanisms shaping the role of ERK1/2 in cellular senescence. Mol Med Rep. 2018, 19(2), 759–770.

Capítulo 3. Evaluación del potencial de las SeNPs como micobactericida

La investigación recogida en el **Capítulo 3** es la referente a la evaluación de las SeNPs como agente bactericida. Las nanopartículas se testaron tanto en *Mycobacterium smegmatis* como en *Mycobacterium tuberculosis*. Los ensayos demostraron la capacidad de las SeNPs para inhibir el crecimiento bacteriano, y los análisis por TEM y cryo-TEM revelaron los daños en la pared bacteriana a causa de esta exposición, y su consiguiente extrusión del material citoplasmático.


Antimycobacterial effect of selenium nanoparticles on Mycobacterium tuberculosis

3.1. Antimycobacterial effect of selenium nanoparticles on Mycobacterium tuberculosis

Hector Estevez, Ainhoa Palacios, David Gil, Juan Anguita, Maria Vallet-Regi, Blanca González, Rafael Prados-Rosales, Jose L. Luque-Garcia

Frontiers in microbiology, 11 (2020)

Abstract

Tuberculosis remains the leading cause of death from a single infection agent worldwide. In recent years, the occurrence of tuberculosis cases caused by drug-resistant strains has spread and is expected to continue to grow. Therefore, the development of new alternative treatments to the use of antibiotics is highly important. In that sense, nanotechnology can play a very relevant role, due to the unique characteristics of nanoparticles. In fact, different types of nanoparticles have already been evaluated both as potential bactericides and as efficient drug delivery vehicles. In this work, the use of selenium nanoparticles has been evaluated to inhibit the growth of two types of mycobacteria: *Mycobacterium smegmatis* and *Mycobacterium tuberculosis*. The results showed that selenium nanoparticles are able to inhibit the growth of both types of mycobacteria by damaging their cell envelope integrity. These results open a new opportunity for the use of this type of nanoparticles as antimycobacterial agents by themselves, or for the development of novel nanosystems that combine the action of these nanoparticles with other drugs.

1. Introduction

Tuberculosis (TB) is a chronic infectious disease transmitted aerially through droplets expelled by an infected person. The disease is caused by the slow-growing tubercle bacillus Mycobacterium tuberculosis (Mtb). TB is the leading cause of death due to infection worldwide, with approximately 1.4 million deceased in 2018 [113] and estimates at 75 million people dying from TB over the next 35 years. In 2018 alone, new TB cases were estimated to be 10.4 million worldwide. Currently, TB treatment requires a six-month regimen of four first-line drugs, which are ineffective at treating infection with multidrug-resistant (MDR) Mtb strains. These strains are rapidly spreading worldwide (more than 480,000 cases reported last year according to the TB alliance) and could cost $16 trillion over the next 35 years. Since microbial resistance to antibiotics increases, there is a call for non-antibiotic therapies that can fill the gaps for bactericidal purposes where antibiotics fail [114]. In the recent years, the combination of nanotechnology and biomedicine has proven to be promising for multiple purposes, including in bactericide applications [115,116,117].

Nanoparticles are highly promising as antimicrobials, complementary to antibiotics, as they act by influencing the bacterial cell wall by direct contact without the need to be endocytosed [118,119]. Their small size implies a greater surface-area-to-volume ratio than bulk material. Also, they may have optical or even magnetic properties [120]. There is a great variety of nanoparticles in use as antimicrobials, such as metal, metal oxide or organic nanoparticles, involving multiple modes of action [121,122,123]. However, nanoparticles affect bacteria in two main lethal pathways, which can occur simultaneously: disruption of membrane potential and integrity, or production of reactive oxygen species (ROS) [124].

Selenium nanoparticles (SeNPs) have already been suggested for multiple biomedical applications due to their antioxidant properties and differential behavior in comparison to other selenospecies [125]. Also, SeNPs have been shown to have antimicrobial activity against different types of bacteria [126]. However, SeNPs have

never been proven before to have an antimicrobial effect on Mtb.

Therefore, in this work, the mycobactericidal capacity of SeNPs has been evaluated on two types of mycobacteria, the fast-growing Mycobacterium smegmatis (Msm) and the slow-growing Mtb, finding an effective inhibition in the mycobacterial growth in a dose-dependent manner. A structural analysis of the mycobacteria subjected to the presence of the SeNPs has been performed by means of electron microscopy to analyze their effect on the cell envelope, showing that SeNPs interact directly with the mycobacteria membrane of Mtb and Msm, compromising their integrity and inducing extrusion of cytoplasmic material.

2. Materials and methods

2.1. Chemicals

Reagents for the synthesis of SeNPs: chitosan, bovine serum albumin, sodium selenite, ascorbic and acetic acid were purchased from Sigma-Aldrich. Reagents for electron microscopy: glutaraldehyde, cacodylate and formaldehyde were purchased from Sigma. Uranyl formate was purchased from Electron Microscopy Sciences (Hatfield, PA, US).

2.2. Synthesis of SeNPs

Chitosan-stabilized SeNPs (Ch-SeNPs) were synthesized following the procedure described by Bai et al. [127]. Briefly, 10 mL of an aqueous chitosan polysaccharide solution (0.5% w/v) were mixed with 7.5 mL of ascorbic acid 0.23 M and 5 mL of acetic acid 2.4 M. Then, 0.25 mL of sodium selenite 0.51 M were slowly added to the previous solution. SeNPs formation was recognized by observing the change of the solution from colorless to red as the reaction progressed. After the synthesis, the colloidal suspension was diluted to 50 mL with distilled water, resulting in final concentrations of 200 mg L−1 of Se and 0.1% of chitosan. Finally, the colloidal suspension was dialyzed for 2 h at room temperature in a ratio of 10 mL against 2 L of distilled water and using a 12 kDa of MWCO membrane.

For control experiments, BSA-SeNPs were also prepared following the same procedure but using an aqueous bovine serum albumin solution (0.5% w/v) instead of the chitosan solution.

2.3. Analytical characterization of the synthesized SeNPs

Transmission electron microscopy (TEM) was performed using a JEOL JEM 1400 instrument operated at 120 kV equipped with a CCD camera (KeenView Camera) and an energy dispersive X-ray spectroscopy (EDS) analyzer. Sample preparation was performed by placing one or two drops of the SeNPs colloidal suspension onto carbon-coated copper grids.

Electrophoretic mobility measurements of the materials suspended in water were used to calculate the zeta potential (ζ) values of the nanoparticles. Measurements were performed in a Zetasizer Nano ZS (Malvern Instruments Ltd., United Kingdom) equipped with a 633 nm "red" laser. The hydrodynamic size of nanoparticles was measured by dynamic light scattering (DLS) with the same Malvern instrument.

2.4. Bacterial strains and culture conditions

Mycobacterium smegmatis mc2155 (Msm) and Mycobacterium tuberculosis H37Rv (Mtb) strains (obtained from the ATCC) were grown in Middlebrook 7H9 medium supplemented with 10% (v/v) OADC supplement (NaCl 8.5 g/L, BSA fraction V 50 g/L, dextrose 20 g/L, 5% (v/v) oleic acid solution 1%, 40 mg/L catalase), 0.5 % (v/v) glycerol and 0.05% Tyloxapol (v/v; Sigma). Cultures were grown at 37 ºC in static standing 25 cm2 flasks with vented caps. Msm-Lux was generated by transforming Msm with the plasmid construct pMV306hsp+Lux (which contains the entire bacterial Lux operon cloned in a mycobacterial integrative expression vector) [128].

2.5. Minimum inhibitory concentration (MIC) assay

Minimum inhibitory concentration (MIC) assay was carried out in 96-well plates diluting exponentially growing Msm or Mtb at an initial density of 1 x 105 bacteria/mL in the presence of two-fold serial dilutions of Ch-SeNPs or BSA-SeNPs starting at 50 µg/mL and including one control sample with no NPs. Plates were incubated at 37 ºC for 7 days (Msm) or for 20 days (Mtb). Bacterial growth was monitored every day for Msm and every week for Mtb and was determined by measuring optical density at 570 nm. The assay was performed in triplicate. MIC values were selected as the minimum concentration able to suppress mycobacterial growth. Alternatively, Msm-lux was submitted to MIC assay and cell viability was assessed by

measuring relative luminescence units (RLUs) at day 2. Correlation between colony forming units (CFUs) was performed according to a previously performed *in vitro* RLUs vs CFUs curve.

2.6. Transmission electron microscopy (TEM) (Negative staining)

Msm cells were fixed with 2% glutaraldehyde in 0.1 M cacodylate at room temperature for 2 h, and then incubated overnight in 4% formaldehyde, 1% glutaraldehyde, and 0.1% PBS. For negative staining of the samples, a drop of the fixed bacterial suspension was applied directly onto a glow-discharged EM grid (QUANTIFOIL. Formvar/Carbon. Cu 400 mesh grids). The sample was allowed to be adsorbed and then blotted with filter paper (Whatman grade No. 1). The grid was washed by touching the surface with two consecutive drops of 0.75% (w/v) uranyl formate, blotting each time, and stained for 1 min with one more drop of the same staining agent. Negative stained samples were examined in a JEOL JEM-1230 (accelerating voltage 100 kV) electron microscope, and images were recorded with a CCD camera ORIUS SC100 (4 × 2.7 k pixel).

2.7. Cryo-electron microscopy (Cryo-EM)

Msm and Mtb cultures were fixed as above prior to vitrification. Grids were prepared following standard procedures and observed at liquid nitrogen temperatures in a JEM-2200FS/CR transmission electron microscope (JEOL Europe, Croissy-sur-Seine, France) operated at 200 kV. An in-column omega energy filter helped to record images with improved signal/noise ratio by zero-loss filtering. The energy selecting slit width was set at 9 eV. Digital images were recorded on an UltraScan4000 CCD camera under low-dose conditions at a magnification of 55,058 obtaining a final pixel size of 2.7 Å/pixel.

3. Results

3.1. Synthesis and Characterization of SeNPs

Selenium nanoparticles were prepared via a redox system in the presence of a biomacromolecule as soft template to control the nucleation and growth of the inorganic nanoselenium. The chemical reduction of selenite with ascorbic acid in the presence of a polysaccharide such as chitosan as stabilizer and capping agent afforded red

elemental selenium in colloidal state [129]. B) 241. Based on our previous work, 0.1 % of chitosan concentration was selected to prepare the SeNPs [13]. Under these conditions, the nanoparticles proved to be colloidally stable. Two months after their synthesis, no flocculated material was present, DLS measurements showed no displacement of the hydrodynamic size distribution and no significant differences in the shape or size of the SeNPs were observed by TEM.

Transmission electron microscopy (TEM) images show well dispersed Ch-SeNPs that exhibit spherical morphology and homogeneous sizes of around 60-80 nm **(Figure 1A**). The energy dispersive spectroscopy analysis (**Figure 1B**) indicates a composition in selenium for the Ch-SeNPs, also being observed in the spectrum the signals for C and O from chitosan and the carbon coated copper grid.

The hydrodynamic size distribution of the Ch-SeNPs measured in the aqueous colloidal suspension (**Figure 1C**) is monomodal and reasonably narrow, with a maximum centered at 105.7 ± 2.5 nm of diameter, which is in concordance with the smaller size of the inorganic nanoparticle determined in the TEM study. The ζ-potential of the Ch-SeNPs in water is in the zone of colloidal stability with a value of + 66.6 ± 4.7 mV. This highly positive value is due to the surface stabilization with chitosan, which possesses an equilibrium for the protonation of the amino groups in water. Therefore, chitosan allows the selenium nanoparticles to form stable colloidal suspensions due to both electrostatic as well as steric stabilization.

3.2. Antimycobacterial activity of SeNPs

We evaluated the ability of SeNPs to inhibit the growth of two different species of mycobacteria: the fast-growing Msm and the slow-growing Mtb. SeNPs were found to be effective in inhibiting mycobacterial growth in a dose-dependent manner, showing MIC values of 0.400 μg/mL for Msm (**Supplementary Fig. S1A**) and 0.195 μg/mL for Mtb (Fig. 2A). To determine whether this inhibition was concomitant to bacterial cell death we generated a luciferase-expressing reporter strain of Msm (Msm-Lux) [16]. Correlation between relative fluorescence units (RLUs) and CFUs was previously determined (**Supplementary Figure S2A**) and used to calculate viable bacteria after treatment of Msm-Lux with SeNPs (**Supplementary Figure**

S2B). We observed a reduction in CFUs as concentration of NPs increased, indicating the bactericidal effect of SeNPs. By this method MIC was similar to that of previously determined by measuring optical density.

To gain insight into the nature of the inhibitory effect of SeNPs, we performed ultrastructural analysis of Msm submitted to 0.400 µg/mL of SeNPs.

Transmission electron micrographs of negative stained samples suggested that Msm exposed to SeNPs manifested reduced integrity of cell envelope leading to extrusion of cytoplasmic material, relative to untreated Msm (**Supplementary Figure S1B and S1C**). To capture the antimycobacterial effect of SeNPs in a close-to-native state, treated (0.195 ug/mL) and untreated Msm and Mtb cells were submitted to cryo-EM. This technique revealed more in detail the membrane damage, both in Msm (**Supplementary Figure S1D and S1E**) and Mtb (**Figure 2B-F**). In

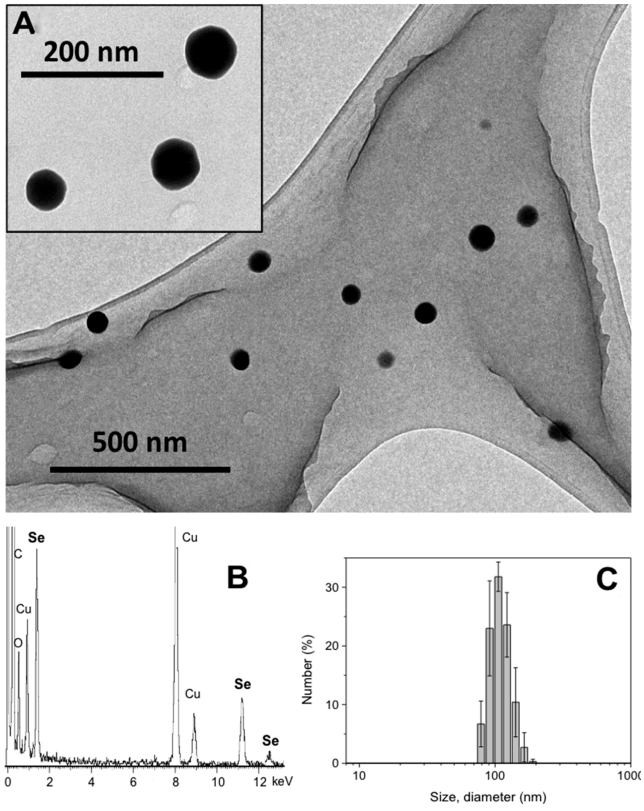

Figure 1. Characterization of the synthesized SeNPs. A) TEM images of a 200 mg L-1 suspension of Ch-SeNPs. B) EDS spectrum of Ch-SeNPs. C) Hydrodynamic size distribution of the Ch-SeNPs in aqueous colloidal suspension measured by dynamic light scattering.

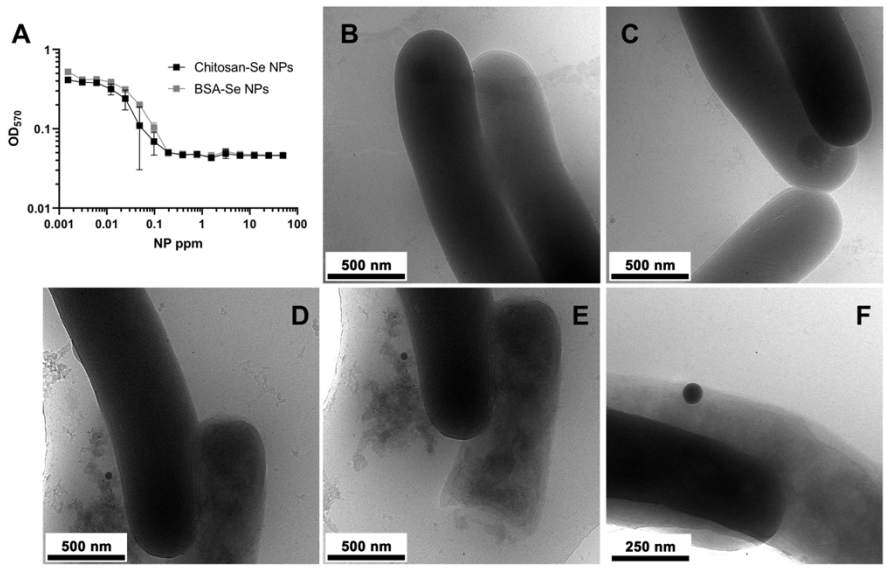

Figure 2. Antimicrobial activity of SeNPs against Mycobacterium tuberculosis. A) MIC assay testing the antibacterial activity of Ch-SeNPs and BSA-SeNPs after 20 days of treatment. (B-E) Ultrastructural analysis by cryo-EM of untreated Mtb cells (B, C) or Mtb cells treated with an inhibitory concentration (0.195 µg/mL) of SeNPs (D-F).

addition, SeNPs could be spotted in direct contact with the mycobacterial cell wall, suggesting a direct connection between the effect of SeNPs and the reduction of the integrity of the mycobacterial cell envelope.

4. Discussion

The rapid spread of antibiotic-resistant Mtb strains makes it necessary to search for alternative treatments. In this sense, the use of nanoparticles with mycobactericidal potential could be especially interesting, since nanoparticles have a high surface area, which means that they contain a high number of active sites to be able to interact with biological entities and, on the other hand, they have a high capacity to penetrate cells and tissues [130,131].

Previous studies have used different types of nanoparticles, either as drug carriers [132] or as bactericidal agents themselves against tuberculosis. In the latter case, the mycobactericidal potential of different metallic nanoparticles such as Ag [133], AgO, AgZnO [134] or Ga [135] nanoparticles, has been evaluated.

Among the different nanoparticles that are being used in biomedicine, Se nanoparticles are especially interesting because of their low toxicity. While Se has a narrow therapeutic window and the

toxicity margins are very delicate, SeNPs possess remarkably reduced toxicity [136]and it has been proposed as a therapeutic agent for different applications without significant side effects [137]. As a matter of fact, it has been demonstrated that SeNPs are less toxic than other inorganic and organic selenospecies [13], showing unique properties such as their capacity for inducing cell cycle arrest [138] without inducing a significant degree of apoptosis [13]. In addition, SeNPs have also been used as a bactericidal agent against Staphylococcus aureus [139] and their anti-biofilm capacity has been demonstrated against S. aureus, Pseudomonas aeruginosa and Proteus mirabilis [140]. However, to date, the potential of Se nanoparticles against Mtb has not been evaluated.

In this study, the mycobactericidal capacity of SeNPs has been demonstrated against two types of mycobacteria, Msm and Mtb, with MIC values of 0.400 µg/mL and 0.195 µg/mL, respectively. Furthermore, to rule out an effect of the chitosan in the Ch-SeNPs bactericidal action, SeNPs stabilized with a protein such as bovine serum albumin (BSA-SeNPs) have been evaluated on Mtb showing an inhibition on the bacterial growth at similar concentrations than Ch-SeNPs (Fig. 2A). Therefore, the mycobactericidal effect is due to the SeNPs themselves and not to the presence of the stabilizing agent chitosan. In agreement with the previously demonstrated bactericidal effect of SeNPs on unrelated bacterial pathogens, we have demonstrated that these NPs can also kill Mycobacteria. Furthermore, our analyses by TEM and cryo-EM have shown that SeNPs come into contact with the cell wall of Mtb and Msm, compromising their integrity and inducing extrusion of cytoplasmic material. These results open a new opportunity for the development of novel nanosystems with high antimycobacterial potential that, alone or in combination with antibiotics, could improve the treatment of multi-drug resistant tuberculosis strains.

Declarations

Funding: This study was supported by Ministerio de Economía y Competitividad (MINECO) grants: CTQ2017-85673-R (JLL-G), SAF2016–77433-R (RP-R), RTI2018-096494-B-100 (JA) and the European Research Council ERC-2015-AdG (VERDI) Proposal No. 694160. CIBER is a public research consortium created by ISCIII whose actions are co-funded by the

European Regional Development Fund. CIC bioGUNE thanks MINECO for the Severo Ochoa Excellence Accreditation (SEV-2016–0644). HE acknowledges Ministerio de Ciencia, Innovacion y Universidades from the Spanish Government for a predoctoral fellowship (PRE2018-084196). AP holds a fellowship form the Department of Education of the Basque Government (PRE_2018_1_0229).
Competing Interests: None declared.
Ethical approval: Not required.

References

[1] Global Tuberculosis Report 2019. Geneva: World Health Organization, 2019.

[2] Chandra Mohana N, Yashavantha Rao HC, Rakshith D, Mithun PR, Nuthan BR, Satish S. Omics based approach for biodiscovery of microbial natural products in antibiotic resistance era. J. Genet. Eng. Biotechnol. 2018; 1:1-8.

[3] Vallet-Regí M, González B, Izquierdo-Barba I. Nanomaterials as Promising Alternative in the Infection Treatment. Int J Mol Sci 2019; 20:3806.

[4] Jayawardana, K.W., Jayawardana, H.S.N., Wijesundera, S.A., De Zoysa, T., Sundhoro, M., Yan, M. Selective targeting of mycobacterium smegmatis with trehalose-functionalized nanoparticles. Chem. Commun. 2015; 51:12028-12031.

[5] Reshma VG, Syama S, Sruthi S, Reshma SC, Remya NS, Mohanan PV. Engineered nanoparticles with antimicrobial property. Curr. Drug Metab. 2017; 11:1040-1054.

[6] Wang, L., Hu, C., Shao, L. The antimicrobial activity of nanoparticles: present situation and prospects for the future. Inter. J. Nanomedicine 2017; 12:1227-1249.

[7] Herman A, Herman AP. Nanoparticles as antimicrobial agents: their toxicity and mechanisms of action. J. Nanosci. Nanotechnol. 2014; 1: 946-57.

[8] Baranwal A, Srivastava A, Kumar P, Bajpai VK, Maurya PK, Chandra P. Prospects of nanostructure materials and their composites as antimicrobial agents. Front. in Microbiol. 2018; 9: 422.

[9] Hoseinzadeh, E., Makhdoumi, P., Taha, P., Hossini, H., Stelling, J., Kamal,

M.A., Ashraf, G.M. A review on nano-antimicrobials: metal nanoparticles, methods and mechanisms. Curr. Drug Metab. 2017; 18: 120-128.

[10] Khan, F., Lee, J.W., Pham, D.T.N., Khan, M.M., Park, S.K., Shin, I.S., Kim, Y.M. Antibiofilm action of ZnO, SnO_2 and CeO_2 nanoparticles towards Gram-positive biofilm formin pathogenic bacteria. Recent Pat. Nanotechnol. 2020;

[12] Reshman, V.G., Syama, S., Sruthi, S., Reshma, S.C., Remya, N.S., Mohanan, P.V. Engineered nanoparticles with antimicrobial property. Curr. Drug Metab. 2017; 18:1040-1054.

[13] Beyth, N., Houri-Haddad, Y., Domb, A., Khan, W., Hazan, R. Alternative antimicrobial approach: nano-antimicrobial materials. Evid. Based Complement. Alternat. Med. 2015; 1-16

[14] Estevez H, Garcia-Lidon JC, Luque-García JL, Cámara C. Effects of chitosan-modified selenium nanoparticles on cell proliferation, apoptosis and cell cycle pattern in HepG2 cells: comparison with other selenospecies. Colloids Surf. B Biointerfaces 2014; 122:184-193.

[15] Huang T, Holden JA, Heath DE, O'Brien-Simpson NM, O'Connor AJ. Engineering highly effective antimicrobial selenium nanoparticles through control of particle size. Nanoscale 2019; 11:14937-51.

[16] Bai Y, Wang Y, Zhou Y, Li W, Zheng W. Modification and modulation of saccharides on elemental selenium nanoparticles in liquid phase. Mater Lett 2008; 62:2311-4.

[17] Andreu N, Zelmer A, Fletcher T, Elkington PT, Ward TH, Ripoll J, Parish T, Bancroft GJ, Schaible U, Robertson BD, Wiles S. Optimisation of bioluminescent reporters for use with mycobacteria. PLoS. ONE. 2010;5:e10777.

[18] Zhang Y, Wang J, Zhang L. Creation of highly stable selenium nanoparticles capped with hyperbranched polysaccharide in water. Langmuir 2010; 26:17617-23.

[19] Singh, R., Nawale, L.U., Arkile, M., Shedbalkar, U.U., Wadhwani, S.A., Sarkar, D., Chopade, B.A. Chemical and biological metal nanoparticles as antimycobacterial agents: A comparative study. Int. J. Antimicrob. Agents 2015; 46:183-188.

[20] Kumarasingam, K., Vincent, M., Mane, S.R., Shunmugam, R., Sivakumar, S., Uma Devi, K.R.

[21] Lu T, Wu Y, Zhao C, Su F, Liu J, Ma Z, Han Q. One-step fabrication and characterization of Fe_3O_4/HBPE-DDSA/INH nanoparticles with controlled drug release for treatment of tuberculosis. Mater. Sci. Eng. C Mater. Biol. Appl. 2018; 93:838-845.

[22] Selim A, Elhaig MM, Taha SA, Nasr EA. Antibacterial activity of silver nanoparticles agains field and reference strains of Mycobacterium tuberculosis, Mycobacterium bovis and multiple drug-resistant tuberculosis strains. Rev. Sci. Tech. 2018; 37:823-830.

[23] Jafari A, Mosavari N, Movahedzadeh F, Nodooshan SJ, Safarkar R, Moro R, Kamalzadeh M, Majidpur A, Boustanshenas M, Mosavi T. Bactericidal impact of Ag, ZnO and mized AgZnO colloid nanoparticles on H37Rv Mycobacterium tuberculosis phagocytez by THP-1 cell lines. Microb. Pathog. 2017; 110:335-344.

[24] Choi SR, Britigan BE, Moran DM, Narayanasamy P. Gallium nanoparticles facilitate phagosome maturation and inhibit growth of virulent Mycobacterium tuberculosis in macrophages. PLosS One 2017; 12:e0177987.

[25] Khurana, A., Tekula, S., Saifi, M.A., Venkatesh, P., Godugu, C. Therapeutic applications of selenium nanoparticles. Biomed. Phamacother 2019; 111:802-812.

[26] Hosnedlova, B., Kepinska, M., Skalickova, S., Fernandez, C., Ruttkay-Nedecky, B., Peng, Q., Baron, M., Melcova, M., Opatrilova, R., Zidkova, J., Bjorklund, G., Sochor, J., Kizek, R. Nano-selenium and its nanomedicine applications: a critical review. Int. J. Nanomedicine 2018; 13:2017-2018.

[27] Lopez-Heras, I., Sanchez-Diaz, R., Anunciacao, D.S., Madrid, Y., Luque-Garcia, J.L., Camara, C. Effect of chitosan-stabilized selenium nanoparticles on cell cycle arrest and invasiveness in hepatocarcinoma cells revealed by quantitative proteomics. J. Nanomed. Nanotechnol. 2014; 5:5.

[28] Tran PA, Webster TJ. Selenium nanoparticles inhibit Staphylococcus aureus growth. Int. J. Nanomed. 2011; 6:1553-1558.

[29] Shakibaie M, Foroontanfar H, Golkari Y, Mohammadi-Khorsand T, Shakibaie MR. Anti-biofilm activity of biogenic selenium nanoparticles and selenium dioxide against clinical isolates of Staphylococcus aureus, Pseudomonas aeruginosa, and Proteus mirabilis. J. Trace Elem. Med. Biol. 2014; 29:235-241.

III. Discusión integradora.

La normativa vigente en la Universidad Complutense de Madrid para la elaboración de una Memoria de Tesis Doctoral, en la versión que permite incluir como tales los artículos publicados o en vías de publicación, requiere la inclusión de una sección que recoja una discusión conjunta de los resultados. A continuación, se discuten los resultados más relevantes y, para ello, se ha seguido la división en 3 Capítulos de forma similar a como se ha divido la parte experimental.

CAPÍTULO 1. DEL POTENCIAL QUIMIOTERAPÉUTICO DE LAS NANOPARTÍCULAS DE SELENIO, AL ESTUDIO DE LOS MECANISMOS MOLECULARES IMPLICADOS EN SU ACCIÓN.

Aunque el selenio ha sido apreciado desde hace décadas por sus propiedades antioxidantes, recientemente se ha sugerido que dicho elemento podría tener un potencial como agente anticancerígeno.

La investigación recogida en este primer capítulo se centra en dos objetivos principales: el de comprobar si las SeNPs exhiben un comportamiento diferente a una selección de las formas orgánicas e inorgánicas de selenio más estudiadas, y el de conocer en profundidad los mecanismos a través de los cuales impiden o limitan la progresión de las células cancerígenas.

Para poder estudiar el comportamiento de las SeNPs en células de hepatocarcinoma (HepG2), se optimizaron las condiciones de síntesis (partiendo de un protocolo ya existente), así como el tipo y concentración de estabilizante para mantener una suspensión homogénea y no floculada (quitosano, 0,5% p/v). La caracterización del material se realizó, fundamentalmente, mediante TEM, DLS y medidas de potencial Z.

El diseño experimental inicial recogió una serie te técnicas bioanalíticas (ensayo de viabilidad por MTT, proliferación y muerte celular, migración, etc.) que permitieran comparan preliminarmente los efectos de las nanopartículas con los otros tipos de especies de selenio, orgánicas e inorgánicas. Algunas de las especies de selenio testadas no influyeron en el crecimiento normal de la población celular. Entre las que sí conseguían inhibirla, en mayor o menor grado, las SeNPs demostraron capacidad para impedir el crecimiento de la población celular sin inducir efecto apoptótico (lo que podría resultar tóxico para células sanas). Por otro lado, y en comparación con las otras especies, las SeNPs probaron ser capaces de arrestar el ciclo celular en su fase previa a mitosis

(S/G2-M) mediante una inhibición parcial de Cdk1, lo cual coincide con las características de los nuevos fármacos quimioterapéuticos en desarrollo, capaces de impedir la rápida proliferación de las células de cáncer sin ser tan agresivos como para inducir un efecto tóxico.

Una vez probado el potencial quimioterapéutico de las SeNPs, la investigación recogida en esta memoria se enfocó en profundizar en el descubrimiento de las rutas celulares afectadas por la acción de este material, así como en los mecanismos moleculares que se suceden para impedir la progresión normal de una población de células cancerígenas *in vitro*.

Con objeto de validar las dianas identificadas previamente en relación con el arresto del ciclo celular, así como para descubrir nuevas dianas terapéuticas sobre las que las SeNPs inciden, se procedió a realizar un experimento de transcriptómica. Este tipo de análisis permite la comparación de los genes que se están expresando activamente en un momento dado (en una población control y en otra expuesta a una concentración dada de SeNPs). La técnica de *microarrays* consiste en la colocación de miles de secuencias génicas en un chip, para que, tras el apareamiento de las bases complementarias de la muestra se pueda estimar la expresión génica. Los resultados confirmaron la inhibición parcial del regulador de ciclo celular Cdk1, así como la alteración de múltiples dianas como la sobreexpresión de p21, consecuencia de la activación de MXD1, o la inhibición de CDCA2 (progresión fase G1), ANGPTL3 (crecimiento celular), o FAM111B (arresto del ciclo a través de la ruta de señalización de p53). Además, las células expuestas a las SeNPs resultaron en una mayor expresión de los tránscriptos de varios supresores tumorales como DUSP5 o EGR1 entre otros.

De forma complementaria, y dado que muchos de los genes relacionados con procesos senescentes resultaron alterados (ADHFE1, SGO1, o C5AR1), se investigó acerca de una potencial inducción del fenotipo senescente por parte de las SeNPs. Para ello, se estudió específicamente la expresión de la enzima ß-galactosidasa. Las células expuestas a las nanopartículas sobreexpresaron dicha enzima, validando los resultados obtenidos por los microarrays de transcriptómica, y señalando una vía más por la cual son capaces de inhibir la progresión tumoral.

Los metabolitos no son únicamente el producto final del genoma, sino que representan unidades modulables para regular rutas biomoleculares. Por lo tanto, y de forma complementaria, se analizaron alteraciones en el metaboloma de células de

hepatocarcinoma humano después de la exposición a SeNPs, mediante el análisis por espectrometría de masas. Se siguió tanto una estrategia de metabolómica dirigida (orientada a metabolitos de rutas energéticas) como otra no dirigida que aportara información global del estado del perfil metabólico. En cuanto al metabolismo energético, los niveles de ATP y de NAD^+ (moléculas clave en procesos de crecimiento celular) se vieron significativamente reducidos. La estrategia no dirigida identificó alteraciones muy relevantes en metabolitos involucrados en el arresto del ciclo celular (tirosina, ácido palmítico o la fosfohistona H3). De igual manera, niveles de metabolitos relacionados con la oncogénesis (prolina, serina, o glicina) disminuyeron. De igual manera, se identificaron alteraciones en metabolitos que participan en el ciclo de los ácidos tricarboxílicos o en la producción de aminoácidos de cadena ramificada (procesos energéticos). El análisis de metabolómica permitió, por una parte, el descubrimiento de un gran número de metabolitos sobre los que las SeNPs ejercen un efecto, consiguiendo así modular rutas metabólicas fundamentales en la progresión tumoral; por otro lado, este análisis también permitió confirmar las observaciones previas respecto al arresto del ciclo celular o la promoción de supresores tumorales indudica por las SeNPs, entre otras.

Puesto que los datos de transcriptómica y metabolómica apuntaban a un daño focalizado en elementos del núcleo celular, se diseñó un experimento de proteómica cuantitativa basado en la metodología SILAC centrado exclusivamente en el subproteoma nuclear. Para ello, se llevó a cabo un protocolo de purificación y aislamiento de proteínas nucleares. De las 47 proteínas alteradas, un gran número estaban relacionadas con el arresto del ciclo celular (CDK1, CCNB1, CCNA2 y CDKN1A), las cuales fueron validadas mediante un experimento de qPCR, que confirmó diferencias significativas en su expresión en comparación con las proteínas de la población control. De igual manera, también se identificaron nuevas proteínas alteradas que podrían considerarse dianas terapéuticas (PLEC, SUMO2, RSU1, o SMARCC1, entre otras).

Puesto que una gran variedad de técnicas bioanalíticas, así como la información aportada por todas las técnologías -omicas ensayadas, apuntaban a un potencial real de las SeNPs como agente quimioterapéutico, se diseñó un experimento *in vivo* para poder evaluarlas en un entorno biológico real. A ratones hembra de doce semanas se les inoculó intradérmicamente tumores de melanoma empleando células B16. Una vez los tumores se desarrollaron hasta un cierto tamaño, se dio inicio a un tratamiento a la mitad de la población con SeNPs en días alternos, mientras que la otra mitad solo fue tratada con el

medio de síntesis. Al final del experimento, el tamaño medio del tumor en los ratones tratados con SeNPs fue aproximadamente seis veces menor que el correspondiente a aquellos que solo se trataron con medio de síntesis, confirmándose así la acción antitumoral de las SeNPs en un ambiente complejo *in vivo*.

CAPÍTULO 2. VEHICULIZACIÓN DE LAS SeNPs. BIOCOMPATIBILIDAD, SELECTIVIDAD, Y ACCIÓN MEJORADA.

Una vez confirmado el potencial de las nanopartículas de selenio como agente antitumoral (*in vivo* e *in vitro*), así como tras haber profundizado en los mecanismos moleculares involucrados en dicha acción, se planteó el diseño de un nanosistema biocompatible que, por un lado, tuviera como eje farmacológico a las SeNPs, pero que por otra parte pudiera contar con elementos para realizar una vectorización selectiva y efectiva hacia las células tumorales. Las nanopartículas de sílice mesoporosa son un excelente agente en el andamiaje de este tipo de sistemas. Son altamente biocompatibles, pueden alojar moléculas en sus poros, así como inmovilizar agentes de targeting en su superficie. Después de una evaluación de receptores de membrana en múltiples líneas celulares de cáncer, se comprobó que la gran mayoría sobreexpresaba receptores de transferrina en su membrana. Es por eso que se propuso el anclaje de esta proteína en la superficie del andamio de mesoporosa de sílice. Dicha proteína debía tener una función dual: la ya comentada de ligando de vectorización para la internalización selectiva en células tumorales como sobreexpresión de receptores de transferrina, y la de matriz para la nucleación de las SeNPs.

Después de la optimización del proceso de síntesis, así como de su posterior caracterización físico-química, se dio comienzo a la evaluación del efecto del nanosistema nombrado como MSNs-Tf-SeNPs en un modelo *in vitro*. En primer lugar, se probó la efectividad de la transferrina como ligando de targeting. Mediante un experimento de citometría de flujo, se comparó la internalización del nanosistema sintetizado en dos cultivos diferentes: HepG2 (sobreexpesan receptores de transferrina en su membrana), y MC3T3 (no expresan receptores de transferrina en su membrana). Los resultados demostraron una internalización muy preferente del nanosistema en células HepG2, confirmando la efectividad del targeting y, por tanto, la selectividad de la

internalización. Posteriormente, se evaluó la viabilidad celular tras la exposición al nanosistema, así como su capacidad para inducir el arresto del ciclo celular. Las conclusiones fueron las mismas que en el caso de las SeNPs, demostrándose así que la vehiculización de las SeNPs en el nanosistema MSNs-Tf-SeNPs no interfiere en sus propiedades antitumorales.

Para poder descubrir alteraciones relacionadas con mecanismos moleculares de acción antitumoral, se llevó a cabo un experimento de transcriptómica. Una gran variedad de procesos moleculares relacionados con el cáncer como el metabolismo energético, crecimiento celular o metabolismo de proteínas se revelaron afectados tras la exposición al nanosistema propuesta. Genes cuya sobreexpresión se asocia con mala prognosis en cáncer como ALDOB, CYP450 o CYP3A estaban significativamente inhibidos, al igual que oncogenes como ID1, 2 y 3, o ANGPTL3. Gran parte de los tránscriptos alterados se relacionan con procesos senescentes. Para poder validar esta última conclusión, se llevó a cabo un experimento para evaluar la expresión de uno de los más conocidos marcadores de senescencia: la β-galactosidasa. Los resultados revelaron niveles de expresión de dicha enzima muy semejantes al control de senescencia con exposición a 10 mg/L de etopósido. De forma análoga al proceso de validación de las SeNPs como agente antitumoral, el último paso en la evaluación de la efectividad del nanosistema antitumoral propuesto, consistió en su validación en un modelo *in vivo*. En este caso se optó por el modelo de embriones de pollo, en los que tras inducir la formación de tumores de mama triple negativo con células MDA-MB-231, fueron tratados con el nanosistema propuesto. La eficacia del nanosistema quedó probada al reducir en un 70% el tamaño de los tumores en comparación con los embriones control tratados con el mismo nanosistema pero sin contener el agente terapéutico, las SeNPs.

CAPÍTULO 3. NANOPARTÍCULAS DE SELENIO DE ACCIÓN BACTERICIDA. LA AMENAZA DE LA TUBERCULOSIS.

Pese a no recibir un gran foco de atención mediática, la tuberculosis se mantiene como primera causa de muerte por infección (1,4 millones en 2018). Dada la aparición exponencial de cepas multirresistentes, urge la necesidad del desarrollo de tratamientos alternativos al uso de antibióticos para el tratamiento de la enfermedad.

Puesto que ya se ha testado una gran variedad de nanopartículas, se decidió evaluar la capacidad de las SeNPs para su aplicación como bactericida. En el trabajo incluido en la presente Tesis Doctoral se evaluó la capacidad de las SeNPs para inhibir el crecimiento de dos cepas bacterianas: *Mycobacterium tuberculosis*, y su equivalente atenuada, *Mybacterium smegmatis.*

Mediante un ensayo MIC (minimum inhibitory concentration) se comprobó, preliminarmente, que la concentración de SeNPs está relacionada de forma inversamente proporcional con la población bacteriana. Además, para profundizar en la naturaleza del efecto inhibitorio, se realizó un análisis ultraestructural por microscopía electrónica de transmisión a bacterias expuestas a una concentración determinada de SeNPs, revelando un compromiso en la integridad de la membrana bacteriana, exponiendo el material citoplásmico. Para poder obtener información de un estado próximo al nativo, se realizó criomicrocopía electrónica de transmisión en ambas cepas, evidenciando en mayor detalle el daño en membrana. Estos resultados permitieron, por tanto, concluir que efectivamente las SeNPs poseen un potencial bactericida, y que podrían resultar un agente muy efectivo en la carrera por conseguir tratamientos alternativos contra la multirresistencia bacteriana.

IV. Conclusiones.

Las conclusiones derivadas de la presente Tesis Doctoral se resumen en los siguientes puntos:

1. Las nanopartículas de selenio tienen un comportamiento único en su efecto sobre un modelo *in vitro* de células tumorales en comparación con otras especies de selenio, tanto orgánicas como inorgánicas. Han demostrado tener un efecto citotóxico que reduce la viabilidad celular y la proliferación. Lejos de tener un efecto apoptótico como el que exhiben otras especies, las SeNPs son capaces de arrestar el ciclo celular mediante la inhibición parcial de CDK1, la cual regula la promoción hacia mitosis, convirtiéndolas en un candidato excepcional a agente quimioterapéutico.

2. Las técnologías -ómicas son de gran utilidad para profundizar en los mecanismos biomoleculares responsables de la acción antitumoral de las SeNPs.

El experimento de transcriptómica reveló múltiples alteraciones en elementos clave para el control del ciclo celular (CDC25, C5AR1, MXD1, etc) así como para la inducción de senescencia (IL-4R, CCL-20, SERPINE-1, etc). La exposición a SeNPs implica la alteración de los niveles normales de varios supresores tumorales (BTG3, RGC32, DUSP5, etc) y de tránscriptos relacionados con la generación de ROS.

Los estudios de metabolómica dirigida revelaron una gran disrupción en el metabolismo energético a causa de la exposición a SeNPs. Por su lado, la metabolómica no dirigida identificó 36 metabolitos alterados después de la exposición. La inhibición de la tirosina y las alteraciones en los niveles normales de ciclina E, B1, PCNA o PTTG1, refuerzan las conclusiones acerca del arresto del ciclo celular. Muchos metabolitos relacionados con la activación de oncogenes (prolina, serina, o glicina, entre otros) resultaron significativamente inhibidos. De igual forma, se revelaron alteraciones en el ciclo del folato, de la metionina o de los ácidos tricarboxílicos, entre otros.

La proteómica, mediante el experimento SILAC, consiguió arrojar luz acerca de las alteraciones en los niveles de expresión de ciertas proteínas y su relación con el efecto quimioterapéutico. Esta vez el análisis se centró en las proteínas de núcleo ya que, experimentos previos, localizaban allí el mayor número de alteraciones. Se comprobó nuevamente el arresto del ciclo celular y se descubrieron niveles muy diferentes a los del control de proteínas clave en el desarrollo tumoral, como por ejemplo: PLEC, SUMO2, RSUI1 o SMARCC1, entre otras.

3. La validación definitiva para poder considerar a las SeNPs un agente quimioterapéutico pasaba por testar su efectividad para inhibir el crecimiento tumoral en un entorno *in vivo*. Las SeNPs demostraron ser capaces de inhibir el crecimiento de un tumor de melanoma B16 inducido a una cohorte de ratones a los cuales se trató con las nanopartículas en días alternos, mientras que una segunda cohorte solo recibió el medio de síntesis como tratamiento, que resulto prácticamente inocuo.

4. La síntesis y caracterización del nanosistema de targeting se desarrolló exitosamente. Las nanopartículas de sílice mesoporosa resultaron ser idóneas tanto para anclar la proteína de vectorización (transferrina), como para no inducir ningún tipo de citotoxicidad. La efectividad de la transferrina como ligando de targeting se comprobó comparando células sin expresión de receptores de transferrina en su membrana (MC3T3), con células que sí los expresaban (HepG2), internalizándose de forma muy preferente en las células HepG2.

Se probó la eficacia de la internalización del nanosistema gracias a la transferrina, y se analizó el estado del ciclo celular mediante citometría de flujo, nuevamente observándose un arresto del ciclo celular. Los experimentos de transcriptómica llevados a cabo refrendaron el arresto del ciclo celular (al igual que con las SeNPs), y además descubrieron nuevos potenciales dianas terapéuticas como por ejemplo EGFR, TGFB1o SPOCK2, entre otras. De igual manera, y ya que muchos de los tránscriptos estaban relacionados con procesos

senescentes, se analizó específicamente la expresión de β-galactosidasa, un marcador del fenotipo senescente. Los resultados de expresión de la proteína estaban en consonancia con los correspondientes al control senescente inducido con etopósido.

5. Nuevamente, una vez se hubieron elucidado los mecanismos moleculares más importantes que intervienen en la acción antitumoral del nanosistema MSNs-Tf-SeNPs, los resultados del experimento *in vivo* siguieron la misma línea. El nanosistema se demostró capaz de impedir la proliferación de las células tumorales en embriones de pollo a los que se le había inducido un tumor triple negativo de mama muy agresivo.

6. Las SeNPs son, además de un agente antitumoral, un potencial bactericida. Debido a su gran prevalencia, los experimentos tuvieron como objeto a *Mycobacterium tuberculosis*, y a su cepa inocua, *Mycobacterium smegmatis*. Se demostró que las SeNPs son capaces de impedir el crecimiento de una colonia bacteriana de estas cepas. Las técnicas de TEM y cryo-EM revelaron daños en la pared bacteriana y la extrusión del material citoplasmático al exterior, confirmándose así su valor como bactericida.

Anexo I. Glosario de abreviaciones

Listado de abreviaturas

DNA: Desoxiribonucleic acid

DNAc: Complementary desoxiribonucleic acid

ADP: Adenosine diphosphate

APTS: Aminopropyltriethoxysilane

RNA: Ribonucleic acid

ATP: Adenosine triphosphate

BSA: Bovine serum albumin

CAM: Chorioallantoic membrane

CCD: Charged coupled device

CDK: Cyclin dependent kinase

CFUs: Colony forming units

Ch-SeNPs: Chitosan-stabilized selenium nanoparticles

COFs: Covalent organic frameworks

Cryo-EM: Cryogenic electron microscopy

Cryo-TEM: Cryogenic transmission electron microscopy

CTAB: Cetyltrimethylammonium bromide

DAPI: 4′,6-diamidino-2-phenylindole

DLS: Dynamic light scattering

DMEM: Dulbecco´s Modified Eagles Medium

DMSO: Dimethyl sulfoxide

EDC: Ethylcarbodiimide

EDTA: Ethylenediaminetetraacetic acid

EDX: Energy dispersive X-ray

EI: Electron ionization

EPR: Enhance permeability and retention

ESI: Electrospray ionization source

FBS: Fetal bovine serum

FITC: Fluorescein isothiocyanate

GAPDH: Glyceraldehyde 3-phosphate dehydrogenase

GC-MS: Gas chromatography mass spectrometry

GO: Gene ontology

HepG2: Hepatocarcinoma cells

HPLC: High performance liquid chromatography

HRP: Horse rabbit peroxidase

ICAT: Isotope-coded affinity tags

ICP: Inductive coupled plasma

iTRAQ Isobaric tags for relative and absolute quantification

LC-MS: Liquid chromatography mass spectrometry

MES: 2-morpholinoethanesulfonic acid

MIC: Minimum inhibitory concentration

MOFs: Metal organic frameworks

MRM: Multiple reaction monitoring

MS: Mass spectrometry

MSM: Mycobacterium smegmatis

MSNs -Tf-SeNPs: Mesoporous silica nanoparticles with transferrin and selenium nanoparticles nanosystem

MSNs: Mesoporous silica nanoparticles

MTB: Mycobacterium tuberculosis

MTT: 3-(4,5-dimethyl-thiazol-2-yl)2,5-diphenyl tetrazolium bromide

MWCO: Molecular weight cut off

NAD^+: Nicotinamide adenine dinucleotide

NADH: 1,4-dihydronicotinamide adenine dinucleotide

NMR: Nuclear magnetic resonance

PBS: Phosphate buffer saline

PCA: Principal component analysis

PCR: Polymerase chain reaction

PFA: Paraformaldehyde

PTMs: Postransductional modifications

QC: Quality control

qPCR: Quantitative Polymerase chain reaction

QqQ: Triple quadrupole

RES: Reticuloendotelial system

RLUs: Relative luminescence units

ROS: Reactive oxygen species

RT: Room temperature

RT-qPCR: Real Time Quantitative Polymerase chain reaction

SASP: Senescence-associated secretory phenotype

Se-MeSeCys: Selenomethyl selenocysteine

$SeCys_2$: Selenocystine

SeMet: Selenomethionine

SeNPs: Selenium nanoparticles

SILAC: Stable Isotope Labelling with Amino Acids

CNS: Central nervous system

SPF: Specific pathogen free

TB: Tuberculosis

TCA: Tricarboxylic acids cycle

TEM: Transmission electron microscopy

TEOS: tetraethylorthosilicate

TESPSA: 3-(triethoxysilyl)propylsuccinic anhydride

Tf: Transferrin

TfR: Transferrin receptor

TGA: Thermogravimetric analysis

TMT: Tandem mass tags

TOF: Time of flight

XRD: X ray diffraction

Anexo II. Técnicas analíticas y bioanalíticas

AII.1. Técnicas de caracterización analítica

En el proceso de desarrollo de un material es imprescindible el empleo de técnicas analíticas que informen sobre parámetros en las distintas etapas de síntesis. Es fundamental el control sobre parámetros como la estabilidad de la suspensión, tamaño, composición, incorporación de agentes químicos, degradación, etc. A continuación, se detallan las que han sido principalmente utilizadas en la presente Tesis Doctoral.

AII.1.1 Potencial Zeta (ζ) y Dispersión de luz dinámica (DLS)

El potencial Zeta (ζ) es una medida de la magnitud de la repulsión o atracción electrostática (o de carga) entre las partículas, y es uno de los parámetros que se sabe que afectan a la estabilidad del material. Existen muchos agentes capaces de modificar el valor del potencial Zeta: pH del medio, fuerza iónica, concentración de cualquier aditivo, temperatura, etc. Valores altos del potencial Zeta se correlacionan con estabilidad eléctrica de la suspensión, mientras que valores bajos suelen corresponder a coagulación o floculación (estabilidad deficiente). Conocer el valor de este parámetro es de gran utilidad ya que se puede reducir el tiempo para producir una formulación, predecir la estabilidad a largo plazo de los materiales y prevenir su envejecimiento acelerado.

Para obtener el valor de potencial Zeta de las nanopartículas, se analiza la movilidad electroforética de los materiales suspendidos en medio acuoso. Las medidas de Potencial Zeta se realizaron empelando un Zetasizer Nano ZS (Malvern Instruments Ltd., Reino Unido) con un láser de 633 nm. Las nanopartículas se dispersan en agua con ultrasonidos y agitación con vórtice y se coloca aproximadamente 1 mL de la suspensión en cubetas DTS1070 (Malvern Instruments).

La técnica de dispersión de luz dinámica (DLS) se fundamenta en irradiar la muestra con un haz láser y monitorizar los fotones dispersos en ángulos específicos durante cortos intervalos de tiempo. Difiere de la dispersión de luz estática en que mide fluctuaciones reales de la intensidad de señal, generalmente con ayuda de un sistema de autocorrelación. Las partículas pequeñas se mueven rápidamente generando fluctuaciones rápidas de la intensidad de dispersión, al contrario que las partículas más grandes. La salida de la señal

es una representación directa del comportamiento de difusión de las partículas en la solución, y por tanto se puede relacionar directamente con su tamaño. La dispersión de luz dinámica en el presente trabajo se midió con el mismo instrumento que el potencial Zeta (Malvern Instruments Ltd., Reino Unido) [141].

AII.1.2 Análisis térmicos

Tanto el análisis termogravimétrico (TGA) como el análisis térmico diferencial (DTA) están basados en la medida de la variación de una propiedad física a consecuencia de un calentamiento controlado.

La termogravimetría mide el peso de la muestra de forma continua mientras aumenta y disminuye la temperatura. Sus resultados son representaciones de el peso respecto a la temperatura, aunque puede sustituirse la temperatura por el tiempo (diagramas isotermos). Puesto que se analiza la pérdida o ganancia de masa, la termogravimetría aporta información acerca de si la muestra se descompone o reacciona con otros componentes.

Por el contrario, el análisis térmico diferencial mide la diferencia de temperatura entre la muestra y un material de referencia inerte (en un intervalo determinado), revelando información acerca de los procesos exotérmicos y endotérmicos que tienen lugar en la muestra. Las medidas de DTA pueden realizarse en condiciones ambientales o bajo atmósfera controlada, y son estrictamente cualitativas (distinguen entre reacciones endotérmicas o exotérmicas y a qué temperatura ocurre). Con un calibrado adecuado de la instrumentación puede convertirse en una técnica semicuantitativa para poder conocer la cantidad de calor involucrado.

AII.1.3 Difracción de rayos X y porosimetría de adsorción de gases

La difracción de rayos X (DRX) es una técnica fundamental para estudiar materiales sólidos con estructuras cristalinas periódicas. Entre otras muchas, sus principales aplicaciones son las de identificar fases mineralógicas, análisis cuantitativo de muestras polifásicas, o estudio de cristales con orden atómico estructural de largo alcance [142].

En el caso de las nanopartículas de mesoporosa de sílice, esta técnica se emplea a bajos ángulos (0,2º a 10º 2θ) puesto que las paredes de sílice no presentan estructura cristalina y, en consecuencia, no muestran reflexiones en altos ángulos (5-80º 2θ). Los análisis de difracción de rayos X a bajos ángulos, no obstante, permiten la caracterización de la estructura mesoporosa de las MSNs, proporcionando información acerca de la topología de los poros, distancia promedio poro-poro, y del tipo de estructura mesoporosa. En el caso del nanosistema MSNs-Tf-SeNPs, puede identificarse la fase cristalina de las nanopartículas nucleadas sobre las MSNs. Para este propósito, es necesario realizar las medidas a ángulos más altos.

Como técnica complementaria para la caracterización de la estructura mesoporosa principalmente, se empleó la porosimetría de absorción de gases. Esta técnica permite conocer la superficie externa e interna de este tipo de materiales. Las medidas consisten en un ciclo de adsorción-desorción de un gas, resultando en un volumen retenido en la superficie del sólido a caracterizar que depende directamente de las condiciones de presión.

La superficie específica (S_{BET}) corresponde a la extensión geométrica de la superficie de las paredes de los poros por gramo de sólido adsorbente, y se determina mediante el método Brunauer-Emmett-Teller (BET). En la presente tesis doctoral, el volumen de poro (Vp) se ha calculado a partir de la cantidad de nitrógeno adsorbido a una presión relativa de 0,98. La distribución del tamaño de poros se estima con la isoterma de desorción (método de Barret-Joyner-Halenda, BJH), y el tamaño del mesoporo se calcula a partir del máximo de la curva de distribución del tamaño de poros [143].

AII.1.4 Microscopía de contraste de fases y microscopía de fluorescencia

Un rasgo común de las muestras biológicas observadas al microscopio, como las células vivas y los componentes intracelulares, es que son, en su mayoría, transparentes. La microscopía de contraste de fases se fundamenta en la relación inversamente proporcional entre la velocidad de la luz y los índices de refracción de los medios por los que se propaga. El contraste obtenido de las células y de sus estructuras intracelulares permite observarlas a pesar de ser transparentes [144].

Además, en el caso de contar con moléculas fluorescentes, podemos acoplar un sistema de fluorescencia al microscopio de contraste de fases. Una lámpara de descarga de arco de Hg emite una radiación que pasa a través de un filtro de excitación selectivo de longitud de onda, y llega a la muestra con una longitud de onda específica. Si se trata de una muestra fluorescente, la luz emitida recorre el camino inverso, pasando por el espejo dicromático, nuevamente a través de un filtro de longitud de onda.

La microscopía de fluorescencia es una técnica no invasiva, altamente sensible y específica, que permite observar dónde se localizan ciertas moléculas o compuestos fluorescentes en el interior celular. Es frecuente el empleo de fluorocromos, que tengan afinidad por ciertas zonas u orgánulos de la célula. Por ejemplo, el DAPI es un fluorocromo específico de ADN que emite en azul, o la faloidina, afín a los filamentos de actina, que permite observar el contorno de la célula (**Figura AI.1**) [145,146].

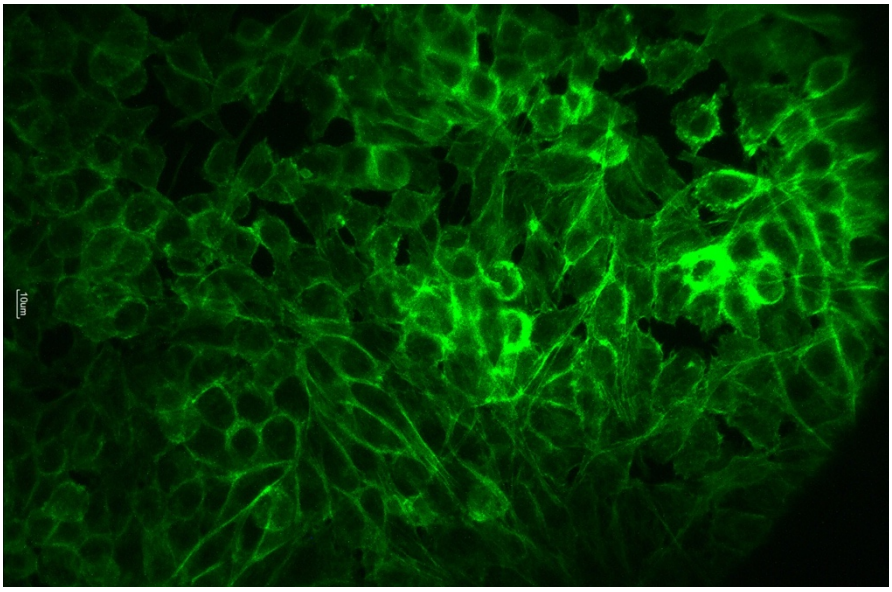

Figura AI.1. Células de hepatocarcinoma (HepG2) cuyos filamentos de actina han sido marcados con faloidina.

AII.1.5 Microscopía electrónica de transmisión (TEM)

El microscopio electrónico de transmisión se emplea para caracterizar y estudiar materiales de diversa naturaleza incluso a escala molecular. El instrumento utiliza un haz de electrones para atravesar la muestra. Parte de los electrones del haz se desviarán por la propia dispersión de la muestra, por lo tanto, se forma una imagen debajo de la muestra cuyas zonas más intensas son inversamente proporcionales a las zonas de mayor masa de

la misma. Esta imagen se aumenta y proyecta sobre una pantalla fluorescente para su visualización en tiempo real. La difracción de electrones permite obtener información acerca de la cristalinidad, mientras que la emisión de rayos X característica de cada muestra revela la composición elemental.

A pesar de que el microscopio electrónico de transmisión puede conseguir resolución molecular, hay muchos factores que pueden limitarla. Las muestras deben ser finas, estar secas y deben poder dispersar los electrones en vacío, por lo que suelen fijarse, estabilizarse, y a veces se introducen metales pesados para generar el contraste necesario para obtener imágenes de alta resolución [147].

El microscopio electrónico de transmisión utilizado en la caracterización de los materiales de la presente Tesis fue el JEOL JEM 1400. Este microscopio tiene una tensión de aceleración de 40 kV a 120 kV, equipado con un sistema de microanálisis tipo SSD (Silicon Drift Detector) refrigerado térmicamente, y una cámara CCD de alta resolución. El material, previa dispersión y homogeneización por ultrasonidos, se deposita sobre una rejilla de cobre para su observación.

La microscopía de transmisión electrónica también se empleó para la caracterización de las bacterias de *Smegmatis tuberculosis*, esta vez mediante tinción negativa. Esta técnica permite, con el empleo de una sustancia opaca a los fotones (alto número atómico), visualizar las cápsulas como entes refringentes sobre una superficie mucho más oscura [148].

Para la caracterización de organismos vivos, es frecuente el uso de la microscopía electrónica criogénica. Esta técnica se fundamenta en el embebido de las estructuras en un entorno vítreo, seguido de observación bajo nitrógeno líquido. La caracterización de dichas bacterias se llevó a cabo mediante un microscopio JEM-2200FS/CR de transmisión electrónica (JEOL Europa, Croissy-sur-Seine, Francia) operando a 200 kV. Para registrar las imágenes fue necesario un filtro de energía omega que mejorara la relación señal/ruido y una cámara UltraScan4000.

AII.1.6 Espectroscopía de energía dispersiva de rayos X

La espectroscopía de energía dispersiva de rayos X (EDX o EDS) es una técnica analítica que se utiliza para conocer la composición de un material sólido. Todas sus variantes dependen de electrones excitantes cerca del núcleo, lo que provoca que aquellos

electrones más lejanos desciendan a niveles de energía para completar los "agujeros" resultantes . Esta técnica trabaja generalmente acoplada tanto a TEM como a SEM (scanning electron microscopy) con el objetivo de identificar y cuantificar la composición elemental de la muestra en áreas concretas de análisis. Para ello se bombardea la muestra con electrones y rayos X. La energía de los fotones emitidos es característica de cada peso atómico del elemento emisor. Esto se debe a que la diferencia de energía entre orbitales aumenta conforme lo hace el peso atómico (ya que aumentan los protones en el núcleo). Así es posible correlacionar la energía emitida con los elementos presentes en la muestra [149].

AII.2 Técnicas bioanalíticas

A continuación se describen las técnicas bioanalíticas que se han empleado para la evaluación funcional de los nanomateriales desarrollados en la presente Tesis Doctoral.

AII.2.1 Evaluación de la actividad microbiana

Uno de los primeros modelos para validar un fármaco en vías de desarrollo son las especies microbianas. Existen dos métodos principales para determinar su susceptibilidad: difusión o dilución. Generalmente los primeros se emplean para compuestos polares, mientras que los segundos para polares y apolares.

Los métodos de difusión se fundamentan en la relación entre la concentración del fármaco necesaria para inhibir una cepa bacteriana y el halo de inhibición de crecimiento de la misma. Para ello, placas de agar son inoculadas por el microorganismo de estudio, y posteriormente se deposita encima un papel de filtro impregnado con el fármaco. Tras dicha incubación puede medirse el halo de inhibición de crecimiento producido por el agente terapéutico. Normalmente las concentraciones evaluadas se ensayan individualmente, sin embargo, puede emplearse un gradiente de concentración del fármaco en medio agar, lo que permite determinar el MIC (concentración mínima inhibitoria) [150].

La composición del papel de filtro puede dificultar la difusión de los agentes de estudio ya que pueden interaccionar con la celulosa. Como alternativa, puede generarse un orificio estéril sobre el agar inoculado con el microorganismo a estudiar. En su interior,

se deposita un volumen del fármaco, y se incuba durante un periodo de tiempo, tras el cual puede evaluarse el halo de inhibición debido a la difusión del agente microbiano por el agar.

Para la determinación de MIC, los métodos de dilución son más adecuados ya que pueden estimar la concentración en agar o en medio de cultivo líquido. La dilución en agar se basa en incorporar diversas concentraciones del agente microbiano en un medio agar fundido, seguido de la inoculación de la especie microbiana de estudio en la parte superior. Tanto para la macrodilución como para la microdilución, se utilizan diluciones seriadas del agente de estudio. Posteriormente se inocula el microorganismo en el medio de cultivo y tras un tiempo determinado puede medirse la MIC. La determinación de este parámetro puede realizarse a nivel visual o bien mediante la medida de la densidad óptica (OD), fundamentada en la turbidez de los cultivos [151].

AII.2.2 Ensayo de viabilidad celular

La viabilidad celular es uno de los parámetros a evaluar en un inicio, cuando se pretende evaluar la citotoxicidad de un fármaco, es decir, los cambios que es capaz de producir en las funciones básicas de las células.

La membrana celular es semipermeable, y envuelve al citoplasma celular, siendo una barrera funcional fundamental. El control de sustancias que la atraviesan está regulado por receptores, transportadores, y rutas de secreción. Es por eso que existen métodos para evaluar la viabilidad celular basados en analizar la integridad de la membrana. Para ello, pueden emplearse tintes o colorantes que sólo atraviesan la membrana en caso de verse comprometida (ej. azul de tripano, yoduro de propidio, etc). De forma alternativa, la integridad de la membrana puede definirse por las sustancias liberadas al medio extracelular que normalmente solo estarían en el interior. Este caso es el de la enzima lactato deshidrogenasa (LDH), la cual se manifiesta sólo si hay daño en la membrana celular, por lo que sus niveles en el exterior pueden correlacionarse con la viabilidad celular.

La evaluación de la viabilidad celular permite obtener información acerca de la dosis (como concentración o intervalo de concentraciones) responsable de una toxicidad letal o subletal. La toxicidad puede testarse mediante múltiples estrategias: observación de cambios morfológicos, cálculo del LD_{50} (concentración a la cual el 50% de células no son

viables), ensayos de crecimiento axonal, adquisición de imágenes de Ca^{2+}, etc. Otro aspecto estrechamente relacionado con la viabilidad celular es la disfunción de la actividad metabólica, por ello existen estudios centrados en la medida de los niveles de ATP o actividad mitocondrial. En el caso de la presente Tesis, el método elegido es el ensayo MTT. El fundamento de este ensayo es una medida de la viabilidad celular entendida como integridad mitocondrial. Una sal de tetrazolio (bromuro de 3-(4,5-dimetiltiazol-2-il)-2,5-difeniltetrazolio) se adiciona al medio de cultivo y es absorbida por las células. Las reductasas mitocondriales de las células viables son capaces de reducir este compuesto a formazán, un compuesto insoluble y violeta (**Figura AI.2**). Al adicionar dimetilsulfóxido (DMSO), se solubiliza el formazán y se puede medir la absorbancia a 595 nm. Esta medida proporciona un porcentaje de viabilidad celular que define la toxicidad del compuesto objeto de estudio [152].

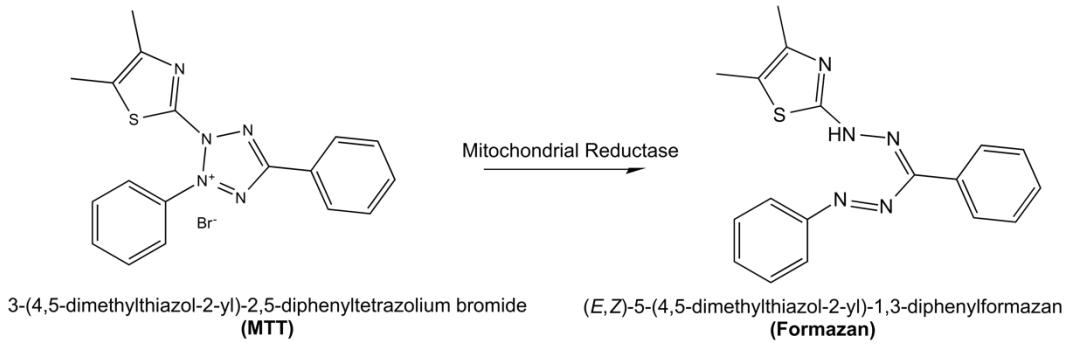

Figura AI.2. Reacción de reducción del compuesto MTT a formazán realizado por las enzimas reductasas mitocondriales.

AII.2.3 Ensayo concentración mínima inhibitoria (MIC)

En microbiología, uno de los factores clave en el estudio de la toxicidad de un material es el estudio de la concentración mínima inhibitoria (MIC). La MIC se define por la concentración más baja de un agente antimicrobiano capaz de inhibir el crecimiento de un microorganismo después de su incubación conjunta. Este parámetro proporciona información acerca de la resistencia de poblaciones de microorganismos ante este tipo de agentes, y permite monitorizar la actividad de fármacos en desarrollo [153]. Experimentalmente, se siembra una concentración constante de microorganismos en

placas multipocillo, a las que se añaden diluciones seriadas del agente a testar (en el caso de la presente Tesis Doctoral: las nanopartículas de selenio). Las placas de bacterias se incuban a 37 ºC y el crecimiento se monitoriza a diario mediante medidas de densidad óptica a 570 nm. Además de determinar la concentración de un determinado fármaco a partir de la cual se inhibe el crecimiento bacteriano (generalmente expresada en μg/mL o mg/L), se establece una clasificación del nivel resistencia de la cepa. Aquellas cepas susceptibles al fármaco se marcan como "s" (susceptible or responding to standard dosing régimen), las que pueden soportar una mayor exposición se marcan como "i" (intermediate or requiring increased exposure), y las que no se ven afectadas como "r" (resistentes.

AII.2.4 Citometría de flujo

La citometría de flujo es una técnica de análisis que permite medir características físicas y químicas de células o partículas suspendidas en medio acuoso. Estas células o partículas se hacen pasar individualmente por un haz luminoso. Tanto la dispersión generada, como la emisión de luz por los fluorocromos presentes en la célula o partícula, aportan información acerca de múltiples parámetros de la célula. En el sistema de detección, a ángulos bajos respecto al haz de luz se sitúa un detector que recoge la dispersión denominada *forward scatter* (FCS), y en ángulo recto respecto al haz, otro que recoge la dispersión *side scatter* (SSC). La FCS está relacionada con el tamaño de las células, mientras que el SSC informa acerca de la complejidad de éstas (**Figura AI.3**). En el caso de la citometría de flujo de fluorescencia, son estos mismo detectores los que recogen la señal de emisión fluorescente.

Una de las ventajas principales de la citometría de flujo es que permite el análisis de un gran número de células en poco tiempo de forma individualizada, además de la posibilidad de incluir múltiples marcajes en ellas para evaluar distintos parámetros. De esta forma, la citometría de flujo es muy útil para evaluar procesos apoptóticos, contenido de DNA (ciclo celular), internalización celular de partículas marcadas con fluoróforos [154], etc.

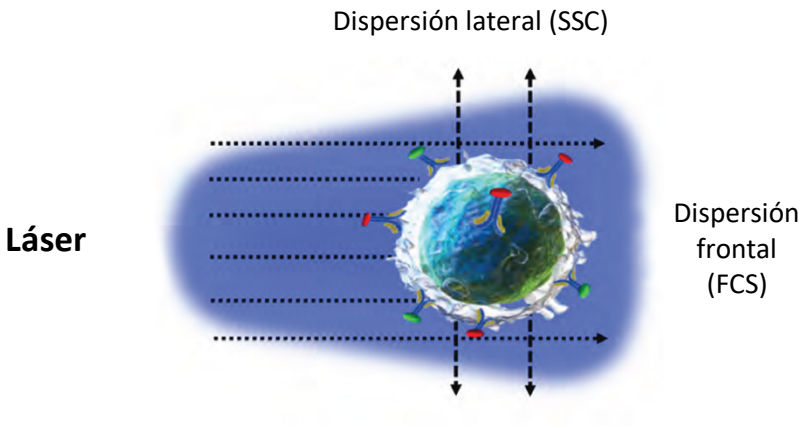

Figura AI.3. Dispersión de luz en citometría de flujo. La desviación frontal (FSC) determina el tamaño celular, mientras que la lateral (SSC) determina la complejidad de la célula.

En concreto, la evaluación del perfil del ciclo celular proporciona información clave para el estudio de los procesos moleculares involucrados en tratamientos quimioterapéuticos **(Figura AI.4).** Para ello son necesarios agentes de tinción específicos de DNA como por ejemplo el yoduro de propidio, o el reactivo Hoechst, el cual presenta afinidad con las regiones ricas en adenina y timina (A-T) [155].

El contenido total de DNA de una célula, va incrementándose conforme progresa el ciclo celular, hasta alcanzar la duplicación del contenido original. En el ciclo pueden diferenciarse cuatro fases principales: fase G1, fase S (síntesis de ADN), fase G2 y fase M (mitosis). De forma teórica, las células en fase G1 tienen una cantidad de ADN que podríamos denominar como "2C", siendo ésta la cantidad unidad de material genético. Por otro lado, las células en fases G2 y M tienen una cantidad "4C" de DNA, mientras que las que se encuentra en fase S, tendrán una cantidad de material genético entre "2C" y "4C". En base a esto y mediante citometría de flujo, se puede correlacionar la intensidad de fluorescencia que proporciona el marcaje de DNA de cada célula, con la cantidad de

material genético de esa célula y, por tanto, determinar así en que fase del ciclo celular se encuentra.

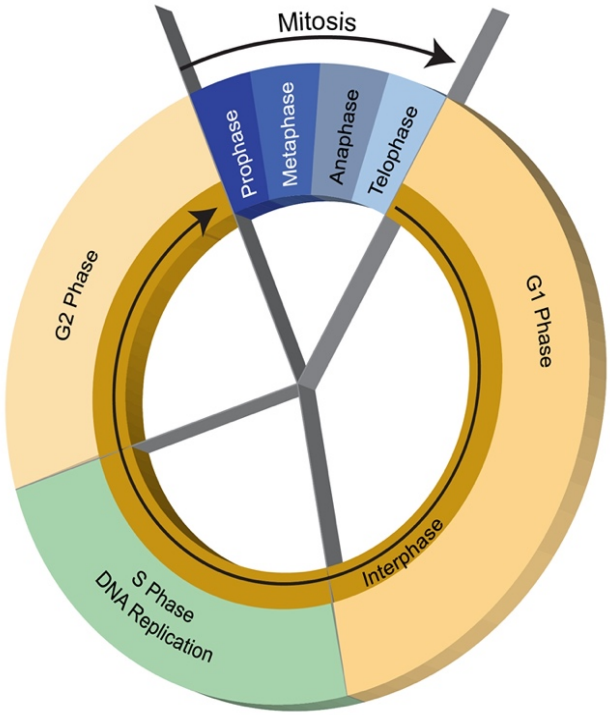

Figura AI.4. Principales fases y subfases del ciclo celular.

AII.2.5 Ensayo de apoptosis

La apoptosis es una forma evolutiva conservada del suicidio celular. La base de su mecanismo es una cascada de enzimas proteolíticas; las caspasas. Estas enzimas consisten en dos unidades principales (~20kDa) y otras dos de menor tamaño (~10kDa), es decir, dos heterodímerosparticipan que forman un tetrámero. Participan en una serie de reacciones impulsadas por señales pro-apoptóticas, ya sea como iniciadoras o como efectoras (escisión proteolítica). Estas caspasas reconoces una secuencia de cuatro aminoácidos, entre los cuales se incluye el residuo de ácido aspártico, que hace las veces de diana para el mecanismo. Para la detección de estas caspasas, y por tanto para la evaluación de la apoptosis, se han desarrollado métodos de inmunoprecipitación, *immuno-blotting*, o empleando sustratos fluorescentes. En la presente Tesis Doctoral, se emplea un kit de APO LOGIX^{TM} SR que emplea el uso de inhibidores de caspasas marcados con sulforodamina. Una vez dentro de la célula, el inhibidor se une

covalentemente a las caspasas y la señal es detectada con un microscopio de fluorescencia. De esta forma, se puede correlacionar de forma cualitativa el grado de inducción de apoptosis de un agente externo, en nuestro caso, las nanopartículas de selenio.

AII.2.6 Ensayo de senescencia

La senescencia celular es un proceso fisiológico que induce cambios en aquellas células que ya no pueden cumplir su función, frenando su proliferación o incluso eliminándolas. En las células senescentes el ciclo celular entra en un estado de parálisis permanente, aunque se mantienen metabólicamente activas. Su fenotipo secretor se expresa, por lo que pueden inducir senescencia a otras células o cáncer. Existen inductores tanto endógenos como exógenos, de naturaleza muy variada. Para evaluar la capacidad de las nanopartículas de selenio para inducir senescencia en células cancerígenas, y por tanto inhibir la proliferación celular de las mismas, se lleva a cabo un ensayo de tinción citoquímica. Este ensayo (Sigma-Aldrich) se fundamenta en la visualización de la expresión de β-galactosidasa la cual sirve como marcador de senescencia.

Para el experimento se disponen células control, células expuestas a Ch-SeNPs, y células expuestas a dos concentraciones de etopósido, 10 y 50 μM (la primera tiene un efecto inductor de senescencia, y la segunda apoptótico). Después del tiempo de exposición, las células se fijan, lavan y tiñen para su observación en un microscopio de contraste de fases.

AII.2.7 Separación de proteínas mediante SDS-PAGE

La separación y purificación de proteínas son etapas necesarias en el estudio y caracterización del proteoma en sistemas biológicos. Los diferentes métodos de separación se fundamentan en características diferenciales de las proteínas como solubilidad, tamaño o carga. La electroforesis en geles de poliacrilamida con SDS (SDS-PAGE) es una de las técnicas de separación de proteínas más ampliamente utilizada. Por acción del SDS, un detergente aniónico que rompe las interacciones hidrofóbicas de las proteínas, éstas se desnaturalizan, perdiendo su conformación tridimensional. Las proteínas desnaturalizadas toman una estructura en forma de bastoncillo con moléculas de SDS cargadas negativamente rodeando la cadena polipeptídica. Se observa un valor

constante de la relación carga/masa después de la formación del complejo SDS-proteína, por lo que la separación se produce dependiendo de su peso molecular, desde el cátodo hasta el ánodo.

En un primer paso, las proteínas se cargan sobre un gel con un tamaño de poro grande, lo que se denomina el gel concentrador o *stacking gel*, con objeto de que todo el volumen de proteína cargado se concentre en una única banda. Posteriormente, la muestra pasa al gel resolutivo (*running gel*), donde se produce la separación de proteínas mediante la aplicación de un voltaje, en función de su tamaño (**Figura AI.5**) . La proporción de acrilamida-bisacrilamida utilizada para polimerizar el gel determina el tamaño de poro, que tiene una incidencia directa en la calidad de la separación. La mayor parte de aplicaciones utilizan entre un 5% y un 20% de entrecruzamiento para el gel resolutivo [156].

Dado que las proteínas son incoloras, para una correcta visualización del proceso de migrado a través del gel, se utilizan tintes como el azul de Coomassie, apreciado por su bajo coste, sencillez y rapidez, con una sensibilidad de entre 0,1-0,5 µg de proteína [157].

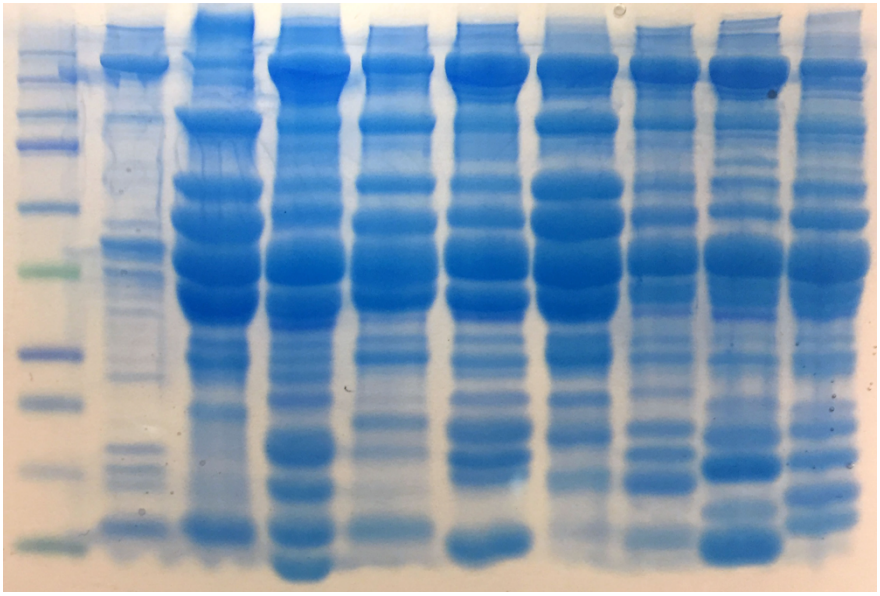

Figura AI.5. Separación de proteínas de varias muestras en gel de poliacrilamida.

AII.2.8 Western blot

Los immunoensayos se fundamentan en la medición de una señal analítica detectable cuando se produce el reconocimiento entre un anticuerpo (Ab) y un antígeno (Ag). Este reconocimiento se da gracias a una región en ambas moléculas denominada "parátopo" en el anticuerpo, y "epítopo" en el antígeno" las cuales presentan alta afinidad (**Figura AI.6**).

La formación de este complejo solo es posible con un antígeno específico, lo cual confiere a este tipo de ensayos una alta sensibilidad y bajos límites de detección. La señal solo puede detectarse si previamente se ha incorporado un marcaje, ya sea fluorescente, luminiscente, radioactivo o enzimático. En la presente Tesis doctoral se ha empleado un tipo de immunoensayo utilizado para evaluar la expresión proteica y que se denomina Western blot. Este ensayo comienza con una separación de las proteínas en gel de poliacrilamida (PAGE) tal y como se detalla en la sección AI.2.7. A continuación se transfieren a un soporte de membrana donde quedan inmovilizadas. Esta transferencia electroforéticas se realiza sobre una membrana de nitrocelulosa (NC) o de fluoruro de polivinildeno (PVDF), aplicando un campo eléctrico orientado perpendicularmente a la superficie del gel. Este tipo de membranas presentan una alta afinidad por las proteínas y gran capacidad de retención.

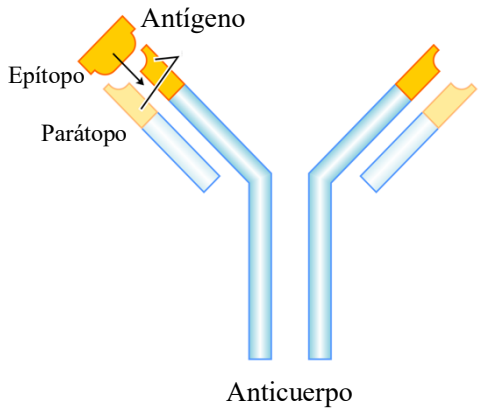

Figura AI.6. Reconocimiento anticuerpo-antígeno.

Una vez transferidas las proteínas desde el gel a la membrana, ésta se incuba con anticuerpos para la detección. En primer lugar se lleva a cabo una etapa de bloqueo para

saturar los sitios libres de la membrana de unión a proteínas (maximizando la relación señal-ruido específica). Para ello se incuba la membrana con caseína o con una disolución de albúmina de suero bovino. Posteriormente, la membrana se lava y se incuba con el anticuerpo primario específico del antígeno de interés. Si este anticuerpo contiene un marcador la detección será directa. Si no lo lleva, es necesaria una segunda incubación con un anticuerpo secundario, capaz de reconocer al anticuerpo primario, y que proporcione la señal analítica.
[158, 159].

AII.2.9 Espectrometría de masas

La espectrometría de masas es una técnica analítica que permite determinar la masa molecular o atómica de un compuesto o elemento según la relación masa/carga (m/z) de los iones formados. Los analitos se cargan eléctricamente (se ionizan) y, en un sistema de alto vacío, se les aplica un gradiente de campo eléctrico en sentido negativo a su carga. Este proceso ocurre en el espectrómetro de masas, que está formado por tres elementos principales: fuente de iones, analizador de masas, y detector [160]. Debido a su alta especificidad, flexibilidad para el diseño experimental, amplio intervalo de tamaños moleculares o posibilidad de automatización entre otras, se ha convertido en una técnica analítica esencial en proteómica o metabolómica, ya sea con fines cualitativos o cuantitativos [161]

Existen cuatro elementos principales que constituyen un espectrómetro de masas: sistema de introducción de la muestra, fuente de ionización, analizador de masas, y detector.

Hay dos sistemas principales de ionización: en fase gaseosa e ionización por desorción. En el primero, la muestra se volatiliza para después ionizarse, empleándose para compuestos térmicamente estables y de pesos moleculares menores a 10^3 Da. Este tipo de ionización suele acoplarse a cromatografía de gases (GC), y la fuente de ionización más utilizada es el impacto electrónico, considerada una fuente “dura” ya que durante el proceso de ionización se produce la fragmentación de la molécula inicial. La ionización por desorción, por el contrario, engloba a las fuentes llamadas “suaves” (electrospray y MALDI), en las que los analitos se transforma directamente en iones gaseosos sin

fragmentarse. Son sistemas aplicables a analitos no volátiles y térmicamente inestables, así como a aquellos compuestos con tamaños mayores a los 10^5 Da [162].

-Ionización química: Un gas reactivo con electrones genera iones que colisionan con las moléculas de la muestra, ionizándolas. La elección del tipo de gas o la diferente afinidad hacia los protones condicionará el grado de ionización del analito.
-Ionización por impacto electrónico: En esta fuente, un chorro de electrones acelerados bombean la muestra ionizándola. La alta energía cinética de los electrones, junto con su baja masa, hace que se produzca un cierto grado de fragmentación, generando iones positivos e incluso la desaparición del ion molecular.
-Ionización mediante desorción por láser asistida por matriz (MALDI): Esta técnica consiste en una co-cristalización de la muestra junto con una matriz (ácido orgánico), la cual se encuentra en una proporción mucho mayor. De esta forma, los analitos se diluyen y se aíslan, evitándose la formación de agregados difíciles de desorber. Esta mezcla es irradiada con un láser de alta potencia de pulsos cortos, de menera que la matriz absorbe energía y se produce el proceso de desorción junto con una transferencia de carga desde la matriz al analito, dando lugar a especies cargadas en fase gaseosa. Esta técnica permite que macromoléculas biológicas no volátiles se ionicen fácilmente.
-Ionización por electrospray (ESI): Se aplica a la muestra un alto voltaje (3-4 kV) en su paso por un capilar o aguja a presión atmosférica, formando pequeñas partículas cargadas

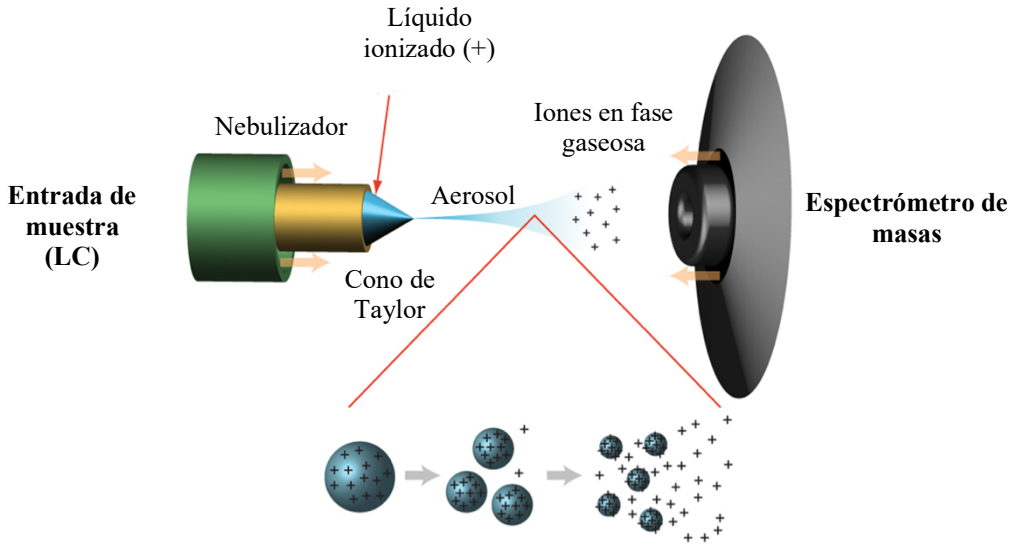

Figura AI.7. Esquema básico de una fuente de ionización por electrospray (ESI).

(**Figura AI.7**). Cuando estas gotas cargadas atraviesan la punta de la aguja, el solvente se evapora progresivamente (ayudado por un flujo de nitrógeno cálido), disminuyendo el tamaño de la gota. En el punto en el que la tensión superficial no puede mantener la carga (límite de Rayleigh), la gota se descompone en otras más pequeñas que transfieren su carga a los analitos, generándose iones que pueden tener una o múltiples cargas dependiendo de su tamaño [163]. Si el capilar tiene un potencial positivo, se retienen los iones negativos y los positivos se desplazan hasta el extremo contrario (ionización en modo positivo). En ese desplazamiento se genera un cono líquido en el extremo del capilar, en cuya punta se acumulan las gotas de analito con carga positiva. A medida que son arrastrados, pierden el solvente hasta la desolvatación completa del analito y su transferencia al analizador de masas. Los iones resultantes pueden presentar diferentes cargas: $[M+H]^+$, $[M+2H]^{2+}$ y $[M+3H]^{3+}$, mayoritariamente. En el caso contrario, ionización en modo negativo, se trabaja con valores de pH muy elevados en comparación con el modo positivo, y son los iones cargados negativamente los que viajan hasta el extremo contrario. Este modo precisa de un alto grado de pureza y bajas concentraciones de sales para que el electrospray se genere de forma correcta. Se suelen emplear disolventes orgánicos y ácidos orgánicos volátiles (ej. ácido fórmico) para formar los cationes y para eliminar las impurezas antes de la ionización. La ionización por electrospray es fácilmente acoplable a la cromatografía de líquidos ya que parte de la muestra en disolución [164,165].

Para el caso particular del análisis de proteínas o péptidos, se desarolló el nanoelectrospray (nanoESI). Estas fuentes, al tener un menor tamaño, minimizan impurezas en la muestra, además de no precisar un sistema de bombeo externo para mantener un flujo constante. La sensibilidad se incrementa sustancialmente respecto a la ionización por electrospray convencional ya que la desorción de los iones de pequeñas gotas es más favorable que de gotas mayores [166].

Un analizador de masas tiene como función la de separar los iones en función de la relación masa/carga (m/z), y enfocarlos a continuación al detector. Los analizadores separan los iones gracias a la energía cinética, velocidad, y momento de fuerza de las mismas, y su elección dependerá de la resolución que se precise, el intervalo y exactitud de masas y velocidad de barrido, entre otros muchos parámetros [167].

-Analizador de tiempo de vuelo (TOF): Un gradiente de voltaje acelera a los iones, los cuales atraviesan una zona tubular. El tiempo que tardan en llegar al detector es dependiente de su relación m/z, es decir, los iones cargados que tengan mayor masa tardarán más en llegar al detector, al contrario de aquellos con menor masa. Es un analizador muy usado para MALDI ya que permite la determinación de masas en un amplio intervalo (100-250.000 u.a.) obteniendo espectros de masas sencillos. La sensibilidad es alta aunque la reproducibilidad no lo es tanto debido al difícil control del proceso de cristalización y producción de iones.

-Analizador de tipo cuadrupolo (Q): Formado por cuatro barras paralelas a las que se les aplica un potencial de corriente continua y lentes con campo eléctrico oscilante. El campo generado filtra los iones con trayectoria estable de camino al detector. Es adecuado para cualquier tipo de interfaces y tiene un bajo coste, aunque el intervalo de trabajo no es muy grande ni la resolución es alta.

-Trampa iónica (IT): Se constituye por un electrodo de entrada, uno anular, y otro de salida. En el anillo se atrapan y mantienen los iones mediante corriente continua y radiofrecuencia. Al aumentar el potencial, las órbitas de los iones más pesados se estabilizan, al revés que los iones más ligeros, los cuales saldrán antes hacia el detector. Las trampas de iones cuadrupolares son económicas y muy útiles con muestras complejas ya que pueden cambiar el escaneo para analitos de diferentes masas y generar espectros MS/MS de los iones detectados. Son altamente sensibles, aunque la resolución y las capacidad de atrapar iones es limitada. Debido a esto se desarrolló la trampa de iones lineal que consiste en cuatro barras paralelas cortadas en tres secciones. Los iones son extraídos de forma radial a través de ranuras en los electrodos mejorando el rango dinámico, la resolución, y la sensibilidad de la técnica.

-Analizador de resonancia iónica en ciclotrón con transformada de Fourier (FT-ICR): Dispone de una celda de trampa de iones que acumula iones gracias a campos magnéticos altos y la resonancia de ciclotrón. Si la velocidad de un ion es lenta y el campo magnético intenso el radio de la trayectoria del mismo disminuye y queda atrapado, oscilando en función de su m/z.

La combinación de analizadores resulta especialmente ventajosa para la identificación de compuestos y la mejora de la sensibilidad, como por ejemplo el triple cuadrupolo (QqQ), el Q-TOF, el TOF-TOF y la combinación de la trampa de iones con el Orbitrap, entre otros.
Especialmente para estudios de metabolómica, se emplea frecuentemente la combinación seriada de tres cuadrupolos (QqQ) donde el primero de ellos (Q1) es un selector de iones precursores, el segundo (Q2) es una celda de colisión, mientras que el tercero (Q3), es un escáner de las masas de iones producto que permite obtener el espectro final. Además, este tipo de combinación es capaz de monitorizar múltiples transiciones de iones en un mismo evento analítico, lo que se conoce como modo MRM (multiple reaction mode).

El proceso de fragmentación en un espectrómetro de masas en tándem (MS/MS) puede llevarse a cabo mediante múltiples métodos. Algunos de ellos son la disociación inducida por colisión (CID), activación inducida por un fotón, disociación por transferencia de electrones (ETD), o activación mediada por electrones (EDC), entre otras [168, 169].

Los detectores son responsables de determinar la abundancia de los iones. El más utilizado en expetrometría de masas es el multiplicador de electrones, el cual es capaz de amplificar la señal del haz de iones hasta 10^6 órdenes de magnitud. Esto es posible gracias a que, cuando un ion cargado golpea una superficie, genera iones secundarios que se liberan de los átomos localizados en la capa externa de dicha superficie. Además, existen otros tipos de detectores como la placa de microcanales (MCP), la copa de Faraday, el contador de centelleo o el contador de fotones multipixel entre muchos otros.

AII.2.10 Proteómica cuantitativa: SILAC

La estrategia SILAC está basada en la adición directa de aminoácidos isotópicos y estables al medio de cultivo celular de dos poblaciones. Una de las poblaciones celulares incorporará los aminoácidos “ligeros” del medio normal de cultivo, mientras que la otra hará lo mismo con los “pesados”, generalmente empleando $^{12}C/^{13}C$ o $^{14}N/^{15}N$. Son suficientes cinco o seis fases mitóticas de la población celular para la incorporación de estos aminoácidos pesados (principalmente L-lisina y L-arginina), completando el marcaje celular al 100%. Tras esto, la población expuesta a este medio “pesado” tendrá todas sus proteínas marcadas con uno o más aminoácidos “pesados”. Una vez se garantiza

el completo marcaje, ambas poblaciones se mezclan en proporción 1:1 y se continúa el proceso analítico con una separación de proteínas por electroforesis en gel y posterior digestión de las mismas con una enzima proteolítica (generalmente tripsina). Después de la digestión se dispone de una mezcla de péptidos cuyas formas "ligera" y "pesada" son químicamente iguales salvo por el átomo pesado. Esto hace que su comportamiento cromatográfico sea idéntico y su detección sea simultánea.

Analíticamente, cada espectro de masas revelará los péptidos en forma de doblete (debido a la diferencia isotópica). El análisis se llevará a cabo relacionando la intensidad relativa de cada uno de los picos en el espectro de MS con la abundancia relativa de la proteína a la cual pertenece dicho péptido en las dos poblaciones [170, 171] (**Figura AI. 8**).
El cociente SILAC obtenido se calcula utilizando la siguiente ecuación, en la cual A y B son las dos poblaciones, I_P es la intensidad del pico del péptido "pesado", I_L la intensidad del pico del péptido "ligero", y *n* la cantidad de péptidos cuantificados:

$$R_{SILAC} = \frac{\frac{I_P A}{I_L A} + \frac{I_P B}{I_L B} + \frac{I_P n}{I_L n}}{n}$$

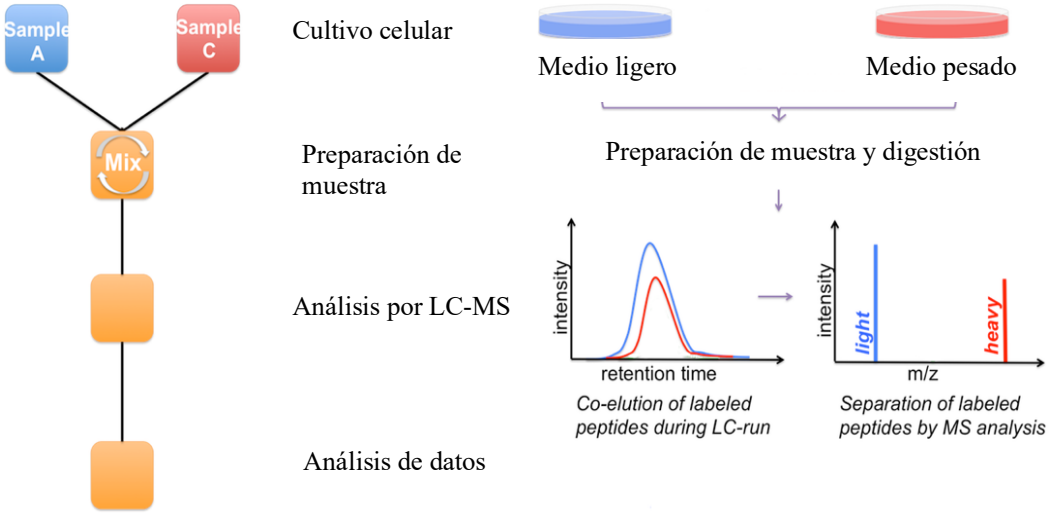

Figura AI.8. Esquema de la estrategia SILAC para la identificación y cuantificación de proteínas.

Al mismo tiempo que se realiza la cuantificación mediante el espectro de MS, se procede a una identificación mediante los espectros de MS/MS de cada péptido. Solo podrán cuantificarse aquellos péptidos que sean identificados, y para ello necesitarán uno de los aminoácidos marcados en su secuencia. Es por esto que generalmente en la estrategia SILAC se marcan los aminoácidos Lys y Arg, y la enzima elegida suela ser tripsina, ya que así todos los péptidos en digestión tendrán en su carbono terminal una Lys o una Arg. Siempre que el cociente SILAC sea distinto a 1, se podrá concluir que la abundancia de esa proteína en ambas poblaciones es diferente, lo cual puede resultar clave en la investigación de la acción de un agente quimioterapéutico.

Si la muestra no es un cultivo celular sino un tejido (cultivo primario), se emplea una variante denominada Super-SILAC. Fundamentalmente, se utiliza una mezcla de líneas celulares representativas de las que, en conjunto, están presentes en dicho tejido. Este *pool* de células será patrón interno tanto para el tejido no tratado como para el tratado. El análisis de las muestras se realiza por espectrometría de masas, aunque la obtención del cociente SILAC será, a su vez, un cociente entre los R_{SILAC} control y tratado [172].

AII.2.11 Análisis de expresión génica

Dentro de la evaluación citotóxica de un material, el estudio de diferencias de expresión génica se ha convertido en un elemento central en la investigación. Dentro de las técnicas más comunes en este campo destacan el Northern Blot, microarrays, hibridación *in situ*, qPCR y qRT-PCR.

En uno de los trabajos de la presente Tesis Doctoral se emplean los microarrays para distinguir diferencias de expresión génica después de la exposición de las células a las nanopartículas. Esta técnica consiste en la inmovilización miles de secuencias génicas sobre una superficie llamada chip. Este proceso lo llevan a cabo robots de precisión que utilizan agujas especiales para depositar las moléculas en las coordenadas correctas del chip (**Figura AI. 9**). En un microarray típico se pueden depositar más de 10.000 dianas (muestras de ADN) El ARN de la muestra biológica es marcado previamente mediante transcripción reversa (en presencia de nucleótidos fluorescentes), para obtener el correspondiente cDNA marcado. El cDNA generado se hibridará con las sondas inmovilizadas en la superficie y dará lugar a una señal fluorescente que puede correlacionarse con la expresión de los genes analizados [173, 174].

Una ventaja de esta técnica es que posibilita la evaluar la expresión diferencial empleando dos marcajes fluorescentes. De esta forma se evitan errores procedentes del empleo de varios procesos de hibridación.

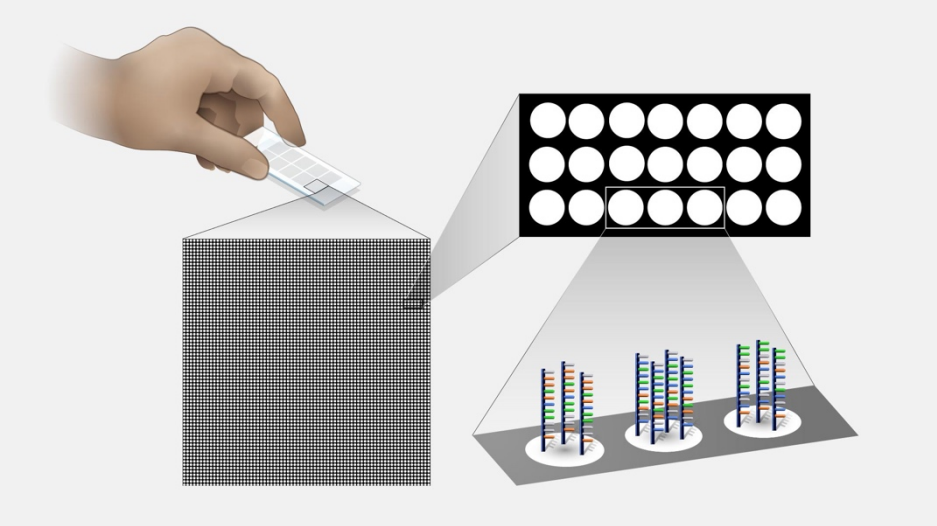

Figura AI.9. Chip para microarrays.

Con el objetivo de evaluar la expresión génica después de la exposición a Ch-SeNPs, se empleó la RT-qPCR como técnica de validación.

La técnica de la reacción en cadena de la polimerasa (PCR) está fundamentada en la obtención de múltiples copias de un fragmento de ADN concreto gracias a la capacidad natural de la ADN polimerasa para replicar hebras de ADN. Para este propósito, el proceso experimental implica ciclos de temperatura que separan las hebras recién formadas después de la replicación para, a continuación, volver a duplicarse.

Dado que muchas etapas se dan a 95 ºC para conseguir la desnaturalización, el desarrollo de la técnica ha incorporado ADN polimerasa termoestable, proveniente de organismos adaptados a la supervivencia en entornos térmicamente extremos.

En un inicio, la temperatura se eleva hasta 94-98 ºC para activar la enzima. Seguidamente, se desnaturaliza el ADN por calentamiento y, a continuación, se hibrida el cebador uniéndose a la secuencia complementaria en el ADN molde (bajando la temperatura hasta 40-68 ºC). La polimerasa une el híbrido de la cadena molde y el cebador, y da comienzo la síntesis de ADN añadiendo los 4 desoxirribonucleótidos-trifosfato (dNTP) complementarios en dirección 5` - 3`. Al final del proceso se lleva a cabo una etapa a 70-74 ºC para garantizar la amplificación total.

Para poder cuantificar la cantidad de ADN presente en la muestra, se lleva a cabo la qPCR, la cual se basa en el empleo de sondas o ácidos nucleicos marcados con fluorescencia, permitiendo la monitorización del producto tras cada ciclo de PCR. En cambio, para detectar el ARN en la muestra es necesario llevar a cabo una RT-qPCR, la cual consta de dos pasos: una transcripción inversa, y la amplificación de la secuencia de ADN deseada [175, 176].

AII.2.12 Metabolómica

Históricamente, el desarrollo de técnicas y métodos para la evaluación del metaboloma no ha seguido el mismo ritmo que otros campos como por ejemplo el de la proteómica o el de la genómica. Esto se debe, principalmente, a la complejidad de las moléculas orgánicas pequeñas en términos físico-químicos. Concretamente, y a diferencia de los genes, RNA mensajeros, o proteínas que codifican información a partir de monómeros, los metabolitos no se producen a partir de una transferencia de información entre residuos dentro de la célula. El rápido desarrollo de la genómica o la proteómica se debe a la tecnología y a las herramientas bioinformáticas acopladas capaces de caracterizar estos elementos. La metabolómica, por el contrario, tiene una gran diversidad de estructuras químicas a analizar, distinguiendo entre metabolitos endógenos y exógenos, en función de su origen. Esta gran diversidad redunda en una gran variedad de polaridades, pesos moleculares grupos funcionales, estabilidad, y reactividad química, entre otras propiedades. Por este motivo, es necesario recurrir a múltiples plataformas y configuraciones analíticas que nos permitan incluir en el estudio la totalidad del metaboloma [177].

Las dos técnicas más empleadas en metabolómica son la resonancia magnética nuclear (RMN) y la espectrometría de masas (MS) acoplada a cromatografía líquida (LC-MS), cromatografía de gases (GC-MS) y, en menor medida, a la electroforesis capilar (CE-MS).

Para evaluar el metaboloma de una población celular es necesario decidir, en un primer lugar, si se pretende estudiar un grupo concreto de metabolitos relacionados entre sí (metabolómica dirigida) o bien el global de metabolitos (metabolómica no dirigida)

[178]. En función de esta decisión y de los atributos de los metabolitos a analizar, variará la preparación de muestra y configuración instrumental [179].

Sin embargo, hay elementos comunes para metabolómica dirigida y no dirigida. Cualquier experimento de metabolómica incluye de una etapa de *quenching* y otra de extracción de metabolómicas.

-*Quenching*: El objetivo principal de este proceso es evitar la progresión de las rutas metabólicas para conservar la integridad de los diferentes compuestos y que las vías enzimáticas no los degraden. Por norma general, se suele realizar mediante la disminución de la temperatura de la muestra, teniendo un efecto directo de detención de rutas metabólicas previo a la lisis celular y extracción de metabolitos.

-Extracción: Normalmente se suelen emplear combinaciones de disolventes orgánicos con agua, por ejemplo en forma metanol, cloroformo y agua, de tal forma que los metabolitos polares se retienen en la fase metanol/agua mientras que los apolares quedan en la fase de cloroformo. Esta mezcla de disolventes permite extraer los metabolitos y que precipiten las proteínas o restos celulares.

-Derivatización: Esta fase se utiliza para aumentar la volatilidad de los compuestos y así poder determinarlos por cromatografía de gases, por ejemplo, a través de la trimetilsililación de los analitos. Uno de los reactivos más comunes es BSTFA, junto con el TMCS (catalizador). La acción de este derivatizante sustituye los hidrógenos activos de grupos químicos como ácidos, alcoholes, aminas, etc., por grupos trimetilsililo (TMS) Previamente a la trimetilsililación es necesario proteger los grupos carbonilo de aldehídos y cetonas de azúcares reductores de procesos de ciclación, además de estabilizar α-cetoácidos frente a la descarboxilación [180,181, 182]. De esta forma, no se introducen grupos TMS en posiciones distintas de un mismo compuesto, previniendo que se formen especies con diferente volatilidad, y por tanto que aparezcan varios picos cromatográficos de un mismo analito.

El reactivo más común es el hidrocloruro de metoxiamina disuelto en piridina [183].

Anexo III. Producciones científicas derivadas y comunicaciones a congresos.

AIII.1. Artículos científicos derivados de la presente Tesis Doctoral.

1. Estevez, H., Garcia-Lidon, J. C., Luque-Garcia, J. L., & Camara, C. (2014). Effects of chitosan-stabilized selenium nanoparticles on cell proliferation, apoptosis and cell cycle pattern in HepG2 cells: comparison with other selenospecies. Colloids and surfaces. B, Biointerfaces, 122, 184–193.

2. Estevez, H., Garcia-Calvo, E., Rivera-Torres, J., Vallet-Regí, M., González, B., & Luque-Garcia, J. L. (2021). Transcriptome Analysis Identifies Novel Mechanisms Associated with the Antitumor Effect of Chitosan-Stabilized Selenium Nanoparticles. Pharmaceutics, 13(3), 356.

3. Estevez, H., Garcia-Calvo, E., Mena, M. L., Alvarez-Fernandez Garcia, R., & Luque-Garcia, J. L. (2023). Unraveling the Mechanisms of Ch-SeNP Cytotoxicity against Cancer Cells: Insights from Targeted and Untargeted Metabolomics. Nanomaterials (Basel, Switzerland), 13(15), 2204.

4. Estevez, H., Garcia-Calvo, E., Sanchez, R., Martin, P., and Jose L. Luque-Garcia, J. L. (2023) Combination of SILAC-based quantitative proteomics and selective enrichment of nuclear proteins to gain insight into the molecular mechanisms responsible for the antitumor effect of selenium nanoparticles. In-vivo validation in a murine melanoma model. Enviado a la revista Small.

5. Estevez, H., Montalvo-Quiros, S., Vallet-Regí, M., Rivera-Torres, J., Gonzalez, B., Luque-Garcia, J.L. (2023) Mesoporous Silica Nanoparticles Functionalized with Transferrin for Target- Oriented Delivery of Selenium Nanoparticles: Deepening into the action mechanisms. Enviado a Acta Biomaterialia

6. Estevez, H., Palacios, A., Gil, D., Anguita, J., Vallet-Regi, M., González, B., Prados-Rosales, R., & Luque-Garcia, J. L. (2020). Antimycobacterial Effect of Selenium Nanoparticles on Mycobacterium tuberculosis. Frontiers in microbiology, 11, 800.

AIII.2. Otros artículos científicos.

[1] Olaya-Abril, A., Prados-Rosales, R., McConnell, M. J., Martín-Peña, R., González-Reyes, J. A., Jiménez-Munguía, I., Gómez-Gascón, L., Fernández, J., Luque-García, J. L., García-Lidón, C., **Estévez, H**., Pachón, J., Obando, I., Casadevall, A., Pirofski, L. A., & Rodríguez-Ortega, M. J. (2014). Characterization of protective extracellular membrane-derived vesicles produced by Streptococcus pneumoniae. Journal of proteomics, 106, 46–60.

[2] Pérez-Pérez, S., Domínguez-Mozo, M. I., Alonso-Gómez, A., Medina, S., Villarrubia, N., Fernández-Velasco, J. I., García-Martínez, M. Á., García-Calvo, E., **Estévez, H**., Costa-Frossard, L., Alvarez-Cermeño, J. C., Luque-Garcia, J. L., Arroyo, R., Villar, L. M., & Alvarez-Lafuente, R. (2020). Acetate correlates with disability and immune response in multiple sclerosis. *PeerJ*, *8*, e10220.

[3] Dominguez-Mozo, M. I., Perez-Perez, S., Villarrubia, N., Costa-Frossard, L., Fernandez-Velasco, J. I., Ortega-Madueño, I., Garcia-Martinez, M. A., Garcia-Calvo, E., **Estevez, H**., Luque Garcia, J. L., Torrejon, M. J., Arroyo, R., Villar, L. M., & Alvarez-Lafuente, R. (2021). Herpesvirus Antibodies, Vitamin D and Short-Chain Fatty Acids: Their Correlation with Cell Subsets in Multiple Sclerosis Patients and Healthy Controls. Cells, 10(1), 119.

[4] Mestre, L., Carrillo-Salinas, F. J., Feliú, A., Mecha, M., Alonso, G., Espejo, C., Calvo-Barreiro, L., Luque-García, J. L., **Estevez, H**., Villar, L. M., & Guaza, C. (2020). How oral probiotics affect the severity of an experimental model of progressive multiple sclerosis? Bringing commensal bacteria into the neurodegenerative process. Gut microbes, 12(1), 1813532.

[5] Cuello, J. P., Martínez Ginés, M. L., García Domínguez, J. M., Tejeda-Velarde, A., Lozano Ros, A., Higueras, Y., Meldaña Rivera, A., Goicochea Briceño, H., Garcia-Tizon, S., de León-Luis, J., Medina Heras, S., Fernández Velasco, J. I., Pérez-Pérez, S., García-Martínez, M. Á., Pardo-Rodríguez, B., Domínguez-Mozo, M. I., García-Calvo, E., **Estévez, H**., Luque-García, J. L., Villar, L. M., … Alvarez-Lafuente, R. (2022). Short-chain fatty acids during pregnancy in multiple sclerosis: A prospective cohort study. European journal of neurology, 29(3), 895–900.

AIII.3. Capítulos de libro

[1] R.C. Prados-Rosales, G. Aragoneses-Cazorla, **H. Estevez**, E. Garcia-Calvo, A. Machuca, J.L. Luque-Garcia, Strategies for membrane protein analysis by mass spectrometry, Advances in Experimental Medicine and Biology 1140 (2019) 289-298.

AIII.4. Comunicaciones a congresos

1. **H. Estévez**, B. González, S. Sánchez-Salcedo, M. Colilla, D. Anunciacao, M. Vallet-Regí, C. Cámara, J.L. Luque-García. Presentación oral. SELENIUM NANOPARTICLES: SYNTHESIS, CHARACTERIZATION AND APPLICATION AS POTENTIAL CHEMOTHERAPEUTIC AGENTS. 14as JORNADAS DE ANÁLISIS INSTRUMENTAL (JAI). Barcelona, 2014.

2. **H. Estevez**, M. Mecha, E. Garcia-Calvo, C. Guaza, J.L. Luque-Garcia*. Póster. UNVEILLING MULTIPLE SCLEROSIS: A PROTEOMIC STUDY OF THE ROLE OF THE KEY PROTEINS IN M1, M2A AND M2C PHENOTYPES. 6th Euchems chemistry congress. Sevilla, 2016.

3. **H. Estevez**, E. Cepria, S. Montalvo-Quiros, R. Sanchez-Diaz, P. Martin, M. Vallet- Regi, B. Gonzalez, J.L. Luque-Garcia. Póster. NOVEL INSIGHTS INTO THE POTENTIAL OF SELENIUM NANOPARTICLES AS A CHEMOTHERAPEUTIC AGENT: BIOMOLECULAR MECHANISMS, IN

VIVO STUDIES AND CELL-SPECIFIC TARGETING. XXI Reunión de la Sociedad Española de Química Analítica. Valencia, 2017.

4. **H. Estevez**, R. Calle-Gil, A. Oberlander, R. Sanchez-Diaz, P. Martin, M. Vallet-Regi,J. Rivera-Torres, B. Gonzalez, J.L. Luque-Garcia. Presentación oral. ANTITUMORAL EFFECT OF SELENIUM NANOPARTICLES: MECHANISMS, IN VIVO ACTIVITY AND SPECIFIC TARGETING. Valladolid, 2019.

5. **Héctor Estévez**. Presentación oral. NUEVOS NANOSISTEMAS HÍBRIDOS COMO HERRAMIENTA FRENTE A CÁNCER Y TUBERCULOSIS. Madrid, 2021.

6. **Hector Estevez**, Ainhoa Palacios, David Gil, Rafael Prados-Rosales and Jose L. Luque-Garcia. Póster. ANTIMYCOBACTERIAL EFFECT OF SELENIUM NANOPARTICLES ON MYCOBACTERIUM TUBERCULOSIS. Oviedo, 2022.

[1] Kieliszek M. (2021). Selenium. *Advances in food and nutrition research*, 96, 417–429.

[2] Barceloux D. G. (1999). Selenium. *Journal of toxicology. Clinical toxicology*, *37*(2), 145–172.

[3] Wessjohann, L., Schneider, A., Abbas, M. & Brandt, W. (2007). Selenium in chemistry and biochemistry in comparison to sulfur. *Biological Chemistry*, 388(10), 997-1006.

[4] Mehdi, Y., Hornick, J. L., Istasse, L., & Dufrasne, I. (2013). Selenium in the environment, metabolism and involvement in body functions. *Molecules* (Basel, Switzerland), 18(3), 3292–3311.

[5] Banerjee, M., Chakravarty, D., Kalwani, P., & Ballal, A. (2022). Voyage of selenium from environment to life: Beneficial or toxic?. *Journal of biochemical and molecular toxicology*, 36(11), e23195.

[6] Hatfield, D. L., Tsuji, P. A., Carlson, B. A., & Gladyshev, V. N. (2014). Selenium and selenocysteine: roles in cancer, health, and development. *Trends in biochemical sciences*, 39(3), 112–120.

[7] Jablonska, E., & Vinceti, M. (2015). Selenium and human health: Witnessing a Copernican revolution? *Journal of Environmental Science and Health. Part C, Environmental Carcinogenesis & Ecotoxicology Reviews*, 33(3), 328–368.

[8] Frost D. V. (1972). The two faces of selenium--can selenophobia be cured?. *CRC critical reviews in toxicology*, 1(4), 467–514.

[9] Casey C. E. (1988). Selenophilia. *The Proceedings of the Nutrition Society, 47*(1), 55–62.

[10] Vinceti, M., Filippini, T., Cilloni, S., & Crespi, C. M. (2017). The Epidemiology of Selenium and Human Cancer. *Advances in cancer research*, 136, 1–48.

[11] Papp, L. V., Lu, J., Holmgren, A., & Khanna, K. K. (2007). From selenium to selenoproteins: synthesis, identity, and their role in human health. *Antioxidants & redox signaling*, 9(7), 775–806.

[12] Mangiapane, E., Pessione, A., & Pessione, E. (2014). Selenium and selenoproteins: an overview on different biological systems. *Current protein & peptide science*, 15(6), 598–607.

[13] Nève J. (1995). Human selenium supplementation as assessed by changes in blood selenium concentration and glutathione peroxidase activity. *Journal of trace elements in medicine and biology : organ of the Society for Minerals and Trace Elements* (GMS), 9(2), 65–73.

[14] Chan, J. M., Darke, A. K., Penney, K. L., Tangen, C. M., Goodman, P. J., Lee, G. M., Sun, T., Peisch, S., Tinianow, A. M., Rae, J. M., Klein, E. A., Thompson, I. M., Jr,

Kantoff, P. W., & Mucci, L. A. (2016). Selenium- or Vitamin E-Related Gene Variants, Interaction with Supplementation, and Risk of High-Grade Prostate Cancer in SELECT. *Cancer epidemiology, biomarkers & prevention* : a publication of the American Association for Cancer Research, cosponsored by the American Society of Preventive Oncology, 25(7), 1050–1058.

[15] Avery, J. C., & Hoffmann, P. R. (2018). Selenium, Selenoproteins, and Immunity. *Nutrients*, 10(9), 1203.

[16] Razaghi, A., Poorebrahim, M., Sarhan, D., & Björnstedt, M. (2021). Selenium stimulates the antitumour immunity: Insights to future research. European journal of cancer (Oxford, England : 1990), 155, 256–267.

[17] Steinbrenner, H., Al-Quraishy, S., Dkhil, M. A., Wunderlich, F., & Sies, H. (2015). Dietary selenium in adjuvant therapy of viral and bacterial infections. Advances in nutrition (Bethesda, Md.), 6(1), 73–82.

[18] Arthur, J. R., McKenzie, R. C., & Beckett, G. J. (2003). Selenium in the immune system. The Journal of nutrition, 133(5 Suppl 1), 1457S–9S.

[19] Bhaskaram P. (2002). Micronutrient malnutrition, infection, and immunity: an overview. Nutrition reviews, 60(5 Pt 2), S40–S45.

[20] Barrett, C. W., Short, S. P., & Williams, C. S. (2017). Selenoproteins and oxidative stress-induced inflammatory tumorigenesis in the gut. *Cellular and molecular life sciences* : CMLS, 74(4), 607–616.

[21] Zhang, Z., Gao, X., Cao, Y., Jiang, H., Wang, T., Song, X., Guo, M., & Zhang, N. (2015). Selenium Deficiency Facilitates Inflammation Through the Regulation of TLR4 and TLR4-Related Signaling Pathways in the Mice Uterus. Inflammation, 38(3), 1347–1356.

[22] Köhrle, J., & Gärtner, R. (2009). Selenium and thyroid. Best practice & research. Clinical endocrinology & metabolism, 23(6), 815–827.

[23] Hoffmann, P. R., Jourdan-Le Saux, C., Hoffmann, F. W., Chang, P. S., Bollt, O., He, Q., Tam, E. K., & Berry, M. J. (2007). A role for dietary selenium and selenoproteins in allergic airway inflammation. Journal of immunology (Baltimore, Md. : 1950), 179(5), 3258–3267.

[24] Solovyev N. D. (2015). Importance of selenium and selenoprotein for brain function: From antioxidant protection to neuronal signalling. Journal of inorganic biochemistry, 153, 1–12.

[25] Akbaraly, T. N., Hininger-Favier, I., Carrière, I., Arnaud, J., Gourlet, V., Roussel, A. M., & Berr, C. (2007). Plasma selenium over time and cognitive decline in the elderly. Epidemiology (Cambridge, Mass.), 18(1), 52–58.

[26] Shahar, A., Patel, K. V., Semba, R. D., Bandinelli, S., Shahar, D. R., Ferrucci, L., & Guralnik, J. M. (2010). Plasma selenium is positively related to performance in

neurological tasks assessing coordination and motor speed. Movement disorders : official journal of the Movement Disorder Society, 25(12), 1909–1915.

[27] Drasch, G., Mail der, S., Schlosser, C., & Roider, G. (2000). Content of non-mercury-associated selenium in human tissues. Biological trace element research, 77(3), 219–230.

[28] Ejima, A., Watanabe, C., Koyama, H., Matsuno, K., & Satoh, H. (1996). Determination of selenium in the human brain by graphite furnace atomic absorption spectrometry. Biological trace element research, 54(1), 9–21.

[29] Whanger P. D. (2001). Selenium and the brain: a review. Nutritional neuroscience, 4(2), 81–97.

[30] Alehagen, U., Opstad, T. B., Alexander, J., Larsson, A., & Aaseth, J. (2021). Impact of Selenium on Biomarkers and Clinical Aspects Related to Ageing. A Review. Biomolecules, 11(10), 1478.

[31] Simonoff, M., Sergeant, C., Garnier, N., Moretto, P., Llabador, Y., Simonoff, G., & Conri, C. (1992). Antioxidant status (selenium, vitamins A and E) and aging. EXS, 62, 368–397.

[32] Pillai, R., Uyehara-Lock, J. H., & Bellinger, F. P. (2014). Selenium and selenoprotein function in brain disorders. IUBMB life, 66(4), 229–239.

[33] Vinceti, M., Mandrioli, J., Borella, P., Michalke, B., Tsatsakis, A., & Finkelstein, Y. (2014). Selenium neurotoxicity in humans: bridging laboratory and epidemiologic studies. Toxicology letters, 230(2), 295–303.

[34] Vinceti, M., Chiari, A., Eichmüller, M., Rothman, K. J., Filippini, T., Malagoli, C., Weuve, J., Tondelli, M., Zamboni, G., Nichelli, P. F., & Michalke, B. (2017). A selenium species in cerebrospinal fluid predicts conversion to Alzheimer's dementia in persons with mild cognitive impairment. Alzheimer's research & therapy, 9(1), 100.

[35] Duffield-Lillico, A. J., Reid, M. E., Turnbull, B. W., Combs, G. F., Jr, Slate, E. H., Fischbach, L. A., Marshall, J. R., & Clark, L. C. (2002). Baseline characteristics and the effect of selenium supplementation on cancer incidence in a randomized clinical trial: a summary report of the Nutritional Prevention of Cancer Trial. Cancer epidemiology, biomarkers & prevention : a publication of the American Association for Cancer Research, cosponsored by the American Society of Preventive Oncology, 11(7), 630–639.

[36] Méplan, C., & Hesketh, J. (2014). Selenium and cancer: a story that should not be forgotten-insights from genomics. Cancer treatment and research, 159, 145–166.

[37] Lin, C. C., Huang, J. F., Tsai, L. Y., & Huang, Y. L. (2006). Selenium, iron, copper, and zinc levels and copper-to-zinc ratios in serum of patients at different stages of viral hepatic diseases. Biological trace element research, 109(1), 15–24.

[38] Bayda, S., Adeel, M., Tuccinardi, T., Cordani, M., & Rizzolio, F. (2019). The History of Nanoscience and Nanotechnology: From Chemical-Physical Applications to Nanomedicine. Molecules (Basel, Switzerland), 25(1), 112.

[39] Food and Drug Administration, Guidance for Industry Considering Whether an FDA-Regulated Product Involves the Application of Nanotechnology Contains Nonbinding Recommendations, 2014.

[40] Sim, S., & Wong, N.K. (2021). Nanotechnology and its use imaging and drug delivery (review). Biomedical reports, 14(5), 42.

[41] Satalkar, P., Elger, B., & Shaw, D. M. (2016). Defining Nano, Nanotechnology and Nanomedicine: Why should it matter?. Science and engineering ethics, 22(5), 1255-1276.

[42] Amir, S.M.M., Sultan, M.T.H., Jawaid, M., Ariffin, A.H., Mohd, S., Salleh, K.A.M., Ishak, M.R., Md Shah, A.U. (2018). Nondestructive testing method for Kevlar and natural fiber and their hybrid composites, in: Durab. Life Predict. Biocomposites, Fibre-Reinforced Compos. Hybrid Compos. Woodhead Publishing, pp. 367–388.

[43] Farokhzad, O. C., ¬ Langer, R. (2006). Nanomedicine: developing smarter therapeutic and diagnostic modalities. Advanced drug delivery reviews, 58 (14), 1456-1459.

[44] Katsuki, S., Matoba, T., Koga, J. I., Nakano, K., & Egashira, K. (2017). Anti-inflammatory nanomedicine for cardiovascular disease. Frontiers in cardiovascular medicine, 4, 87.

[45] Bozzuto, G., & Molinari, A. (2015). Liposomes as nanomedical devices. International journal of nanomedicine, 10, 975–999.

[46] Guimarães, D., Cavaco-Paulo, A., & Nogueira, E. (2021). Design of liposomes as drug delivery system for therapeutic applications. International journal of pharmaceutics, 601, 120571.

[47] Chauhan A. S. (2018). Dendrimers for Drug Delivery. Molecules (Basel, Switzerland), 23(4), 938.

[48] Nune, S. K., Gunda, P., Thallapally, P. K., Lin, Y. Y., Forrest, M. L., & Berkland, C. J. (2009). Nanoparticles for biomedical imaging. Expert opinion on drug delivery, 6(11), 1175–1194.

[49] Shi Kam, N. W., Jessop, T. C., Wender, P. A., & Dai, H. (2004). Nanotube molecular transporters: internalization of carbon nanotube-protein conjugates into Mammalian cells. Journal of the American Chemical Society, 126(22), 6850–6851.

[50] Lin W. (2015). Introduction: Nanoparticles in Medicine. Chemical reviews, 115(19), 10407–10409.

[51] Probst, C. E., Zrazhevskiy, P., Bagalkot, V., & Gao, X. (2013). Quantum dots as a platform for nanoparticle drug delivery vehicle design. Advanced drug delivery reviews, 65(5), 703–718.

[52] European Commission, Scientific Committee on Emerging and Newly Identified Health Risks SCENIHR, (2010).

[53] Vallet-Regi, M., & Tamanoi, F. (2018). Overview of Studies Regarding Mesoporous Silica Nanomaterials and Their Biomedical Application. The Enzymes, 43, 1–10.

[54] Frickenstein, A. N., Hagood, J. M., Britten, C. N., Abbott, B. S., McNally, M. W., Vopat, C. A., Patterson, E. G., MacCuaig, W. M., Jain, A., Walters, K. B., & McNally, L. R. (2021). Mesoporous Silica Nanoparticles: Properties and Strategies for Enhancing Clinical Effect. Pharmaceutics, 13(4), 570.

[55] Akhter, F., Rao, A. A., Abbasi, M. N., Wahocho, S. A., Mallah, M. A., Anees-ur-Rehman, H., & Chandio, Z. A. (2022). A Comprehensive Review of Synthesis, Applications and Future Prospects for Silica Nanoparticles (SNPs). Silicon, 14(14), 8295–8310.

[56] Loganathan, S., Tikmani, M., & Ghoshal, A. K. (2013). Novel pore-expanded MCM-41 for CO2 capture: synthesis and characterization. Langmuir : the ACS journal of surfaces and colloids, 29(10), 3491–3499.

[57] Lu, J., Liong, M., Zink, J. I., & Tamanoi, F. (2007). Mesoporous silica nanoparticles as a delivery system for hydrophobic anticancer drugs. Small (Weinheim an der Bergstrasse, Germany), 3(8), 1341–1346.

[58] Wu, S. H., Hung, Y., & Mou, C. Y. (2011). Mesoporous silica nanoparticles as nanocarriers. Chemical communications (Cambridge, England), 47(36), 9972–9985.

[59] Vivero-Escoto, J. L., Slowing, I. I., Trewyn, B. G., & Lin, V. S. (2010). Mesoporous silica nanoparticles for intracellular controlled drug delivery. Small (Weinheim an der Bergstrasse, Germany), 6(18), 1952–1967.

[60] Maranhão, R. C., Vital, C. G., Tavoni, T. M., & Graziani, S. R. (2017). Clinical experience with drug delivery systems as tools to decrease the toxicity of anticancer chemotherapeutic agents. Expert opinion on drug delivery, 14(10), 1217–1226.

[61] Wang, X., Yang, L., Chen, Z. G., & Shin, D. M. (2008). Application of nanotechnology in cancer therapy and imaging. CA: a cancer journal for clinicians, 58(2), 97–110.

[62] Bregoli, L., Movia, D., Gavigan-Imedio, J. D., Lysaght, J., Reynolds, J., & Prina-Mello, A. (2016). Nanomedicine applied to translational oncology: A future perspective on cancer treatment. Nanomedicine : nanotechnology, biology, and medicine, 12(1), 81–103.

[63] Bangham, A. D., Standish, M. M., & Watkins, J. C. (1965). Diffusion of univalent ions across the lamellae of swollen phospholipids. Journal of molecular biology, 13(1), 238–252.

[64] Farokhzad, O. C., & Langer, R. (2009). Impact of nanotechnology on drug delivery. ACS nano, 3(1), 16–20.

[65] Liu, Y., Miyoshi, H., & Nakamura, M. (2007). Nanomedicine for drug delivery and imaging: a promising avenue for cancer therapy and diagnosis using targeted functional nanoparticles. International journal of cancer, 120(12), 2527–2537.

[66] Bharali, D. J., & Mousa, S. A. (2010). Emerging nanomedicines for early cancer detection and improved treatment: current perspective and future promise. Pharmacology & therapeutics, 128(2), 324–335.

[67] Bareford, L. M., & Swaan, P. W. (2007). Endocytic mechanisms for targeted drug delivery. Advanced drug delivery reviews, 59(8), 748–758.

[68] Roggers, R., Kanvinde, S., Boonsith, S., & Oupicky, D. (2014) The practicality of mesoporous silica nanoparticles as drug delivery devices and progress toward this goal. AAPS PharmSciTech, 15(5), 1163-1171.

[69] Davis, M.E., Chen, Z. G., & Shin, D. M. (2008). Nanoparticle therapeutics: an emerging treatment modality for cancer. Nature reviews. Drug discovery, 7(9), 771-782.

[70] Zaman K. (2010). Tuberculosis: a global health problem. Journal of health, population, and nutrition, 28(2), 111–113.

[71] Strausz J. (2007). Tuberkulózis 2006 [Tuberculosis 2006]. Orvosi hetilap, 148(18), 829–831.

[72] Cardona P. J. (2018). Pathogenesis of tuberculosis and other mycobacteriosis. Patogénesis de la tuberculosis y otras micobacteriosis. Enfermedades infecciosas y microbiologia clinica (English ed.), 36(1), 38–46.

[73] Denholm J. (2010). The most recent report from the World Health Organization found that, worldwide, approximately 5% of new tuberculosis cases are caused by multidrug-resistant strains (MDR TB). Journal of travel medicine, 17(3), 216.

[74] Robledo J. (2019). Biomedica : revista del Instituto Nacional de Salud, 39(3), 431–433.

[75] Luo, X., Zeng, X., Gong, L., Ye, Y., Sun, C., Chen, T., Zhang, Z., Tao, Y., Zeng, H., Zou, Q., Yang, Y., Li, J., & Sun, H. (2022). Nanomaterials in tuberculosis DNA vaccine delivery: historical perspective and current landscape. Drug delivery, 29(1), 2912–2924.

[76] Macêdo, D. C. D. S., Cavalcanti, I. D. L., Medeiros, S. M. F. R. D. S., Souza, J. B., Lira Nogueira, M. C. B., & Cavalcanti, I. M. F. (2022). Nanotechnology and tuberculosis:

An old disease with new treatment strategies. Tuberculosis (Edinburgh, Scotland), 135, 102208.

[77] Okamoto, Y., Taguchi, K., Yamasaki, K., Sakuragi, M., Kuroda, S., & Otagiri, M. (2018). Albumin-Encapsulated Liposomes: A Novel Drug Delivery Carrier With Hydrophobic Drugs Encapsulated in the Inner Aqueous Core. Journal of pharmaceutical sciences, 107(1), 436–445.

[78] Richter, A., Rudolph, I., Möllmann, U., Voigt, K., Chung, C. W., Singh, O. M. P., Rees, M., Mendoza-Losana, A., Bates, R., Ballell, L., Batt, S., Veerapen, N., Fütterer, K., Besra, G., Imming, P., & Argyrou, A. (2018). Novel insight into the reaction of nitro, nitroso and hydroxylamino benzothiazinones and of benzoxacinones with Mycobacterium tuberculosis DprE1. Scientific reports, 8(1), 13473.

[79] De Maio, F., Palmieri, V., De Spirito, M., Delogu, G., & Papi, M. (2019). Carbon nanomaterials: a new way against tuberculosis. Expert review of medical devices, 16(10), 863–875.

[80] Tăbăran, A. F., Matea, C. T., Mocan, T., Tăbăran, A., Mihaiu, M., Iancu, C., & Mocan, L. (2020). Silver Nanoparticles for the Therapy of Tuberculosis. International journal of nanomedicine, 15, 2231–2258.

[81] Singh, R., Nawale, L., Arkile, M., Wadhwani, S., Shedbalkar, U., Chopade, S., Sarkar, D., & Chopade, B. A. (2016). Phytogenic silver, gold, and bimetallic nanoparticles as novel antitubercular agents. International journal of nanomedicine, 11, 1889–1897.

[82] Huang, S. H., Yang, T. C., Tsai, M. H., Tsai, I. S., Lu, H. C., Chuang, P. H., Wan, L., Lin, Y. J., Lai, C. H., & Lin, C. W. (2008). Gold nanoparticle-based RT-PCR and real-time quantitative RT-PCR assays for detection of Japanese encephalitis virus. Nanotechnology, 19(40), 405101.

[83] Dahlgren, P. N., Bishop, K., Dey, S., Herbert, B. S., & Tanaka, H. (2018). Development of a New Monochrome Multiplex qPCR Method for Relative Telomere Length Measurement in Cancer. Neoplasia (New York, N.Y.), 20(5), 425–431.

[84] Estevez, H., Garcia-Calvo, E., Rivera-Torres, J., Vallet-Regí, M., González, B., & Luque-Garcia, J. L. (2021). Transcriptome Analysis Identifies Novel Mechanisms Associated with the Antitumor Effect of Chitosan-Stabilized Selenium Nanoparticles. Pharmaceutics, 13(3), 356.

[85] Xia, I. F., Kong, H. K., Wu, M. M. H., Lu, Y., Wong, K. H., & Kwok, K. W. H. (2022). Selenium Nanoparticles (SeNPs) Immunomodulation Is More Than Redox Improvement: Serum Proteomics and Transcriptomic Analyses. Antioxidants (Basel, Switzerland), 11(5), 964.

[86] Saquib, Q., Siddiqui, M. A., Ahmad, J., Ansari, S. M., Faisal, M., Wahab, R., Alatar, A. A., Al-Khedhairy, A. A., & Musarrat, J. (2018). Nickel Oxide Nanoparticles Induced Transcriptomic Alterations in HEPG2 Cells. Advances in experimental medicine and biology, 1048, 163–174.

[87] Alsagaby S. A. (2022). Transcriptomics-Based Investigation of Molecular Mechanisms Underlying Apoptosis Induced by ZnO Nanoparticles in Human Diffuse Large B-Cell Lymphoma. International journal of nanomedicine, 17, 2261–2281.

[88] Betts J. C. (2002). Transcriptomics and proteomics: tools for the identification of novel drug targets and vaccine candidates for tuberculosis. IUBMB life, 53(4-5), 239–242.

[89] Kumari, S., Kumar, A., Samant, M., Singh, N., & Dube, A. (2008). Discovery of novel vaccine candidates and drug targets against visceral leishmaniasis using proteomics and transcriptomics. Current drug targets, 9(11), 938–947.

[90] Sivapalan, L., Kocher, H. M., Ross-Adams, H., & Chelala, C. (2021). Molecular profiling of ctDNA in pancreatic cancer: Opportunities and challenges for clinical application. Pancreatology : official journal of the International Association of Pancreatology (IAP) ... [et al.], 21(2), 363–378.

[91] Mathys, H., Davila-Velderrain, J., Peng, Z., Gao, F., Mohammadi, S., Young, J. Z., Menon, M., He, L., Abdurrob, F., Jiang, X., Martorell, A. J., Ransohoff, R. M., Hafler, B. P., Bennett, D. A., Kellis, M., & Tsai, L. H. (2019). Single-cell transcriptomic analysis of Alzheimer's disease. Nature, 570(7761), 332–337.

[92] Domon, B., & Aebersold, R. (2006). Mass spectrometry and protein analysis. Science (New York, N.Y.), 312(5771), 212–217.

[93] Rozanova, S., Barkovits, K., Nikolov, M., Schmidt, C., Urlaub, H., & Marcus, K. (2021). Quantitative Mass Spectrometry-Based Proteomics: An Overview. Methods in molecular biology (Clifton, N.J.), 2228, 85–116.

[94] Gioria, S., Urbán, P., Hajduch, M., Barboro, P., Cabaleiro, N., La Spina, R., & Chassaigne, H. (2018). Proteomics study of silver nanoparticles on Caco-2 cells. Toxicology in vitro : an international journal published in association with BIBRA, 50, 347–372.

[95] Sund, J., Alenius, H., Vippola, M., Savolainen, K., & Puustinen, A. (2011). Proteomic characterization of engineered nanomaterial-protein interactions in relation to surface reactivity. ACS nano, 5(6), 4300–4309.

[96] Evans, C., Noirel, J., Ow, S. Y., Salim, M., Pereira-Medrano, A. G., Couto, N., Pandhal, J., Smith, D., Pham, T. K., Karunakaran, E., Zou, X., Biggs, C. A., & Wright, P. C. (2012). An insight into iTRAQ: where do we stand now?. Analytical and bioanalytical chemistry, 404(4), 1011–1027.

[97] Gygi, S. P., Rist, B., Gerber, S. A., Turecek, F., Gelb, M. H., & Aebersold, R. (1999). Quantitative analysis of complex protein mixtures using isotope-coded affinity tags. Nature biotechnology, 17(10), 994–999.

[98] Ong S. E. (2012). The expanding field of SILAC. Analytical and bioanalytical chemistry, 404(4), 967–976.

[99] Olsen, J. V., Ong, S. E., & Mann, M. (2004). Trypsin cleaves exclusively C-terminal to arginine and lysine residues. Molecular & cellular proteomics : MCP, 3(6), 608–614.

[100] Fernández, M. N., Muñoz-Olivas, R., & Luque-Garcia, J. L. (2019). SILAC-based quantitative proteomics identifies size-dependent molecular mechanisms involved in silver nanoparticles-induced toxicity. Nanotoxicology, 13(6), 812–826.

[101] Edelmann, M. J., Shack, L. A., Naske, C. D., Walters, K. B., & Nanduri, B. (2014). SILAC-based quantitative proteomic analysis of human lung cell response to copper oxide nanoparticles. PloS one, 9(12), e114390.

[102] Garcia-Calvo, E., Cabezas-Sanchez, P., & Luque-Garcia, J. L. (2021). In-vitro and in-vivo evaluation of the molecular mechanisms involved in the toxicity associated to CdSe/ZnS quantum dots exposure. Chemosphere, 263, 128170.

[103] Johnson, C. H., Ivanisevic, J., & Siuzdak, G. (2016). Metabolomics: beyond biomarkers and towards mechanisms. Nature reviews. Molecular cell biology, 17(7), 451–459.

[104] Zeki, Ö. C., Eylem, C. C., Reçber, T., Kır, S., & Nemutlu, E. (2020). Integration of GC-MS and LC-MS for untargeted metabolomics profiling. Journal of pharmaceutical and biomedical analysis, 190, 113509.

[105] Schymanski, E. L., Jeon, J., Gulde, R., Fenner, K., Ruff, M., Singer, H. P., & Hollender, J. (2014). Identifying small molecules via high resolution mass spectrometry: communicating confidence. Environmental science & technology, 48(4), 2097–2098.

[106] Wei, Y., Jasbi, P., Shi, X., Turner, C., Hrovat, J., Liu, L., Rabena, Y., Porter, P., & Gu, H. (2021). Early Breast Cancer Detection Using Untargeted and Targeted Metabolomics. Journal of proteome research, 20(6), 3124–3133.

[107] Shang, X., Zhong, X., & Tian, X. (2016). Metabolomics of papillary thyroid carcinoma tissues: potential biomarkers for diagnosis and promising targets for therapy. Tumour biology : the journal of the International Society for Oncodevelopmental Biology and Medicine, 37(8), 11163–11175.

[108] Luan, H., Wang, X., & Cai, Z. (2019). Mass spectrometry-based metabolomics: Targeting the crosstalk between gut microbiota and brain in neurodegenerative disorders. Mass spectrometry reviews, 38(1), 22–33.

[109] McGarrah, R. W., Crown, S. B., Zhang, G. F., Shah, S. H., & Newgard, C. B. (2018). Cardiovascular Metabolomics. Circulation research, 122(9), 1238–1258.

[110] Rico, C. M., Wagner, D., Abolade, O., Lottes, B., & Coates, K. (2020). Metabolomics of wheat grains generationally-exposed to cerium oxide nanoparticles. The Science of the total environment, 712, 136487.

[111] Lv, M., Huang, W., Chen, Z., Jiang, H., Chen, J., Tian, Y., Zhang, Z., & Xu, F. (2015). Metabolomics techniques for nanotoxicity investigations. Bioanalysis, 7(12), 1527–1544. https://doi.org/10.4155/bio.15.83

[112] Chen, Z., Han, S., Zhang, J., Zheng, P., Liu, X., Zhang, Y., & Jia, G. (2021). Metabolomics screening of serum biomarkers for occupational exposure of titanium dioxide nanoparticles. Nanotoxicology, 15(6), 832–849. https://doi.org/10.1080/17435390.2021.1921872

[113] Global Tuberculosis Report (2019). Geneva: World Health Organization.

[114] Chandra Mohana, N., Yashavantha Rao, H. C., Rakshith, D., Mithun, P. R., Nuthan, B. R., & Satish, S. (2018). Omics based approach for biodiscovery of microbial natural products in antibiotic resistance era. Journal, genetic engineering & biotechnology, 16(1), 1–8.

[115] Vallet-Regí, M., González, B., & Izquierdo-Barba, I. (2019). Nanomaterials as Promising Alternative in the Infection Treatment. International journal of molecular sciences, 20(15), 3806.

[116] Jayawardana, K. W., Jayawardena, H. S., Wijesundera, S. A., De Zoysa, T., Sundhoro, M., & Yan, M. (2015). Selective targeting of Mycobacterium smegmatis with trehalose-functionalized nanoparticles. Chemical communications (Cambridge, England), 51(60), 12028–12031.

[117] Reshma, V. G., Syama, S., Sruthi, S., Reshma, S. C., Remya, N. S., & Mohanan, P. V. (2017). Engineered Nanoparticles with Antimicrobial Property. Current drug metabolism, 18(11), 1040–1054.

[118] Wang, L., Hu, C., & Shao, L. (2017). The antimicrobial activity of nanoparticles: present situation and prospects for the future. International journal of nanomedicine, 12, 1227–1249.

[119] Herman, A., & Herman, A. P. (2014). Nanoparticles as antimicrobial agents: their toxicity and mechanisms of action. Journal of nanoscience and nanotechnology, 14(1), 946–957.

[120] Baranwal, A., Srivastava, A., Kumar, P., Bajpai, V. K., Maurya, P. K., & Chandra, P. (2018). Prospects of Nanostructure Materials and Their Composites as Antimicrobial Agents. Frontiers in microbiology, 9, 422.

[121] Hoseinzadeh, E., Makhdoumi, P., Taha, P., Hossini, H., Stelling, J., Kamal, M. A., & Ashraf, G. M. (2017). A Review on Nano-Antimicrobials: Metal Nanoparticles, Methods and Mechanisms. Current drug metabolism, 18(2), 120–128.

[122] Khan, F., Lee, J. W., Pham, D. N. T., Khan, M. M., Park, S. K., Shin, I. S., & Kim, Y. M. (2020). Antibiofilm Action of ZnO, SnO2 and CeO2 Nanoparticles Towards Grampositive Biofilm Forming Pathogenic Bacteria. Recent patents on nanotechnology, 14(3), 239–249.

[123] Reshma, V. G., Syama, S., Sruthi, S., Reshma, S. C., Remya, N. S., & Mohanan, P. V. (2017). Engineered Nanoparticles with Antimicrobial Property. Current drug metabolism, 18(11), 1040–1054.

[124] Beyth, N., Houri-Haddad, Y., Domb, A., Khan, W., & Hazan, R. (2015). Alternative antimicrobial approach: nano-antimicrobial materials. Evidence-based complementary and alternative medicine : eCAM, 2015, 246012.

[125] Estevez, H., Garcia-Lidon, J. C., Luque-Garcia, J. L., & Camara, C. (2014). Effects of chitosan-stabilized selenium nanoparticles on cell proliferation, apoptosis and cell cycle pattern in HepG2 cells: comparison with other selenospecies. Colloids and surfaces. B, Biointerfaces, 122, 184–193.

[126] Huang, T., , Holden, J. A., , Heath, D. E., , O'Brien-Simpson, N. M., , & O'Connor, A. J., (2019). Engineering highly effective antimicrobial selenium nanoparticles through control of particle size. Nanoscale, 11(31), 14937–14951.

[127] Bai Y, Wang Y, Zhou Y, Li W, Zheng W (2008). Modification and modulation of saccharides on elemental selenium nanoparticles in liquid phase. Mater Lett; 62:2311-4.

[128] Andreu, N., Zelmer, A., Fletcher, T., Elkington, P. T., Ward, T. H., Ripoll, J., Parish, T., Bancroft, G. J., Schaible, U., Robertson, B. D., & Wiles, S. (2010). Optimisation of bioluminescent reporters for use with mycobacteria. PloS one, 5(5), e10777.

[129] Zhang, Y., Wang, J., & Zhang, L. (2010). Creation of highly stable selenium nanoparticles capped with hyperbranched polysaccharide in water. Langmuir : the ACS journal of surfaces and colloids, 26(22), 17617–17623.

[130] Singh, R., Nawale, L. U., Arkile, M., Shedbalkar, U. U., Wadhwani, S. A., Sarkar, D., & Chopade, B. A. (2015). Chemical and biological metal nanoparticles as antimycobacterial agents: A comparative study. International journal of antimicrobial agents, 46(2), 183–188.

[131] Kumarasingam, K., Vincent, M., Mane, S. R., Shunmugam, R., Sivakumar, S., & Uma Devi, K. R. (2018). Enhancing antimycobacterial activity of isoniazid and rifampicin incorporated norbornene nanoparticles. International journal of mycobacteriology, 7(1), 84–88.

[132] Lu, T., Wu, Y., Zhao, C., Su, F., Liu, J., Ma, Z., & Han, Q. (2018). One-step fabrication and characterization of Fe3O4/HBPE-DDSA/INH nanoparticles with controlled drug release for treatment of tuberculosis. Materials science & engineering. C, Materials for biological applications, 93, 838–845.

[133] Selim, A., Elhaig, M. M., Taha, S. A., & Nasr, E. A. (2018). Antibacterial activity of silver nanoparticles against field and reference strains of Mycobacterium tuberculosis, Mycobacterium bovis and multiple-drug-resistant tuberculosis strains. Revue scientifique et technique (International Office of Epizootics), 37(3), 823–830.

[134] Jafari, A., Mosavari, N., Movahedzadeh, F., Nodooshan, S. J., Safarkar, R., Moro, R., Kamalzadeh, M., Majidpour, A., Boustanshenas, M., & Mosavi, T. (2017). Bactericidal impact of Ag, ZnO and mixed AgZnO colloidal nanoparticles on H37Rv Mycobacterium tuberculosis phagocytized by THP-1 cell lines. Microbial pathogenesis, 110, 335–344.

[135] Choi, S. R., Britigan, B. E., Moran, D. M., & Narayanasamy, P. (2017). Gallium nanoparticles facilitate phagosome maturation and inhibit growth of virulent Mycobacterium tuberculosis in macrophages. PloS one, 12(5), e0177987.

[136] Khurana, A., Tekula, S., Saifi, M. A., Venkatesh, P., & Godugu, C. (2019). Therapeutic applications of selenium nanoparticles. Biomedicine & pharmacotherapy = Biomedecine & pharmacotherapie, 111, 802–812.

[137] Hosnedlova, B., Kepinska, M., Skalickova, S., Fernandez, C., Ruttkay-Nedecky, B., Peng, Q., Baron, M., Melcova, M., Opatrilova, R., Zidkova, J., Bjørklund, G., Sochor, J., & Kizek, R. (2018). Nano-selenium and its nanomedicine applications: a critical review. International journal of nanomedicine, 13, 2107–2128.

[138] Lopez-Heras, I., Sanchez-Diaz, R., Anunciacao, D.S., Madrid, Y., Luque-Garcia, J.L., Camara, C (2014). Effect of chitosan-stabilized selenium nanoparticles on cell cycle arrest and invasiveness in hepatocarcinoma cells revealed by quantitative proteomics. J. Nanomed. Nanotechnol.; 5:5.

[139] Tran, P. A., & Webster, T. J. (2011). Selenium nanoparticles inhibit Staphylococcus aureus growth. International journal of nanomedicine, 6, 1553–1558. https://doi.org/10.2147/IJN.S21729

[140] Shakibaie, M., Forootanfar, H., Golkari, Y., Mohammadi-Khorsand, T., & Shakibaie, M. R. (2015). Anti-biofilm activity of biogenic selenium nanoparticles and selenium dioxide against clinical isolates of Staphylococcus aureus, Pseudomonas aeruginosa, and Proteus mirabilis. Journal of trace elements in medicine and biology : organ of the Society for Minerals and Trace Elements (GMS), 29, 235–241.

[141] Clogston, J. D., & Patri, A. K. (2011). Zeta potential measurement. Methods in molecular biology (Clifton, N.J.), 697, 63–70.

[142] Bunaciu, A. A., Udriştioiu, E. G., & Aboul-Enein, H. Y. (2015). X-ray diffraction: instrumentation and applications. Critical reviews in analytical chemistry, 45(4), 289–299.

[143] Pasqua, L., De Napoli, I. E., De Santo, M., Greco, M., Catizzone, E., Lombardo, D., Montera, G., Comandè, A., Nigro, A., Morelli, C., & Leggio, A. (2019). Mesoporous silica-based hybrid materials for bone-specific drug delivery. Nanoscale advances, 1(8), 3269–3278.

[144] Mann, C., Yu, L., Lo, C. M., & Kim, M. (2005). High-resolution quantitative phase-contrast microscopy by digital holography. Optics express, 13(22), 8693–8698.

[145] Sanderson, M. J., Smith, I., Parker, I., & Bootman, M. D. (2014). Fluorescence microscopy. Cold Spring Harbor protocols, 2014(10), pdb.top071795.

[146] Bastiaens, P. I., & Squire, A. (1999). Fluorescence lifetime imaging microscopy: spatial resolution of biochemical processes in the cell. Trends in cell biology, 9(2), 48–52.

[147] Burghardt, R. C., & Droleskey, R. (2006). Transmission electron microscopy. Current protocols in microbiology, Chapter 2.

[148] Mörgelin M. (2017). Negative Staining and Transmission Electron Microscopy of Bacterial Surface Structures. Methods in molecular biology (Clifton, N.J.), 1535, 211–217.

[149] Slater, T. J., Lewis, E. A., & Haigh, S. J. (2016). Energy Dispersive X-ray Tomography for 3D Elemental Mapping of Individual Nanoparticles. Journal of visualized experiments : JoVE, (113), 52815.

[150] Hausdorfer, J., Sompek, E., Allerberger, F., Dierich, M. P., & Rüsch-Gerdes, S. (1998). E-test for susceptibility testing of Mycobacterium tuberculosis. The international journal of tuberculosis and lung disease : the official journal of the International Union against Tuberculosis and Lung Disease, 2(9), 751–755.

[151] Balouiri, M., Sadiki, M., & Ibnsouda, S. K. (2016). Methods for in vitro evaluating antimicrobial activity: A review. Journal of pharmaceutical analysis, 6(2), 71–79.

[152] Marks, D. C., Belov, L., Davey, M. W., Davey, R. A., & Kidman, A. D. (1992). The MTT cell viability assay for cytotoxicity testing in multidrug-resistant human leukemic cells. Leukemia research, 16(12), 1165–1173.

[153] Andrews J. M. (2001). Determination of minimum inhibitory concentrations. The Journal of antimicrobial chemotherapy, 48 Suppl 1, 5–16.

[154] Darzynkiewicz, Z., Bedner, E., & Smolewski, P. (2001). Flow cytometry in analysis of cell cycle and apoptosis. Seminars in hematology, 38(2), 179–193.

[155] Riccardi, C., & Nicoletti, I. (2006). Analysis of apoptosis by propidium iodide staining and flow cytometry. Nature protocols, 1(3), 1458–1461.

[156] Matsumoto, H., Haniu, H., & Komori, N. (2019). Determination of Protein Molecular Weights on SDS-PAGE. Methods in molecular biology (Clifton, N.J.), 1855, 101–105. https://doi.org/10.1007/978-1-4939-8793-1_10

[157] Brunelle, J. L., & Green, R. (2014). Coomassie blue staining. Methods in enzymology, 541, 161–167.

[158] Taylor, S. C., & Posch, A. (2014). The design of a quantitative western blot experiment. BioMed research international, 2014, 361590.

[159] Hnasko, T. S., & Hnasko, R. M. (2015). The Western Blot. Methods in molecular biology (Clifton, N.J.), 1318, 87–96.

[160] Domon, B., & Aebersold, R. (2006). Mass spectrometry and protein analysis. Science (New York, N.Y.), 312(5771), 212–217.

[161] Bantscheff, M., Schirle, M., Sweetman, G., Rick, J., & Kuster, B. (2007). Quantitative mass spectrometry in proteomics: a critical review. Analytical and bioanalytical chemistry, 389(4), 1017–1031.

[162] Chapman J. R. (1996). Mass spectrometry. Ionization methods and instrumentation. Methods in molecular biology (Clifton, N.J.), 61, 9–28.

[163] Tycova, A., Prikryl, J., Kotzianova, A., Datinska, V., Velebny, V., & Foret, F. (2021). Electrospray: More than just an ionization source. Electrophoresis, 42(1-2), 103–121.

[164] Wilm, M. (2011). Principles of electrospray ionization. Molecular & Cellular proteomics: MCP, 10(7), M111.009407.

[165] Tycova, A., Prikryl,, J., Kotzianova, A., Datinska, V., Velebny, V., & Foret, F. (2021) Electrospray: More than just an ionization source. Electrophoresis, 42 (1-2), 103-121.

[166] Fenn, J. B., Mann, M., Meng, C. K., Wong, S. F., & Whitehouse, C. M. (1989). Electrospray ionization for mass spectrometry of large biomolecules. Science (New York, N.Y.), 246(4926), 64–71.

[167] Li, C., Chu, S., Tan, S., Yin, X., Jiang, Y., Dai, X., Gong, X., Fang, X., & Tian, D. (2021). Towards Higher Sensitivity of Mass Spectrometry: A Perspective From the Mass Analyzers. Frontiers in chemistry, 9, 813359.

[168] Banerjee, S., & Mazumdar, S. (2012). Electrospray ionization mass spectrometry: a technique to access the information beyond the molecular weight of the analyte. International journal of analytical chemistry, 2012, 282574.

[169] Aebersold, R., & Goodlett, D. R. (2001). Mass spectrometry in proteomics. Chemical reviews, 101(2), 269–295.

[170] Chen, X., Wei, S., Ji, Y., Guo, X., & Yang, F. (2015). Quantitative proteomics using SILAC: Principles, applications, and developments. Proteomics, 15(18), 3175–3192.

[171] Deng, J., Erdjument-Bromage, H., & Neubert, T. A. (2019). Quantitative Comparison of Proteomes Using SILAC. Current protocols in protein science, 95(1), e74.

[172] Shenoy, A., & Geiger, T. (2015). Super-SILAC: current trends and future perspectives. Expert review of proteomics, 12(1), 13–19.

[173] Angres B. (2005). Cell microarrays. Expert review of molecular diagnostics, 5(5), 769–779.

[174] Sealfon, S. C., & Chu, T. T. (2011). RNA and DNA microarrays. Methods in molecular biology (Clifton, N.J.), 671, 3–34.

[175] Ma, H., Bell, K. N., & Loker, R. N. (2020). qPCR and qRT-PCR analysis: Regulatory points to consider when conducting biodistribution and vector shedding studies. Molecular therapy. Methods & clinical development, 20, 152–168.

[176] Navarro, E., Serrano-Heras, G., Castaño, M. J., & Solera, J. (2015). Real-time PCR detection chemistry. Clinica chimica acta; international journal of clinical chemistry, 439, 231–250.

[177] Bujak, R., Struck-Lewicka, W., Markuszewski, M. J., & Kaliszan, R. (2015). Metabolomics for laboratory diagnostics. Journal of pharmaceutical and biomedical analysis, 113, 108–120.

[178] Schrimpe-Rutledge, A. C., Codreanu, S. G., Sherrod, S. D., & McLean, J. A. (2016). Untargeted Metabolomics Strategies-Challenges and Emerging Directions. Journal of the American Society for Mass Spectrometry, 27(12), 1897–1905.

[179] Patti, G. J., Yanes, O., & Siuzdak, G. (2012). Innovation: Metabolomics: the apogee of the omics trilogy. Nature reviews. Molecular cell biology, 13(4), 263–269.

[180] Clish C. B. (2015). Metabolomics: an emerging but powerful tool for precision medicine. Cold Spring Harbor molecular case studies, 1(1), a000588.

[181] Bowling, F. G., & Thomas, M. (2014). Analyzing the metabolome. Methods in molecular biology (Clifton, N.J.), 1168, 31–45.

[182] Patti, G. J., Yanes, O., & Siuzdak, G. (2012). Innovation: Metabolomics: the apogee of the omics trilogy. Nature reviews. Molecular cell biology, 13(4), 263–269.

[183] Wang, Y., Xu, L., Shen, H., Wang, J., Liu, W., Zhu, X., Wang, R., Sun, X., & Liu, L. (2015). Metabolomic analysis with GC-MS to reveal potential metabolites and biological pathways involved in Pb &Cd stress response of radish roots. Scientific reports, 5, 18296.